Extraction and recovery process of Poly-β-hydroxybutyrate from recombinant *Escherichia coli*

Yao LING

A thesis submitted for the degree of

Doctor of Philosophy

Department of Chemical Engineering

Faculty of Engineering

The University of Adelaide

January 1999

STATEMENT

The work described in this thesis contains no material which has been accepted for the award of any other degree or diploma in any university or other tertiary institution and, to the best of my knowledge and belief, contains no material previously published or written by another person, except where due reference has been made in the text.

I give consent to this copy of my thesis, when deposited in the University Library, being for loan and photocopying.

20.8.99

ACKNOWLEDGEMENT

I would like to express my gratitude to the people who have provided valuable assistance and encouragement throughout this work.

To my supervisors, Drs. Anton Middelberg and David Williams, for their patient, kind and valuable supervision. Without their encouragement and advice, the implementation of this thesis would not have been possible.

To Dr. Connor Thomas for his advice and help; Prof. Richard Jarrett who conducting the statistical work which forming an important part of this thesis; Chris Mansell for training and assisting me to operate pilot plant equipment and his technical help for conducting experiments; Richard ven Wegen for doing the production cost estimation. Thanks are also given to the peoples in the Department who gave help and advice during the study.

And to my husband, Wei Qi, for his kind support and utmost understanding throughout my studies.

SUMMARY

In response to the increasing concern about the disposal of petroleum-derived plastic, the development of biodegradable plastic has drawn much research attention. Poly-β-hydroxybutyrate (PHB) and its copolymer are considered to be the potential candidate. However, their high production cost has restricted their widespread use. PHB extraction and recovery has received less attention on a scientific basis comparing with PHB formation and processing of the purified product, despite its importance in determining overall production cost and altering properties of the final product. The industrial extraction method in use is complex in procedure and also involves the treatment with expensive chemical materials, which raised the production cost and also resulted in the low product quality. The aim of this study is to develop the process for PHB recovery from recombinant *E. coli*, using homogenization and centrifugation as the basic unit operations, with effects directed to reduce the PHB overall production cost.

The use of homogenization and centrifugation for PHB recovery was investigated and characterized. Homogenization was found efficient in PHB release from recombinant *E. coli* and high disruption efficiency was obtained after two passes of homogenization. Repeated centrifugation effected cell debris removal, while ensure a reasonable PHB collection efficiency. The fractionation was improved by incorporating NaOCl digestion into the process, which facilitated other cellular components removal such as protein and DNA as well. DNA denaturation and adherence to PHB granules during treatment were eliminated by restructuring unit operations sequence. A process which combined three homogenizer passes, three centrifuge passes, coupled with mild NaOCl treatment was established giving PHB purity of 96.5% and recovery rate of 79.5%, with negligible DNA and protein contamination levels.

For the simulation of the fractionation of cell debris and PHB, some fundamental work was conducted subsequently. Debris comminution of *E. coli* cell containing PHB by homogenization was characterized using Cumulative Sedimentation

Analysis (CSA), and PHB granules released were sized by an Analytical disc centrifuge (CDS). Both size distribution can be described by the Boltzmann function. The mathematical model for the prediction of cell debris size obtained after homogenization was validated. The effect of fermentation on cell debris comminution was discussed. The evidence about the effectiveness of freeze and thaw treatment of *E. coli* cells on following debris comminution by homogenization was presented. Chemical treatment (NaOH and NaOCl) on cell debris size reduction was assessed. NaOCl was recommended for the use of PHB recovery because of the impact of NaOH on PHB aggregation. NaOCl at mild condition showed less effect on cell debris micronisation compared with NaOH, but more efficient than that by having additional homogenization pass.

Particle fractionation in a disc-stack centrifuge was described by grade-efficiency curves. The simulation of the fractionation of cell debris and PHB granules confirmed that repeated centrifugation effected the fractionation of cell debris with PHB granules and indicated that cell debris removal and PHB collection in a given operation condition vary with the centrifugation feedrate and the homogenization passage prior to centrifugation. The importance of the first centrifugation on the overall cell debris removal was identified. The significance of the micronisation of cell debris prior to the centrifugation on the overall purification was highlighted. The significance of NaOCl treatment on cell debris fractionation was identified.

Cell debris digestion by NaOCl was modelled using response surface methodology, and expressed as a function of NaOCl concentration, cell concentration and the number of homogenization passes prior to centrifugation. PHB stability during the treatment was also investigated and modelled. Cell concentration (B) and NaOCl concentration (C) were identified as major effects on cell debris micronization, and their effect can be well summarized by the ratio B/C. It was recommended that the sole use of NaOCl treatment was unlikely to provide sufficient cell debris size reduction, while maintaining a high PHB collection, and other unit operations such as multiple homogenization should be included in association with NaOCl treatment. The Boltzmann function was also

reassessed statistically for the expression of cell debris size distribution and it was found that the Boltzmann function might not be the best model for the expression of cell debris size digested with NaOCl.

Based on the information obtained in the preceding studies, the PHB recovery process was finally optimized through the simulation of cell debris and PHB fractionation. The optimal process which met the cell debris removal target (〈95% cell debris removal) at the minimum overall production cost was then identified, involving 6 passes homogenization and 2 passes centrifugation, incorporating NaOCl treatment at a concentration of 0.85 g/L active chlorine. The process was demonstrated at pilot scale, a cell debris removal of 96.11% and PHB recovery rate of 93.65%, were achieved, and the estimated PHB production cost was US$6.57 /kg PHB. The efficiency on DNA and protein removal was also revealed. The results obtained can be simply extrapolated to full-scale PHB manufacture. It is believed that the optimal process was competitive to the existing industrial method in use in terms of PHB purity and recovery, but with significant reduction on production cost.

TABLE OF CONTENTS

Chapter One

1.1 Introduction 1

1.2 PHB intracellular formation 6

1.2.1 PHB production by *A. eutrophus* 6

1.2.2 PHB production by recombinant *E. coli* 10

1.3 Extraction of intracellular PHB 14

1.3.1 Laboratory methods for PHB recovery 14

1.3.1.1 Solvent extraction 14

1.3.1.2 Differential digestion treatment 15

1.3.1.3 Dispersion of sodium hypochlorite and chloroform 16

1.3.2 Large scale extraction of PHB 18

1.3.2.1 Enzymatic treatment 18

1.3.2.2 Cell disruption by heat shock 20

1.3.2.3 High pressure homogenization 20

1.3.2.4 Conclusion 21

1.3.3 Inclusion bodies recovery by homogenization and Centrifugation 21

1.3.4 Summary 23

1.4 PHB characterization 24

1.4.1 PHB intracellular degradation and depolymerase 24

1.4.2 Native morphology and morphology conversion of PHB 25

1.4.3 Existence of PHB amorphous state 26

1.4.4 PHB granule size and density 28

1.5 PHB contaminants, and their impact on PHB properties and recovery process 31

1.6 Scope of research 34

Chapter Two: Materials and methods 37

2.1 PHB production by fermentation 38

2.1.1 Bacterial strain and its maintenance 39

2.1.2 Shake flask culturing 40
2.1.3 Fed-batch fermentation protocol 40
2.1.4 Fermentation results 42
2.2 Cell disruption by homogenization 44
2.3 Particle fractionation by centrifugation 46
2.4 Analytical methods 48
2.4.1 Centrifugal Disc photoSedimentometer (CDS) 48
2.4.2 Cumulative sedimentation analysis 50
2.4.3 Sodium Dodecyl Sulphate-Polyacrylamide Gel Electrophoresis 55
2.4.4 Staining and visualizing of PHB granules 57
2.4.5 Dry cell weight measurement 58
2.4.6 Glucose determination 58
2.4.7 Cell lyophilization 62
2.4.8 PHB extraction by chloroform 62
2.5 Analysis of contaminants 64
2.5.1 Bio-Rad protein assay for protein measurement 64
2.5.2 DNA determination by diphenylamine assay 65
2.5.3 Residual cell debris quantification by SDS-PAGE 67
2.6 Characterization of PHB physical properties 68
2.6.1 PHB analysis by gas chromatography 68
2.6.2 Molecular weight determination by HPLC 73
2.6.3 PHB crystallization and glass transition analysis by DSC 75
2.6.4 PHB thermal stability analysis by TGA 76

Chapter Three: PHB recovery by homogenization and centrifugation 78
3.1 Introduction 79
3.2 Experimental work 80
3.2.1 Fermentation 80
3.2.2 Extraction process 80
3.2.3 Analysis 82
3.3 Results and discussion 85
3.3.1 PHB release by homogenization 85

3.3.2 Process A: Repeated centrifugation and PHB purity 85
3.3.3 Process B: Preliminary study of NaOCl effect on PHB recovery 87
3.3.4 Process C: An initial optimized process for PHB recovery from recombinant *E. coli*. 89
3.3.5 Conclusions 91

Chapter Four: Particle size analysis and fractionation simulation **92**

4.1 Modelling **93**
4.1.1 Modelling the recovery process 93
4.1.2 Cell debris micronization by homogenization: Modelling 94
4.1.3 Modelling study of centrifugation 96
4.1.4 Data collection and parameter determination 102
4.1.5 Summary 103

4.2 Experimental Work **104**
4.2.1 Fermentation 104
4.2.2 Cell debris size measurement by CSA 105

4.3 Results and discussion **107**
4.3.1 PHB stability under homogenization 107
4.3.2 Cell debris comminution by homogenization 110
4.3.3 Effect of fermentation on cell debris comminution 114
4.3.4 Effect of freeze-thaw on PHB and cell debris comminution 119
4.3.5 Conclusions 120

4.4 Simulation study of particle fractionation **122**
4.4.1 Performing a simulation 122
4.4.2 Simulation of the general effects 123
4.4.2.1 Multiple homogenization on PHB fractionation 124
4.4.2.2 Multiple centrifugation on PHB fractionation 125
4.4.3 Simulation study of the extraction processes 126
4.4.3.1 Process A 126
4.4.3.2 Process B 129
4.4.3.3 Process C 131
4.4.4 Conclusions 134

Chapter Five: Modelling cell debris digestion using response surface methodology 135

5.1 Introduction 136

5.2 Literature review of chlorination and preliminary investigation 138

5.2.1 Chemistry of chlorination 138

5.2.2 Mechanism of chlorination for cell material 140

5.2.2.1 Chlorine as a disinfectant 140

5.2.2.2 Solubilisation of cellular materials by NaOCl 142

5.2.2.3 Chlorination on nucleic acids 144

5.2.3 Dechlorination 145

5.2.4 Factors effecting NaOCl digestion 147

5.3 Factorial experimental design and response surface methodology 149

5.3.1 Factorial design and response surface methodology 149

5.3.2 Selection of factors and response variables 150

5.3.3 pH in NaOCl treatment condition on cell debris digestion and PHB stability 151

5.3.4 Experimental design 155

5.3.4.1 Overview 155

5.3.4.2 Design for Experiment I 155

5.3.4.3 Design for Experiment 2 157

5.4 Experimental Work 159

5.4.1 Fermentation 159

5.4.2 Homogenization and NaOCl treatment 159

5.4.3 Cell debris size measurement by CSA 160

5.4.4 PHB stability analysis 161

5.5 Developing regression models 162

5.5.1 Analysis for Experiment I 162

5.5.2 Analysis for Experiment II 165

5.5.3 Effect of B/C as a single factor on cell debris digestion 168

5.6 Discussion 170

5.6.1 Effect of cell concentration and NaOCl concentration on cell debris

digestion 170
5.6.2 Contour plotting analysis 174
5.6.3 Cell debris distribution and the Boltzmann function 177

Chapter Six: Optimization of PHB recovery process 181

6.1 Simulation and optimization of PHB recovery process 182

6.1.1 Defining the basic process flowsheet 182
6.1.2 Simulation strategy 184
6.1.2.1 Criteria for particle fractionation 184
6.1.2.2 Models and parameters used in simulation 185
6.1.2.3 Variables involved in PHB recovery process 186
6.1.3 Operational variables selection 188
6.1.4 Simulation 191
6.1.4.1 The effect of NaOCl concentration on CDR and PC 191
6.1.4.2 The effect of first-centrifuge feedrate on CDR and PC 194
6.1.4.3 The effect of homogenization and centrifugation 198
6.1.5 Summary: Process conditions for the optimized PHB recovery process 202

6.2 Experimental demonstration of the process 205

6.2.1 Definition for the optimal PHB recovery process 205
6.2.2 Experimental work 205
6.2.3 Characterization of the optimized PHB recovery process 209
6.2.4 Conclusion 215

6.3 Sensitivity analysis and further discussion 216

6.3.1 The effect of PHB size distribution on PHB production cost 216
6.3.2 The effect of cell concentration on production cost 219
6.3.3 PHB production cost allocation 221
6.3.4 Sensitivity analysis and further reduction of PHB production cost 223
6.3.5 Conclusion 224

Chapter Seven: Overall conclusions 225

7.1 PHB host --recombinant *E. coli* cells 225

7.2 A summary of the existed PHB recovery methods 226
7.3 Homogenization 226
7.4 NaOCl treatment 228
7.5 Centrifugal fractionation 229
7.6. Simulation and optimization of PHB extraction process 230
7.7 A process for PHB recovery from recombinant *E. coli* 231
7.8 Areas of interest for further research 233

REFERENCES 235

Appendix A **251**
A1 Operating procedure for SDS-PAGE analysis 251
A2 Modification of sample preparation for SDS-PAGE analysis 256
Appendix B Determination of PHB concentration by GC 259
Appendix C Impacts of chemical treatment and incomplete re-suspension on PHB granules and cell debris size 261
Appendix D Simulation procedure of cell debris fractionation 269
Appendix E Statistical analysis for model development 275
Appendix F Suspension viscosity 295

CHAPTER 1

1.1 INTRODUCTION

An increasing volume of petroleum-derived synthetic plastics is manufactured worldwide for various applications including use as coatings, structures and packing materials. They are more economical and easier to use industrially than many natural polymers. As a result, waste plastic has been become one of the main components of municipal waste. For example, in South Korea, 1.3 millions tons of waste plastics was generated in 1993, with a predicted annual increase of 30% (Chang, 1994). The disposal of waste plastics is currently a significant worldwide problem.

Major existing methods of solid waste disposal include incineration, recycling, landfill and composting. Unlike natural polymers, most synthetic plastics cannot be assimilated into the ecosystem, limiting the capacity of conventional waste-disposal methods. Recycling is seen as a method of reducing the problem. However, only about 25% of plastic waste is recyclable (Chang, 1994). An alternative solution is to develop biodegradable plastics.

Several types of biodegradable polymer are under development, including poly-hydroxyalkanoates (PHAs), aliphatic polyesters, polylactides, and polysaccharides. PHAs represent the family of polyesters which are accumulated by various microorganisms as an intracellular carbon and energy reserve material.

Microbial PHA accumulation generally occurs in response to a lack of essential nutrients such as nitrogen or phosphorus with an excess of carbon source such as sugar (Doi, 1990). By feeding different substrates during accumulation, PHAs with varying monomer units and side-chain compositions are produced. More

than 90 different PHA monomer units have been identified in various bacteria (Steinbuchel and Valentin, 1995).

PHAs are biodegradable thermoplastics with a wide range of applications (Doi, 1990). The physical properties of PHAs compare favourably with a range of synthetic thermoplastics and elastomers. They can be processed by conventional polymer processing equipment. PHAs are completely biocompatible and biodegradable in our environment. PHAs are naturally derived from renewable carbohydrate resources, and can be degraded into water and carbon dioxide in aerobic conditions, or methane and water under anaerobic conditions, within months. PHAs degradation in the environment, mainly in soil, sludge or seawater, are by the action of microorganisms (Doi, 1990). Some microorganisms, such as bacteria and fungi, excrete extracellular PHA depolymerases that degrade the microbial polyesters and utilize the decomposed compounds as nutrients. PHAs also show the ability to be recycled, facilitating entry into existing recycling schemes.

Poly(3-hydroxybutyrate) (PHB) was the first identified biodegradable polymer in microorganisms (Anderson and Dawes, 1990), and is the best characterized and studied member of the PHA family. PHB has many properties similar to isotactic polypropylene (Table 1.1). However, PHB is stiffer, more brittle, and has a remarkably lower breakage extension than polypropylene (Holmes, 1985). That is due to its native exceptional stereochemical regularity and crystalline structure (Mitomo *et al.*, 1987). Its brittleness is developed further during storage as a result of increasing crystallinity. Since PHB has a high melting point but a relatively low thermal degradation temperature, its stability during thermal processing has to be considered.

The problems associated with PHB mechanical properties are overcome by the copolymer poly-(3-hydroxybutyrate-co-3-hydroxyvalerate) P(3HB-co-3HV). Microbial P(3HB-co-3HV) is formed by supplementing carbohydrate feeding (e.g., glucose) with a compound containing an uneven number of carbons such as

propionic acid (Doi, 1990). P(3HB-co-3HV) has many useful thermomechanical properties compared with PHB. Incorporating comonomer 3HV into the PHB chain reduces crystallinity and makes the polymer tougher and more flexible. Its toughness and flexibility are regulated by varying the 3HV fraction. P(3HB-co-3HV) has a low melting temperature, which decreases with increasing 3HV fraction, thus removing concern about thermal degradation during processing. P(3HB-co-3HV) is of industrial interest and has been produced industrially by ZENECA Bio Products (UK) using *Alcaligenes eutrophus* as the host (Byrom, 1992). The product was sold at a price of US $16 /kg under the tradename 'Biopol' (Lee, 1995).

Table 1.1. A comparison of the physical and thermal properties of PHB and Polypropylene

Property	Units	PHB	Polypropylene
Melting temperature	°C	179	176
Glass transition temperature	°C	4	-10
Crystallinity	%	60-80	50-70
Molecular weight (M_w)	daltons	10^6	2×10^5
Density	g/cm^3	1.250	0.905
Tensile strength	MPa	40	38
Young's modulus	GPa	3.5	1.7
Extension to break	%	6	400
UV resistance		good	poor
Solvent resistance		poor	good
O_2 permeability (25mm film)	$cm^3/m^2/atm/day$	45	1700

A successful PHA market depends not only on the material properties but also the economics of manufacture. Despite its advantages over other materials, the PHA market is very small, incomparable with the large demand for biodegradable plastics. The key impediment affecting its market performance is the high production cost and thus high selling price. Compared with petroleum-derived polymers, such as polypropylene which sells at a price of less than US $1 /kg,

P(3HB-co-3HV) is not acceptable for many applications. Further exploitation of this technology for a commodity product requires a substantial reduction in present manufacturing cost. Considerable effort has been devoted to the development of better bacterial strains, more efficient fermentation strategies, and more economic recovery processes.

A. eutrophus was the first microorganism employed for the industrial production of PHB and P(3HB-co-3HV), because of its ability to accumulate a large amount of PHA (Byrom, 1987). Research into the development of superior bacterial strains by recombinant DNA techniques has been carried out extensively. Recombinant *E. coli* harbouring *A. eutrophus* PHB synthesis genes has been used for PHB synthesis in recent years with increased PHB productivity. In the meantime, some progress has been made in the improvement of fermentation control techniques. Carbon source is the major contributor to total substrate cost. Cheap carbon substrates, such as sucrose and dairy cheese whey, have been investigated for PHA cost reduction.

PHA extraction and recovery has received less attention compared with fermentation and host strain selection. Nevertheless, PHA extraction and purification becomes increasingly important in determining overall process costs. It is estimated that over two-thirds of the overall PHA production cost lies in downstream recovery. The quality of extracted PHA, and thus its application, are also dependent on the selected recovery process. Existing PHA extraction processes are generally inefficient. An efficient extraction process is required, which gives high product yield and efficiency at low production cost, while ensuring good product quality.

In this chapter, a literature review covering aspects of PHA production and recovery is provided. PHB production methods by the fermentation of *A. eutrophus* and *E. coli* are described in Sections 1.2.1 and 1.2.2, respectively. Existing recovery methods are reviewed in Section 1.3, and PHB characterization

is described in Section 1.4. PHB contaminants and their impacts are reviewed in Section 1.5. Finally the scope of research is outlined in Section 1.6.

1.2 PHB INTRACELLULAR FORMATION

More than 300 different microorganisms are capable of accumulating PHAs in response to unbalanced nutrient conditions (Steinbuchel, 1991). However, only a few can accumulate PHA to a level that suggests further investigation may be worthwhile. To select a microorganism for economic PHA production, a number of factors need to be considered, including growth rate, PHA accumulation rate, the substrates utilized, and PHA yield. PHA recovery is also important as it affects the final product cost significantly.

A glucose-utilizing mutant *A. eutrophus* H16 was the first microorganism selected and employed since 1982 for the industrial production of PHB and subsequently P(3HB-co-HV) (Byrom, 1987 and 1992). Reasons for choosing *A. eutrophus* as a PHA producer include the ability to accumulate PHA to high content with high molecular weight, and utilize various economically acceptable substrates. Consequently, *A. eutrophus* is the most studied microorganism in terms of PHA production. The *A. eutrophus* genes involved in PHB synthesis were cloned and expressed in *E. coli* in the early 1990s. Since then, PHA production in recombinant *E. coli* has been studied extensively, and it shows promise as an alternative for PHA production. In this section, PHB production using *A. eutrophus* and recombinant *E. coli* are briefly reviewed.

1.2.1 PHB production by *A. eutrophus*

A. eutrophus is a gram-negative bacterium, easy to grow, and it can accumulate PHB to a level of 60-95% of its biomass as intracellular granules in a simple medium. PHB formation in *A. eutrophus* is now well understood as a result of genetic and biochemical studies in recent years. PHB metabolism in *A. eutrophus* is clearly identified and it is found that PHB biosynthesis and biodegradation are regulated at the enzymatic level. PHB biosynthesis genes of *A. eutrophus* have been cloned and sequenced. Fermentation control and substrate requirement have

also been investigated for efficient PHB production. These have improved PHB production significantly.

Fermentation control

PHB accumulation in *A. eutrophus* occurs only when its growth is limited by the lack of an essential nutrient but with an excess of carbon sources such as glucose (Doi, 1990). Fed-batch fermentation is the mode mostly used. The fermentation can be divided into two stages: cell growth and PHB accumulation. During the first stage, cell grows under unlimited conditions, and very little PHB is produced. After the culture achieves the desired cell concentration, the supply of an essential nutrient is terminated and an excess of carbon source maintained. This initiates PHB accumulation.

Fermentation control is crucial for obtaining high PHB yield (Lee, 1996b). Since the residual cell concentration (defined as the cell concentration minus PHB concentration) is mostly achieved during the first stage and remains approximately constant while PHB is accumulated, any increase in cell concentration during the second stage is largely due to PHB accumulation. Because PHB is accumulated intracellularly, the cell concentration obtained before nutrient limitation is one of the factors determining PHB yield. Furthermore, cells from different growth stages vary in their capability to accumulate PHB. To optimize PHB yield, it is therefore necessary to choose the right time to introduce nutrient limitation. Byrom (1987) reported that in an *A. eutrophus* fermentation, the first cell growth stage took approximate 60 h before phosphate limitation was imposed: massive PHB accumulation occurred up to 75% (wt/wt) of the total dry biomass during the next 48 h.

The two stage fermentation affects the size and size distribution of PHB granules. The average number of PHB granules per *A. eutrophus* cell was fixed in the early accumulation stage and remained constant throughout PHB accumulation (Ballard *et al.*, 1987). PHB accumulation resulted solely from an increase in PHB granule mean diameter. Physical constraints due to cell size were the major factor limiting

PHB accumulation. Synthesis ceased when the PHB content reached about 80% because of the intracellular volume constraints, despite PHB synthase activity remaining relatively high. A reasonably high cell concentration obtained within a relative short time will be essential to achieve high PHB content, and thus high PHB productivity.

Nutrient requirement

PHB accumulation is initiated by the limitation of an essential nutrient, such as nitrogen, oxygen, phosphorus, sulfur or magnesium (Doi, 1990). Nitrogen and phosphate limitation are the mostly used. Phosphate limitation was employed at industrial scale by ZENECA (Byrom, 1987). Ammonium hydroxide (NH_4OH) was employed for pH control and also served as nitrogen source in *A. eutrophus* fermentation (Kim *et al.*, 1994a and 1994b). Nitrogen limitation, therefore, can be imposed simply by switching NH_4OH supply to another base such as NaOH.

As well as nutrient limitation, an excess of carbon source is essential for PHB accumulation. An optimum range of carbon concentration exists for a given strain. For example, glucose concentration was controlled between 10 and 20 g/L for *A. eutrophus* NCIMB 11599 (Kim *et al.*, 1994a). This control can be achieved using an on-line glucose analyzer or by monitoring the CO_2 evolution rate using mass spectrometry (Kim *et al.*, 1994a and 1994b). The DO-stat feeding strategy is also useful for PHB fed-batch fermentation. It can prevent the large fluctuations of glucose concentration in the culture due to the intermittent feeding (Rhee *et al.*, 1993).

Copolymer P(3HB-co-3HV) was accumulated in *A. eutrophus* by supplementing propionic acid along with glucose into the growth medium when cells were in the growth limiting stage (Byrom, 1992). The 3HB fraction in P(3HB-co-3HV) is regulated by varying the ratio of propionic acid to glucose in the feed solution (Doi, 1990). One major problem associated with copolymer production is the toxicity of co-substrates. Co-substrates such as propionic acid are toxic in excess of 0.1% in the culture, thus preventing polymer synthesis. For copolymer with a

low fraction of 3HV, the toxicity of propionic acid does not affect PHB accumulation because propionic acid is added in the cell growth limiting stage. However, the feeding rate of co-substrate must be carefully controlled. Co-substrates are also relatively expensive, which raises product cost. Furthermore, the feeding of co-substrates requires the modification of the existing fermentation strategies and makes the process of scaling up more difficult.

Biochemistry of PHB formation

Under unbalanced nutrient supply conditions, PHB synthesis in *A. eutrophus* undergoes a sequence of three enzymatic reactions after the conversion of carbon source to acetyl-CoA (Anderson and Dawes, 1990). Firstly, acetyl-CoA molecules are condensed to acetoacetyl-CoA catalysed by β-ketothiolase and free acetyl-coenzyme A is released. The intermediate acetoacetyl-CoA is then reduced into R-3-hydroxybutyryl-CoA by NADPH dependent acetoacetyl-CoA reductase. Finally, R-3-hydroxybutyryl-CoA is linked together to form a growing linear chain of PHB by the action of the PHB synthase (Figure 1.1).

Intracellular PHB degradation occurs simultaneously with PHB synthesis but at different rates (Figure 1.1). The presence of excessive carbon source accelerates PHB synthesis, while PHB degradation becomes dominant when the carbon source is depleted (Kawaguchi and Doi, 1992).

PHB degradation is initiated by PHB depolymerase to form R-3-hydroxybutyric acid. NAD specific dehydrogenase oxidizes the acid to acetoacetate which is then converted to acetoacetyl-CoA (Figure 1.1). Acetoacetyl-CoA is an intermediate to not only PHB synthesis but also PHB degradation. 3-Ketothiolase catalyzes the reversible condensation of two acetyl-CoA molecules into acetoacetyl-CoA. 3-ketothiolase appears to be the key enzyme in both PHB degradation and PHB synthesis.

The production of copolymer P(3HB-co-3HV) utilizes a similar pathway. The supplemented propionic acid is converted into propionyl-CoA in the first instance.

The enzymes involved in PHB synthesis have a relatively broad specificity. β-ketothiolase is able to incorporate propionyl-CoA with acetyl-CoA to form acetopropionl-CoA, which is then reduced and synthesized to give random copolymer P(3HB-co-3HV).

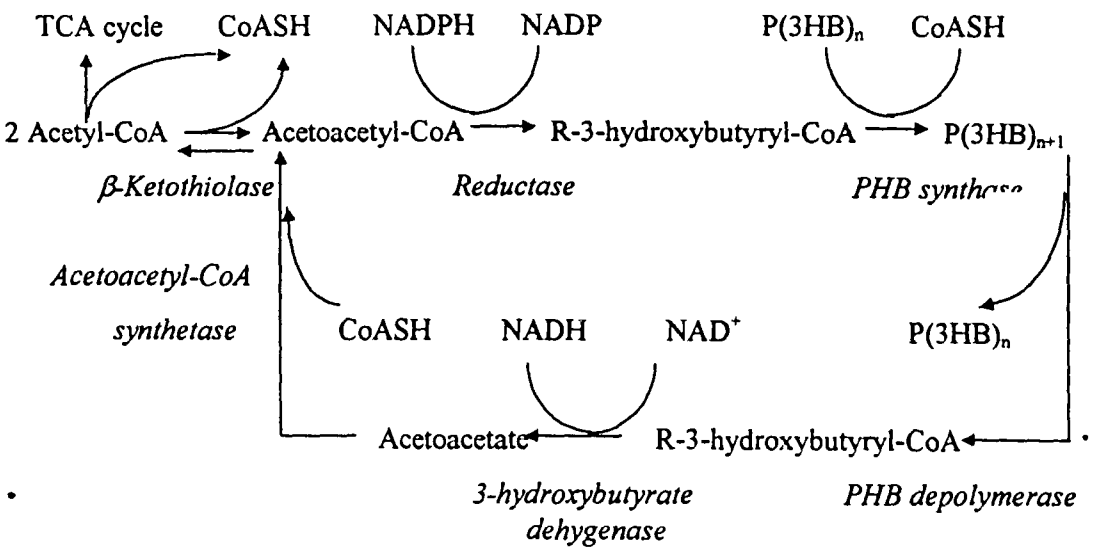

Figure 1.1. PHB metabolic pathway in *A. eutrophus*

1.2.2. PHB production by recombinant *E. coli*

E. coli is a widely used bacterium for the production of various recombinant proteins. *E. coli* has been the best studied microorganism in every respect. It grows rapidly and can utilize a relatively wide range of carbon sources. Fed-batch fermentation techniques giving high cell density and high product yield are well established (Lee, 1996a). The cloning of PHB synthesis genes of *A. eutrophus* into *E. coli* enables this PHB negative bacterium to produce PHB efficiently with high accumulation rates and high yields (up to 95% of dry cell weight) (Slater *et al.*, 1988). The PHB biosynthesis in recombinant *E. coli* and the productivity vary greatly depending on the gene expression system, selected medium and fermentation techniques applied.

Expression system

PHB biosynthesis genes of *A. eutrophus* were cloned and expressed in *E. coli* independently by three research groups (Slater *et al.*, 1988; Schubert *et al.*, 1988; Peoples *et al.*, 1989a and 1989b). The structural genes are located in a single operon in the order phbC, phbA and phbB encoding PHB synthase, β-ketothiolase and acetoacetyl CoA reductase, respectively. The expression of PHB biosynthesis genes in *E. coli* with the native *A. eutrophus* promoter is constitutive and nutrient limitation is not required during PHB synthesis (Peoples *et al.*, 1989b).

PHB accumulation depends on the expressed enzyme levels encoded by three genes. To achieve a high PHB expression, a high genes dosage is required, which can be obtained by using high copy number plasmids (Janes, 1990). A stable plasmid is necessary because recombinant plasmid containing the PHB synthesis genes may be lost rapidly from host cells during PHB accumulation (Lee *et al.*, 1994). The presence of antibiotics can maintain stable regeneration of plasmid containing cells, but this is not economically feasible at industrial scale.

PHB synthesis varies significantly among different *E. coli* strains because of the different expression levels of PHB synthetic genes (Lee and Chang, 1995). Among ten *E. coli* strains transformed with the same plasmid, PHB yield from glucose varied from 0.46 to 0.04 g PHB/g glucose, and productivity varied between 0.2 and 0.02 g.PHB/g residual cell mass.h (Lee and Chang, 1995b). These differences result from strain metabolic differences, including the concentrations of metabolites and the rates of metabolite formation. Introducing PHB biosynthesis genes into *E. coli* strains results in the establishment of a new metabolic pathway, which will compete and cooperate with the existing metabolic system.

Culture medium and metabolic engineering

PHB accumulation in recombinant *E. coli* is strongly dependent upon culture medium. *E. coli* produces higher levels of PHB in complex medium than in minimal medium. A PHB yield of 89 g/L was obtained in 42 h by a pH-stat fed-

batch culture of *E. coli* XL1-Blue in LB medium supplemented with glucose (Lee *et al.*, 1994b).

Despite the high PHB concentration, using expensive complex medium is not economical at large scale. It is estimated that approximately one third of the production cost was attributed to the medium, when culturing recombinant *E. coli* in LB medium with glucose as the carbon source (Douglas, 1991). Recently, a PHB yield of 177 g/L has been achieved on a glucose-based minimal medium (Wong *et al.*, 1998). This will reduce medium cost.

Fermentation

Unlike *A. eutrophus*, PHB formation by recombinant *E. coli* is a one-step process not requiring nutrient limitation. PHB is accumulated during cell regeneration and division. Fed-batch fermentation is employed to achieve a high cell concentration with high PHB content. pH-stat with a high limit can be employed for control. Under this approach, nutrients are added intermittently once glucose becomes depleted, typically indicated by a sharp rise of pH. In the early growth stage, the majority of the residual cell concentration is produced but with low PHB accumulation. In the stationary growth stage, PHB accumulation dominants the increase in cell concentration (Kim *et al.*, 1992). The physical occupation of PHB granules in the cytoplasm suppresses cell regeneration causing a slowdown of cell growth. This trend continues until growth ceases. For recombinant *E. coli* XL1-Blue growing in a semi-defined medium, once the P/X (defined as the ratio of PHB concentration to cell concentration) reached 50% in the early stationary phase, no further residual cell growth occurred, but PHB accumulation continued at a gradually reduced rate until the fermentation was terminated (Lee *et al.*, 1994).

Even through recombinant *E. coli* does not require any specific nutrient limitation, PHB synthesis becomes more efficient at a reduced cell growth rate when an excessive carbon source is provided. This is because the reduced cell growth due to the presence of PHB granules increases acetyl-CoA availability for PHB synthesis.

Advantages

Preliminary studies indicated that recombinant *E. coli* carrying the PHB biosynthesis genes is an economically more attractive candidate compared to the conventional PHB producer *A. eutrophus*. Well established gene construction techniques make it possible to develop PHB host strains with high PHB expression levels; a high cell density is relatively easy to achieve by modifying the available culture techniques; *E. coli* can utilize a number of carbon sources including sucrose and lactose, providing other opportunities for reducing production cost. The absence of intracellular PHB depolymerases is also an advantage as PHB will not be degraded once synthesized.

Utilization of recombinant *E. coli* also facilitates downstream PHB extraction, further reducing production cost. The *E. coli* cell wall becomes fragile because of PHB accumulation, simplifying PHB release. This phenomenon has not been observed in *A. eutrophus* (Lee, 1996). Genetically mediated lysis can also be employed to enhance PHB release in a gentle and efficient manner (Fidler *et al.*, 1992). The stable morphological structure of PHB granules is also beneficial for PHB extraction (Section 1.4). In the next section, methods available for PHA recovery are reviewed in some detail.

1.3. EXTRACTION OF INTRACELLULAR PHB

Intracellular PHB granules are protected and isolated from their environment by the cell wall, which provides mechanical strength and maintains concentration gradients between the cell and its surrounding. To recover PHB, it must first be liberated from the cell wall and then separated from non-PHB cellular material. There are generally two approaches to achieve the PHB recovery. One is to solubilize PHB using specific PHB solvents followed by precipitation and another is to solubilize non-PHB cellular material and maintain PHB granules intact followed by solid-liquid fractionation. The property and quality of the extracted polymer is affected by the chosen extraction method, specifically its molecular organization and molecular weight. The major non-PHB components comprise proteins, nucleic acids and lipids, and the extraction methods vary in the rate and extent of the removal of these contaminating biochemicals.

1.3.1. Laboratory methods for PHB recovery

The existing methods for PHB recovery at laboratory scale include solvent extraction, differential digestion, and the use of a dispersion of chloroform and hypochlorite. A common disadvantage is the need to use a large amount of chemical, thus raising production cost.

1.3.1.1. Solvent extraction

Solvent extraction uses organic solvents to solubilize and thus extract PHB from its biological source. The solubilized PHB is then separated from insoluble cellular material by filtration or centrifugation. The co-extracted cellular lipids in crude PHB solution are removed by slowly adding precipitates such as diethyl ether, hexane or methanol. To improve the solvent extractability, pretreatment of cell material, for example by lyophilization or milling, is required. A typical solvent extraction procedure using chloroform is described in Section 2.4.8.

The solvents used in the extraction are normally chlorinated organic solvents, such as methylene chloride, dichloroethane, and chloroform (Doi, 1990). The resultant PHB purity and recovery are high without molecular weight degradation. However, the chloroform solution containing more than 5% PHB (w/v) tends to be very viscous (Holmes and Lim, 1990), and the removal of insoluble cell material from PHB crude solution becomes difficult. A large quantity of solvent is thus required. Apart from the high chemical expense, the method also involves working with toxic and/or explosive, volatile solvents. Also, the downstream solvent recovery and recycle has to be considered. All these considerations restrict its application. Currently, solvent extraction is only used at laboratory scale for analytical purposes (Berger *et al.*, 1989; Hahn *et al.*, 1994; Lee *et al.*, 1995).

1.3.1.2. Differential digestion treatment

Sodium hypochlorite and sodium hydroxide solution digest microbial cell material effectively, mainly due to alkaline lysis and also through oxidation by hypochlorite. Differential digestion uses sodium hypochlorite or sodium hydroxide solution to release intracellular PHB and solubilize other non-PHB cellular material. The released PHB is then collected by centrifugation. The extraction conditions are harsh and severe PHB degradation often occurs.

Digestion of cell material by hypochlorite is affected by the cell mass and NaOCl conditions, treatment time, and pH. Under an optimized condition, PHB of 95% purity was extracted from *A. eutrophus* cells with about 50% molecular weight reduction (Berger *et al.*, 1989). PHB degradation was slightly improved if pretreating *A. eutrophus* cell mass with surfactants, such as SDS and Triton X-100 (about 60%) (Ramsay *et al.*, 1990). PHB degradation can also be reduced by the addition of sodium bisulfite ($NaHSO_3$), which anti-oxidizes the excessive hypochlorite, protecting the released PHB granules from further attack (Roh *et al.*, 1995). The resulting loss of molecular weight was reduced from 30% to 14% for PHB from *A. eutrophus*. Hypochlorite digestion appears to be more active in alkaline conditions due to a combination of alkaline lysis and oxidation. Hence

PHB purity could be increased by using high pH solutions, instead of by raising hypochlorite concentration (Roh *et al.*, 1995). Unfortunately, while the purity of the extracted PHB improved, the available PHB molecular weight decreased.

Hypochlorite digestion has been applied to recombinant *E. coli* (Hahn *et al.*, 1994). PHB in recombinant *E. coli* was less susceptible to hypochlorite degradation than that in *A. euthophus,* probably as a consequence of the differences in PHB morphology (Hahn *et al.*, 1995). Under mild conditions, PHB degradation was minimal (Middelberg *et al.*, 1995), suggesting that dilute hypochlorite can be employed as a cheap and simple method to recover PHB from recombinant *E. coli.*

Unlike sodium hypochlorite, sodium hydroxide digestion of cell material is solely due to alkaline lysis. The optimal condition for *A. eutrophus* cell mass with a concentration of 40 g/L was 1 N NaOH at 30°C for 1 h, yielding a PHB purity of 88.4% with a recovery of 90.8% (Lee *et al.*, 1995). Only a slight reduction in molecular weight was observed. Using NaOH digestion, the pretreatment is simple, involving only the cell harvest from cell broth by centrifugation with no milling and lyophilization required as for the hypochlorite treatment. This method shows some promise of achieving satisfactory scale up.

1.3.1.3. Dispersion of sodium hypochlorite and chloroform

The method is a combination of solvent extraction and differential digestion, based on the hydrophobicity of PHB and the hydrophilicity of the cell wall surface. The PHB-containing cell mass is suspended in a dispersion of hypochlorite solution and chloroform. When the PHB is released from cell mass by the action of hypochlorite, it migrates immediately from the aqueous phase to the organic chloroform phase. The chloroform serves as a shield protecting PHB from severe degradation (Hahn *et al.*, 1993 and Hahn *et al.*, 1994). The remaining non-PHB cellular material in the aqueous phase is subject to further solubilisation. The dispersion forms three layers after centrifugation; the hypochlorite aqueous phase is on the top, while the PHB containing chloroform

phase is on the bottom with remaining cell debris forming a layer in between. PHB is recovered by non-solvent precipitation and filtration from the organic phase.

This method possesses the advantages of both differential digestion and solvent extraction. PHB degradation is reduced significantly due to the protection of chloroform. PHB molecular weight could be regulated by adjusting hypochlorite concentration and reaction time. The non-PHB cellular material trapped in aqueous phase is readily removed from PHB solution and thus the viscosity of the solvent phase is significantly reduced. PHB specific solubility in chloroform and the suitable ratio of chloroform to hypochlorite assure high purity of the extracted PHB.

Hypochlorite concentration, treatment time and the ratio of chloroform to aqueous phase are the main factors being considered for maximizing PHB recovery while minimizing PHB degradation (Hahn *et al.*, 1994). The optimized condition for PHB extraction from *A. eutrophus* was 90 min treatment time with 30% hypochlorite concentration and 1:1 (v/v) chloroform-to-aqueous phase ratio. This treatment yielded a PHB purity of over 97% with 91% recovery (Hahn *et al.*, 1994).

The dispersion method has been applied for PHB extraction from *A. eutrophus* and recombinant *E. coli* in a laboratory scale with a remarkable reduction in PHB degradation (Hahn *et al.*, 1994; Hahn *et al.*, 1995). However, this process is unlikely to be satisfactory at industrial scale. A large amount of solvent is required to reduce the viscosity of the extraction solution, enabling easy separation of the soluble PHB polymer from insoluble non-PHB cellular material. This causes not only a large solvent recovery cost, but also a considerable solvent loss, even if a relatively efficient solvent recovery procedure is available.

1.3.2. Large scale extraction of PHB

The process development to produce PHB in bulk quantities has come a long way since PHB was first described. One of the major problems is the lack of an efficient extraction process. Solvent extraction was scaled up for PHB recovery from *Alcaligenes latus* (Haenggi, 1990). The process used methylene chloride to dissolve PHB from insoluble non-PHB material, followed by PHB precipitation. The process did not go into commercial production because of some unknown reasons.

The existing process for PHB and copolymer P(3HB-co-3HV) recovery from *A. eutrophus* is based on enzymatic digestion of non-PHB cellular material. It involves several complex steps, including cell rupture, enzymatic and detergent digestion, extensive washing and centrifugation, and final product decoloration. Cell disruption was initially implemented by heat shock, which was later replaced by high-pressure homogenization (Harrison, 1990). A detailed description of this process is given below.

1.3.2.1. Enzymatic treatment

Like differential digestion treatment, enzymatic treatment aims to solubilize non-PHB cellular material and leave PHB intact (Holmes, 1990). Since the proteinaceous materials form at least 40% by weight of the non-PHB cellular material, a proteolytic enzyme was employed. The enzyme of choice was required to be ineffective at solubilizing peptidoglycan, as the solubilized peptidoglycan may form masks enclosing the PHB granules with entrapped impurities, making subsequent PHB fractionation difficult. Prior to the treatment, the cell broth was subjected to heat shock at a temperature of at least 100°C. This step caused partial cell disruption and some nucleic acids were released and denatured. It significantly reduced cell suspension viscosity, ensuring the efficient subsequent operation and separation. The residual cell material was

further solubilised by surfactants and by heating the suspension to a temperature above 80°C. After washing and re-suspension, the residual material was treated with hydrogen peroxide, in an attempt to remove the discoloration of PHB caused by thermal treatment. The treatment with hydroxygen peroxide effected little or no further solubilization of non-PHB cellular material, but aided the separation of the PHB from aqueous medium by centrifugation due to a reduction in viscosity.

This method proved practical and was industrially applicable. It was employed by ZENECA in a commercial process by further modification and scaled up for continuous operation. The heat shock was conducted by heating the harvested cell broth at neutral or slightly acidic pH at 150°C through the injection of high pressure steam, and the condition maintained for 60 seconds before rapid release to atmospheric pressure. The process was then followed by alkaline serine protease and a non-ionic detergent treatment, washing to remove soluble debris, and treatment with hydrogen peroxide (Harrison, 1990).

In the commercial process, heat shock achieved the release of a significant amount of cytoplasmic materials, and resulted in sufficient cell wall permeation which facilitated further aqueous extraction. The release of nucleic acids and subsequent hydrolysis by heat shock eliminated the high suspension viscosity. Since the process was developed for PHB recovery from *A. eutrophus*, the presence of endogenous depolymerases was also considered. The inactivation of endogenous depolymerase was achieved simultaneously during heat shock. The treatment with alkaline serine protease effected the removal of a majority of proteins and nucleic acids, which was further enhanced by non-ionic detergent treatment. No significant reduction in molecular weight was found during protease and detergent treatment. The incorporation of hydrogen peroxide treatment at 80°C into the extraction method reduced color and odor in the final product but caused a 14% reduction in molecular weight.

1.3.2.2. Cell disruption by heat shock

Heat shock in continuous mode was both difficult to control and expensive in energy consumption. Fusion of PHB granules was observed after heat shock. This may facilitate downstream solid-liquid separation, but prevents the removal of the entrapped non-PHB material and reduces product quality. Further investigation found that heat shock did not achieve complete cell disruption and complete nucleic acid release, influencing the hydrolysis and solubilisation of nucleic acids. Most importantly, heat shock enhanced PHB degradation with about a 50% reduction in molecular weight composed to its starting value. The removal of the peptidoglygen wall material did not appear to be affected by heat shock.

The effectiveness of the heat shock process can be improved by operating under alkaline conditions (Harrison, 1990). This enables high levels of cell disruption to occur at a reduced temperature, thereby reducing PHB degradation. An optimized operation condition was pH 9, 140°C and 30 seconds, resulting in a soluble protein release of 85% and less than 20% degradation of PHB molecular weight.

1.3.2.3. High pressure homogenization (HPH)

Improved cell disruption at equivalent energy requirements can be achieved by HPH (Harrison, 1990). HPH has less harmful impacts on PHB molecular weight in comparison with heat shock, and the resultant molecular weight of the purified product is two-fold greater compared with the process involving heat shock. While PHB granules fuse together after heat shock, HPH maintains PHB granule morphology and results in the release of discrete granules of native size, which prevents the entrapment of cytoplasmic materials within the polymer granules. HPH is well suited to continuous operation.

HPH was incorporated into the PHB extraction process in place of heat shock (Harrison, 1990). HPH yielded a slight improvement in the reduction of

contaminanting biochemicals, especially protein and DNA. This may be due to the prevention of entrapment of non-PHB materials within the polymer granule aggregates. A PHB product containing 1.2% protein, approximately 0.2% lipid and negligible nucleic acid, phosphorus and sulphur was obtained. HPH did not affect enzyme activity. Inactivation of the intracellular depolymerase was achieved spontaneously during protease treatment.

1.3.2.4. Conclusion

The PHB extraction process for *A. eutrophus* is generally efficient if there is no high requirement on PHB purity (Harrison, 1990). The complexity in processing and the use of expensive enzymes raises PHB production cost significantly, especially when high PHB purity is required. Further solvent treatment needs to be considered. In terms of product quality, the major problem is low purity, colouring, odour due to the presence of contaminants over certain levels, and also the compacted PHB structure with high crystallinity caused by repeated centrifugation (Harrison, 1990). A reduction in molecular weight of the extracted PHB is also a problem that needs to be solved (Harrison, 1990).

1.3.3. Inclusion body recovery by homogenization and centrifugation

Homogenization and centrifugation are common unit operations to recover recombinant protein inclusion bodies from host cells formed during fermentation (Middelberg, 1996; Wong, 1996). Homogenization releases the inclusion bodies from the cells and yields a mixture containing inclusion bodies, soluble protein, and insoluble cell wall material. Cell wall is comminuted during homogenization and appears as small cell debris that remains insoluble. Centrifugation is used to fractionate insoluble inclusion bodies from other cellular material after cell disruption. Large, dense inclusion bodies are sedimented in the concentrate while small, light cell debris is discharged along with supernatant. Fractionation efficiency can be enhanced by optimizing centrifugation conditions (e.g., feedrate), despite perfect fractionation never being achieved. Some inclusion

bodies are lost into the supernatant representing product loss and some cell debris appears in the concentrate representing product contaminant. Purity can be enhanced through multiple centrifugation passes, minimizing the need for expensive chemicals and enzymes. Chemical and enzymatic treatment for further purification can be considered if a high purity product is required (Middelberg, 1996).

Due to the similarity of physical properties of recombinant protein inclusion bodies and intracellular PHB (see Section 1.4), this technique may be adapted for PHB fractionation in a scaled-up process. In addition, intracellular PHB granules comprise predominantly PHB (Lundgren *et al.*, 1964) and cellular contaminants such as nucleic acids and proteins found in the extracted PHB are mainly introduced during the extraction. The use of centrifugation to wash the PHB granules after release from host cells instead of PHB dissolution, may avoid the risks of incorporating contaminants into the PHB. Despite the widespread use of centrifugation for the recovery of inclusion bodies, this technique has not been thoroughly investigated as a method for the collection of PHB granules.

Fractionation by centrifugation is dictated by the relative sedimentation-velocity distributions of the granules and cell debris (e.g., size and density) (Hoare and Dunnill, 1989). PHB granule size is dictated by fermentation and has been characterized as described in Section 1.4. Cell debris size can be regulated by mechanical or chemical treatment. Homogenization effects cell debris comminution accompanying inclusion bodies release. The cell suspension is fed through a homogenizer a number of times to ensure that all the cells are broken and the cell wall is comminuted to a size which allows efficient separation from the inclusion bodies. Chemical treatment has also shown strong potential for cell debris digestion (Lee *et al.*, 1995; Williamson and Wilkinson, 1958). Sodium hypochlorite (NaOCl) effects cell debris digestion and has a less significant impact on PHB in mild treatment conditions (Berger *et al.*, 1989; Middelberg *et al.*, 1995). The techniques are also available to monitor and characterize debris minimization (Wong, 1997).

1.3.4. Summary

The PHB recovery methods reviewed are based on chemical or enzymatic solubilisation to achieve the separation of PHB granules from non-PHB cellular material. There is no straightforward pure mechanical approach for PHB recovery. The laboratory scale methods have been well established but few have been successfully scaled up. The existing large scale process is limited to PHB recovery from *A. eutrophus,* and high production cost and low quality of the extracted PHB are considerable problems. Improving PHB recovery and purification, and developing effective and cost-optimal recovery schemes, are important for PHB produced with recombinant *E. coli.* Homogenization and centrifugation could be employed as major unit operations in the PHB recovery process due to the similar physical properties of recombinant protein inclusion bodies and PHB granules.

Comparing with *A. eutrophus*, the recovery of PHB from recombinant *E. coli* could be easier due to the larger PHB granule size, higher crystallinity, and the possible introduction of genetically-mediated cell wall lysis. Higher crystallization makes *E. coli* PHB much more resistant to some extraction processes with less consequent molecular-weight reduction.

1.4. PHB CHARACTERISATION

PHB appears as intracellular discrete granules within host microorgrams. The *in vivo* PHB granule from wild type microorganisms possess a coating membrane about 2 nm thick, composed of lipids and proteins representing about 0.5% and 2% of the granule weight, respectively (Griebel *et al.*, 1968). The coating membrane lipids function to stabilize the interface between the hydrophobic contents of the granule and its aqueous environment, while the membrane proteins are associated with the activities of PHB polymerase and depolymerase (Lundgren *et al.*, 1964). PHB is the predominant component in native granules with lipids and proteins representing contaminants but in very small quantities.

The extracted PHB is highly crystalline, and has identical X-ray diffractograms even from different microorganims, indicating uniformity in crystal structure (Lundgren *et al.*, 1965). Some of its properties are similar to polypropylene, as shown in Table 1.1.

To develop a PHB extraction process, some knowledge about native PHB granules is required. Native PHB morphology determines its accessibility to extraction methods as it relates to the PHB stability and resistance to treatment conditions. PHB granule size distribution plays an important role, especially in a size-based particle fractionation process such as centrifugation. The intracellular depolymerase has also to be considered as it affects PHB yield and process design. A general review about these properties is given in this section.

1.4.1. PHB intracellular degradation and depolymerase

The most attractive feature of PHB and its copolymer is their ability to undergo rapid biodegradation. Intracellular PHB is degraded serving as a carbon and energy source under conditions of carbon starvation by the host microorganism. The metabolic pathway of PHB intracellular degradation is well understood (Section 1.2.1). PHB accumulation accompanies its degradation but at a different

rate. PHB degradation was about 10 times lower than that of PHB accumulation (Kawaguchi and Doi, 1992).

PHB degradation is catalyzed by intracellular PHB depolymerase. Kawaguchi and Doi (1992) suggested that PHB intracellular depolymerase was an exo-type hydrolase which hydrolyzed an ester bond of PHB at the terminus of polymer chain and released a monomeric 3-hydroxybutyric acid as the product. Assuming PHB depolymerase is a serine-esterase with a hydroxy group as an active site (E-OH), the proposed reaction scheme of PHB degradation can be described as follows:

$$E\text{-}OH + P(3HB)_n \longrightarrow P(3HB)_{n-1}O\text{-}E + \text{R-3-hydroxybutyric acid}$$

$$P(3HB)_{n-1}O\text{-}E + H_2O \longrightarrow P(3HB)_{n-1} + E\text{-}OH$$

The number of PHB molecular chains and the polydispersity remain almost constant during the degradation.

The intracellular PHB depolymerase has been isolated from some bacteria and characterized (Doi, 1990). However, it was not detected in recombinant *E. coli* (Lee *et al.*, 1994). Its activation on PHB granules is very susceptible because it is active only on native amorphous PHB granules. Treatments such as freeze and thaw cycles, repeated centrifugation, and proteolytic attack, render granules partially or completely inactive as a substrate for hydrolysis. This finding led to extensive studies of PHB morphology (Section 1.4.2).

1.4.2. Native morphology and morphology conversion of PHB

PHB from natural origins has exceptional stereochemical regularity. The PHB chain is linear and chiral centres possess only the R-stereochemical configuration, which implies that the polymer is completely isotactic and capable of crystallization (Mitomo *et al.*, 1987). The *in vivo* PHB was expected to be crystalline. Due to

PHB sensitivity to intracellular depolymerase, the existence of the two morphological states was postulated (Merrick and Doudoroff, 1964).

The *in vivo* PHB is in an amorphous state and becomes crystallized irreversibly during various treatments (Barham, 1990). ^{13}C-NMR spectroscopy and X-ray diffraction studies confirmed the *in vivo* PHB from *A. eutrophus* and other wild type microorganisms existed as an amorphous elastomer (Barnard and Sanders, 1988; Barnard and Sanders, 1989; Kawaguchi and Doi, 1990). An amorphous state for PHB in recombinant *E. coli* was also suggested by the TEM study of Lee (1996).

The amorphous PHB granules *in vivo* serve as a carbon storage material that participates in PHB metabolism. The PHB amorphous state is critical for maintaining PHB sensitivity to the intracellular enzyme system for PHB synthesis and degradation. Its inactivation is irreversible, accompanied by crystallization. The conversion from a native state to the inactive crystalline state can be induced by various treatments. Some of these treatments typically form part of the PHB extraction processes, such as centrifugation, freeze-thaw cycling, prolonged storage at 4°C, drying, sonication, enzyme treatment, exposure to solvents such as acetone, and acidic and alkaline conditions (Harrison *et al.*, 1992; Kawaguchi and Doi, 1990). However, the PHB morphological state was not affected by exposure to pressure, shear or cavitation experienced under homogenization, but the released PHB became more susceptible to change its configuration (Harrison, 1990).

1.4.3. Existence of PHB amorphous state

It seems impossible to give a plausible explanation for nascent PHB appearance in non-crystalline state on the basis of crystallization kinetics. One would expect that PHB with its exceptional stereochemical regularity and low glass transition temperature of ca. 6-9°C to crystallize rapidly at room temperature or normal cell growth temperature (30°C -37°C). It is possible that some special components

exist within *in vivo* PHB, which act as plasticizers to maintain PHB in the amorphous state.

Water is an integral component of PHB granules (Mas *et al.*, 1985). Barnard and Sander (1988) postulated that water could act as a PHB plasticizer within granules. This suggestion was supported by Harrison *et al.* (1992). Besides, Kawaguchi and Doi (1990) also found that the removal of lipid fraction in PHB native granules by enzymatic hydrolysis altered polymer mobility. However, lipid is unlikely to be a dominant effect due to its relatively small quantity. Once native PHB granules are subject to some chemical and physical treatments which induce the alteration of the native polymer-plasticizer arrangement, the loss of plasticizers occures with concomitant compaction of PHB granules, resulting in a drop in glass transition temperature and the formation of a crystalline structure. The extent of plasticizer loss depends on the treatment conditions, and determines the resultant crystallinity.

The assumption of the existence of plasticizers seems to be generally acceptable after extensive studies. However, Koning and Lemstra (1992) have questioned the existence of plasticizers, and postulated that native granules did not contain effective plasticizers and that the amorphous state of PHB *in vivo* could be explained from the crystallization kinetics of submicrometric granules being dominated by homogeneous nucleation. The *in vivo* PHB granules were free of extraneous particles because the granule membrane formed a barrier against the entry of other cell constituents (Lundgren *et al.*, 1964), and the disruption of the granule membrane by various treatments allowed extraneous particles acting as nucleation sites and induces the crystallization.

Both models give satisfactory explanation for PHB crystallization in recombinant *E. coli*. It was found that the lyophilized PHB derived from recombinant *E. coli* had higher crystallinity (60%) than that from *A. eutrophus* (16%) (Hahn *et al.*, 1995). Like other microoganisms, PHB from recombinant *E. coli* is in the amorphous state (Lee, 1996), but does not possess a coating-like granule

membrane. According to the first assumption, lyophilization to remove the PHB plasticizer water is easier for recombinant *E. coli* than that from *A. eutrophus*, resulting in high crystallinity. Alternatively, the lack of a granule membrane makes extraneous particle invasion easier, inducing high crystallinity. This characteristic will benefit PHB recovery from recombinant *E. coli* because of the improved PHB stability and resistance to the extraction conditions, corresponding to a variation in the extent and rate of PHB recovery and contaminant removal. PHB from recombinant *E. coli* was very resistant to hypochlorite treatment due to high crystallinization induced during the treatment (Hahn *et al.*, 1995).

1.4.4. PHB granules size and density

PHB granules synthesized by *A. eutrophus* and *Bacillus megaterium* were typically spherical with diameters in the range of 0.1-0.8 μm (Lafferty *et al.*, 1988), whereas the average diameters of PHB from recombinant *E. coli* were in the range of 1.13-1.25 μm determined by photosedimentation (Middelberg *et al.*, 1995).

PHB granule size is dictated by the nature of the host cells. Apart from PHB accumulation capacity which varies dramatically from one bacterium to another, the intracellular physical constraint is one of the major factors controlling PHB size. Recombinant *E. coli* cells undergo considerable change in response to the over-accumulation of PHB. For example, cells were heavily distorted due to PHB protrusion, resulting in a fragile call wall structure (Lee, 1996)

Fermentation conditions affect PHB size. As described in Section 1.2.1, the average number of PHB granules in *A. eutrophus* was fixed in the early PHB accumulation stage and the diameter of the PHB granules increased throughout the period of PHB accumulation under physical constraints due to intracellular space limitation. PHB granules from *A. eutrophus*, therefore, are highly homogeneous in size with relatively low polydispersity. However, the PHB granules from recombinant *E. coli* are highly heterogeneous in size and shape because of the non-synchronous nature of PHB accumulation during fermentation. PHB accumulation

occurs along with cell division and regeneration of new PHB granules. The total amount of PHB and the average number of PHB granules each cell possesses differ significantly. The size distribution of PHB granules, therefore, becomes broader compared with that from *A. eutrophus*. Moreover, the mean PHB granule size in *E. coli* increases with increasing PHB concentration (Middelberg *et al.*, 1995), which implies that PHB diameter increases throughout the fermentation.

Large PHB granules can also be produced by aggregation or flocculation. PHB released from *E. coli* cells is able to form aggregates in some ionic solutions (Dennis, 1991). Calcium chloride ($CaCl_2$) was recommended as a suitable aggregation agent based on the speed and size of aggregation formation. A 100% PHB aggregation rate was attainable at a $CaCl_2$ concentration of 10 mM under the conditions tested (Dennis, 1991). Some cell debris may be incorporated into the PHB aggregates if high $CaCl_2$ concentration is used. It is interesting to note that the addition of $CaCl_2$ produced aggregation only if the PHB was from *E. coli*, but no aggregates were formed if PHB was produced from *A. eutrophus*.

PHB crystalline density was reported as 1.260 g/cm^3 from X-ray diffraction studies, while the amorphous density was 1.177 g/cm^3 obtained from extrapolations of the data of specific volume changes during the heating of glassy PHB (Barham *et al.*, 1984). The density of *in vivo* PHB and the isolated solid from *A. eutrophus* was estimated to be 1.16 g/cm^3 and 1.24 g/cm^3, respectively, using Percoll density gradients (Mas *et al.*, 1985; Pedros-Alio *et al.*, 1985). The difference is most likely due to the different techniques used.

PHB accumulation results in an increase in host cell volume and cell density. PHB granules appear as tightly compacted inclusion bodies compared with other cellular components. The change in cell volume and cell density for *A. eutrophus* was significant according to the result of Pedros-Alio *et al.* (1985), and the cell volume was found to increase linearly with PHB content. A mathematical model predicting cell volume and density changes in response to PHB accumulation was postulated by Mas *et al.* (1985). The relationship between cell buoyant density

and inclusion bodies formation was further studied by Hwang (1996). This can be used to monitor PHB accumulation during cultivation.

1.5. PHB CONTAMINANTS, AND THEIR IMPACT ON PHB PROPERTIES AND THE RECOVERY PROCESS

The non-PHB cellular material (termed NPCM) generally comprise nucleic acids, lipids, polysaccharide, proteinaceous material including glycoproteins, and the cell wall construction material including phospholipids, peptidoglycans, lipopolysaccharides and other carbohydrates. The proteinaceous material forms at least 40% by weight of the NPCM (Holmes and Lim, 1990).

Insufficient removal of NPCM during the extraction process has impacts on resulting PHB properties and thus on its application. For example, one of the significant impacts is the decoloration and offensive odour appearing after heat processing, which is unacceptable for a variety of applications. Nucleic acids are identified as a major cause of product decoloration (Harrison, 1990). Both 4.2% RNA and 0.3% DNA by mass can result in considerable browning of the material. The degradation in color quality also occurs when protein is present in excess of 2% by mass. In addition, introducing foreign agents during the purification process can also cause quality degradation due to their incomplete removal after treatment. For example, the use of non-ionic ethoxylates (Tritons X100 and Triton X102) as solubilization agents can result in color degradation if it remains in excess of 1% by mass (Harrison, 1990). Despite the detrimental impact of nucleic acids on PHB properties, little attention has been paid to their effective removal during the development of PHB recovery. The focus has always been on protein removal mainly because of its large composition in NPCM.

Because of the complexity in composition and properties of components, the removal of NPCM can be achieved progressively through each processing step of recovery. The expense of recovery is thus determined by the required PHB purity and acceptable contaminant levels. Optimization of the fractionation process is to obtain the PHB with a purity that meets its application requirement but at relatively low cost.

The presence of intracellular nucleic acids also has a strong impact on the PHB recovery process. Cell disruption by either mechanical or chemical methods produces a highly viscous suspension due to the release of nucleic acids (Higgins *et al.*, 1978). Further study indicated that it was mainly DNA that contributed to the increase in suspension viscosity (Agerkvist and Enfors, 1990). The release of PHB is accompanied by the release of intracellular nucleic acids due to the similarity in size of the bacterial nucleoplasm and PHB granules (Harrison, 1990). High viscosity of the cell suspension drastically slows down the particle sedimentation during the physical fractionation such as centrifugation, and causes low particle collection and therefore low yield.

The decrease in viscosity to a level which enables efficient processing of the suspension must be considered. The hydrodynamic properties of nucleic acids are mainly dependent upon their molecular weight. Therefore, a reduction in suspension viscosity can be achieved by either breakage of the long molecular chains of nucleic acids or the decrease in their concentration. DNA chain is shear-sensitive and can be irreversibly degraded to small fragments during homogenization (Agerkvist and Enfors, 1990). The dramatic increase in viscosity after cell disruption can be decreased through multiple homogenization. The suspension viscosity, therefore, is a function of the number of homogenizer passes. It is also reported that heating shock prior to cell disruption causes denaturation and solubilization of some nucleic acids in the cells thus reducing the viscosity of cell disintegrates, facilitating the subsequent purification process (Holmes and Lim, 1990). However, high temperatures may result in the denaturation of protein which inhibits its adoption in protein inclusion body recovery. Intracellular PHB is more resistant to high temperatures compared to protein inclusion bodies.

Some methods have been reported that reduce the nucleic acids concentration, for example, the addition of $MnSO_4$ that precipitates nucleic acids (Higgins *et al.*, 1978). However, this is inapplicable in practice because the precipitated nucleic acids adheres to solid particles preventing their late removal and causes high

nucleic acids contamination. The use of nuclease enzyme to hydrolyze nucleic acids is another alternative for the reduction of viscosity (Harrison, 1990). Nuclease enzyme treatment is a routine procedure in laboratory studies, but its use on a large scale process is precluded because of its cost and especially in this case involving the production of a commodity product such as PHB. In the current commercial PHB production process, nucleic acids are found to be removed effectively together with proteins after protease and detergent treatment (Harrison, 1990).

In general, nucleic acids are one of the major concerns in PHB recovery and have a significant impact on not only the extracted PHB properties but also the PHB extraction process.

1.6. SCOPE OF THE RESEARCH

The aim of this research is to develop a process for PHB extraction and recovery from recombinant *E. coli* using homogenization and centrifugation as basic unit operations, aiming to achieve a reduction in overall PHB production cost. The fractionation of insoluble cell debris from the liberated PHB granules forms the core of this research. The research focuses on each unit operation in terms of its impact on particle size. Interactions between unit operations to optimize the overall recovery process are also considered. As the physical structure of PHB and P(3HB-co-3HV) granules is similar, the study can be easily extrapolated to the recovery of PHB copolymer. Through this study, a systematic understanding of inclusion body fractionation from a scientific and practical perspective is obtained.

A general description of the techniques and assays applied in this study is given in Chapter 2, including particle size methods, techniques for characterizing the extracted PHB, and assays for contaminants. Homogenization and centrifugation operation conditions throughout this study are also presented. The recombinant *E. coli* fermentation for PHB production is described, which provides cell material for extraction studies.

In Chapter 3, a series of PHB recovery processes using homogenization and centrifugation are conducted and characterized as a preliminary investigation. Incorporating NaOCl treatment into the recovery process is also investigated, and its importance in terms of improving both PHB purity and recovery is identified. These provide practical information on the basic structure of possible PHB fractionation processes and their performance, guiding subsequent studies.

The aim of Chapter 4 is to prepare homogenization and centrifugation models for subsequent process simulation and further optimization. It begins with a literature review on the existing modelling studies in terms of cell debris comminution by homogenization and the particle fractionation in a centrifuge. PHB size is dictated by fermentation, while cell debris size is determined by the unit

operations in the recovery process. The effect of homogenization on cell-debris micronization for PHB-containing *E. coli* cells is studied. The effect of fermentation conditions and freeze-thaw prior to homogenization on cell debris comminution by homogenization is also investigated. Further discussion is given regarding the use of the Boltzmann function and the cell debris reduction model by homogenization for describing cell debris size. PHB and cell debris data are collected by Centrifugal Disc photoSedimentometer and Cumulative Sedimentation Analysis (Sections 2.4.1 and 2.4.2), respectively. This allows the determination of parameters for cell debris reduction models and also simulation of the PHB and cell debris fractionation processes developed in Chapter 3. Particle fractionation is predicted by use of a grade-efficiency curve. The dominant centrifuge operating conditions affecting PHB recovery and cell debris removal are defined, and the effects on product yield and purity are discussed. The function of NaOCl treatment in the extraction process is further defined.

PHB stability influences unit operation performance and also attainable PHB yield. PHB stability during release and cell-debris comminution by homogenization is therefore investigated by monitoring the granule size during each homogenizer pass by CDS in Chapters 3 and 4.

Chapter 5 provides statistical models of cell debris size as a function of NaOCl treatment conditions using response surface methodology. PHB degradation under NaOCl treatment is also investigated and modelled. These allow the prediction of cell debris size and PHB degradation as a function of NaOCl treatment conditions in a defined experimental range. The modelling study also identifies major factors in terms of cell debris minimization by NaOCl treatment.

Chapter 6 presents a simulation study of PHB recovery processes. Using information from the studies above, a basic extraction process comprising homogenization, centrifugation and NaOCl treatment is defined, and the main system variables are established. PHB fractionation from cell debris is simulated as a function of the number of homogenization and centrifugation passes, the first-pass centrifuge feedrate, and NaOCl concentration. A cell-debris removal

target is then set and the cost-optimal strategy defined. Optimization is then performed. An optimal extraction process is selected, which meets the cell-debris-removal target at minimum overall production cost. A demonstration of the optimized extraction process is then conducted at pilot scale, and characterized in terms of cell debris removal and PHB collection during centrifugation. Sensitivity study and further reduction of the production cost are also conducted.

Apart from insoluble cell debris, the removal of other intracellular components such as nucleic acids and protein is also considered. Their impact on product quality and the recovery process is reviewed in Chapter 3. In addition, the preliminary investigation in Chapter 3 provides information on the removal of these contaminants by homogenization and centrifugation. The effect of NaOCl treatment on DNA and protein removal is also identified, which aids process optimization. The final DNA and protein removal in the optimized recovery process was characterized.

An overall conclusion is made in Chapter 7. The results from the preceding studies are summarized. Some recommendations for further research are also made.

CHAPTER 2

MATERIALS AND METHODS

To develop a PHB extraction process, it is necessary that methods of assessing process performance are selected and reliable techniques for the characterization of PHB and contaminants quantitation are available. This chapter will describe the production of PHB by fermentation, followed by the basic unit operation of extraction, namely homogenization and centrifugation. This will be followed by a detailed description of the analytical methods employed to quantify the physical and chemical characterization of the PHB and its contaminants.

2.1. PHB PRODUCTION BY FERMENTATION

Microbial fermentation is used for the expression of bioproducts in microorganisms. Once an expression system has been constructed, productivity can be enhanced by increasing cell growth and cell density, and by improving product formation intracellularly through an optimized fermentation strategy. Fermentation modes include batch, continuous, and fed-batch modes.

Fed-batch mode is most commonly employed to obtain a high cell density. During fermentation, nutrient mixture is fed into a fermenter periodically to increase the concentrations of consumed medium components. Nutrient feeding regulates the cell growth rate as well as product formation rate. Correspondingly, oxygen consumption and heat generation in the fermenter are then regulated (Fieschko, 1989). Acetate is a major inhibitory byproduct in the production of recombinant proteins by fermentation (Anderson *et al.*, 1984). However, in fed-batch fermentation acetate formation can be effectively eliminated. Continuous fermentation is generally not employed for the production of recombinant products, mainly due to the high possibility of plasmid loss over long periods (Dwivedi *et al.*, 1982).

Fed-batch fermentation techniques for recombinant *E. coli* are well established, leading to the efficient and high-level production of various protein and non-protein products such as PHB (Lee, 1996b). One of the major concerns in terms of the optimization of a fermentation system is the selection of a suitable feeding strategy. Various nutrient feeding methods have been developed (Lee, 1996b). With regarding to feedback orientated feeding methods, DO-stat and pH-stat are the most commonly used. The DO-stat method is based on the observation that dissolved oxygen concentration increases rapidly as soon as the major substrate is depleted. Substrate concentration can thus be maintained within a desired range by automatically feeding the predetermined amount of nutrients if DO rises above a preset value. Medium pH will also give a quick response if carbon substrates

become depleted (Suzuki *et al.*, 1986). pH begins to rise when the carbon substrate become depleted. This is mainly because of an increase in the concentration of ammonium ions excreted by growing cells. In a semi-defined or complex medium, the presence of nitrogen sources such as yeast extract can support further cell growth even if the carbon substrate becomes depleted. In this case, DO does not change substantially, making the DO-stat method difficult. The use of pH-stat for carbon feeding control in a semi-defined or complex medium is superior.

In this study, a genetically engineered *E. coli* strain was employed for PHB production by fed-batch fermentation using the pH-stat feeding strategy. Unlike *A. eutrophus*, the accumulation of PHB in recombinant *E. coli* does not require the limitation of an essential nutrient source and no induction is needed as the PHB expression in the strain is constitutive (Lee, 1996b). PHB accumulation, therefore, accompanies cell growth, although distinct phases of maximum cell growth and PHB accumulation are observed. The expression system uses a semi-defined medium containing yeast extract to improve PHB production (Lee and Chang, 1996). Glucose is the major carbon source.

2.1.1. Bacterial strain and its maintenance

A non-K-12 *E. coli* strain Toppl [F', *proAB*, $lacI^q$, ZΔ *M15*. In*10*, (tet^R)] (Stratagene, California, USA) was chosen and transformed with plasmid pJM9123 (Slater *et al.*, 1992). Transformants were selected using kanamycin (50 μg/mL). Plasmid pJM9123 contains the *phb* operon originally isolated from *A. eutrophus*. The transformed strain was stored in 15% v/v glycerol with 1% w/v peptone at −70°C. Fresh stocks were prepared by streaking a loopful of glycerol stock onto an Oxiod Nutrient Agar plate, and incubated overnight at 37°C prior to transferring into a sterile glycerol solution using a loop. These glycerol stocks were stored at −70°C.

2.1.2. Shake flask culturing

Shake flask cultures of recombinant *E. coli* Topp1 (pJM9123) was prepared as inoculums for the fed-batch fermentation using a single bacterial colony from fresh Oxoid Nutrient Agar plates. The growth medium used was a modified R-medium (Lee *et al.*, 1994). Salts and trace elements compositions are listed in Table 2.1. Nutrient composition is in Table 2.2. To prevent precipitation in highly-concentrated media, glucose, yeast extract, casamino acids and salt solution were separately autoclaved and mixed aseptically prior to inoculation. The initial culture of 20 mL was incubated at 37°C for 24 h, and subcultured afterwards by addition of the flask contents into 200 mL of fresh medium. The subculture was incubated for another 24 h before inoculating the fermenter.

Table 2.1. Media composition (salts and trace elements)

Solution	**Composition**
Salts	KH_2PO_4, 13.5 g/L; $(NH_4)_2HPO_4$, 4.0 g/L; citric acid, 1.7 g/L; $MgSO_4$. $7H_2O$, 1.4 g/L, 1.0 mL/L trace solution.
Trace elements	$FeSO_4.7H_2O$, 10.0 g/L; $CaCl_2.2H_2O$, 2.0 g/L; $ZnSO_4.7H_2O$, 2.2 g/L; $MnSO_4.4H_2O$, 0.5 g/L; $CuSO_4.5H_2O$, 1.0 g/L;$(NH_4)_6Mo_7O_{24}.4H_2O$, 0.1 g/L; $Na_2B_4O_7.10H_2O$, 0.02 g/L; 5M HCl/L.

Table 2.2. Shake-flask media composition (nutrients and selection antibiotic)

	Fermentation I	**Fermentation II**	**Fermentation III**
Glucose	20 g/L	20 g/L	20 g/L
Nutrient buffer	Yeast extract, 5.0 g/L; Casamino acid, 5.0 g/L.	yeast extract, 5.0 g/L	yeast extract, 5.0 g/L
Kanamycin	50 μg/mL	50 μg/mL	50 μg/mL

2.1.3. Fed-batch fermentation protocol

Three fermentations were conducted in a 20 L Chemap CF-2000 fermenter with an initial medium volume of 12.5 L. Media and feeding solution compositions for the three fermentations are summarised in Tables 2.1 and 2.3. Fermentation was

inoculated from shake flask cultures with media composition listed in Tables 2.1 and 2.2. During fermentation, culture temperature was controlled at 37°C. Dissolved oxygen concentration (DOT) was maintained at approximately 80% of air saturation by automatically adjusting the air inlet flowrate. Pure oxygen or oxygen-enriched air (75% oxygen/25% air) was used as required. Culture pH was kept at 6.8 by the addition of 14% (v/v) NH_4OH. Foaming was controlled by a mechanical foam breaker and the automatic addition of chemical antifoam (1% v/v) as required.

A pH-stat feeding strategy with a high limit was employed. The pH setpoint was 6.80. As soon as glucose depleted, medium pH rose rapidly giving an on-time indication for feeding. Feeding was manually operated using an electronic balance. When the pH was higher than 6.85, 350 mL of nutrient feeding solution was added to bring the glucose concentration to 20 g/L, calculated assuming a total medium volume of 12.5 L. Glucose concentration in the culture was measured off-line using an UV-method (Fermentation I) (Section 2.4.6) or a glucose analyser (YSI 2700 SELECT, Yellowspring Instrument, USA) (Fermentation II and III) (Section 2.4.6), which assisted pH-stat control thus preventing glucose depletion or overfeeding. Glucose concentration was maintained at less than 20 g/L throughout the operation of all three fermentations.

The fermentation was terminated by the addition of formaldehyde (0.02% v/v final concentration) at an optical density (OD) (600 nm) (UNICAM 8625 UV/VIS spectrophotometer) of 84 (Fermentation I), or 100 (Fermentation II), or 124 (Fermentation III). Culture was stored overnight at 10°C in the fermenter before being frozen (-18°C) in 2 L bottles. During the fermentation, samples were taken at 2 h intervals for the measurement of OD, glucose concentration (Section 2.4.6), dry cell weight (DCW) (Section 2.4.5), and PHB content (Section 2.6.1).

2.1.4. Fermentation results

PHB exists in the form of granules in *E. coli* Topp1(pJM9123) cells (Figure 2.1). Figure 2.2 illustrates the features of cell growth and PHB accumulation during the fermentation (Fermentation I). A final cell concentration of 42.3 g/L with PHB content of 52.0 % (w/w) was obtained (Table 2.4). This compares with a dry weight of 175 g/L and a PHB content of 37% for an optimized fed-batch fermentation using *E. coli* XL1- Blue[pSY105] and a yeast-based medium (Lee and Chang, 1995b). PHB and cell concentration did not increase after 22 h. This may have been caused partially by operational problems. Table 2.4 summarises the results for the three fermentations. No attempt was made to optimize the fermentation process nor to extend to high cell concentrations, as the sole aim was to create material for downstream recovery studies. However, *E. coli* Topp1[pJM9123] seems to hold promise for high-cell-density PHB fermentation following further optimisation.

Table 2.3. Medium compositions for fed-batch fermentations

Solutions	**Fermentation I**	**Fermentation II**	**Fermentation III**
Glucose	30.0 g/L	20.0 g/L	20.0 g/L
Nutrient Buffer	Yeast extract, 5.0 g/L; Casamino acid, 5.0 g/L.	Yeast extract, 5.0 g/L;	Yeast extract, 5.0 g/L;
Nutrient Feeding	Glucose, 700 g/L; Yeast extract, 70 g/L.	Glucose, 700 g/L; Yeast extract, 35.0 g/L; $MgSO_4.7H_2O$, 20.0 g/L.	Glucose, 700 g/L; Yeast extract, 35.0 g/L; $MgSO_4.7H_2O$, 20.0 g/L.
Kanamycin	50 μg/mL	50 μg/mL	50 μg/mL

Table 2.4. Fermentation results

	Fermentation I	Fermentation II	Fermentation III
Culture time (h)	47	28	53
OD (600 nm)	84	100	124
Cell concentration (DCW) (g/L)	42.3	42.1	43.3
PHB content % (w/w)	52.2	57.8	60.5

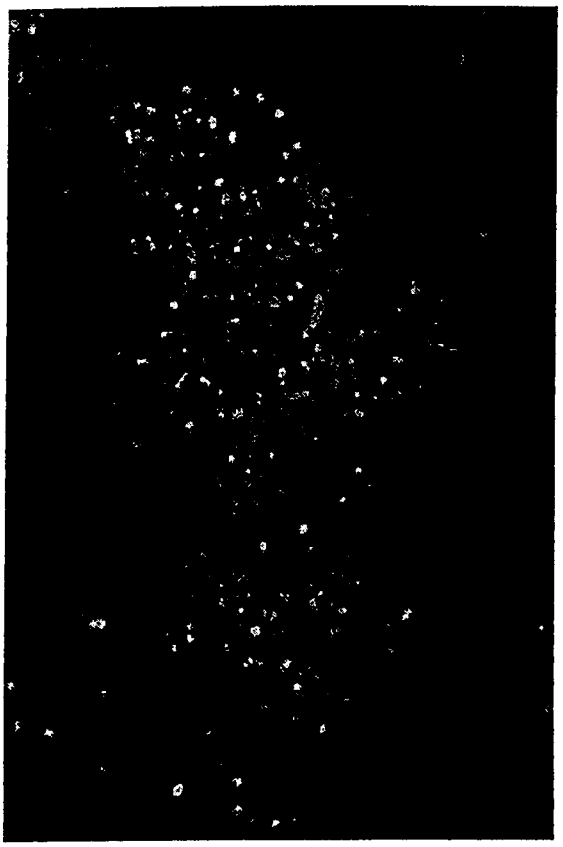

Figure 2.1. Nile Blue A stained *E. coli* Topp1(pJM9123) containing PHB granules (orange fractions). Cells were taken from Fermentation I.

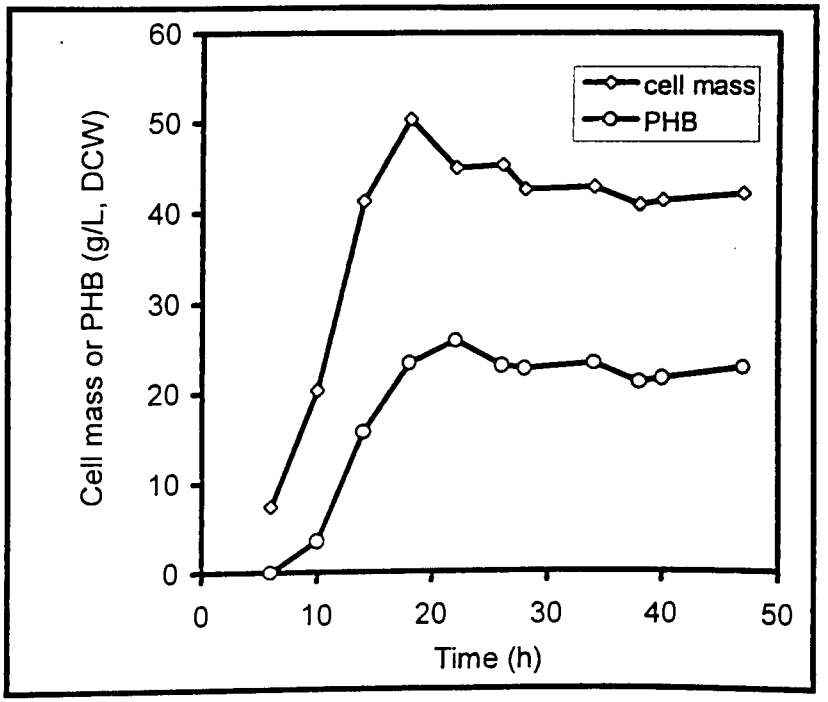

Figure 2.2. Time course of cell growth and PHB accumulation during the fermentation of recombinant *E. coli* Topp1(pJM9123) in Fermentation I.

2.2. CELL DISRUPTION BY HOMOGENIZATION

To recover the intracellular products formed during fermentation, they must be released from the host cells by cell disruption, followed by fractionation and purification. There are many techniques for cell disruption including physical, chemical, enzymatic, and mechanical methods. High-pressure homogenization is one of the most widely-used mechanical methods at process scale. Homogenization has been used for yeast disruption, and the release of intracellular products from *E. coli* and other cells. The method has been recently reviewed by Middelberg (1995). The use of homogenization for the release of PHB granules from *A. eutrophus* was also investigated by Harrison *et al.* (1991).

The mechanism of cell disruption by homogenization continues to be debated.. Cells generally experience a combination of shear-stress, turbulence, cavitation and impingement when passing through a homogenizer. Recent work also suggests a mechanism related to inertia during acceleration (Kleinig and Middelberg, 1998). Variables affecting homogenizer disruption efficiency include feed temperature, operating pressure, the number of homogenization passes, and the homogenizer valve design (Kleinig *et al.*, 1995). Disruption performance is also affected by the type of microorganism, cell growth conditions, the presence of inclusion bodies, and any pretreatment (Harrison *et al.*, 1991).

Feed cell concentration is one of major concerns for the homogenization operation as it directly affects process cost. Recent research has shown that increasing feed cell concentration reduces disruption efficiency due to an increase in feed viscosity and the associated homogenizer valve gap. However, the impact is less than that due to fermentation and homogenization conditions (Kleinig *et al.*, 1995 and Wong *et al.*, 1997). It has been suggested that the optimal feed concentration is the maximum that does not lead to operational problems due to high feed viscosity (Kleinig *et al.*, 1995).

Along with the release of intracellular products, the comminution of cell debris is also achieved by homogenization. Variables affecting performance are similar to that of cell disruption (Wong *et al.*, 1997). The cell debris size in a homogenate affects the subsequent downstream separation performance. In practice, to fractionate insoluble inclusion bodies from cell debris, multiple homogenization passes may be employed to obtain a large enough size difference between the cell debris and inclusion bodies. A detailed review of cell debris comminution by homogenization is given in Section 4.1.2.

In this study, homogenization was employed in the PHB extraction process as a unit operation for the release of PHB granules from recombinant *E. coli,* and for the comminution of cell debris. It was conducted with an APV-Gaulin 15MR APV high-pressure homogenizer, fitted with a ceramic cell-disruption (CD) valve. The operation pressure was 55.2 MPa and the feed temperature was approximately 10°C in all cases. This condition assured over 80% of cell disruption after the first homogenization pass (see the relevant sections for details). Specific operational details are given in the relevant sections of subsequent chapters.

2.3. PARTICLE FRACTIONATION BY CENTRIFUGATION

Centrifugation has been widely used in the biotechnology industry for the separation of small biological particles. Examples include harvesting cells from fermentation broth (Aronsson and Zadorecki, 1987), the removal of insoluble cell material (e.g., cell debris) from soluble products after cell disruption (Aronsson and Zadorecki, 1987), and the fractionation of insoluble products (e.g., inclusion bodies) from contaminating insoluble particles (e.g., cell debris) (Hoare and Dunnill, 1989; Middelberg, 1996). Existing industrial centrifuges can generally be classified into four basic types according to bowl design. They are the tubular-bowl centrifuge, the multichamber centrifuge, the scroll centrifuge and the disc-stack centrifuge. The most common type of centrifuge found in biotechnology is the disc-stack centrifuge, which is further classified by the method of solid discharge, namely batch, intermittent, and continuous design.

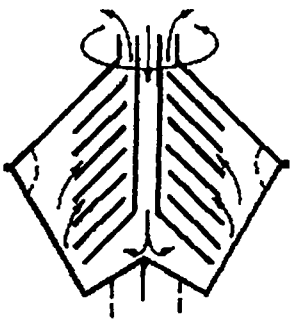

Figure 2.3. Disc stack centrifuge (batch mode)

Figure 2.3 illustrates the mass flow within a batch-mode disc-stack centrifuge. Suspension is fed from the top of the rotating bowl and distributes into narrow disc spaces, where particles suspended are subjected to centrifugal force moving towards the disc underside. Settled particles then slide along the disc underside surface and are finally collected in the sediment holding space. Clarified liquid flows out through an annular slit near the feed inlet. The design of stacked conical discs gives a large sedimentation area in a compact volume, and also minimizes the particle settling distance and thus settling time.

Particle fractionation by centrifugation is never perfect. For a given feed suspension, fractionation performance is affected by centrifuge separation area, bowl rotating speed and throughput (flowrate).

Centrifugation was employed in this study for the fractionation of PHB granules from insoluble non-PHB cell material (e.g., cell debris) in *E. coli* homogenate. It was achieved in a Veronesi KLE-160 solid-bowl disc-stack centrifuge with a fixed operating speed of 8400 r.p.m. The equivalent separation area (Σ) was 3775 m^2. The feedrate (Q) employed was between 300 and 900 mL/min or between 1.32×10^{-9} m s^{-1} and 3.97×10^{-9} m s^{-1} after normalization (Q/Σ). PHB paste after batch operation was removed from the inner bowl surface. The PHB collection efficiency for each centrifugation pass was estimated by comparing the PHB size distributions in feed and supernatant suspension as measured by CDS (Section 2.4.1). Specific experimental details are given in the relevant sections. In all cases, the density of PHB granules was assumed to be 1260 kg/m^3 (Middelberg *et al.*, 1995). As explained in Section 4.1.4, the assumed density does not affect the model predictions.

To optimize disc-stack centrifuge fractionation performance, models are reviewed and some centrifugal effects are studied based on the simulation (see Sections 4.1.3 and 4.4, respectively). PHB fractionation by centrifugation is finally optimized by adjusting the centrifugal flowrate and homogenate properties (e.g., cell debris size) (Chapter 6).

2.4. ANALYTICAL METHODs

2.4.1. Centrifugal Disc photoSedimentometer (CDS)

Centrifugal disc photosedimentation (CDS) was employed in this study to measure the size and size distribution of *E. coli* whole cells and PHB granules.

Figure 2.4 shows a schematic diagram of a Joyce-Loebl disc centrifuge (DCF4, Applied Imaging Ltd, Gateshead, UK). Sample is loaded onto the inner radius of a rotating fluid annulus (the spin fluid). The particles contained in the sample start from nearly the same initial radius, sedimenting under the applied centrifugal force towards the outer edge of the rotor where a detector records absorbance as a function of time. To prevent convective transport, a density gradient is formed throughout the spin fluid prior to sample injection.

The time taken, t, for a particle with a Stokes diameter D to reach the detector is given by Equation 2.1,

$$t = \frac{18\mu}{\Delta\rho\omega^2 D^2} Ln(\frac{r}{r_0}) \qquad (2.1)$$

where μ is the spin-fluid viscosity (Pa.s), ω is the disc angular velocity (rad/s), $\Delta\rho$ is the density difference between the particle and the fluid (kg/m^3), and r and r_0 are the detector and start radii of the instrument (m), respectively. A plot of the detected absorbance versus particle Stokes' diameter, D, is obtained. The extinction coefficient has to be considered when particle size approaches the source light wavelength (Middelberg *et al.*, 1990). Since t is proportional to $1/D^2$ by Equation 2.1, high resolution can be achieved during sedimentation.

A number of references cite centrifugal disc photosedimentation for sizing biological particles, including the size determination of inclusion bodies (Taylor *et al.*, 1986; Olbrich, 1989; Middelberg *et al.*, 1990; Thomas *et al.*, 1991; Wong *et al.*, 1996), cell debris (Olbrich, 1989; Thomas *et al.*, 1991) and PHB granules (Middelberg *et al.*, 1995). However, its performance suffers from some inherent

disadvantages as described by Middelberg *et al.* (1990), including baseline drift and errors in assumed extinction coefficients.

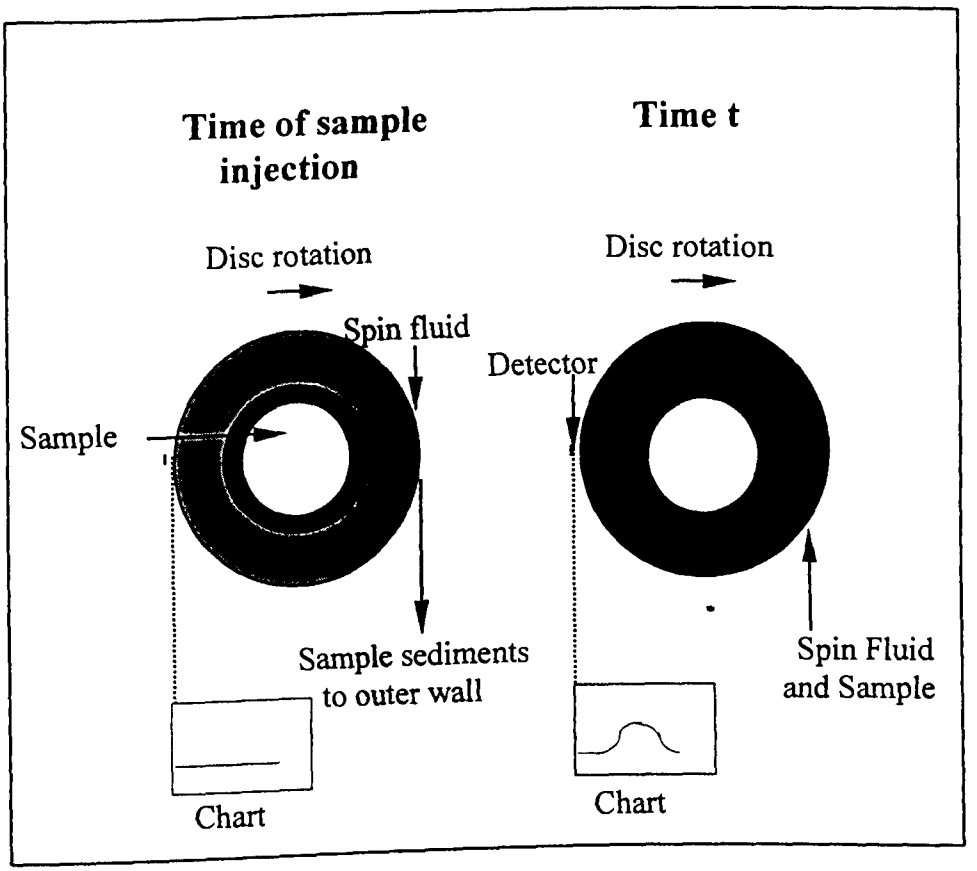

Figure 2.4. Schematic diagram of the Joyce-Loeble disc centrifuge (Middelberg, 1992)

A method based on the machine settings and operating conditions summarized in Table 2.5 was used in this thesis. Cell disruption efficiency by homogenization was estimated by comparing the areas under the normalized size distribution curves prior to, and after, homogenization. PHB collection efficiency during each centrifugation pass was also estimated by CDS (Section 2.3), assuming a density of 1085 kg/m^3 for whole *E. coli* cells and 1260 kg/m^3 for PHB granules (Wong *et al.*, 1997; Middelberg *et al.*, 1995).

Table 2.5. Operating conditions for Joyce-Loebl DCF4 analytical disc centrifuge (Middelberg, 1992)

	Ethanol-Water Method
Spin Fluid (SF)	20 mL water
Buffer Fluid (BF)	1.5 mL 20% v/v Ethanol-Water
Sample Volume and Suspension	0.5 mL 20% v/v Ethanol-Phosphate Buffer
Disc Speed	8000 r.p.m.
Gain	6.0
r_o (cm) (Equation 2.1)	4.01
r (cm) (Equation 2.1)	4.82
μ (cP) (Equation 2.1)	1.14
Time = 0 s	Inject SF
Time = 60 s	Inject BF
Time = 90 s	Boost 70
Time = 150 s	Boost 70
Time = 210 s	Boost 20
Time = 300 s	Inject sample

2.4.2. Cumulative sedimentation analysis

Cumulative Sedimentation Analysis (CSA) is a newly-developed method for sizing *E. coli* cell debris (Wong *et al.*, 1997). It is based on particle sedimentation under centrifugal force, coupled with Sodium Dodecyl Sulfate-Polyacryalmide Gel Electrophoresis (SDS-PAGE) analysis of proteins associated with the sedimented debris particles. It provides reliable measurement as no sample pretreatment (e.g., separation of granules and debris) is required. The presence of inclusion bodies in the homogenate system does not affect the measurement of cell debris (Wong *et al.*, 1997). This technique was used extensively in this study to measure the debris size in homogenized or chemically-treated *E. coli* cell suspensions containing PHB granules.

2.4.2.1. Theory

CSA is based on Stokes' law. A brief explanation of the theoretical basis of CSA is provided based on the work of Wong *et al.* (1997), as the technique is relatively

new. The sedimentation of an individual particle in a homogenous suspension under a specific force is described by Equation 2.2,

$$D^2 = \frac{18\eta}{F_a}\frac{1}{\Delta\rho}\frac{H}{t_e} \qquad (2.2)$$

where H is the effective settling height for a particle with Stokes' diameter D in an effective time t_e; $\Delta\rho$ is the density difference between the particle and suspending fluid; F_a is the acceleration due to a specific force, and η is the viscosity of the liquid continuous phase. As F_a, $\Delta\rho$ and η are constant, a D^2 distribution can be expressed as a function of the effective time t_e for a fixed settling height H.

The cumulative oversize fraction (W) of particles of size greater than D can be related to the weight percent (F) of the particles sedimented in time t_e, by Equation 2.3 (Wong *et al.*, 1997).

$$W(t_e) = F - t_e\frac{dF}{dt_e} = F - \frac{dF}{dLnt_e} \qquad (2.3)$$

To obtain the curve of F as a function of t_e, a series of sedimentation tests are carried out in a centrifuge using a swing-out rotor (Figure 2.5). Centrifugation speeds and times are selected to ensure the whole particle size range is covered at reasonable resolution. The cumulative oversize curve W as a function of Stokes' diameter D is finally plotted using Equations 2.2 and 2.3.

With reference to Figure 2.5, the effective settling time is calculated with Equation 2.4,

$$t_e = t_1 \times \frac{R_{Lm}\omega^2}{g} \qquad (2.4)$$

where ω is the angular velocity, R_{Lm} is the log mean radius given by Equation 2.5,

$$R_{Lm} = \frac{R_f - R_i}{Ln(\frac{R_f}{R_i})} \qquad (2.5)$$

where R_i and R_f represent the initial and final radii of the particle settling range.

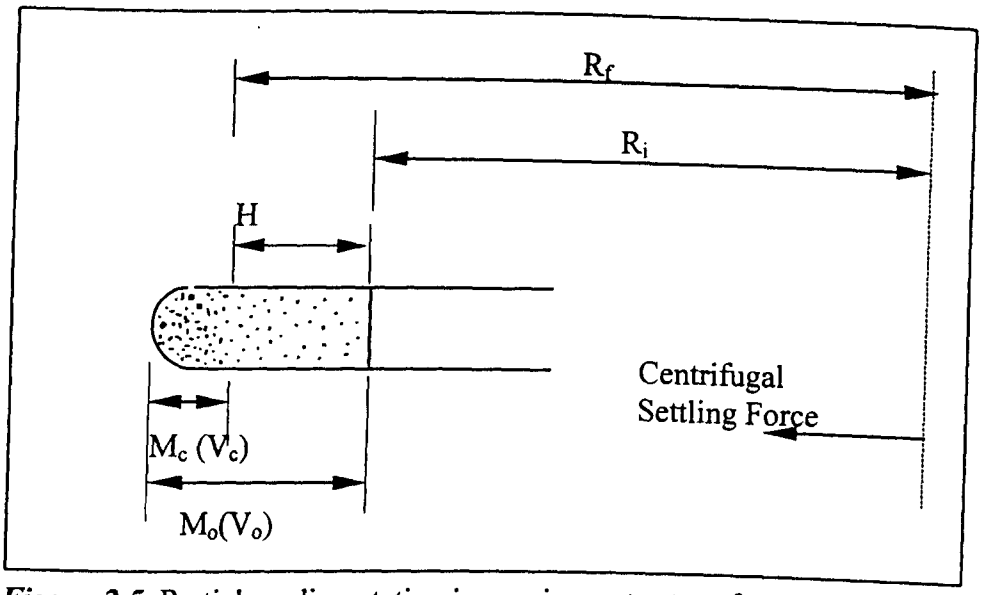

Figure 2.5. Particle sedimentation in a swing-out rotor of a centrifuge. (Wong *et al.*, 1997)

To minimize inaccuracies in measuring dry weights, SDS-PAGE is employed to determine $F(t_e)$. This is done by quantitating the relative concentrations of outer membrane proteins in supernatant and concentrate fractions following centrifugation. $F(t_e)$ is calculated using Equation 2.6 or 2.7,

$$F(t_e) = 1 - \frac{I_s}{\frac{V_s}{V_s + V_c}(I_s + I_c)} \qquad (2.6)$$

$$F(t_e) = \frac{M_c - \frac{V_c}{V_o} M_o}{\frac{V_o - V_c}{V_o} M_o} = \frac{I_c - \frac{V_c}{V_o} I_o}{\frac{V_o - V_c}{V_o} I_o} \qquad (2.7)$$

where I_o, I_c and I_s are relative intensity of a specific protein band for the unsedimented sample, the concentrate and the supernatant, respectively, determined from SDS-PAGE gel by densitometry. V_o, V_c and V_s represent the volumes corresponding to total particle contents of M_o, M_c and M_s, respectively.

2.4.2.2. CSA method specifics

The operating procedure of CSA can be divided into three steps: (1) sedimentation under centrifugal force, (2) SDS-PAGE analysis for protein

quantification, and (3) data interpretation. The sedimentation and data interpretation are described in this section, whilst SDS-PAGE analysis is defined in Section 2.4.3.

Sedimentation under centrifugal force

1. Dilute the homogenized or chemical-treated cell suspension to a reasonable concentration with PBS buffer and mix well.
2. Pipette 25 mL of sample into a 50 mL centrifuge tube and centrifuge it using a HB-6 swing-out rotor in a Sorvall RC-5C refrigerated centrifuge (Du Pont, USA) for a predetermined time. Table 2.6 lists the assigned centrifugation times and speeds used in this study, which covers the full range of recombinant *E. coli* cell debris and inclusion body distributions. The centrifuge chamber temperature was set at 10-15°C.
3. Remove the top 20 mL supernatant into another 50 mL tube carefully after sedimentation without disturbing the bottom concentrates.
4. Centrifuge supernatants (20 mL) and the concentrates (5 mL) at 27,600×g for 4 h and 2 h, respectively, enabling the sedimentation of all particles down to a Stokes' diameter of 0.07μm.
5. Collect the final clarified supernatants for viscosity measurement using a Haake Rotovisco RV 100 concentric cylinder viscometer at 10°C.
6. Mix the pellets sedimented from supernatants and concentrates with SDS-PAGE sample buffer. The samples are ready for SDS-PAGE analysis.

To reduce the operating time and work load, and to prevent other possible variables being introduced during the long time operation, the CSA operating procedure conducted in Chapter 5 was simplified by taking 10 samples instead of 15 for constructing the cumulative fraction curve $F(t_e)$ using the assigned centrifugation times and speeds listed in Table 2.7. Also, after sedimentation, the supernatant was discarded and only the concentrate was further pelleted and analyzed by SDS-PAGE.

Numerical analysis and data interpretation

F was obtained as a function of effective settling time (t_e) using Equation 2.6 or 2.7 as explained above. Data were analyzed in TABLE CURVE 2D (Jandel Scientific, AISN Software) to give a best-fit curve. The slope of the curve at a specific t_e was then determined by differentiation at the point under consideration. Oversize cumulative fraction W was obtained as a function of t_e and further as a function of the Stokes' diameter D using Equations 2.2 and 2.3. A cell debris density of 1085 kg/m^3 was assumed as justified by Wong *et al.* (1997).

The Boltzmann function (Equation 2.8) was used to fit the cell debris size distribution. Median diameter (D_{50}) and distribution width (w) were obtained by non-linear regression of the cumulative oversize curve using GENSTAT 3.1 (NAG Ltd, UK).

$$1 - W(D) = \frac{1}{\left[1 + \exp\left(\frac{D - D_{50}}{w}\right)\right]} \qquad (2.8)$$

Table 2.6. Centrifuge times and speeds for samples separation by CSA (I)

Sample No.	Speed (r.p.m.)	RCF (×g)	Time (min)	T_{eff} (seconds)	D (μm)
1	2500	1021	15	671891	1.162
2	2500	1021	20	895855.6	1.006
3	2500	1021	25	1119820	0.900
4	2500	1021	35	1567747	0.761
5	3000	1471	35	2258723	0.634
6	4000	2615	30	3441718	0.513
7	4000	2615	40	4588957	0.445
8	5000	4086	30	5377766	0.411
9	5000	4086	40	7170355	0.356
10	6000	5884	40	10325592	0.296
11	7000	8008	40	14052912	0.254
12	9000	13239	40	23232581	0.198
13	13000	27622	40	48472721	0.137
14	13000	27622	70	84827261	0.103
15	13000	27622	120	145000000	0.079

Table 2.7. Centrifuge time and speed for sample separation by CSA (II)

Samples No.	Speed (r.p.m.)	RCF (×g)	Time (min)	T_{eff} (seconds)	D (μm)
1	2500	1021	15	671891	1.162
2	2500	1021	25	1119820	0.900
3	3000	1471	35	2258723	0.634
4	4000	2615	40	4588957	0.445
5	5000	4086	30	5377766	0.411
6	5000	4086	40	7170355	0.356
7	6000	5884	40	10325592	0.296
8	7000	8008	40	14052912	0.255
9	13000	27622	40	48472721	0.137
10	13000	27622	120	145000000	0.079
11	13000	27622	300	362500000	0.050

2.4.3. Sodium Dodecyl Sulphate-Polyacrylamide Gel Electrophoresis (SDS-PAGE)

SDS-PAGE analysis is a laboratory technique for protein separation, quantitation, and characterisation. SDS-PAGE separates proteins based on molecular weight. The anionic detergent sodium dodecyl sulphate (SDS) is selected as a charge agent that binds the protein. In most cases, the net charge of protein per mass unit following SDS binding is approximately constant. The amount of SDS bound to protein, and hence the resulting negative charge, are roughly proportional to protein molecular weight.

Polyacrylamide gel functions as a molecular sieve to fractionate proteins during electrophoresis. The gel is formed by copolymerisation of acrylamide monomers with a cross-linking agent N,N'-Methylene-bisAcrylamide to give a three-dimensional lattice. The pore size within the gel matrix, which determines the resolution of protein separation, depends on the relative concentrations of monomer and cross-linking agent. As the SDS-protein complex migrates across the polyacrylamide gel in an electrophoresis field, the proteins are gradually separated according to their molecular weights to form protein bands. These are visualized by staining with coomassie blue stain solution (see Appendix A1 for solution preparation). The stain bound to a given protein band is approximately

proportional to the protein mass, allowing quantitation by scanning densitometry. The molecular weight of a given band is estimated using a standard protein mixture with well-defined molecular weights.

The limitation of SDS-PAGE for protein quantification in CSA was reviewed by Wong (1996). Sample preparation prior to SDS-PAGE analysis may introduce errors and is considered in this section. A detailed description of the SDS-PAGE operating procedure used throughout this thesis is presented in Appendix A.

2.4.3.1. Method description

SDS-PAGE analysis was conducted with 12% acrylamide separating gel and a 4.0% stacking gel using a PROTEIN IIxi vertical electrophoresis cell (Bio-Rad Laboratories, Australia). Gel was stained overnight in coomassie brilliant blue G-250 solution (Bio-Rad Laboratories, Australia), followed by destaining in a destain solution. Prior to drying in a gel drier (Model 583, Bio-Rad Laboratories, Australia), the destained gel was reconditioned in a gel conditioner and hydrated in a glycerol-water solution. The intensity of a specific protein band was determined quantitatively by a densitometry (Model 300A, Molecular Dynamics, California, USA). The preparation of buffers and solutions, and the full operating procedure for SDS-PAGE in the current work, are provided in Appendix A.

2.4.3.2. Modification of sample preparation for SDS-PAGE analysis

Before loading onto the gel, the protein sample is denatured and solubilized by boiling with sample buffer containing SDS. The boiling time affects the protein solubilization yield. At least 4 min was recommended to achieve reasonable protein solubilization (Bio-Rad Operation Manual). Overboiling may result in protein degradation and thus a band shift on the gel slab. The optimal boiling time may also vary with sample size and operating conditions. Therefore validation of sample boiling time is required. Furthermore, storage of samples prior to SDS-PAGE analysis is required during each batch of CSA analysis because of the large number of samples involved. It needs to be determined

whether the protein remains stable during the prolonged storage (at 4°C) and has an impact on SDS-PAGE analysis. Examination of the effect of prolonged storage is thus required. Brief experiments were conducted to investigate these effects, and the results presented in full in Appendix A.

The experimental results show that the detectable protein band intensity varied with sample boiling time. Under the condition tested, 10 min gave the highest protein response and thus highest protein solubilization yield. A boiling time of 10 min was therefore applied for all the samples prepared for SDS-PAGE analysis in this study. The detectable cell membrane protein of *E. coli* became unstable after prolonged storage according to the experimental result. To minimizing errors, it was required to complete sample preparation within 5 days, giving a detectable protein intensity of over 96% compared to the original sample (prior to storage).

2.4.4. Staining and visualizing of PHB granules

PHB granules exhibit a strong orange fluorescence when stained with Nile blue A. The cultured *E. coli* Topp1 (pJM9123) cells were washed with MilliQ water and heat-fixed onto a clean microscope slide. They were stained with a filtered 1% (w/v) aqueous solution of Nile Blue A at 55°C in a waterbath for 10 min (Ostle and Holt, 1982). The slide was then immersed in 8% aqueous acetic acid for 1 min after rinsing with slowly running tap water to remove excess stain. The stained sample smear was rinsed again and blotted on tissue paper before being covered carefully with a cover slip using Movoil containing anti-bleaching agent as a mounting medium. PHB granules were observed as scattered fluorescence dots at an excitation wavelength of 460 nm, using an Olypus BHS Microscope with a BH2-RFC UV fluorescent attachment. Nile blue A appears to be a more specific stain for PHB than other stains.

PHB granules can also be visualized after staining with Crystal Violet. The heat-fixed sample smear was covered with Crystal Violet reagent for 1 min, and then

rinsed with tap water to remove excess stain. PHB granules were then observed as clear zones under an Olympus BHS Microscope.

2.4.5. Dry cell weight (DCW) measurement

1. Pre-heat Eppendorf tubes (1.5 mL) in an oven at 105°C for at least 24 h. Store them in a desiccator and weigh after cooling down.
2. Pipette 1 mL of cell broth from a shake flask culture or a fermentation into the pre-weighed tube and centrifuge at a speed of 13,000 rpm for 10 min in a Micromax bench centrifuge.
3. Remove the supernatant carefully with a pipette, and rinse the cell pellet twice with distilled water.
4. Re-heat the pellet in a tube at 100°C for 24 h before reweighing.
5. Repeat the measurements four times and take the average weight as the dry cell weight (g/L).

2.4.6. Glucose determination

2.4.6.1. UV-Method

Glucose concentration in culture medium supernatant was monitored spectrophotometrically by using a Boehringer Mannheim Analysis Kit (Catalog No. 716251). Glucose was converted into gluconate-6-phosphate with release of a UV-detectable complex (NADPH) by the following two enzymic reactions:

Reaction I: $$\text{D-Glucose} + \text{ATP} \xrightarrow{\text{Catalyst HK}} \text{G-6-P} + \text{ADP}$$

Reaction II: $$\text{G-6-P} + \text{NADP} \xrightarrow{\text{Catalyst G-6-P-DH}} \text{Gluconate-6-phosphate} + \text{NADPH} + \text{H}$$

NADPH formed from the reactions was stoichiometric with glucose in the sample, and was detected by measuring sample supernatant absorbance at 340 nm using a spectrophotometer.

This assay was conducted as detailed in the instructions of the analysis kit using a UNICAM 8625 spectrophotometer. Glucose concentration was determined relative to a calibration curve employing pure D-glucose as a standard. The linearity of the calibration curve covered a range from 0 to 20 g/L glucose.

2.4.6.2. Glucose analyser

An alternative to the above kit is to use the YSI Model 2700 SELECT Biochemistry Analyser (Yellowspring Instruments, USA) for the measurement of glucose concentration in fermentation media. The key technology applied in this YSI instrument is an enzyme sensor. With reference to Figure 2.6, the sensor probe is fitted with a three-layer membrane with immobilized glucose oxidase enzyme in the middle layer. The sample injected into a sample chamber diffuses through the membrane. Once past the polycarbonate membrane, substrate D-glucose contained in the sample is rapidly oxidized, catalysed by the oxidase enzyme in the middle layer, producing hydrogen peroxide (H_2O_2) (Reaction I). H_2O_2 is electrochemically oxidized further at the platinum anode and electrons are then released (Reaction II), resulting in a rise in probe signal current. Once equilibrium between H_2O_2 formation and H_2O_2 oxidation is achieved, the signal current is linearly proportional to H_2O_2 concentration and, therefore, to the concentration of the glucose in the sample. The polycarbonate layer functions to limit sample diffusion and controls the rate of Reaction I, providing improved linearity and measurement stability. To prevent substrates other than H_2O_2 contributing to sensor current, a subsidiary inner layer containing a thin film of cellulose acetate is attached to the membrane.

Reaction I: β-D-glucose + O_2 $\xrightarrow{\text{Glucose Oxidase}}$ D-Glucono-δ-lactone + H_2O_2

Reaction II: H_2O_2 $\xrightarrow{\text{Pt anode}}$ $2H^+ + O_2 + 2e^-$

The YSI Glucose analyser provides a direct reading of glucose concentration in the sample solution. This method is faster, easier and more economical than the UV-method, and is capable of high accuracy.

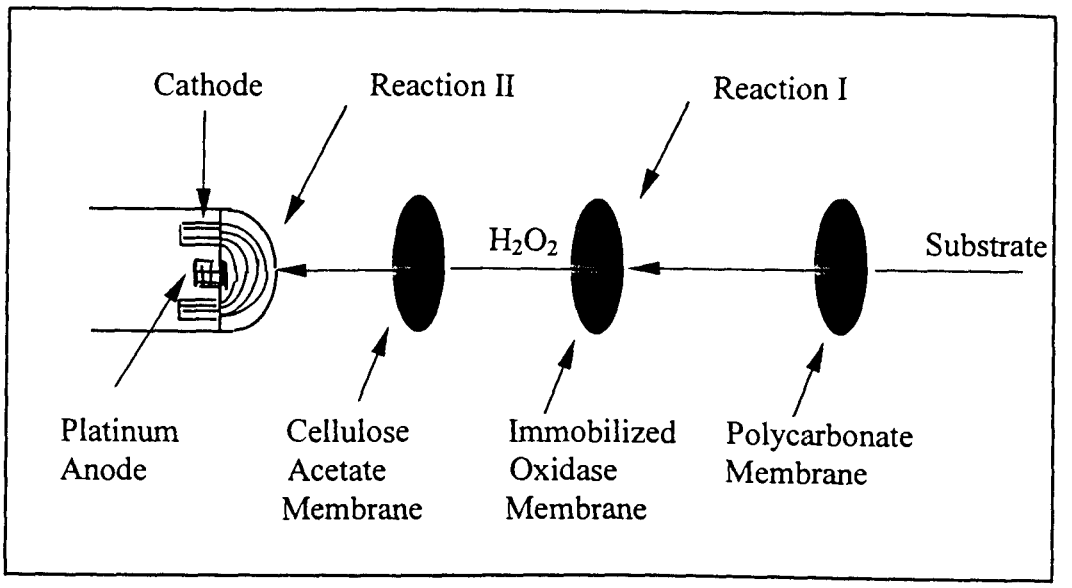

Figure 2.6. Sensor probe and enzyme membrane

The YSI Glucose analyser provides a direct reading of glucose concentration in the sample solution. This method is faster, easier and more economical than the UV-method, and is capable of high accuracy.

Mutarotation of glucose

Mutarotation of glucose can cause measurement uncertainty for a freshly prepared glucose solution when using this glucose analyzer. When solid D-glucose is dissolved in water, α and β anomers start to equilibrate, and the optical rotatory power of the solution gradually changes until it reaches a constant (Stryer, 1981; Finar, 1963). This process is termed mutarotation. As a result, the reading on the sensor probe may be lower than expected before the mutarotational equilibrium is achieved. The time taken to achieve mutarotational equilibrium varies with glucose concentration as shown in Figure 2.7. For D-glucose aqueous solution with a concentration within 25 g/L, 5 h incubation at room temperature is generally required to reach equilibrium. Stability was maintained for one week. The time for mutarotation equilibrium is also buffer dependent. The dilutant in this study was a phosphate buffer solution containing 40 g/L NaH_2PO_4 and 10 g/L Na_2HPO_4. The presence of phosphate can accelerate the mutarotational

equilibration. The equilibration can also be accelerated by raising the incubation temperature (YSI User's manual).

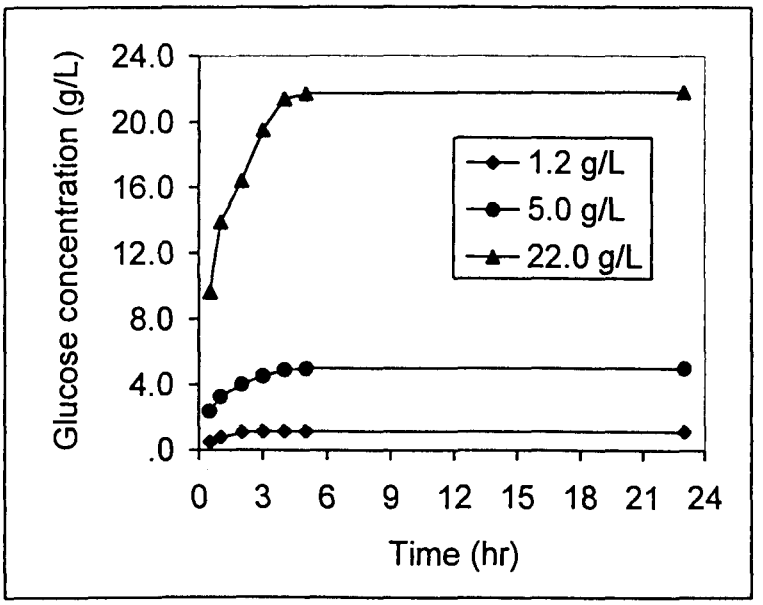

Figure 2.7. Mutarotational equilibrium of glucose as a function of time.

Operating procedure

1. Prepare the glucose calibration standard by dissolving D-glucose powder (AnalaR grade, Chem-Supply, South Australia) in phosphate buffer (40 g/L NaH_2PO_4 and 10 g/L Na_2HPO_4), and allow to stand for at least 3 h before measurement. The standard concentration was approximately 2.5 g/L, corresponding to a detection limit of 25.0 g/L.
2. Prepare the sample buffer with the buffer powder YSI 2357.
3. Install the fresh probe membrane and check the linearity of the membrane response using the glucose standard and its dilute solutions.
4. Take cell suspension from a fermentation and centrifuge at 13,000 rpm for 5 min using a Micromax bench centrifuge. Remove the supernatent.
5. Dilute the supernatant with MilliQ water to a concentration within the detection range.
6. Repeat the measurement in triplicate and take the average value.
7. Check periodically the linearity of membrane response during the test. Discard the membrane on appearance of non-linearity.

2.4.7. Cell lyophilization

1. Pellet the cell sample in a centrifuge and rinse twice with MilliQ water.
2. Remove the cell pellet into a 8 mL or 12 mL Kimble glass culture tube using a pipette, fix onto the tube bottom by freezing with dry ice.
3. Attach the tube to one of the sample ports in an Edwards Modulyo Freeze Drier using an adapter.
4. The working temperature and vacuum were about minus 50°C and 2.5 bar pressure. A minimum of 24 h was required for lyophilization, depending on sample volume.

2.4.8. PHB extraction by chloroform

Chloroform is the most widely used solvent for PHB extraction. Lyophilization of cell mass prior to extraction is required.

PHB extraction with Soxhlet apparatus

1. Crush lyophilized cell samples (typical masses) into a fine powder before placing into a glass-wool sample tube, and inserting into a Soxhlet apparatus containing 150 mL of chloroform (analytical grade, BDH Chemicals, Victoria, Australia).
2. Set up a Soxhlet apparatus and sit it onto a heater. Maintain the chloroform boiling for 2 to 3 h.
3. Precipitate PHB from crude chloroform by slowly adding a mixture of methanol (analytical grade, BDH Chemicals, Victoria, Australia) and water (7:3 v/v) after cooling to ambient temperature.
4. Filter the precipitate with a filter paper. Re-dissolve and re-precipitate once more to wash out insoluble non-PHB cell material.
5. Air dry the final precipitate and store at room temperature.

PHB extraction by centrifugation

1. Suspend the lyophilized cell fine powder (approximately 3 g) in hot acetone for 20 min.
2. Mix the powder after drying with 50 vol of chloroform and incubate at ambient temperature for 48 h. Chloroform was analytical grade (BDH Chemicals, Victoria, Australia).
3. Centrifuge the suspension at 27,600 ×g for 2 h using a HB-6 swing-out rotor in a Sorvall RC-5C refrigerated centrifuge (Du Pont, USA). Collect the supernatant containing the extracted soluble PHB.
4. Precipitate PHB in supernatant by non-solvent (5 × the vol of chloroform) and filtrate it. The non-solvent was a mixture of methanol and water (7:3 v/v) and methanol was the analytical grade (BDH Chemicals, Victoria, Australia).

2.5. ANALYSIS OF CONTAMINANTS

The primary objective of any PHB extraction process is to remove the non-PHB cell material from PHB. The major contaminants include soluble cellular protein, DNA, and insoluble cell debris. To evaluate the performance of a PHB recovery process and identify the key unit operation in terms of contaminant removal, reliable contaminant quantification methods are required.

2.5.1. Bio-Rad protein assay for total protein measurement

The Bio-Rad Protein Assay, based on the Bradford assay (Bradford, 1976), is a rapid and reliable dye-based method for measuring soluble protein concentration. When protein binds Coomassie Brilliant Blue G-250 in acidic conditions, the maximum absorbance of the dye shifts from 465 nm to 595 nm. The observable differential colour change of the dye is developed in response to changes in protein concentration. Protein concentration can, therefore, be quantified by measuring the reaction mixture absorbance at 595 nm after the colorimetric reaction, and relating it to a standard calibration curve. Bovine serum albumin (BSA) is commonly used as a protein standard.

The method is less sensitive to interference from many commonly-used biochemical reagents and non-protein components, and eliminates problems associated with the Lowry and Biuret assays. The disadvantage of this assay is slight variability in the protein-to-dye binding ratio between different protein types, meaning the result is not strictly quantitative. The final protein concentration is therefore expressed in mg/mL of BSA equivalent.

The procedure described below is adapted from the Bio-Rad Protein Assay Instruction Manual. It is applied for the measurement of total protein concentration in *E. coli* cell suspension and the recovered PHB pellets throughout this thesis.

Reagent

Bio-Rad Protein Assay kit II (Catalogue No. 500-0002), contains 450 mL dye reagent concentrate and lyophilized bovine serum albumin standard (Bio-Rad Laboratories Inc. Australia). The range of measurable protein concentration was from 200 to 1,400 μg/mL before dilution with reagent.

Experimental procedure

1. Prepare dye reagent by diluting 1 part stock dye reagent concentrate with 4 parts MilliQ water. Filter with Whatman #1 filter paper to remove particles before use.
2. Suspend sample powder in MilliQ water to give a concentration of about 2 mg/mL. Allow to stand for 4 h, shaking intermittently for good dissolution.
3. Prepare 5 dilutions of the protein standard.
4. Pipette 100 μL of sample solution and each standard into a clean and dry test tube. Add 5.0 mL of diluted dye working reagent to each tube and vortex.
5. Measure absorbance at 595 nm with a UV/VIS spectrophotometer after incubating at room temperature for 10 min.
6. Samples and standards were assayed in duplicate or triplicate. An average measurement was taken to establish a standard curve and calculate protein concentration.

2.5.2. DNA determination by diphenylamine assay

DNA quantification by diphenylamine assay is based on the determination of DNA deoxyribose. Deoxyribose reacts quantitatively with diphenylamine in the presence of acetic acid, sulphuric acid and acetaldehyde, producing a blue-colour, which is measured spectrophotometrically (Burton, 1956). Improved sensitivity is obtained by incubating test samples with 7% perchloric acid as it minimizes interference from proteinaceous materials and also maximizes DNA extraction from sample pellets (Burton, 1968). For liquid samples including cell broth and homogenates, incubation with 7% perchloric acid at 70°C for 20 min was applied throughout this study. For lyophilized PHB powder, incubation was extended to

30 min to ensure complete extraction of DNA from re-suspended solid sample. Experimental results showed no significant destruction on deoxyribose during the incubation. After perchloric acid treatment, the sample mixture was centrifuged to remove insoluble PHB granules prior to the addition of diphenylamine working reagent for the colour development reaction. DNA concentration was then determined relative to the standard curve.

Table 2.8. Reagents and preparation of diphenylamine assay

Reagents	Preparation
diphenylamine reagent	Dissolve 3.0 g diphenylamine in 200 mL glacial acetic acid. Stable for 3 months at 4°C.
1.6% aqueous acetaldehyde	Add 0.5 mL acetaldehyde to 25 mL MilliQ water. Stable for 3 months at 4°C.
7% perchloric acid	Add 10 mL of perchloric acid to 90 mL of MilliQ water. Stable for 3 months at 4°C.
5mM NaOH	Add 40 mg NaOH to 200 mL MilliQ water. Stable for 3 months at 4°C.
DNA Standard	Dissolve 1 mg standard DNA (sodium salt from calf thymus, purchased from Sigma-Aldrich Pty. Ltd., NSW, Australia) in 1 mL 5mM NaOH solution.

Experimental procedure

1. Prepare the reagents as summarized in Table 2.8.
2. Prepare DNA standard: dilute DNA stock solution to give concentrations of 0, 100, 200, 300, 400 and 500 mg/L DNA. Treat as normal samples.
3. Suspend lyophilized sample powder in MilliQ water at a concentration of about 2 mg/mL and allow to stand for 4 h for maximum dissolution.
4. Mix 1.0 mL of sample suspension with 1.0 mL of 7% perchloric acid in a glass test tube. Incubate at 70°C in a water bath for 30 minutes for the PHB sample powder or 20 min for the liquid sample.
5. After cooling, centrifuge the sample at 13,000 rpm for 8 min (Micromax Bench Centrifuge) to remove insoluble PHB granules. Remove 1 mL of supernatant and mix with 2 mL of diphenylamine working agent prepared immediately before use by adding 0.3 mL of H_2SO_4 and then 0.1 mL of aqueous acetaldehyde to 20 mL of diphenylamine reagent. Incubate for 16 to 20 h at 30°C in a water bath.

6. Measure absorbance using a UV/VIS spectrophotometer at 600 nm and determine DNA concentration from the established standard curve.

2.5.3. Residual cell debris quantification by SDS-PAGE

Removal of cell debris is a major concern in terms of inclusion body recovery from host cells. The SDS-PAGE technique enables the identification and quantification of insoluble proteins associated with cell debris. Two specific debris-associated *E. coli* outer membrane proteins, OmpA and OmpC/F, with molecular weights ranging from 31 to 45 kDa, were identified (Wong *et al.*, 1997). Cell debris can be quantified by measuring the relative concentration of one of the outer membrane proteins in samples, assuming it is evenly distributed over the *E. coli* cell envelope. This method was used to monitor cell debris removal in each unit operation in the PHB recovery process.

Experimental procedure

1. Re-suspend the sample powder in MilliQ water at a concentration of less than 4 g/L and allow to stand for 4 h with intermittent shaking for good dissolution.
2. Fill a centrifuge tube with 20 mL of sample suspension and centrifuge at 27,600 ×g for 4 h using a HB-6 swing-out rotor in a Sorvall RC-5C refrigerated centrifuge (Du Pont, USA). All the cell debris with a size above 0.07 μm is sedimented under these conditions.
3. Remove the supernatant and dissolve the pelleted sample with SDS sample buffer. Conduct SDS-PAGE analysis with a 12% acrylamide separating gel and a 4% stacking gel, followed by densitometry of one outer membrane protein band (Section 2.4.3). Cell debris is quantified relatively by comparing the intensities of the same protein band between samples (e.g., by comparing a centrifuged sample with a feed sample, giving total removal).

2.6. CHARACTERISATION OF PHB PHYSICAL PROPERTIES

2.6.1. PHB analysis by gas chromatography

PHB concentration in microbial cell mass is determined by gas chromatography (GC) following conversion to 3-hydroxybutyric acid methylester by incubation with chloroform and acidified methanol (Braunegg *et al.*, 1978). Under mild acidic conditions, PHB extracted from cell materials by chloroform is depolymerized and dehydrated to its component monomer 3-hydroxybutyric acid (HB), followed by HB methanolysis. The resulting 3-hydroxybutyric acid methylester (3-HBME) is determined by GC. The composition of the copolymer P(3HB-3HV) can also be determined as it forms 3-HBME and 3-hydroxyvalerio acid methylester (3-HVME). The esters can be differentiated in GC retention time. Benzoic acid is employed as an internal standard to correct errors in injection volume. Benzoic acid is converted into benzoate methylester that has a longer GC retention time than that of 3-HBME and 3-HVME.

There are some other methods reported for PHB determination, for example, turbidmetric measurement (Williamson and Wilkinson, 1958), spectrophotometric determination (Law and Slepecky, 1961), capillary isotachophoresis (Sulo *et al.*, 1996), fluorescence method (Page and Tenove, 1996), and thermogravimetric method (Hahn and Chang, 1995). However, the GC method developed by Braunegg *et al.* (1978) remains the most common one used in laboratories. The GC method does not require PHB extraction from cell materials and is thus superior to many other methods. It is also rapid, reliable and reasonably accurate. The GC method was employed throughout this study for the determination of PHB concentration.

2.6.1.1. Experimental procedure

Sample preparation

Lyophilized cell material was suspended with a mixture containing 2 mL chloroform, 2 mL acidified methanol (3% v/v sulphuric acid) and 200 μL internal standard solution (approximately 0.4 g benzoic acid in 100 mL methanol) in a tightly sealed tube and incubated at 100°C for 3.5 h. After adding 1 mL of deionized water and mixing, two phases were formed. Insoluble non-PHB material accumulated at the interface. The top phase was removed and discarded. The remaining organic phase was directly injected into the GC. In parallel with sample treatment, standard PHB was employed to construct a calibration curve. The detailed procedure is given in Appendix B.

GC instrument and operating conditions

A computer-controlled gas chromatograph (Shimadzu GC-17A) equipped with a double flame ionization detector (FID) and fitted with a packed column (10% CARBOWAX 20M on chromosorb WAM 80/100, 1/8th, Alltech Associates, Pty. Ltd., NSW, Australia) was used in the study. The analysis employed the following temperature-programmed operating conditions: start at 100°C, hold for 1 min, ramp to 180°C at a rate of 8°C/min and hold for 5 min before termination. The injection volume varied between 0.5 μL and 2 μL. Nitrogen was the carrier gas at a flow rate of 30 mL/min. Detection was by FID. Figure 2.8 shows a typical chromagraph under the above condition with identificable peaks of 3-HBME and benzoate methylester.

PHB quantitation

The quantity of PHB was determined from the quotient (Q) of the peak areas of 3-HBME and benzoate methylester. It was calculated from the average Q value obtained from three replicate GC injections with reference to the constructed calibration curve. Figure 2.9 presents a typical calibration curve used in the analysis. Calibration was made only within the linear range. The composition

and concentration of copolymer in a cell sample, for example PHB/HV, were determined by employing a PHB/HV copolymer as a calibration standard.

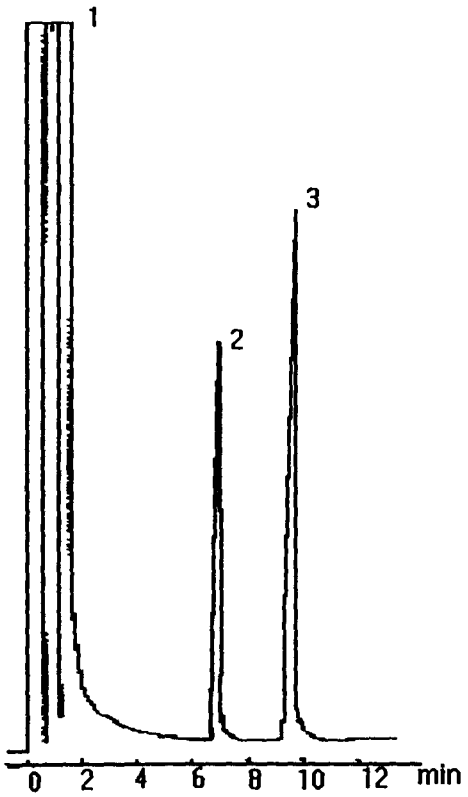

Figure 2.8. Typical chromatogram of the reaction solution on the packed column. Peak 1: solvent mixture; Peak 2: 3-HBME; Peak 3: benzoate methylester.

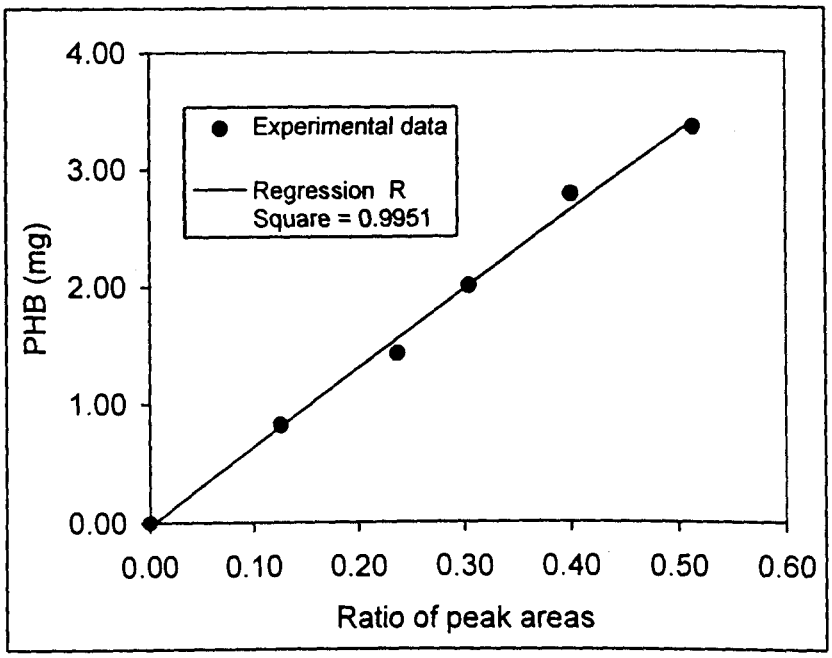

Figure 2.9. A typical PHB calibration curve.

2.6.1.2. Optimization of GC method for PHB analysis

GC was employed throughout this thesis for PHB analysis. Concerns about accuracy and reproducibility are common with such a method. In this section, the optimization of operating conditions is discussed with the emphasis on developing the final sample treatment procedure for enhanced sensitivity and reliability.

Incubation conditions

After mixing cell sample containing PHB with acidified methanol and chloroform, the sample mixture was incubated. Two major processes, namely PHB extraction from the cell material and subsequent methanolysis, occur during incubation. The incubation conditions, therefore, affect the reliability and accuracy of the measurement. It is necessary to determine the optimum incubation time at a fixed incubation temperature. Shortening the incubation time may not ensure complete PHB extraction and the completion of methanolysis. On the other hand, longer incubation may lead to the decomposition of hydroxybutyric acid and the formation of secondary products in the presence of sulphuric acid (Riis and Mai, 1988). This restricts the optimal incubation time to a narrow range.

An experiment was conducted to obtain the optimal incubation time for recombinant *E. coli* cells containing PHB. Approximately 5 mg of lyophilized recombinant *E. coli* cell mass from shake flask culture was weighed and mixed with MeOH/3%H_2SO_4 and $CHCl_3$ in tubes which were incubated at 100°C for various times. Figure 2.10 illustrates the ratio of the intensity of 3-HBME to benzoate methylester (per sample mass unit) as a function of incubation time. At a temperature of 100°C, 3.5 h of incubation time was necessary to obtain a high response of 3-HBME for the cell material. Further incubation caused the degradation of 3-HBME. Secondary products were not detectable. An incubation time of 3.5 h was therefore selected throughout this study.

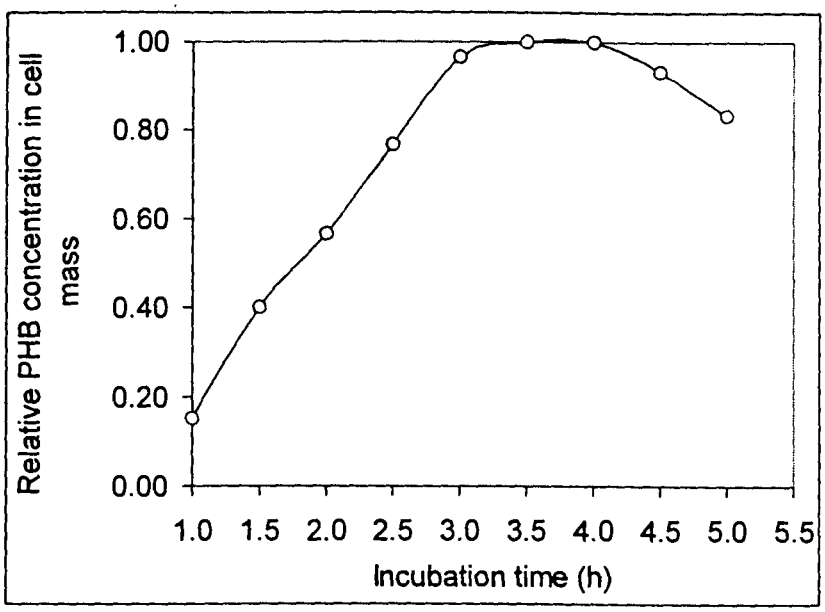

Figure 2.10. Detected PHB relative concentration in recombinant *E. coli* cell mass as a function of incubation time (at a temperature of 100°C).

Methylester partition

In Braunegg's method, water was added to the reaction mixture after incubation to extract sulphuric acid and cell debris from the organic phase containing the methylesters of HB, HV, and benzoic acid. Due to solubility in water, methylesters may not completely move into the organic layer and thus cause inaccuracy (Jan *et al.*, 1995). To eliminate methylester loss due to its partition between chloroform and water, the chloroform layer was carefully withdrawn with a finnpipette after water extraction. Water remaining in the collected chloroform solution can be further absorbed by the addition of sodium sulphate.

Cell mass lyophilization

Lyophilization treatment was required for all cell samples prior to PHB analysis using the GC method in this study. Lyophilization improves PHB extraction efficiency from *E. coli* cells. This improvement was demonstrated by comparing the detectable PHB concentration in cell samples with and without lyophilization, as described below.

E. coli cell broth from three different sources (shake flask cultures A, B and C) were pipetted into tubes in duplicate and centrifuged. The supernatant was

discarded. Half of the samples were lyophilized. The wet pellets and lyophilized samples were analyzed using Braunegg's method. Table 2.9 lists the PHB concentration measured by GC. Note that the detected PHB from the wet sample was much less than that from the lyophilized sample. This suggests that lyophilization enhances the permeabilisation of chloroform through the cell wall and eases PHB extraction during incubation.

Table 2.9. GC-detected PHB concentration in cell mass

Sample	PHB concentration (g/L)		
	Source A	Source B	Source C
wet cell pellets	6.45	8.79	11.57
lyophilized powder	10.76	13.77	20.1

2.6.2. Molecular weight determination by HPLC

A well-established method for determining molecular weight and molecular weight distribution of linear polymers is to use High Performance Liquid Chromatography (HPLC), coupled with the universal calibration (Grubisic *et al.*, 1967). Universal calibration is based on the linear relationship of $Log([\eta]M)$ to HPLC retention time or retention volume and the Mark-Houwink equation (Equation 2.9). Molecular weight can be calculated from Equation 2.9 if the Mark-Houwink constants, α and K, are available.

$$[\eta] = K \times M_v^{\alpha} \qquad (2.9)$$

$$Log[\eta]M_v = LogM_v^{1+\alpha} + LogK$$

In the above equations, $[\eta]$ is the intrinsic viscosity and M_v is the viscosity-average molecular weight. α and K represent Mark-Houwink constants. Linear polystyrene with low polydispersity is normally used as a calibration standard to construct a calibration curve.

Microbially-produced PHB has a linear configuration (Doi, 1990). PHB molecular weight from some microbiological sources has been determined by light scattering and osmometric analysis, and a separation technique has also been

introduced to fractionate PHB with low polydispersity (Miyaki *et al.*, 1977; Marchessault *et al.*, 1970; Akita *et al.*, 1976). This makes it possible to estimate the Mark-Houwink constants for PHB. With known Mark-Houwink constants of standard polystyrene and PHB at a specific temperature, PHB molecular weight and its distribution can be determined

HPLC operating conditions

A Shimadzu LC-10A HPLC system, equipped with a PLgel 10 μm Mixed-B 30037.5 column (Polymer Laboratories Inc., Amherst, USA) and a Shimadzu RID-6A refractive-index detector were employed. A guard column was attached prior to the sample column to protect it from contamination. A Shimadzu two-channel vacuum degasser was also connected to degas the mobile phase. During operation, the oven temperature of the HPLC system was stabilized at 40°C. Chloroform served as the eluent and the solvent. Eluent flow rate was set at 0.8 mL/min.

Sample preparation

Solvent-extracted PHB was re-dissolved in chloroform at 50°C at a concentration of approximately 0.5% (wt/vol). The solution was filtered to remove all chloroform-insoluble contaminants before injection. Injection volume was 50 μL. Calibration standards were a series of 12 polystyrenes with molecular weight in the range of 2×10^3 to 2×10^6 Da. The standard was prepared in a similar manner as PHB samples at a concentration of 0.1 % (wt/vol).

Calculation

The Mark-Houwind constants (α and K) for polystyrene and PHB (at 30°C) are 0.794, 4.9×10^{-5}, and 0.78, 1.18×10^{-4}, respectively. The retention volume was measured in triplicate and the average value was taken for the calculation. Figure 2.11 is the universal calibration curve of polystyrene standard. The molecular weight of PHB was then calculated using Equation 2.9.

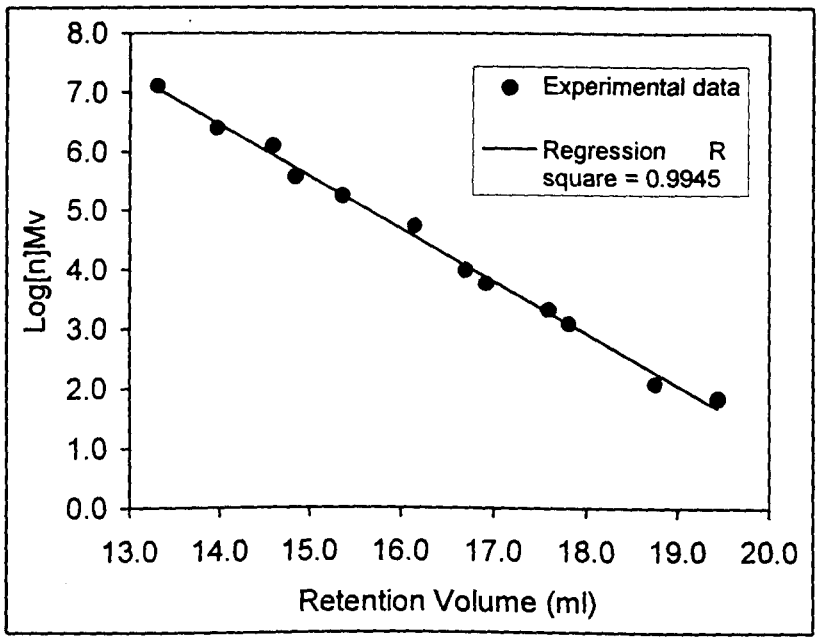

Figure 2.11. The universal calibration curve for PHB molecular weight determination.

2.6.3. PHB crystallization and glass transition analysis by DSC

Differential Scanning Calorimetry (DSC) is a technique for detecting thermal effects accompanying physical or chemical change in a sample by means of programmed heating or cooling. A polymer will undergo major physical change in its morphological state at transition points (the glass transition temperature for amorphous polymer and the crystallization temperature for crystalline polymer). A change in enthalpy occurs and this can be followed by calorimetry. Microbial-sourced PHB is in a highly crystalline state after extraction due to its native exceptional stereochemical regularity, and an endotherm in the DSC thermogram appears around the melting point. The crystallinity of PHB can be estimated by measuring the enthalpy of fusion and comparing that with 146 J/g for 100% crystalline PHB (Barham *et al.*, 1994). PHB glass transition can also be monitored using DSC. The amorphous state of PHB is obtained after quenching the sample from the fusion point to a low temperature (about -100°C).

A DuPont 2200 Thermal Analyser was used for this analysis. Standard indium was for temperature calibration and nitrogen as the carrier gas. Lyophilized

sample of about 10 mg was weighed and encapsulated in a standard aluminium pan and placed into the sample chamber. A thermal cycle was programmed and is listed below:

1. Equilibrate at 25°C
2. Ramp to 200°C at 10°C/min
3. Isothermal for 5.0 min
4. Ramp 50.0°C/min to -100°C
5. Iso-track for 5.0 min
6. Ramp 10.0°C/min to 200.0°C.

Figure 2.12 illustrates a typical DSC thermogram of PHB under the stated operating condition. Morphological transition of polymer is temperature-dependent. At a heating rate of 10°C/min, the peak point of the fusion endotherm was taken as the melting temperature. PHB sample crystallinity was estimated by normalizing the peak area and comparing with the value 146 J/g for heat fusion of 100% crystalline. The inflection point of the specific heat increment at the glass transition range in the second scan was taken as the glass transition temperature.

2.6.4. PHB thermal stability analysis by TGA

Thermal Gravimetric Analysis (TGA) provides kinetic information on degradation, oxidation, and evaporation by measuring the weight change of a sample continuously while its temperature is increased at a constant rate. TGA is mainly used to study thermal decomposition and polymer stability, indicating the temperature at which a thermal event occurs.

Analysis was conducted with a 2200 DuPont Thermal Analyser. Lyophilized sample was placed into the sample chamber with a sample pan, and scanned in the temperature range of 25°C to 350°C at a rate of 10°C/min. Nitrogen was the carrier gas at a flow rate of 20 mL/min. Figure 2.13 is a typical TGA thermogram of PHB, illustrating PHB weight change as a function of temperature. PHB

degradation commenced at a temperature of 250°C under the stated operating conditions.

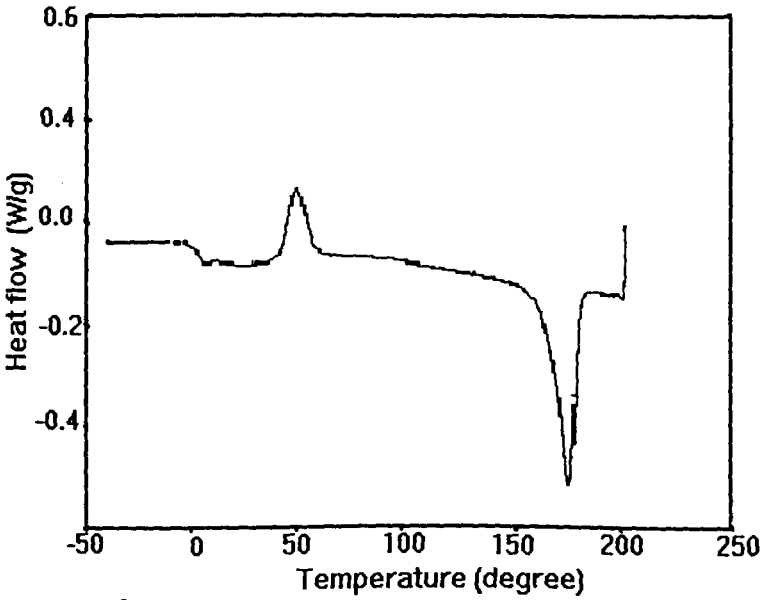

Figure 2.12. Typical DSC thermogram of PHB

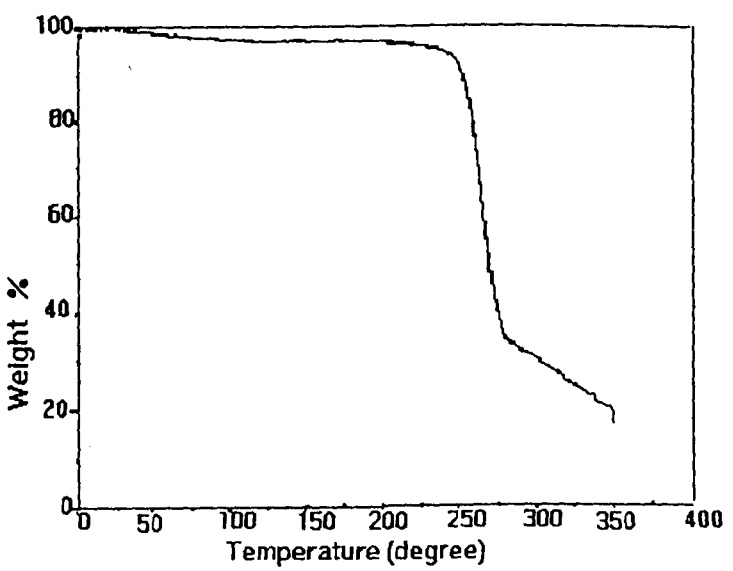

Figure 2.13. A typical TGA thermogram of PHB

CHAPTER 3

PHB RECOVERY BY HOMOGENIZATION AND CENTRIFUGATION

In this chapter, a series of PHB extraction processes involving homogenization and centrifugation were conducted and characterized as a preliminary investigation to provide the basic experimental information for further process optimization.

3.1. INTRODUCTION

A number of PHB recovery methods have been developed in the past few decades as reviewed in Section 1.3. Most are limited to laboratory only and have not been tested at pilot nor production scale. The current industrial method for PHB recovery involves thermal shock and stepwise enzymatic digestion, which has been further modified by incorporating high-pressure homogenization for cell disruption (Section 1.3.2). A high disruption efficiency for PHB release from *A. eutrophus* was obtained using high-pressure homogenization, and key factors affecting disruption have been thoroughly investigated (Harrison *et al.*, 1991). However, the process for classifying PHB from non-PHB cellular components following cell disruption has received scant attention. The removal of non-PHB cell material in the current process is based on solubilization using enzymes and detergents, coupled with multiple centrifugation passes (Section 1.3.2). This approach raises total production cost and yields a relatively low PHB quality which is unacceptable for some applications. More importantly, rational optimization of the centrifugal separation using model-based simulation has not been attempted.

In this chapter, a process for PHB extraction from recombinant *E. coli* employing homogenization and disc-stack centrifugation is investigated. This approach is based on the method for inclusion body processing (see Section 1.3.3) and the PHB recovery process for *A. eutrophus* (Section 1.3.2). The effect of NaOCl on cell debris digestion and PHB fractionation is also tested as it degrades debris (see Section 1.3.1.2). A preliminary process involving homogenization and centrifugation, coupled with NaOCl treatment, is established. Process performance is defined both in terms of PHB recovery and the removal of key contaminants (protein, cell debris and DNA as reviewed in Section 1.5). The PHB purity and recovery attained by the process are comparable to those obtained from the existing PHB recovery process for *A. eutrophus* (Harrison, 1990). Further optimization is undertaken in subsequent chapters.

3.2. EXPERIMENTAL WORK

3.2.1. Fermentation

The bacterial strain employed in this experiment was *E. coli* Topp1(pJM9123). Details of this strain are given in Section 2.1. A fed-batch fermentation (Fermentation I) was conducted in a 20 L Chemap CF-2000 Fermenter with an initial medium volume of 12.5 L. A 3×400 mL shake-flask culture was prepared as inoculum to obtain a high inoculum concentration. The growth medium was an adaptation of the defined R-medium, supplemented with glucose and yeast extract. The compositions of the medium and feeding solutions are given in Section 2.1. Culture temperature was controlled at 37°C. Dissolved oxygen concentration was maintained at 80% saturation by automatically adjusting aeration. Pure oxygen was used when required. Culture pH was kept at 6.9 by the addition of 14% (v/v) ammonia-water. Feeding strategy was pH-stat with a high limit. A mixture of glucose and yeast extract was fed intermittently when pH reached its high limit. The fermentation was terminated at a cell concentration of 42.3 g/L (DCW) (Section 2.1), giving a total volume of 18 L. The culture was stored in the fermenter overnight at 10°C before being frozen at -18°C.

During the fermentation, samples were taken regularly to measure PHB concentration (Section 2.6.1), DCW (Section 2.4.5), glucose concentration (Section 2.4.6) and optical density (OD) at 600 nm (UNICAM 8625 Spectrophotometer).

3.2.2. Extraction process

Three different extraction processes were examined using the frozen cell material from Fermentation I. Each was analysed in terms of PHB purity and recovery. Each process is summarised in Figure 3.1.

Homogenization

Frozen cell material from Fermentation I was thawed overnight at 4°C and then diluted 10 times with PBS buffer (6.5 g/L NaCl and 1.37 g/L KH_2PO_4, adjusted to pH 6.9 with 2 M NaOH). Homogenization was conducted with an APV-Gaulin high-pressure homogenizer (15MR, CD valve) at a pressure of 55.2 MPa. During the homogenization, cell disruption and PHB release were monitored using an analytical disc centrifuge (DCF4, Applied Imaging Ltd, Gatesheak, U.K.) as described in Section 2.4.1. The feed temperature was approximately 10°C for each pass.

Centrifugation

Centrifugation was carried out in a Veronesi KLE-160 solid-bowl disc-stack centrifuge with a fixed operating speed of 8400 r.p.m. (Σ=3775 m^2). The feedrate for each centrifuge pass is indicated in Figure 3.1. For re-centrifugation, the sedimented paste was removed from the solid-bowl and re-suspended in PBS buffer (as above), with assistance of a hand-held electric mixer. The suspension was adjusted to its initial volume. The feed temperature was approximately 10°C for each centrifugation pass.

Hypochlorite treatment

Commercial sodium hypochlorite (Fistons technical grade, FSE Australia, 100 g/L active chlorine) was diluted with MilliQ water to give sodium hypochlorite stock solution (NaOCl) with 17 g/L active chlorine (Middelberg *et al.*, 1995). This was added to the homogenates in Batches B and C, respectively, to give the final concentration of 0.85 g/L active chlorine (1.5% relative to stock concentration) as shown in Figure 3.1. The mixture was then incubated for 1 h in an homogenization tank with circulation prior to centrifugation. The temperature was maintained between 10°C -15°C during treatment.

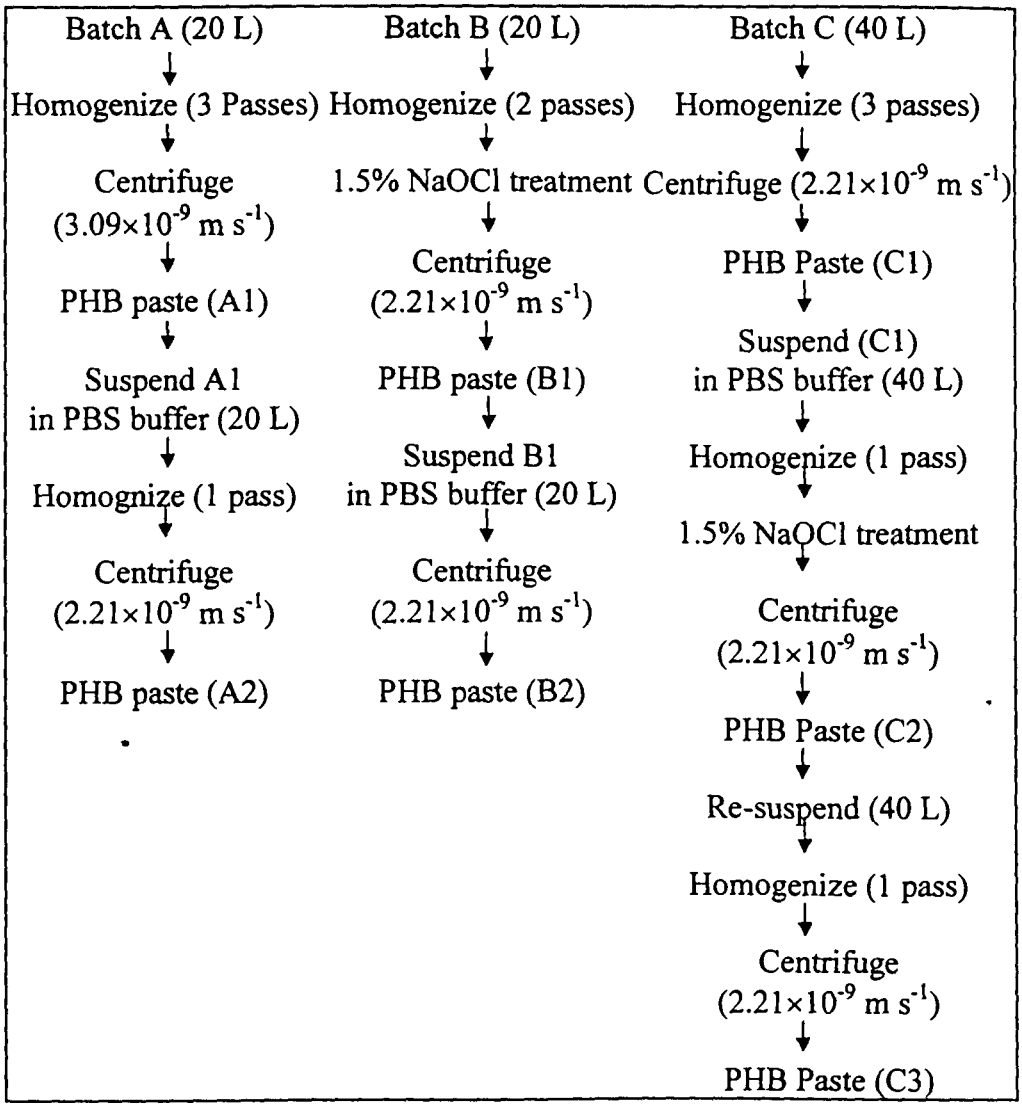

Figure 3.1. PHB recovery protocols for Batches A, B and C.

3.2.3. Analysis

Disc centrifuge analysis

Centrifuge feeds and supernatants were analyzed by an Applied Imaging DCF4 disk centrifuge (Gateshead, U.K.) with the standard water spin fluid scheme (Section 2.4.1). A density difference of 260 kg/m^3 between PHB and spin fluid was employed (Middelberg *et al.*, 1995). The relative amount of particles present in the tested sample was obtained by integrating the area under its size

comparing the results from the centrifuge feed and supernatant. No extinction correction was applied to the data (Middelberg *et al.*, 1995).

Dry weight measurement

Dry cell weight (DCW) was measured by pipetting 1 mL of cell broth into a pre-heated and weighed 1.5 mL Eppendorf tube, which was then analysed as described in Section 2.4.5. Measurements were triplicated.

Contaminant analysis

A small amount of sedimented wet paste after each centrifuge pass was collected for PHB purity and contaminant analysis. Each sample was freeze-dried, and crushed into fine powder before being suspended in MilliQ water at a concentration of about 2 mg/mL. The suspension was allowed to stand for at least 4 h with magnetic stirring to allow sufficient dissolution prior to protein and DNA analysis. Total protein and DNA concentration in the suspension were determined as described in Sections 2.5.1 and 2.5.2, respectively. All the results presented were calculated on the basis of dry cell weight.

PHB measurement

PHB concentration was measured by gas chromatography as described in Section 2.6.1. Approximately 10 mg of lyophilized paste from the centrifuge concentrate was suspended in chloroform using a 5 mL volumetric flask. 0.5 mL of the suspension was taken for GC analysis. The measurement was triplicated. The operating procedure is given in Section 2.6.1.

Cell debris quantification by SDS-PAGE

Relative cell debris concentration in the extracted PHB sample was approximated by SDS-PAGE with a 12% acrylamide separating gel and a 4% stacking gel, followed by densitometry of an outer membrane protein band between 31 and 45 kDa (Wong *et al.*, 1996). The 100 μL sample suspension prepared for protein analysis above was boiled with 400 μL of sample buffer for 5 min before loading onto the gel. Cell debris content in samples was determined relative to the initial homogenate. The operating procedure for SDS-PAGE is given in Section 2.4.3.

onto the gel. Cell debris content in samples was determined relative to the initial homogenate. The operating procedure for SDS-PAGE is given in Section 2.4.3.

RESULTS AND DISCUSSION

3.3.1. PHB release by homogenization

Figure 3.3 shows the particle size distributions in cell suspension and homogenates measured by CDS as a function of the number of homogenization passes. The data are normalised to the same cell concentration for comparison. The mean diameter of PHB granules is approximately 0.65 μm after three homogenizer passes, which is smaller than previous work (Middelberg *et al.*, 1995) but larger than that of typical protein inclusion bodies (Middelberg, 1996).

As shown in Figure 3.3, the complete release of PHB was achieved after two homogenizer passes for the PHB-containing *E. coli* cells under the conditions tested. Surprisingly, the third homogenizer pass apparently resulted in some breakage of PHB granules. This warrants further investigation as the stability of PHB granules under homogenization determines the suitability for scale-up. A further discussion of PHB stability during homogenization is given in Section 4.3.1.

3.3.2. Process A: Repeated centrifugation and PHB purity

The composition of PHB paste recovered by centrifugation in three extraction batches is detailed in Table 3.1. In Process A, PHB with a purity of 90.2% w/w (dry basis) was achieved after two centrifugal passes (A2). This is comparable to that obtained by Harrison (1990) for *A. eutrophus* using a complex enzyme and surfactant treatment at laboratory scale. Protein and nucleic acids are important contaminants that must be removed from crude PHB extracts (Section 3.1.1). Protein removal was effected by centrifugation and protein content was reduced to 9% of its starting concentration by two centrifugal passes. Similarly, total DNA was reduced significantly from 5.2% to 0.62% (w/w) after two centrifuge passes. Multiple homogenization passes result in the fragmentation of nucleic acid, and also the disentanglement of nucleic acids from cell debris along with the cell

debris comminution. This improves the removal of DNA and contributes to a reduction in suspension viscosity thus improving handling characteristics of homogenates. The removal of cell debris by centrifugation was also very efficient, with 75% removal achieved on the first centrifuge pass and a further 19.7% with the second pass. Generally, a significant reduction in all key contaminants (protein, DNA, and debris) was achieved by repeated centrifugation. However, the resultant protein and DNA content were not below the limits reported to cause PHB decolouration in thermal processing (Harrison, 1990). Further treatment is clearly required to reach a high purity, especially with reference to DNA.

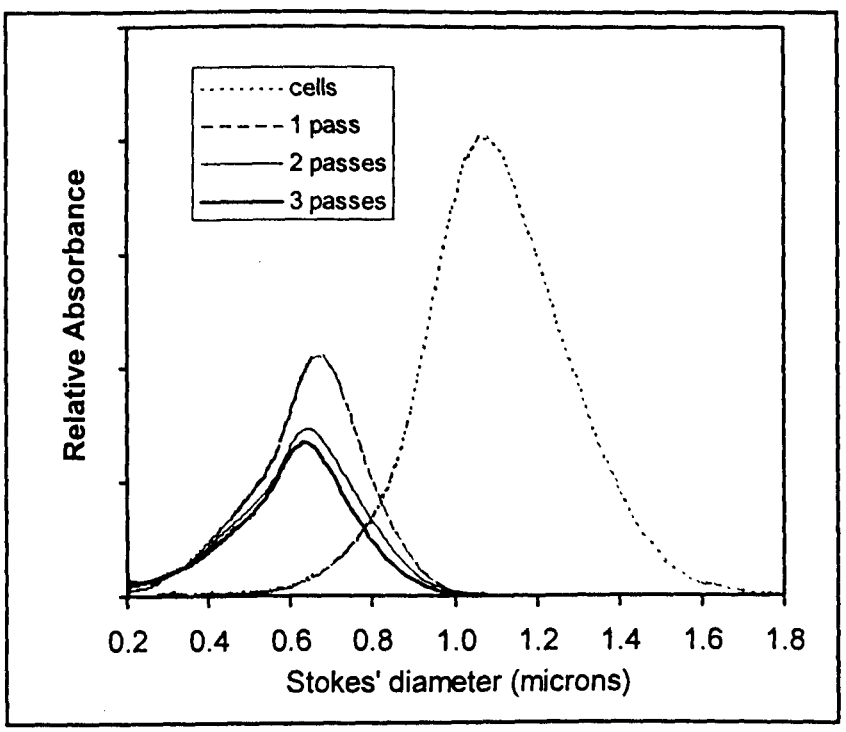

Figure 3.3. Size distributions for whole cells and PHB granules in homogenates measured by CDS. N is the number of homogenization passes.

Multiple centrifugation improves purity but with significant PHB loss. PHB collection efficiencies were 76% and 95% for the two centrifugal passes, respectively. The high viscosity of the suspension could be one of the major reasons giving low PHB collection in the first centrifugation. The increase in viscosity after homogenization was significant as a consequence of nucleic acid

release (Section 3.1.1), and it would become severe at high cell concentrations. In the commercial PHB extraction process from *A. eutrophus*, heatshock prior to homogenization was conducted for both the deactivation of endogenous depolymerase and also the denaturation and solubilisation of nucleic acids (Harrison, 1990; Holmes and Lim, 1990). This unit operation eliminated the impact of viscosity for the following process. Re-suspension and re-centrifugation evidently improved PHB purity but this was offset by additional PHB loss. According to Wong (1996), the improvement in purity becomes less significant after the third centrifuge pass, whereas further granule loss to the supernatant occurs with increasing the number of centrifugal passes. In an attempt to improve recovery without compromising purity, the second centrifugation study employed chemical treatment to reduce contaminant levels (Section 3.3.3).

Table 3.1. Results for PHB fractionation by centrifugation.

Extraction Process		PHB (% w/w)	Protein (% w/w)	DNA (% w/w)	Cell Debris Removal(%)	Collection Efficiency (% per pass)
Cell broth		52.0	25	5.2	0	
Process A	A1	79.1	9.0	1.2	75.0	76
	A2	90.2	2.3	0.62	94.3	95
Process B	B1	82.1	3.9	2.2	85.4	92
	B2	94.0	1.0	1.9	94.3	97
Process C	C1	70.2	9.1	1.2	60.8	82
	C2	90.8	0.54	0.15	92.4	99
	C3	96.5	< 0.01	0.03	96.5	98

3.3.3. Process B: Preliminary study of NaOCl effect on PHB recovery

Both NaOH and NaOCl were suggested as cell debris digestion agents for PHB recovery (Section 1.3.1). The use of NaOH was precluded as it led to the formation of PHB aggregation in the PHB homogenate even though significant debris reduction can be achieved (Appendix C). NaOCl was therefore selected and introduced into Process B. The operating procedure and conditions for

Process B are given in Figure 3.1 with results summarised in Table 3.1. NaOCl treatment under mild conditions (0.85 g/L active chlorine) did not result in significant PHB degradation in the process, as suggested previously (Middelberg *et al.*, 1995). PHB recovery increased from 76% to 92% by reducing the centrifuge feedrate (Q/Σ) from 3.09×10^{-9}m s^{-1} (A1) to 2.21×10^{-9}m s^{-1} (B1), which confirms the importance of feedrate on particle collection efficiency. Despite the reduced feedrate, improved removal of protein and cell debris was achieved on the first centrifuge pass, presumably due to cell debris micronisation together with a reduction in suspension viscosity during NaOCl treatment. The reduction in viscosity in turn may enhance PHB collection efficiency. This confirms previous work that employed NaOCl to digest non-PHB biomass (Berger *et al.*, 1989; Hahn *et al.*, 1995). Surprisingly, final debris removal for Sample B2 was no greater than that for A2. This may be due to a reduction in the total number of homogenizer passes from 4 to 2 for Process B. Total protein removal was also improved by NaOCl treatment and was reduced to 1% after two centrifugation passes (B2) compared with 2.3% (A2). The value of 1% is below the limit reported to cause significant decoloration in thermal processing (Harrison, 1990).

It is noted that DNA removal does not follow the same trend as protein and debris removal. There is less DNA removal (56%) in the first centrifuge pass in Process B. Further, approximately 50% of the DNA in Sample A1 is removed by re-centrifugation, whereas only 14% of the DNA in Sample B1 is removed. A possible reason for reduced DNA removal is the effect of NaOCl on DNA structure. Partial denaturation of the DNA may promote adherence to PHB granules, thus preventing separation. The inclusion of an extra homogenization step between Sample A1 and A2 may also enhance DNA removal through improved re-suspension of the paste, and destruction of DNA through shear. The incomplete re-suspension of PHB paste after centrifugation in the experimental conditions is examined in Appendix C. Inserting additional homogenization step between centrifugation is also necessary in terms of the cell debris comminution and thus removal.

Generally, the introduction of NaOCl at a relatively low concentration effects the degradation of non-PHB cellular material and has a negligible impact on PHB granules. Incorporating hypochlorite treatment into the PHB recovery process can lead to high PHB recovery while improving the removal of debris and protein. The result also suggests that introduction of hypochlorite treatment after the first centrifuge pass may lead to high DNA removal along with the high protein and debris removal.

3.3.4. Process C: An initial optimized process for PHB recovery from recombinant *E. coli.*

Based on the information obtained in Processes A and B, the PHB recovery process was further modified (Process C) (Figure 3.1). It was decided to introduce the NaOCl treatment after the first centrifugal fractionation (i.e., after removal of considerable DNA) to overcome the problem of DNA contamination. The study presented in Appendix C emphasized the impact of incomplete re-suspension on cell debris comminution and thus its removal. An additional homogenization step was therefore introduced after centrifugation to enhance paste re-suspension and hence the dispersion of granules and residual debris. This process gave both high PHB purity (96.5%) and recovery (81%) (Table 3.1). High PHB recovery is attributed to the reduction in feedrate (C1) and the effect of NaOCl treatment on homogenate viscosity (C2). A comparison of C1 and A1 reconfirms that collection efficiency was improved as the feedrate decreased from 3.09×10^{-9} m s^{-1} to 2.21×10^{-9} m s^{-1}, but with a penalty of decreased cell debris removal (75% to 60.8%). NaOCl treatment caused a drop in total protein to 0.54% after the first centrifugation and further to a level below 0.01% after the second pass. DNA removal was enhanced in Process C as expected. The significant decrease in DNA content from 0.62% (A2) to 0.15% (C2) was evidently attributed to NaOCl treatment. Homogenization effects DNA fragmentation and thus its removal (C3).

This recovery process yielded a very pure PHB product with negligible DNA and protein contamination. This process is competitive in terms of PHB purity and recovery with the industrial method described by Harrison (1990), but does not require enzyme, detergent and hydrogen peroxide washing. The remaining protein and DNA contents are below the levels reported to cause PHB decoloration in thermal processing (Harrison, 1990). This fractionation process was conducted at pilot scale, and the results obtained can be extrapolated to full-scale PHB manufacture with some confidence.

The fractionation process will be further studied in terms of the micronization of cell debris and their collection efficiency during centrifugation in Chapter 4. Further process simplification would be possible by using a continuous rather than solid-bowl disc-centrifuge, thus simplifying paste re-suspension and re-centrifugation. Savings are also possible by optimizing the NaOCl treatment regime. Optimisation of the NaOCl treatment and the whole recovery process will be addressed in Chapters 5 and 6.

A specific limitation of Process C is the low cell concentration employed. Due to the limited cell material, the concentration was approximately 4.2 g/L. Because cell concentration does not affect the disruption efficiency significantly (Kleinig *et al.*, 1995) and particle size is only slightly affected by a change in cell concentration (Agerkvist and Enfors, 1990), the available results may extend to relatively high cell concentrations if the increase in cell concentration does not generate significant increases in viscosity (Wong, 1996). The possibility of using a higher cell concentration is addressed in Chapter 6 along with optimisation of NaOCl digestion regime. Obviously, a strong correlation between cell debris digestion and NaOCl treatment conditions exists, which will be addressed in Chapter 5.

3.3.5. Conclusions

The use of homogenization and centrifugation for PHB recovery from recombinant *E. coli* was investigated in this chapter. Homogenization was an efficient method of PHB release, with a high disruption efficiency obtained after two homogenizer passes. Repeated centrifugation effected cell debris removal while ensuring a reasonable PHB collection efficiency. An improved PHB collection efficiency was obtained by incorporating NaOCl digestion into the process. The problem associated with DNA denaturation and thus its adherence to PHB granules was overcome by restructuring the unit operation sequence. An extra homogenization step inserted between two centrifugation passes in the process conditions improved the dispersion of PHB paste and thus enhancing the removal of protein and DNA, and also cell debris. Finally, a process which included three homogenizer passes, three centrifuge passes, coupled with mild NaOCl treatment, was established, which gave a PHB with 96.5% purity and 79.5% recovery rate with negligible DNA and protein contaminants. The process is ready for scale-up.

CHAPTER 4

PARTICLE SIZE ANALYSIS AND FRACTIONATION SIMULATION

A preliminary investigation of PHB recovery by the use of homogenization, centrifugation, and NaOCl treatment was conducted in Chapter 3. The aim of this chapter is to prepare homogenization and centrifugation models for process simulation and further optimization performed in Chapter 6. To achieve this, the existing models are reviewed. CSA (Section 2.4.2) is used to measure debris size following cell disruption by homogenization. The data are fitted to the models to obtain the model parameters. The simulation is also set up based on the processes conducted in Chapter 3, which provides information for further optimization of the PHB recovery process.

4.1. MODELLING

4.1.1. Modelling the recovery process

A preliminary investigation of PHB recovery from recombinant *E. coli* was conducted in Chapter 3 by the use of homogenization and centrifugation. After release by homogenization, PHB was fractionated from non-PHB cellular material by repeated centrifugation and yielded acceptable PHB recovery rate and purity. The experiment also indicated that PHB yield and purity were enhanced by incorporating hypochlorite treatment into the process. The process can be further optimized through simulation.

Figure 4.1 describes the main steps to achieve the optimization of this recovery process. Centrifugal fractionation of non-PHB insoluble material (i.e., cell debris) from PHB granules is dictated by their relative sedimentation velocity distributions (e.g., size and density). Optimizing the process, therefore, can be made through the simulation of the particle size related fractionation in the three unit operations (i.e., homogenization, centrifugation and NaOCl treatment) defined in the preliminary investigation. This chapter deals with the fractionation of cell debris and PHB in homogenization and centrifugation, while Chapter 5 will focus on the establishment of models for PHB and cell debris by NaOCl treatment. This enables the overall process simulation and optimization conducted in Chapter 6.

The existing modelling study on homogenization and centrifugation is reviewed in the following sections. Cell debris size is affected by homogenization and NaOCl treatment, and will be measured by CSA (Section 2.4.2) in this chapter. PHB granule size dictated by fermentation is measured by CDS (Section 2.4.1). The model parameters are thus determined by fitting those particle size data to the models. With the basic information on particle fractionation from the modelling study, and sensitive measurement of PHB and cell debris size, the settling

behaviour of PHB and cell debris and their fractionation in a disc-stack centrifuge can be predicted and optimized further.

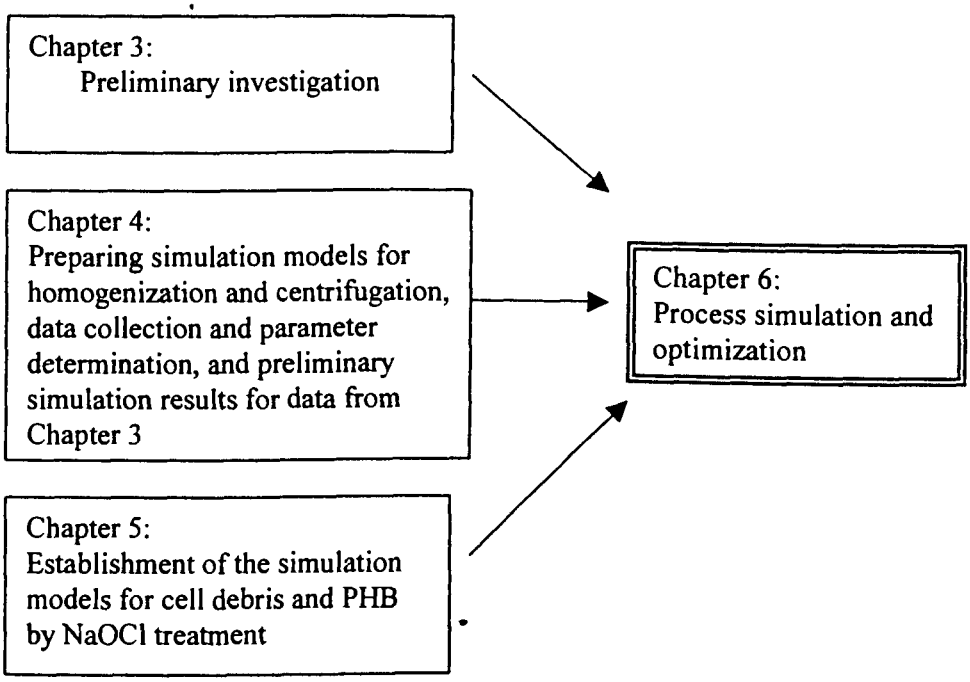

Figure 4.1. The main steps to optimize the PHB recovery process.

4.1.2. Cell debris comminution by homogenization: Modelling

Homogenization is the most commonly used mechanical method for large-scale cell disruption and cell debris comminution. The homogenizer disruption efficiency is affected by suspension temperature, cell concentration, homogenizer operating pressure, the number of homogenizer passes and homogenizer valve design (Hetherington *et al.*, 1971; Keshavarz-Moore *et al.*, 1990; Kleinig *et al.*, 1995; Harrison *et al.*, 1991; Agerkvist and Enfors, 1990). When cell material is passed through a homogenizer, not only intracellular material is released but also the cell debris is comminuted. The system variables which affect cell disruption efficiency, such as the number of homogenizer passes, will affect debris comminution as well. Cell debris comminution increases the size difference between cell debris and inclusion bodies and thus facilitates their fractionation.

The modelling study of debris comminution requires the sensitive measurement of debris size. However, cell debris is comparatively difficult to characterize mainly

due to the sensitive physical and chemical properties, and the small size range (Wong, 1996). Significant variation in debris physical properties such as size and shape appears following some pretreatments, resulting in high measurement uncertainty. However, the CSA method (described in Section 2.4.2) is not interfered by the presence of inclusion bodies when sizing *E. coli* cell debris. It has a broad size measurement range that other methods are not able to achieve. For example, many methods have low sensitivity when the size is below than 0.2 μm, the region where most of cell debris size is located. The method thus provides a means to the characterization and modelling study of cell debris size.

Cell debris size is reduced with each homogenization pass (Olbrich, 1989; Agerkvist *et al.*, 1990; Thomas *et al.*, 1991; Bailey *et al.*, 1995). It was also found that the ease of cell debris comminution is consistent with cell disruption efficiency by homogenization (Wong *et al.*, 1997). Cell disruption efficiency varies with the strain, cell growth phase and whether or not cells are induced, resulting in differences in the extent of cell debris-size reduction. The higher the cell disruption efficiency, the smaller the resulting cell debris will be.

The *E. coli* cell debris distribution after homogenization can be described using the Boltzmann function (Equation 2.8, Wong *et al.*, 1997). The Boltzmann function has been applied to describe yeast whole cell and cell debris distribution disrupted by homogenization (Siddiqqi *et al.*, 1996). The median diameter D_{50} and parameter w can be obtained by regression of the experimental data. The application of the Boltzmann equation to describe the cell debris distribution significantly improves the ability to compare effects of process variables on cell debris size.

Cell debris size reduction of recombinant *E. coli* cells during homogenization has been modelled based on grinding theory using a particle population balance (Wong, 1996). The cumulative undersize distribution of debris after the N^{th} homogenizer pass $P(x_i, N)$ can be estimated from the particle distribution after the $N\text{-}1^{th}$ homogenizer pass $P(x_i, N\text{-}1)$ using Equation 4.1.

$$P(x_i, N) = 1 - [1 - P(x_i, N-1] * \exp(-\alpha x_{i-1}^{a}) \quad (4.1)$$

It is assumed that the cell debris distribution in a homogenate is derived from two processes: the disruption of whole cells to debris P_{dc} and subsequent cell debris comminution P_{dd}. It can be estimated by Equation 4.2 according to the proportion of whole cells and debris in a given homogenate.

$$D_N \times P_d(x_i, N) = (D_N - D_{N-1}) \times P_{dc}(x_i, N) + (D_{N-1}) P_{dd}(x_i, N) \quad (4.2)$$

The constant α in Equation 4.1 is same for both processes while a is replaced with a_c in Equation 4.3 for cell disruption and a_d in Equation 4.4 for debris comminution, respectively.

$$P_{dc}(x_i, N) = 1 - [1 - P_c(x_i, N-1] * \exp(-a_c x_{i-1}^{a}) \quad (4.3)$$

$$P_{dd}(x_i, N) = 1 - [1 - P_d(x_i, N-1] * \exp(-a_d x_{i-1}^{a}) \quad (4.4)$$

The cell debris distribution as a function of homogenizer passes can be predicted if the initial whole cell distribution and the cell disruption efficiency of each homogenizer pass are given.

4.1.3. Modelling study of centrifugation

Following the ever-increasing application of centrifugation, a need has arisen for a simple and widely acceptable models that enable the evaluation of centrifuge separation capacity and the prediction of particle separation performance under certain operating conditions. However, such a method has not been available. The existing modelling work is either based on assumptions which are rarely met in real operation or use semi-empirical expressions based on experimental work. Wide variations have existed between individual interpretations. In this section, some fractionation models of centrifuge operation are reviewed in relation to the prediction and optimization of PHB fractionation from cell debris.

Stokes' law

The sedimentation of a solid particle under the influence of a force can be described by Stokes' law. If the force acting on a particle is gravity, its settling velocity V_g is expressed by Equation 4.5,

$$V_g = \frac{(\rho_s - \rho_l)D^2}{18\mu} g \tag{4.5}$$

where ρ_s and ρ_l are the densities of particle and fluid phase, respectively, μ is the fluid viscosity, g is the gravitational constant, and D is particle diameter.

In a centrifuge field, the particle moves under a centrifugal force and the settling velocity V_c is described by Equation 4.6,

$$V_c = \frac{(\rho_s - \rho_l)D^2}{18\mu} \omega^2 r \tag{4.6}$$

where ω and r are the angular velocity of the rotating bowl and the radius, respectively.

Stokes' law simplifies the movement of particles by assuming particles are small, inert and spherical, and move in an infinite diluted suspension with a laminar flow pattern. Equations 4.5 and 4.6 are valid only if the hindered settling or turbulent settling of particles is negligible and the Reynolds number is smaller than 0.1 (i.e., $R_e = V_r \rho_l D/\mu < 0.1$).

Sigma Model

The sigma model for a disc stack centrifuge was established on the basis of Stokes' law and a plug flow assumption. As shown in Figure 2.3, the flow containing solid particles were evenly distributed between disc spaces. Within each space, the flow moves parallel to the disc surface at the same angular velocity without axial and radial mixing. The overall fraction of particles collected, f, is then related to the fluid flowrate Q and velocity V, and is given by Equation 4.7,

$$\begin{aligned} fQ &= V\Sigma \qquad & V\Sigma < Q \\ f &= 1 \qquad & V\Sigma \geq Q \end{aligned} \tag{4.7}$$

The Sigma factor Σ is the equivalent settling area of a centrifuge, defined as the settling area of a gravitational settling tank (1 metre deep) which possesses the same separation capacity as the given centrifuge. It can be calculated from Equation 4.8,

$$\Sigma = \frac{2\pi N\omega^2}{3g\tan\varphi}(R_a^3 - R_b^3) \tag{4.8}$$

where ω is the centrifuge angular velocity, N is the number of discs, φ is the angle between the axis and disc surface, and R_a and R_b are the disc outer and inner radii, respectively.

Use of the Sigma model for the prediction of centrifugal recovery has led to serious errors mainly due to the simplified plug-flow assumption. The real flow pattern between discs is more complicated than assumed. Besides, particles may not follow Stokes' law and an intermediate law between Stokes' law and Newtow's law might exist (Frampton, 1963). To modify the Sigma model, empirical factors were introduced for fitting the model to the experimental data (Frampton, 1963; Ambler, 1959). However, these factors were strongly restricted by experiments and can be evaluated only by experimental observation. There is a need for further characterization of the flow hydrodynamics between discs, to support the correction of the Sigma model and the establishment of a practical and acceptable model.

Grade Efficiency

To evaluate the separation efficiency of a centrifuge, the concept of grade efficiency is used. It is defined as the fraction of particles collected with a diameter D in a centrifugal system as a function of dimensionless particle diameter D/D_c, where D_c, known as the critical particle size or the theoretical separation limit, is a function of the centrifuge design and operation condition. Grade efficiency can be determined experimentally using Equation 4.9.

$$T(D) = \frac{\text{Sedimented portion of particle with a diameter } D}{\text{Total particles with a diameter } D \text{ in feed stream}} \tag{4.9}$$

Grade efficiency characterizes the separation capacity of a given separation system, and is dependent upon centrifuge design and the feature of the feed including flowrate. In practice, the grade efficiency reveals its statistical character, even though it was originally derived from a theoretical concept. The value of grade efficiency is only the probability of particle sedimentation and a large uncertainty exists for predicting the sedimentation of a small number of particles. For example, when a single particle with a size of D passes through a centrifuge, the possibility of sedimentation is 100% or 0% depending on the operation. The establishment of a meaningful grade efficiency requires the consideration of a large number of particles covering a wide size range.

Grade efficiency in an ideal disc centrifuge

For the particles following Stokes' law, the grade efficiency in a disc centrifuge is expressed by Equation 4.10,

$$T(D) = (D/D_c)^2 \qquad \text{for } D < D_c \qquad (4.10)$$

$$T = 1 \qquad \text{for } D \geq D_c$$

the critical particle size D_c is given by Equation 4.11,

$$D_c = \sqrt{\frac{18\mu Q}{\Delta\rho\Sigma g}} \qquad (4.11)$$

where $\Delta\rho$ is the density difference between particle and aqueous fluid and μ is the fluid viscosity.

According to this model, a particle with a diameter larger than D_c will have a grade efficiency value of unity. However, experimental work has recorded large deviations from this prediction as illustrated in Figure 4.2. In a real disc centrifuge, the flow condition is more complex and does not follow the laminar flow pattern assumption. As a result, particles of similar size may be subjected to different conditions because of the different location within the centrifuge, resulting in deviation in separation performance. Furthermore, the uneven surface properties of particles of the same diameters can also cause difference in separation efficiency. To meet the particle performance in a real centrifuge, grade efficiency can be corrected by incorporating a more realistic flow pattern and/or introducing empirical factors.

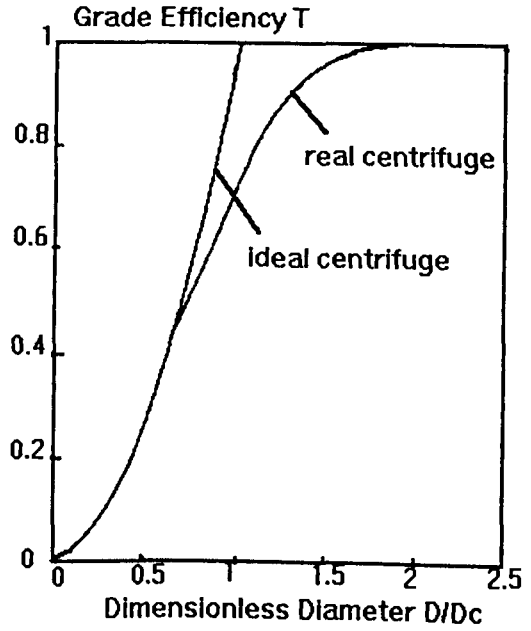

Figure 4.2. The grade-efficiency curve of an ideal centrifuge and a real centrifuge (Mannweiler, 1989)

Lateral mixing model

The model given by Equation 4.12 was used by Mannweiler (1989) for describing the separation of biological particles in a disc-stack centrifuge.

$$T(D) = 1 - \exp\left[-k\left(\frac{D}{D_c}\right)^n\right] \tag{4.12}$$

The model assumes plug flow in the axial direction and complete mixing in the lateral direction. Particles are evenly suspended across the lateral section perpendicular to the disc surface (Licht, 1980). Two empirical parameters k and n are introduced. They vary with different separation systems and can be determined by regression of experimental data.

Particle separation prediction

The use of grade efficiency enables the prediction of the particle separation in a given centrifuge. The particle size distribution in the discharged aqueous overflow and the sedimented particle phase can be predicted if the particle size distribution in the feed is known. This is the necessary information for the

selection of the optimum centrifugal operation conditions and also for the design and operation of subsequent downstream processes.

For a given separation system, the overall collection efficiency E_T can be estimated from grade efficiency $T(D)$ and the particle size distribution (by volume) in the feed suspension $F_0(D)$, given by Equation 4.13,

$$E_T = \int_{D_{min}}^{D_{max}} T(D) dF_0(D) \tag{4.13}$$

where D_{max} and D_{min} are the maximum and minimum particle size present in the feed suspension. The particle size distribution in the discharged supernatant $F_l(D)$ is given by Equation 4.14,

$$F_l(D) = 1 - T(D)F_0(D) \tag{4.14}$$

and the particle size distribution in the concentrate $F_s(D)$ is given by Equation 4.15,

$$F_s(D) = T(D)F_0(D) \tag{4.15}$$

Modelling Study of Bioprocessing

There are a few reports on the modelling of biological particle separation in large-scale centrifuges. The model introduced by Mannweiler (1989) was employed for the prediction of collection efficiency of *E. coli* inclusion bodies and cell debris (Wong *et al.*, 1996; Wong, 1997; Olbrich, 1989; Jin, 1992) and yeast cell debris (Clarkson *et al.*, 1996) after homogenization. The experimental study of collection efficiency relies on particle size characterization and some modelling were developed in association with size analysis methods. Middelberg *et al.* (1991) presented a model for inclusion body collection efficiency from disc centrifuge as a function of Stokes' diameter which was measured by CDS. Jin *et al.* (1994) reported an efficient method for on-line monitoring and control of inclusion body collection by measuring turbidity, which may result in the establishment of an empirical centrifugal model.

4.1.4. Data collection and parameter determination

The simulation of PHB fractionation from cell debris by homogenization and centrifugation bases on the information of particle size. PHB granule size can be measured by CDS, while cell debris size is characterized by CSA. Details regarding these techniques are given in Sections 2.4.1 and 2.4.2, respectively. Both size distributions of cell debris and PHB granules are expressed by Boltzmann functions (Equation 2.8).

Cell debris size distribution after multiple homogenization can be predicted by cell debris size reduction model (Equation 4.1) under certain homogenization conditions if the cell size distribution prior to homogenization and the cell disruption efficiency of each homogenizer pass are given. The initial cell size distribution can be measured by CDS, and the cell disruption efficiency after each homogenizer pass can be estimated using CDS data (Middelberg *et al.*, 1990). The parameters α, a_c and a_d in Equation 4.1 are obtained by regression of the experimental data.

Grade efficiency curves of PHB and cell debris under certain centrifugation conditions can be determined experimentally using Equation 4.9 by measuring their size distributions in the concentrate and supernatant. Equation 4.12 will be used in this study for the prediction of PHB and cell debris fractionation performance in a disc-stack centrifuge. Two empirical parameters k and n can be obtained by regression to the experimental data.

In this study, the centrifugal fractionation is performed in a Veronesi KLE-160 solid-bowl disc-stack centrifuge with an average bowl rotational speed of 8400 rpm (Σ=3775 m^2). The parameters k and n are valued at 0.16 and 2.6 for PHB granules and 0.13 and 2.1 for cell debris, respectively. These parameters were obtained for recombinant *E. coli* cell debris and protein inclusion bodies fractionated in the same centrifuge as used in this study (Wong, 1996). The recommended feedrate (Q/Σ) in the simulation study is from 1.32×10^{-9} m s^{-1} to

3.97×10^{-9} m s^{-1} as this is the range of model and parameter confidence. The density of whole cells and the resulting cellular debris was taken as 1085 kg/m^3 (Hwang, 1996), and PHB-granule density was taken as 1260 kg/m^3 (Middelberg *et al.*, 1995). These densities are approximate and only used to transform distributions to a size basis for presentation. In simulation, the settling-velocity distribution is the critical determinant of performance, and this is not affected by the assumed density (Middelberg, 1998).

4.1.5. Summary

The PHB recovery process will be optimized through simulation. As the centrifugal fractionation of insoluble cell debris from PHB is particle size dependent, the sensitive measurement of PHB and cell debris size and effective prediction models are essential. CSA and CDS will be employed for sizing PHB and cell debris, respectively. The cell debris size reduction model (Equation 4.1) will be used for the prediction of homogenization performance, while the settling behaviors of PHB and cell debris in a disc-stack centrifuge will be simulated by the use of the grade efficiency model (Equation 4.12).

4.2. EXPERIMENTAL WORK

The purpose of conducting these experiments is to characterize the debris size of PHB containing *E. coli* subject to different process conditions, namely multiple homogenization, fermentation batch effects and pretreatment by freeze-thaw cycling. Together with the size data of cell debris by chemical treatment presented in Appendix C, these data are used subsequently in simulation and optimization. CSA was employed as the major measurement method.

4.2.1. Fermentation

The cell material for the experimental work came from two fermentations. (Fermentations I and II). Fermentation I was described in Section 2.1. Some cell broth was taken for homogenization after storage at 10°C overnight following fermentation termination, while the remaining cells were stored at -18°C for subsequent use.

Fermentation II was conducted in a similar manner. The composition of the initial medium (12.5 L) was based on the defined R-medium, supplemented with 30.0 g/L glucose, 5.0 g/L yeast extract, and 5.0 g/L casamino acid. The fermentation started by inoculation from a shake flask culture (1.2 L incubated overnight). During the fermentation, nutrient feeding solution containing 700 g/L glucose and 70 g/L yeast extract was fed in intermittently under pH-stat control. The whole fermentation lasted 27.5 h with a final OD of 85 at 600 nm (UNICAM 8625 Spectrophotometer) and a cell concentration (DCW) of 42.1 g/L with 57.8 % PHB content (defined as the ratio of PHB concentration to cell concentration w/w). The fermentation was terminated by the addition of formaldehyde (0.02% v/v of the final concentration). The culture remained overnight in the fermenter before homogenization and CSA analysis. A detailed description about the medium composition and fermentation protocol is given in Section 2.1.

4.2.2. Cell debris size measurement by CSA

Two batches of CSA analysis were conducted employing fresh harvested cells from Fermentation I and II. The experimental procedure is detailed in Sections 4.2.2.1. In Section 4.2.2.2, CSA analysis is briefly described.

4.2.2.1. CSA analysis of fresh cell material

The fresh cell broth harvested from both Fermentation I and II was diluted in PBS buffer (1.37 g/L KH_2PO_4, 6.5 g/L NaCl, adjusted pH to 6.9 with 2M NaOH) to give an optical density of 12-15 at 600 nm. Five discrete homogenizer passes were conducted at 55.2 MPa in an APV-Gaulin high-pressure homogenizer (15MR) with a ceramic cell disruption valve. The feed temperature was approximately 10°C for each pass. 1 L of homogenate was collected after each pass. The cell debris size was determined by CSA. Cell disruption and PHB release by homogenization were monitored by an Applied Imaging DCF4 Disc Centrifuge (Gateshead, U.K.) with a standard water spin fluid scheme (Middelberg *et al.*, 1990). The density of whole cells and the resulting cellular debris was taken as 1085 kg/m^3 (Hwang, 1996), and PHB granule density was taken as 1260 kg/m^3 (Middelberg *et al.*, 1995).

4.2.2.2. CSA analysis

The sample treatment procedure for CSA analysis is detailed in Section 2.4.2. The centrifugation for the fractionation and sedimentation was conducted in a Sorvall RC-5C refrigerated centrifuge (Du Pont, USA) using a HB-6 Swing-out rotor. It was followed by SDS-PAGE analysis as described in Section 2.4.3. 15 groups of fractionation spin speed and spin time were allocated covering the cell debris size distribution range. The supernatant after centrifugal sedimentation was collected and the viscosity measured by a Haake Rotovisco RV 100 concentric cyclinder viscometer at 10°C.

Numerical analysis was done as follows: the weight percentage of protein as a function of effective settling time $F(t_e)$ was firstly obtained by scanning with a densitometer and the results stored as an ASCII file. It was then pasted into TABLE CURVE 2D (Jandel Scientific, AISN, Software) to find the fitted curves. The cumulative cell debris undersize distribution $W(D)$ was obtained using Equations 2.2 and 2.3 as previously described (Section 2.4.2).

4.3. RESULTS AND DISCUSSION

4.3.1. PHB stability under homogenization

PHB stability during homogenization and centrifugation is of some concern. It may well determine the success of high-pressure homogenization and centrifugation for PHB release from hosting cells, and subsequent PHB fractionation. As particle collection by centrifugation is strongly size dependent (Wong, 1996), PHB breakage not only represents PHB yield loss, but also complicates the subsequent fractionation process. More centrifuge passes may be needed with consequent increased yield loss. Harrison (1990) found that PHB granules from *A. eutrophus* were not altered during homogenization except for some deformation of the granules by fusion after multiple homogenizer passes. The homogenization performance of recombinant *E. coli* containing PHB granules has not been reported. PHB in recombinant *E. coli* may be susceptible to the damage during homogenization due to the lack of a membrane surrounding the PHB (Section 1.4).

PHB stability during homogenization can be monitored by CDS. The homogenization pattern of PHB hosting *E. coli* differs from that of *E. coli* with recombinant protein inclusion bodies (Wong, 1996). Figure 4.3 presents the typical particle size distribution of PHB containing *E. coli* cells and its homogenate as a function of the number of homogenizer passes. For comparison, data have been normalized to the same cell concentration. Fresh cells from Fermentation II were used in this test. As shown, the initial homogenizer pass produces large particles with a broad distribution range. This can be explained by the two step cell disruption mechanism proposed by Harrison (1990). The initial stage of cell disruption by homognization involves only the breakage of the cell-wall envelope with much of the cell-wall still associated with the PHB. The liberation of PHB is achieved through further homogenizer passes that result in the gradual decrease in particle mean diameter and the narrowing of the size distribution. According to the crystallization mechanism of native PHB proposed

by Koning and Lemstra (1992), the gradual volume shrinkage of PHB and thus the shift of particle mean diameter towards the small size direction may also be attributed partially to PHB morphological transformation from amorphous to crystalline state, which is induced by introducing foreign particles during homogenization. The density difference between the PHB amorphous state and the crystalline state (Barham *et al.*, 1984) will allow a marked granule volume reduction if a high percentage of morphological transformation occurs from the amorphous to crystalline state. The released PHB will become denser and rigid with high crystallinity, and stable in the subsequent centrifugation process. It was reported (Hahn *et al.*, 1995) that about 60% of crystallinity was formed in the extracted PHB from recombinant *E. coli* by differential digestion. It was also noted that after four homogenizer passes, PHB distribution became stable, with a mean diameter of approximate 0.50 μm. Completely free PHB may exist after this pass. Note that it is not possible to obtain information on debris size from these CDS plots for the reasons outlined in Section 2.4.1, namely errors in baseline and extinction corrections, and low sensitivity for cell debris.

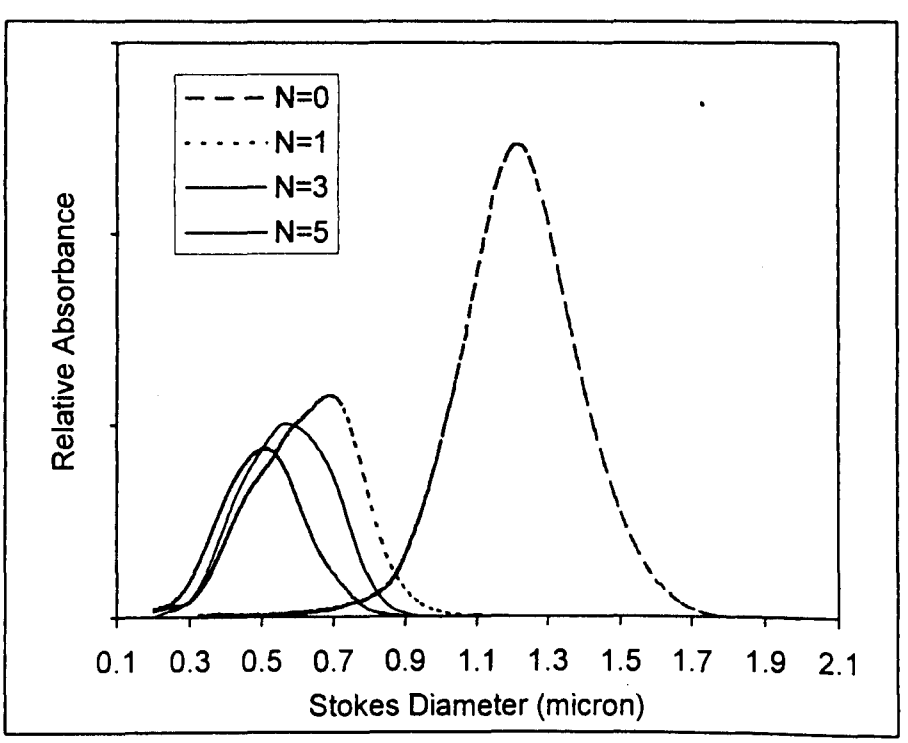

Figure 4.3. Size distributions for *E. coli* cells and PHB granules in the homogenate from Fermentation II measured by CDS. N is the number of homogenizer passes

The same homogenization conditions were repeated on the fresh cells from Fermentation I. The size distribution of whole cells and PHB in homogenate as a function of the number of homogenizer passes is presented in Figure 4.4. Again, the first homogenizer pass produced large particles with a broad distribution and a high percentage of free PHB is obtained after two homogenizer passes. The PHB mean diameter after two homogenizer passes was centred at 0.62 μm. It is noted that homogenization caused particle breakage after three homogenizer passes. This has also been observed during homogenization using frozen cells containing PHB granules from same fermentation batch (Fermentation I) in Section 3.3.1.

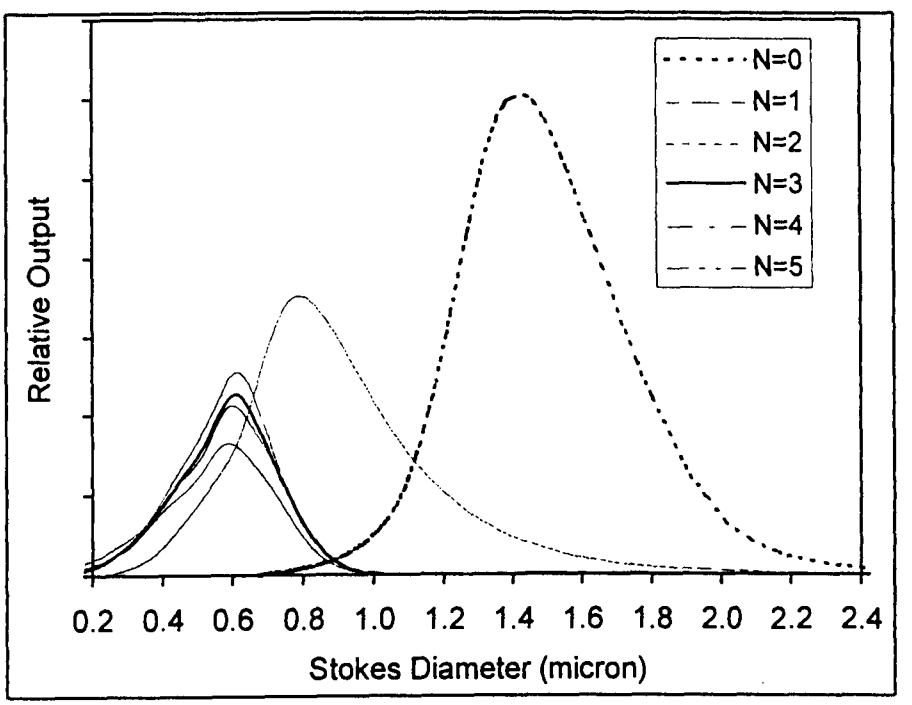

Figure 4.4. Particle size distribution of *E. coli* cells and the homogenate from Fermentation I as a function of the number of homogenizer passes (N).

The liberation of PHB from its host cells and surrounding cell debris, and PHB stability during homogenization vary with fermentation and homogenization conditions. The instability of PHB during homogenization and its dependency on fermentation conditions can not be concluded at this stage as the investigation is limited to only two fermentations. However, only a small percentage of PHB breakage was observed (Figure 4.4) and this will not have a significant impact on the final PHB yield. In general, homogenization is a satisfactory method for releasing PHB at large scale and shows high disruption efficiency.

4.3.2. Cell debris comminution by homogenization

Cell debris is comminuted with each homogenizer pass, accompanied by the gradual release of inclusion bodies (Wong *et al.*, 1997). Debris size of the fresh *E. coli* cells from Fermentation I was measured by CSA after each homogenizer pass. Figure 4.5 presents the cumulative oversize distributions of cell debris as a function of the number of discrete homogenizer passes. Smooth curves are regressions of the Boltzmann function (Equation 2.8) with parameters D_{50} and w listed in Table 4.1. The size distribution of whole cells measured by CDS is also included for comparison. The Boltzmann equation describes the debris size distribution for *E. coli* homogenate containing PHB granules very well as it did for *E. coli* containing protein inclusion bodies (Wong *et al.*, 1997) and yeast debris (Siddiqqi *et al.*, 1996). Evidently, repeated homogenization causes micronization of cell debris as expected. The median diameter of debris decreases from 0.65 μm after the first homogenizer pass to 0.36 μm after five homogenizer passes. Median debris size D_{50} and distribution width w after each homogenizer pass are comparable with those for *E. coli* containing recombinant protein inclusion bodies under similar homogenization conditions (Wong *et al.*, 1997).

It is noted that following an increase in the number of homogenizer passes, the extent of reduction on debris median diameter is reduced. There is an approximate 0.15 μm reduction in D_{50} from the first homogenizer pass to the second one compared with a reduction of 0.02 μm as the number of passes increases from four to five. This implies that cell debris size reduction is strongly size-dependent in accord with the debris-reduction model of Wong *et al.* (1997). Debris with large size experiences high levels of comminution. Multiple homogenizer passes, therefore, are generally required to achieve micronization of debris with a narrow distribution. For a given homogenizer condition and cell type, a minimum cell debris size may exist.

It is also revealed that the parameter w decreases following the gradual decrease in D_{50}, resulting in a narrowing of the cell-debris distribution. The linear correlation of D_{50} and w can be viewed by plotting D_{50} against w, and can be expressed by a simplified equation (Equation 4.16) established using linear regression.

$$w = 0.322 * D_{50} \tag{4.16}$$

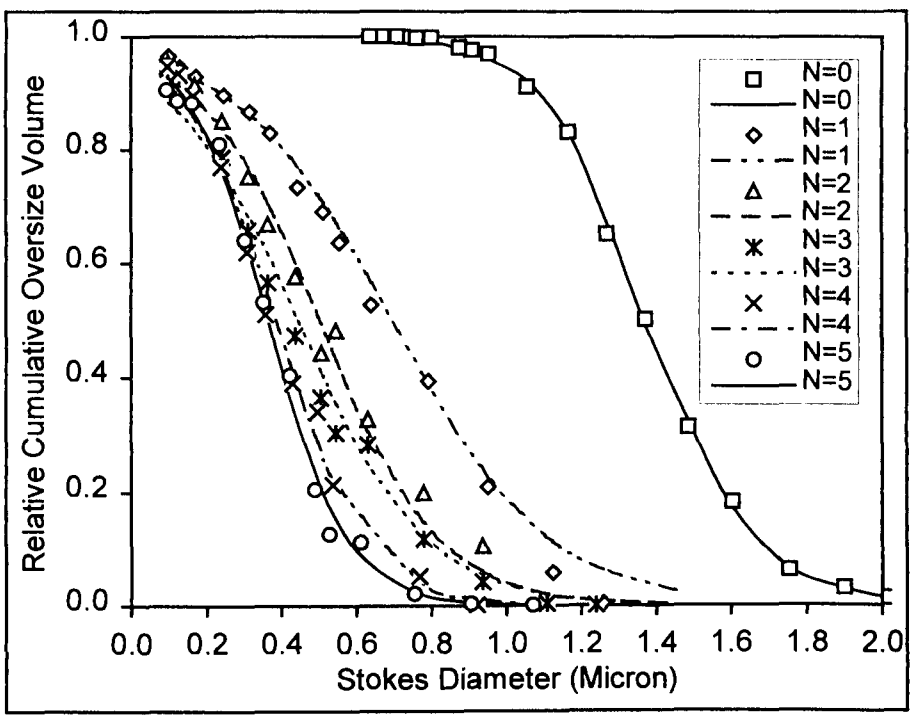

Figure 4.5. Cumulative oversize distributions of cell debris in homogenates of Fermentation I as a function of the number of homogenizer passes (N). Smooth curves were obtained by regression to the Boltzmann equation with parameters given in Table 4.1.

The use of the debris size reduction model (Equation 4.1) to simulate debris size distribution for PHB bearing *E. coli* cells disrupted by homogenization is confirmed (Figure 4.6). Smooth curves are obtained by the regression of the experimental data to Equation 4.1. The value of parameters a_C, a_d and α were 1.24, 0.844 and 2.12, respectively. The initial cell size distribution was obtained from CDS. An assumption of 90% disruption for the first homogenization pass and 100% for the second pass was made because of the difficulty in measuring disruption efficiency accurately. Figure 4.7 is a parity plot for the relative

cumulative undersize distribution. It confirms that Wong's model (Equation 4.1) provides an excellent estimate of cumulative undersize distribution.

Table 4.1. Median Diameters (D_{50}, μm) and Boltzmann parameters (w, μm) for cell debris in N passes homogenates from Fermentation I and II measured by CSA. (Errors represent standard deviation of the mean by regression of the Boltzmann equation 2.8)

		Fermentation I (fresh cells)	Fermentation II (fresh cells)
D_{50}	N=1	0.65 ± 0.010	0.69 ± 0.017
	N=2	0.50 ± 0.016	0.50 ± 0.013
	N=3	0.44 ± 0.017	0.42 ± 0.013
	N=4	0.38 ± 0.010	0.36 ± 0.001
	N=5	0.36 ± 0.010	0.32 ± 0.014
w	N=1	0.20 ± 0.009	0.20 ± 0.012
	N=2	0.17 ± 0.016	0.17 ± 0.013
	N=3	0.16 ± 0.018	0.16 ± 0.012
	N=4	0.12 ± 0.010	0.11 ± 0.007
	N=5	0.10 ± 0.009	0.10 ± 0.013

The values of constants α, a_c and a_d depend upon cell material and homogenizer operation conditions and design. The constant α has a value over 2 and is within the range suggested (Wong *et al.*, 1997), emphasizing the importance of particle size in size reduction during homogenization as stated above. The magnitude of cell disruption represented by a_c is larger than a_d as expected, due to the release of a large amount of cytoplasmic material. Both a_c and a_d are close to the values obtained from *E. coli* containing recombinant protein inclusion bodies (a_c = 1.5 ± 0.10, a_d = 0.85 ± 0.10, and α = 2.3 ± 0.13, Wong *et al.*, 1997).

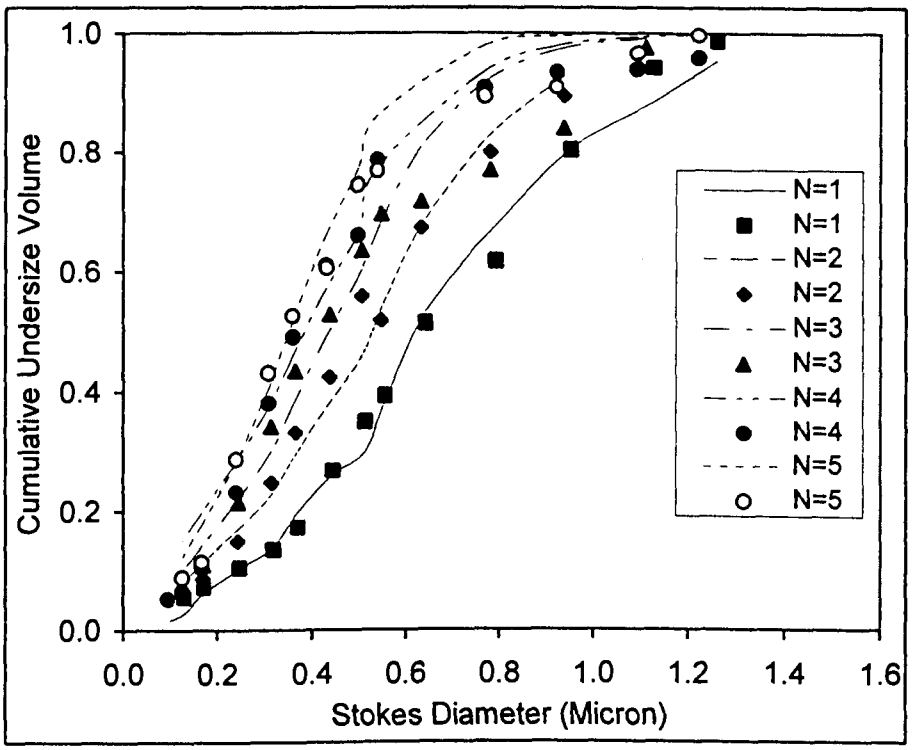

Figure 4.6. Cumulative undersize distributions for homogenates from Fermentation I as a function of homogenizer passes (N). Smooth curves were obtained by regression to Equation 4.1 with parameters $\alpha = 2.12$, $a_c = 1.24$ and $a_d = 0.844$.

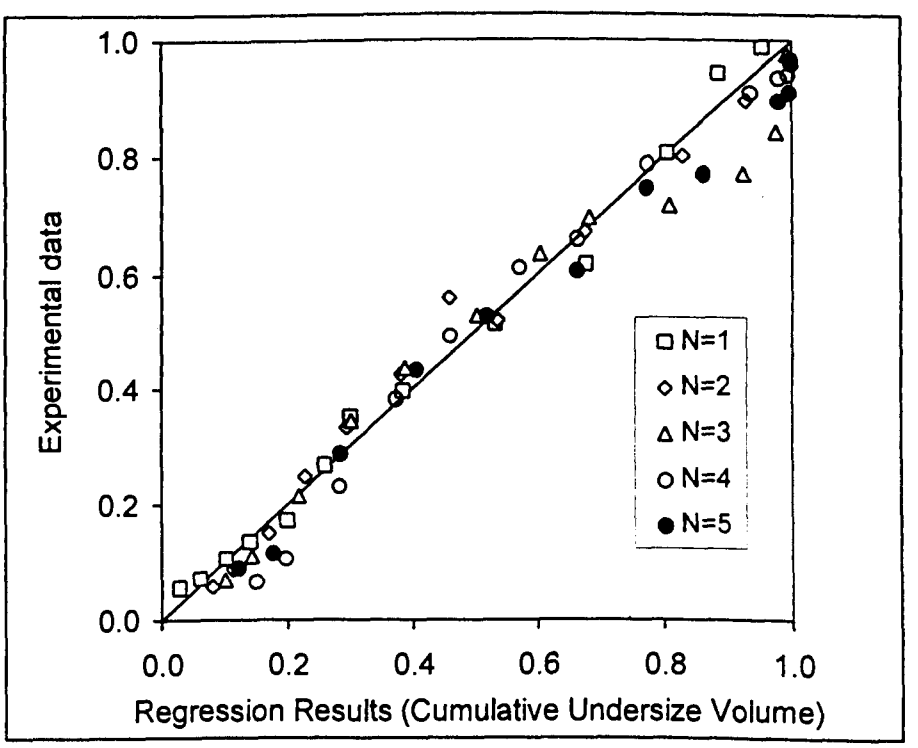

Figure 4.7. Parity plot of CSA experimental data of relative cumulative undersize volume versus the regressed values to the model (Equation 4.1).

4.3.3. Effect of fermentation on cell debris comminution

To investigate the influence of fermentation conditions on cell debris comminution by homogenization, a similar experiment and analysis was conducted on the cell material from Fermentation II.

Figure 4.8 shows the cumulative oversize distribution of cell debris as a function of the number of homogenizer passes; results of regression to the Boltzmann equation are provided in Table 4.1. The experimental data were also regressed to the cell debris size reduction model (Equation 4.1) giving α, a_c and a_d values of 2.05, 1.03 and 1.13, respectively. Results are shown in Figure 4.9. Figure 4.10 shows a good agreement between experimental D_{50} data and the simulation based on Equation 4.1, which confirms again the applicability of the model for *E. coli* containing PHB.

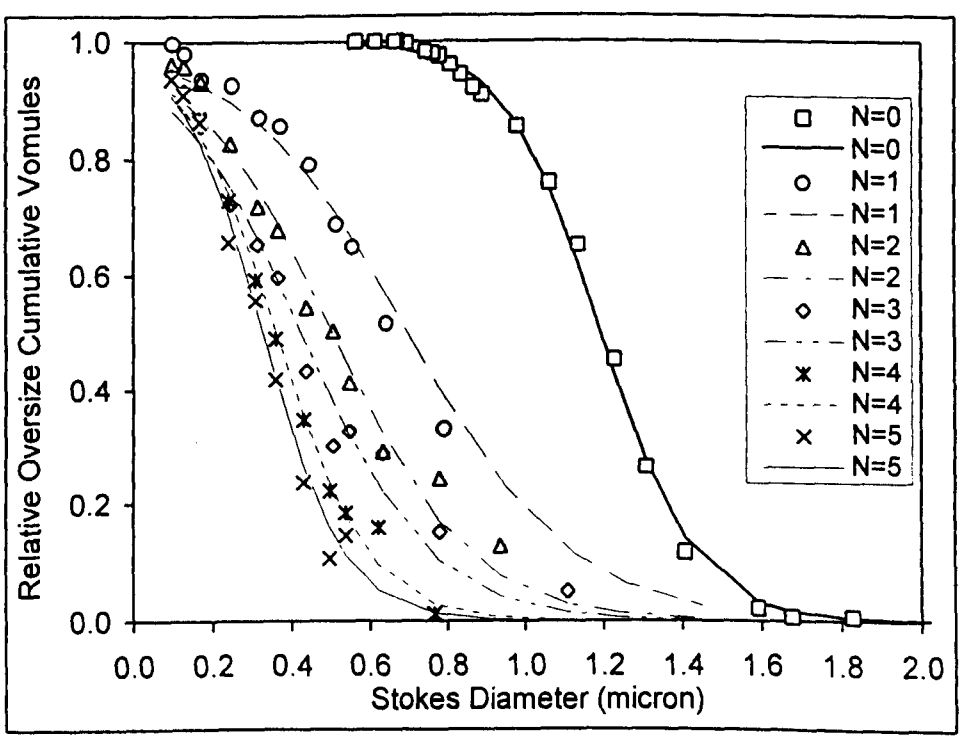

Figure 4.8. Cumulative oversize distributions of cell debris in homogenates of Fermentation II as a function of the number of homogenizer passes (N). Smooth curves were obtained by regression to the Boltzmann equation giving parameters in Table 4.1.

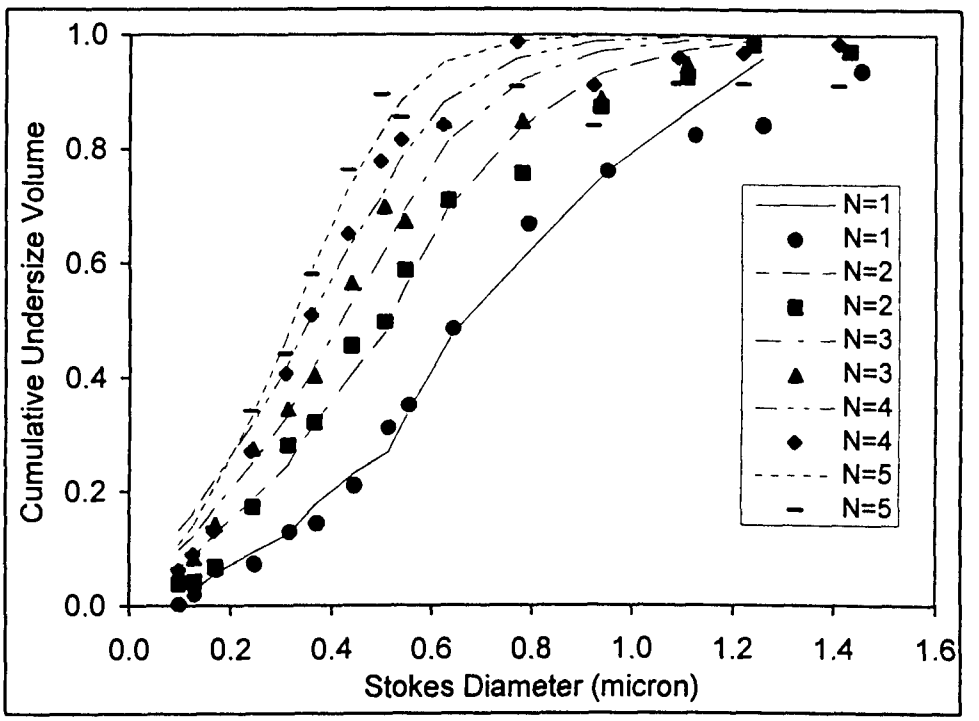

Figure 4.9. Cumulative undersize distribution for homogenates as a function of homogenizer passes (N). Smooth curves were obtained by regression to Equation 4.1 giving parameters $\alpha = 2.05$, $a_c = 1.03$ and $a_d = 1.13$

Variations in cell debris size between Fermentations I and II exist (Table 4.1). Since the samples after fermentation were treated and tested under similar conditions, the differences in cell debris size could be attributed to the fermentation.

Fermentation dictates the cell disruption characteristics, namely the size distribution and cell wall characteristics. For PHB accumulation in *E. coli*, cell size is mainly determined by PHB accumulation as over 50% by weight of cell material in most harvested cells is PHB. Since the majority of PHB accumulation takes place as cell growth slows, the rapid increase in cell volume occurs to accommodate the PHB (Lee *et al.*, 1994). A considerable size difference is, therefore, expected for cells taken from different stages of PHB accumulation. Table 4.2 lists the size of whole cells and released PHB from Fermentations I and II obtained by CDS and regressed to the Boltzmann equation 2.8. The cells from Fermentation I have a larger median diameter and thus larger PHB granules.

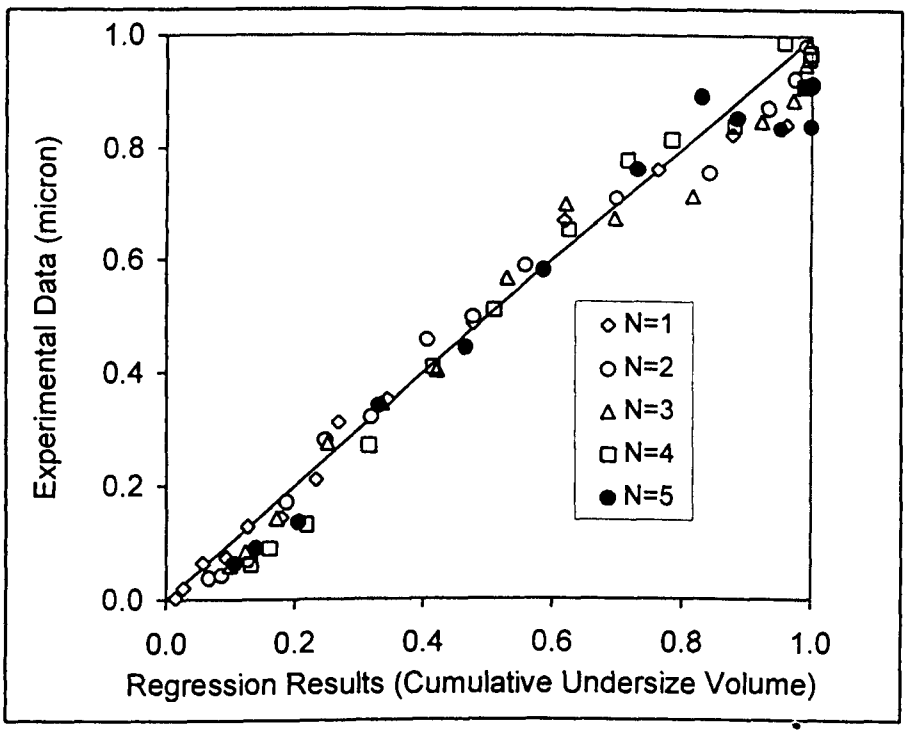

Figure 4.10. Comparison of experimental cumulative undersize volume data with the regressed data to the cell debris size reduction model (Equation 4.1).

To clarify the fermentation effect on cell debris comminution, the change in cell wall structure during PHB accumulation should be understood. Firstly, the cell wall becomes fragile because of the presence of the large volume of the developing intracellular PHB, leading to easier cell wall disruption as observed by Lee (1996) using TEM. However, the slight improvement in cell disruption efficiency is hardly revealed by CDS analysis due to insufficient sensitivity, and other methods may be considered such as by measuring the release of biochemicals (e.g., protein or DNA (Middelberg, 1995)). It is expected that cells from Fermentation I have a larger cell disruption rate than that from Fermentation II because the former has larger intracellular PHB volume and should generate small cell debris. However, by comparing the size of cell debris after multiple homogenizer passes (Table 4.1), it was found that small cells with small PHB size generated small cell debris size after multi-homogenization passes. It is suggested that the second change described below may occur in cell wall structure accompanying PHB accumulation .

Table 4.2. The Boltzmann parameters (D_{50} and w) for *E. coli* cells and the released PHB granules after three homogenizer passes from Fermentation I and II. The parameters α, a_c and a_d in cell debris size reduction model (Equation 4.1) are also included.

		Fermentation I		Fermentation II
		fresh cells	frozen cells	fresh cells
Whole cells	D_{50} (μm)	1.38	1.17	1.20
	w (μm)	0.139	0.125	0.118
PHB in 3 passes homogenates	D_{50} (μm)	0.584	0.377	0.473
	w (μm)	0.084	0.086	0.073
	α	2.12	2.29	2.05
	a_c	1.24		1.03
	a_d	0.84	0.96	1.13

The present understanding is that cell wall strength is attributed solely to the peptidoglycan layer. The thickness of the peptidoglycan layer and the degree of crosslinkage between adjacent polysaccharide chains will therefore determine the resistance of the cell wall to rupture (Middelberg *et al.*, 1992). The transition from the exponential phase to stationary phase during *E. coli* cell growth results in an increase in the degree of peptidoglycan crosslinkage. This trend may be further developed during stationary phase. For PHB accumulation in *E. coli*, the increase in cell volume during PHB accumulation stage, the accompanying increase in cell wall thickness and peptidoglycan cross-linkage, make cell debris hard to comminute. As a result, large cells will generate large debris size after multiple-pass homogenization, while small cells with small PHB granules give small debris size. This is consistent with the experimental results presented in Table 4.1. This difference is not evident after the first homogenizer pass because a large fraction of cell debris is still associated with PHB granules, which shifts the measurement towards large sizes.

The explanation becomes clear looking at the parameters of the cell debris reduction model (Equation 4.1). Fermentations I and II have close α values. a_c and a_d represent the capability of cell disruption and cell debris comminution. Fermentation I has higher a_c than Fermentation II, meaning higher cell disruption

and PHB release rate, while a_d from Fermentation I was lower than that from Fermentation II, implying a lower level of cell debris comminution.

E. coli cells initially appear rod-shaped, but during PHB accumulation the cell becomes increasingly spherical. Since size and shape also affect cell disruption, some variation with harvest time and PHB accumulation should be expected.

Comparison between *A. eutrophus* and recombinant *E. coli*

PHB accumulation by recombinant *E. coli* has a significant influence on both PHB yield and disruption as discussed above. However, an increase in cell size in excess of 30% in stationary phase caused little change in the ease of disruption for *A. eutrophus* (Harrison *et al.*, 1991). A difference between *A. eutrophus* and recombinant *E. coli* is expected in terms of cell wall structure in response to the PHB accumulation.

A. eutrophus is known to be capable of naturally producing PHB as an energy and carbon reserve material in response to nutrient limitation. When PHB is accumulated in stationary phase, PHB volume starts to expand within *A. eutrophus* cells but there are physical constraints due to volume limitation. *A. eutrophus* should be able to regulate such volume constrictions by growing cell wall to allow more PHB accommodation, and/or strengthening the cell wall to compensate for the developing weakness of the cell wall, thus preventing the extrusion of intracellular materials. PHB extrusion has never been observed in *A. eutrophus* (Lee, 1996). It was reported (Harrison, 1990) that when the PHB fraction in the cells was less than 58%, PHB accumulation was accompanied by cell wall growth and cell envelope expansion in a cylindrical shape. However, at a PHB content in excess of 58%, cell wall growth ceased and the cells became increasingly spherical in response to the internal pressure. However, cell wall self-regulation will not occur for recombinant *E. coli* overexpressing a plasmid-encoded product, as metabolic energy is directed solely to product formation. A weaker wall structure is therefore expected. This has been observed for *E. coli* expressing protein at high levels leading to the formation of a recombinant inclusion body (Wang *et al.*, 1997).

4.3.4. Effect of freeze-thaw cycling on PHB and cell debris comminution

E. coli cell disruption for PHB release and the subsequent cell debris comminution by homogenization are influenced by cell pretreatment. Table 4.2 includes the size of whole cells and PHB released from frozen cells in comparison with fresh cells from Fermentation I. The median diameter of cells containing PHB and the PHB granules after the freezing and thawing cycle decreased markedly comparing with fresh cells from the same fermentation batch (see Figure 4.11). This can be explained in terms of PHB crystallization. The freezing and thawing cycle initiates the crystallization of *in vivo* PHB (Harrison *et al.*, 1992), and a density difference exists between amorphous and crystalline PHB states (Barham *et al.*, 1984). Since PHB normally constitutes over 50% of total cell weight, the transition from the amorphous to crystalline state would result PHB granule and hosting cell shrinkage.

Freezing and thawing is one physical method for cell disruption through the formation and subsequent melting of ice crystals (Haphins, 1991). The formation of large ice crystal during gradual freezing causes extensive cell wall damage. Figure 4.11 illustrates that freezing and thawing recombinant *E. coli* enhances cell debris comminution efficiency by comparing debris size distributions in homogenates of fresh and thawed cell materials from Fermentation I. The data for frozen cell material are cited from Appendix C, while the data for fresh cells from Section 4.3.2.

Assuming complete cell disruption (100%) after the second homogenizer pass for pretreated cells from Fermentation I, the debris data after two and three homogenizer passes were regressed to the debris size reduction model (Equation 4.1) with α and a_d equal to 2.29 and 0.96, respectively. The high α and a_d values imply a high level of cell debris comminution compared to fresh cell material (α = 2.12, a_d = 0.84) (see Table 4.2).

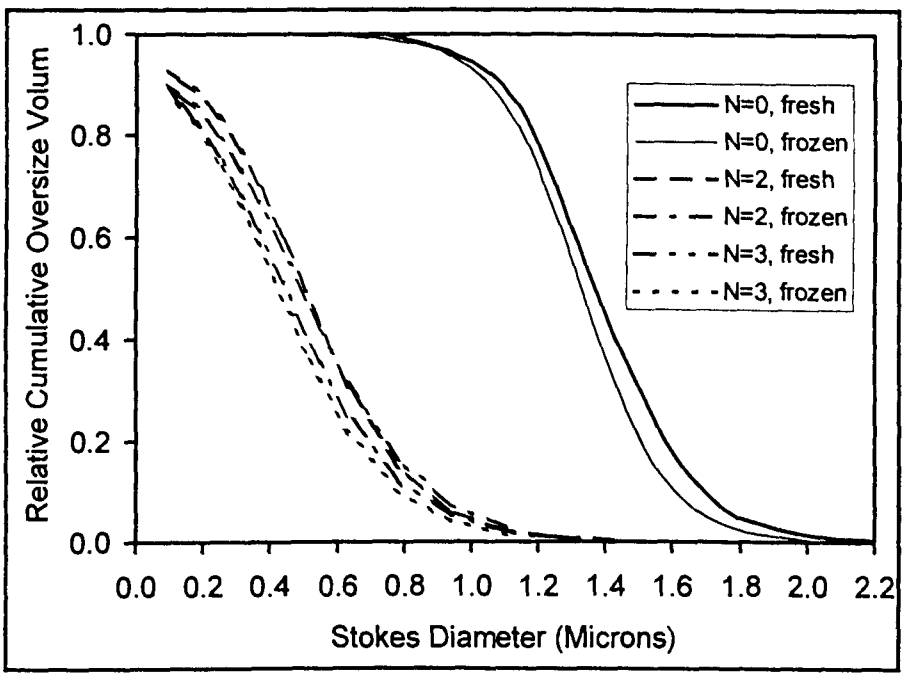

Figure 4.11. Comparison of size distributions of cells and homogenate from fresh and thawed cell material from Fermentation I: N=0, whole cells; N=2, two-pass homogenate; N=3, three-pass homogenate.

4.3.5. Conclusions

Homogenization is efficient for PHB release from *E. coli* cells and also cell debris comminution. Debris size can be predicted by the debris size reduction model (Equation 4.1). A reduction in cell debris size by homogenization is affected by the fermentation conditions, cell type and the cell pretreatment. Large *E. coli* cells possessing large PHB granules will result in high cell disruption efficiency, but with relatively large cell debris size after multiple homogenization passes. Small cells with a lower PHB content have low cell disruption efficiency but with small debris size. Freezing and thawing shrinks both the whole cells and PHB granules due to PHB crystallization, and results in physical damage to the cell wall. This gives smaller cell debris under similar homogenization conditions. Since PHB fractionation from cell debris by centrifugation depends on cell debris size reduction by homogenization, the interaction of fermentation,

homogenization, and cell pretreatment in terms of cell debris size reduction has to be taken into account.

4.4. SIMULATION STUDY OF PARTICLE FRACTIONATION

Cell debris represents the insoluble contaminant in PHB homogenate and thus is a major concern during centrifugal fractionation. Based on the information of PHB granules and cell debris size obtained in the previous sections, the settling characteristics of PHB granules and cell debris in a disc stack centrifuge can be studied, and PHB collection efficiency and cell debris removal can be predicted by simulation. In this section, the simulation conditions and procedure for PHB and cell debris fractionation are firstly described. It is followed by the simulation of some general effects on PHB fractionation, such as repeated homogenization and repeated centrifugation. The PHB fractionation performance is then further examined by simulation of the extraction processes conducted in Chapter 3. The information obtained will aid the development of a fractionation scheme and the optimization of overall PHB recovery process in Chapter 6.

4.4.1. Performing a simulation

The operating conditions of homogenization and centrifugation in this study are described in Sections 2.2 and 2.3. The simulation is carried out based on these conditions. The grade-efficiency of PHB granules and cell debris in the disc-stack centrifuge is expressed by Equation 4.12 with k and n equal to 0.16 and 2.6 for PHB granules, and equal to 0.13 and 2.1 for cell debris, in a *E. coli* homogenate system. These parameter values were obtained for recombinant *E. coli* cell debris and protein inclusion bodies produced by homogenization and fractionated in the same centrifuge used in this study (Wong, 1996). D_c in Equation 4.12 is calculated by Equation 4.11. The density difference between particle and aqueous fluid $\Delta\rho$ is 260 kg/m^3 for PHB and 85 kg/m^3 for *E. coli* cell debris.

Debris size reduction by homogenization is predicted by the use of the debris size reduction model (Equation 4.1). The parameters α, a_c and a_d, are listed in Table 4.2. The whole cells and PHB size are sized by CDS. CDS measurement also

provides the information of cell disruption rate, which is required for the use of Equation 4.1.

Simulation is conducted in Excel. With the known grade-efficiency curves and the particle size distribution in feed suspension, the overall collection efficiency can be estimated using Equation 4.13. The particle size distribution collected in the concentrate or discharged in the supernatant is then given by Equation 4.14 or 4.15. A detailed procedure of the simulation is given in Appendix D.

4.4.2. Simulation of the general effects

Multiple homogenization and multiple centrifugation are the general processes employed to achieve high product purity at large scale. The effect of multiple homogenization and multiple centrifugation on PHB purity and recovery are discussed by simulation in this section.

The simulation bases on the data for the cell material from Fermentation I after freeze-thaw pretreatment. The size distribution of whole cells and PHB granules are described by the Boltzmann function (Equation 2.8). The median diameter D_{50} and Boltzmann parameter w are 1.17 micron and 0.125 micron are for whole cells containing PHB granules, and 0.377 micron and 0.086 micron for PHB granules, respectively. The size of cell debris in two-pass and three-pass homogenates is given in Table 4.1. Parameters α and a_d in debris size reduction model (Equation 4.1) equal to 2.29 and 0.96, respectively (Section 4.3.4). It is assumed that the re-suspension of PHB paste collected from centrifugation is complete and that the homogenization contributes to the cell debris size reduction but without impact on PHB granule size.

4.4.2.1. Multiple homogenization on PHB fractionation

A process is assumed which involves multiple homogenization prior to one pass centrifugation. The effect of repeated homogenization and the centrifuge feedrate on the removal of cell debris is simulated and presented in Figure 4.12. The simulation was limited to the normalized centrifuge feedrates (Q/Σ) between 1.32 $\times 10^{-9}$ m s^{-1} to 3.97 $\times 10^{-9}$ m s^{-1} as this is the confidence range for the models and parameters. The cell debris size after the second and third homogenizer pass measured by CSA were listed in Table 4.1, while the debris size after the fourth and fifth pass were estimated by the size reduction model (Equation 4.1). A viscosity of 1.5 $\times 10^{-3}$ Pa s after two-pass homogenization was assumed in the simulation. It dropped to 1.4 $\times 10^{-3}$ Pa s after the third pass and remained constant for subsequent homogenization passes. Cell debris removal depends strongly on the centrifuge feedrate and the number of homogenizer passes as expected. Operated at same centrifuge feedrate rate, debris removal increases significantly as the number of homogenization pass increases. Clearly, a strong interaction exists between homogenization and centrifugation.

The number of homogenizer passes prior to centrifugation affects the cell debris removal significantly as illustrated in Figure 4.12. The removal of cell debris decreases from 73.0% to 69.0% at the same feedrate ($Q/\Sigma = 3.09 \times 10^{-9}$ m s^{-1}) if using two homogenizer passes instead of three passes. The improvement of debris removal becomes less significant after multiple homogenizer passes probably because of the reduced effect on debris size reduction by homogenization.

Figure 4.12 also includes the curve describing PHB overall collection efficiency as a function of centrifuge feedrate. Note that the PHB size distribution is relatively insensitive to the number of homogenizer passes as the extent of the observed granule breakage is low (Section 4.3.1). However, PHB recovery decreases concomitantly with the increase of debris removal as the feedrate increases. The size of PHB granules in the simulation was small (D_{50} = 0.38

micron, w = 0.086 micron). PHB collection will become less sensitive to feedrates with an increase in PHB granule size.

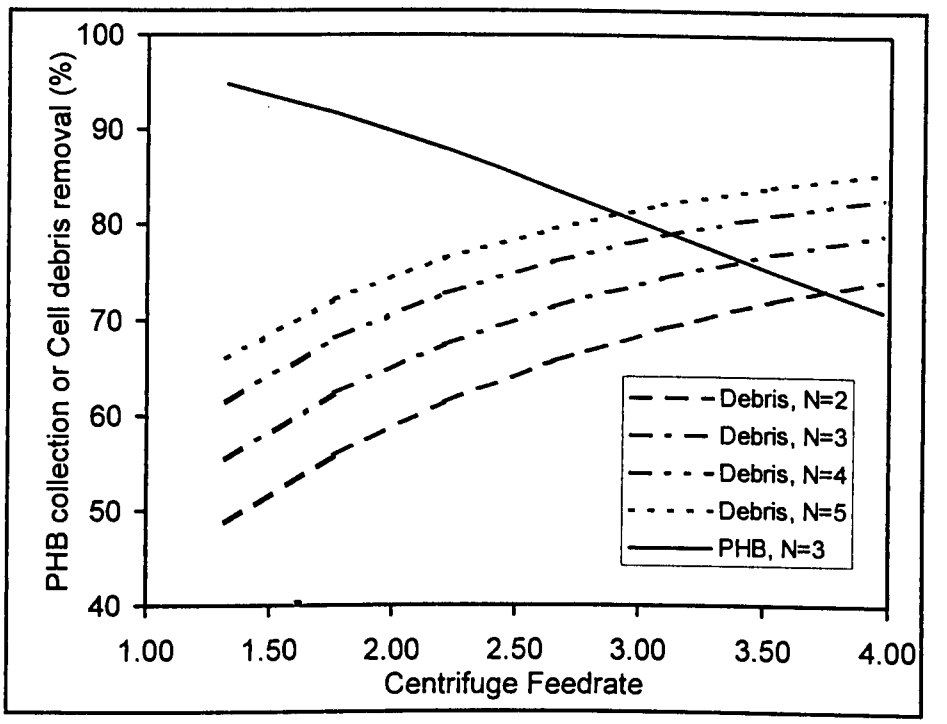

Figure 4.12. PHB collection and cell debris removal (%) by the centrifugation as a function of centrifuge feedrate Q/Σ ($m\ s^{-1} \times 10^9$). N is the number of the homogenizer passes.

To enhance PHB collection, a low centrifuge feedrate is necessary. As shown in Figure 4.12, by decreasing feedrate from 3.09×10^{-9} m s^{-1} to 2.21×10^{-9} m s^{-1}, increases PHB in a three-pass homogenate from 80.2% to 88.5%. This is offset by a reduction in debris removal efficiency from 73.0% to 67.0%. However, under the same operating conditions 72.5% cell debris removal is then attainable if N is increased to 4. The selection of operating conditions will be a compromise between the PHB collection and cell debris removal levels.

4.4.2.2. Repeated centrifugation on PHB fractionation

Repeated centrifugation improves inclusion bodies purity (Wong, 1996). Re-suspension reduces the suspension viscosity, thus PHB loss through the supernatant can be minimized. Since PHB collection becomes less sensitive to the change on feedrate after re-suspension, high feedrate can be employed with

improved debris removal while maintaining high PHB collection efficiency. In this study, a process is assumed which involves five discrete centrifugation passes after three homogenizer passes. The suspension viscosity is assumed to be 1.4 $\times 10^{-3}$ Pa.s for the first centrifugation and 1.2 $\times 10^{-3}$ Pa.s for the second and 1.1 $\times 10^{-3}$ Pa.s for the subsequent passes. The centrifugation is operated at a feedrate (Q/Σ) of 3.09 $\times 10^{-9}$ m s^{-1}. The attainable PHB recovery and the cell debris removal by repeated centrifugation are simulated and presented in Figure 4.13. As shown, cell debris removal is enhanced by multiple centrifugation. The majority of cell debris removal is achieved in the first two passes (92.7%). After a further centrifuge pass, 95.7% cell debris is removed. PHB loss shows similar trend but less sensitive compared to debris removal. The use of multiple centrifugation results in high PHB purity, but at the expense of a long processing time and also a relatively low PHB collection, which therefore raises total production cost. It is not economically acceptable sometimes. Since the remaining low level of cell debris is not a dominant contaminant affecting PHB properties compared to DNA and protein (Harrison, 1990), the operating conditions of centrifugation will mainly depend on the levels of DNA and proteins in the yielded PHB and its application requirement.

4.4.3. Simulation study of the extraction processes

4.4.3.1. Process A

Process A involved two-pass centrifugation after three homogenizer passes (Chapter 3). Extra homogenization was incorporated between centrifugation to ensure sufficient re-suspension due to the limitation of the discharge of the centrifuge used. Figure 4.14 illustrates the simulation of the relative volume collection of cell debris as a function of debris size for each unit operation. The comparison between the simulation and experimental results in terms of PHB recovery and cell debris removal is given in Table 4.3. About 73.0% volume fraction of debris removal was achieved at an expense of 19.8% PHB loss in the first centrifugation operated at a normalized feedrate (Q/Σ) of 3.09 $\times$ 10^{-9} m s^{-1},

compared with the actual results of 76% PHB collection and 75% cell debris removal. The second centrifugation operated at 2.21 × 10^{-9} m s^{-1} had an overall PHB collection of 98.1% and debris removal of 72.1%. This gave a total PHB collection of 78.0% and debris removal of 92.5%. The simulation matches the experimental data reasonably well. The deviation is possibly a consequence of the inaccuracy in the viscosity measurement. The viscosity used in the simulation is 1.4 ×10^{-3} Pa s for the first centrifugation and 1.2 ×10^{-3} Pa s for the second one. Actual viscosity could be higher, leading to a high removal of cell debris. The inaccurate viscosity may also be the reason why the predicted PHB collection efficiency was higher than the experimental value for both centrifugation passes. Furthermore, the parameters of Equation 4.12 used in the simulation were determined for recombinant protein granules with a median diameter of approximate 0.45 μm. Extrapolation to PHB granules with a different size range may also introduce errors.

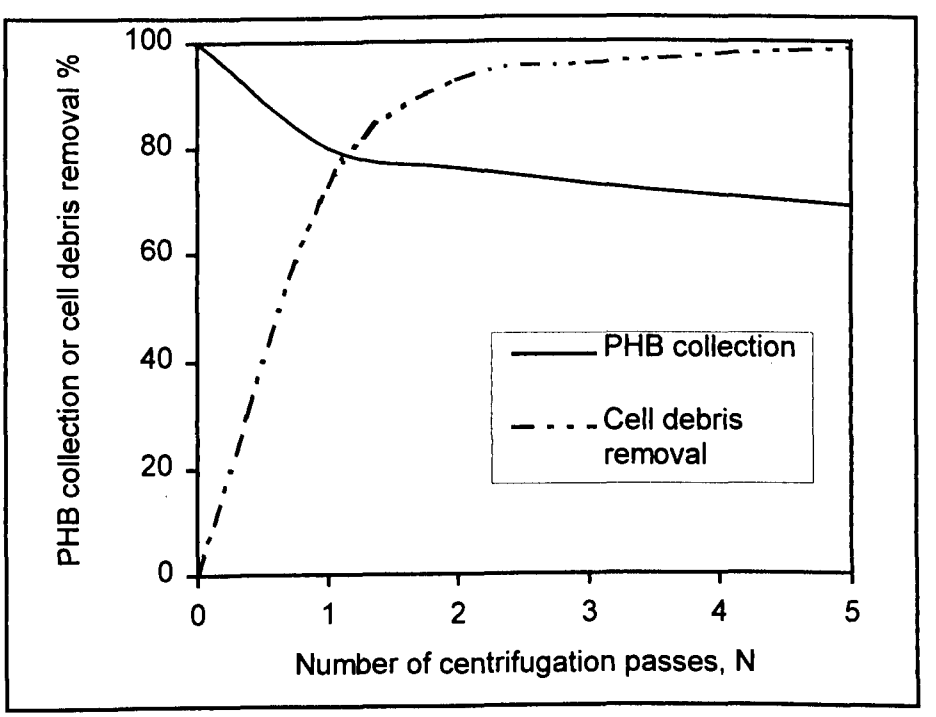

Figure 4.13. Simulation of PHB collection and cell debris removal as a function of the number of centrifuge passes after three homogenizer passes. The centrifuge feedrate is 3.09 ×10^{-9} m s^{-1}.

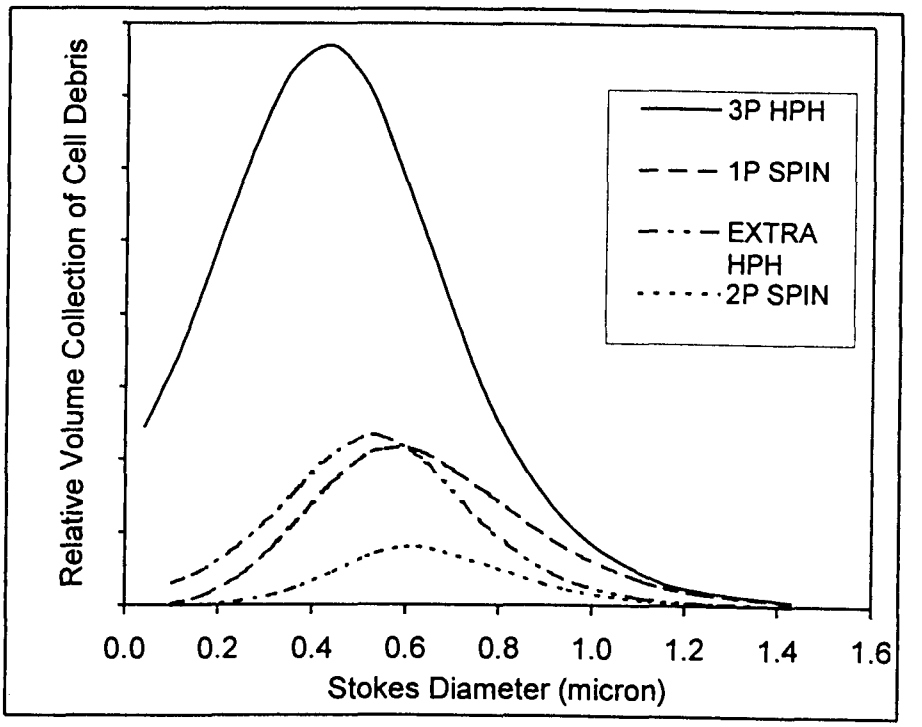

Figure 4.14. Simulation of relative volume collection of cell debris as a function of debris size in Process A after three homogenizer passes (3P HPH), the first centrifugation (1P SPIN), re-suspension (extra HPH) and the second centrifugation (2P SPIN).

Table 4.3. The simulation results of PHB recovery and cell debris removal by two passes centrifugation in Process A compared with the experimental results.

	Simulation		Experiment	
	First centrifugation	Second centrifugation	First centrifugation	Second centrifugation
PHB collection %	80.2	98.0	76	95
Cell debris removal %	73.0	72.0	75	77

Both the simulation and the experimental results of Process A indicate that the majority of cell debris removal and PHB loss occurred in the first centrifugation. The pretreatment prior to the first centrifugation (i.e., the number of homogenization passes) and the operating conditions of the first centrifugation (i.e., centrifuge feedrate) need to be defined in terms of the optimization of the whole fractionation process.

4.4.3.2. Process B

The use of NaOCl at a relatively low concentration effects the digestion of non-PHB cellular material, and has negligible impact on PHB granules in recombinant *E. coli* (Hahn *et al.*, 1994). NaOCl treatment improved not only cell debris removal but also PHB collection efficiency in Process B (Chapter 3).

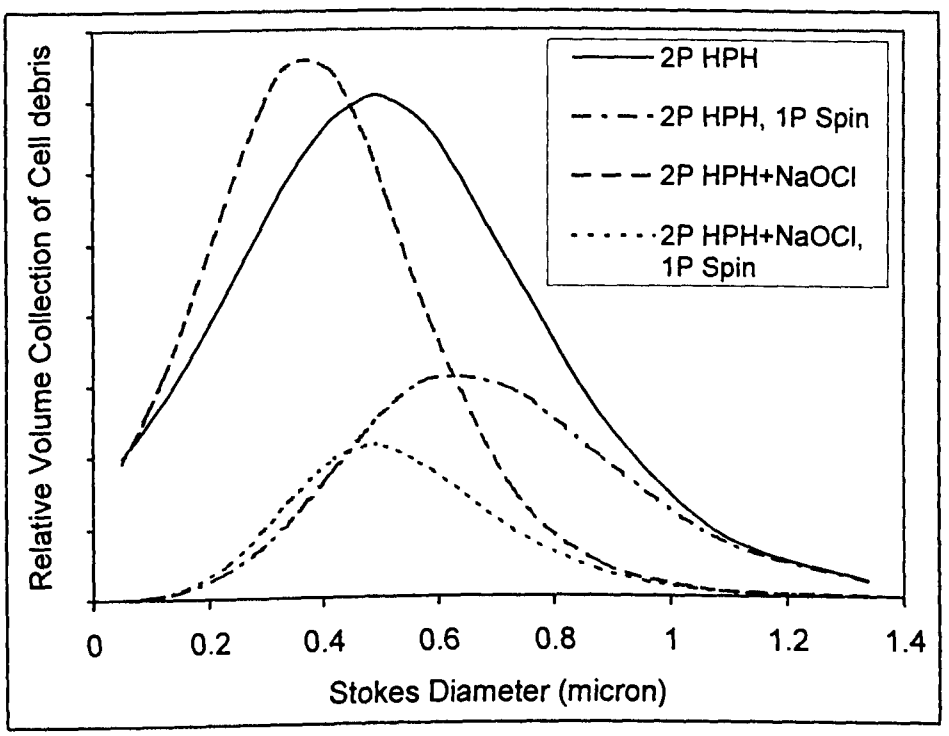

Figure 4.15. Simulation of fractionation of cell debris in two-pass homogenate with NaOCl treatment prior to (2P HPH+NaOCl) and after centrifugation (2P HPH+NaOCl , 1P SPIN), compared to that without NaOCl treatment prior to (2P HPH) and after centrifugation (2P HPH, 1P SPIN)).

Cell debris digestion by NaOCl treatment was identified in Appendix C. For the two-pass homogenate, NaOCl treatment (0.85 g/L active chlorine) reduced the debris median diameter and the distribution width from 0.480 micron to 0.371 micron and from 0.171 micron to 0.123 micron, respectively (see Appendix C). The contribution of this NaOCl treatment on cell debris fractionation was simulated, and compared with that without NaOCl treatment (Figure 4.15). The centrifugation was operated at a feedrate of 2.21×10^{-9} m s^{-1}. According to the simulation, NaOCl treatment raised the cell debris removal from 62.0% to 81.1%, which is significantly larger than the value of 69.5% brought above by increasing

the feedrate to 3.09 $\times 10^{-9}$ m s^{-1}, or 67.0% by adding one more homogenizer pass prior to the centrifugation. The improved debris removal was also attributed by reduced suspension viscosity as the viscosity was reduced from 1.5 $\times 10^{-3}$ Pa.s to 1.3 $\times 10^{-3}$ Pa.s. These confirm further the effectiveness of incorporating NaOCl treatment into PHB recovery process in terms of cell debris removal.

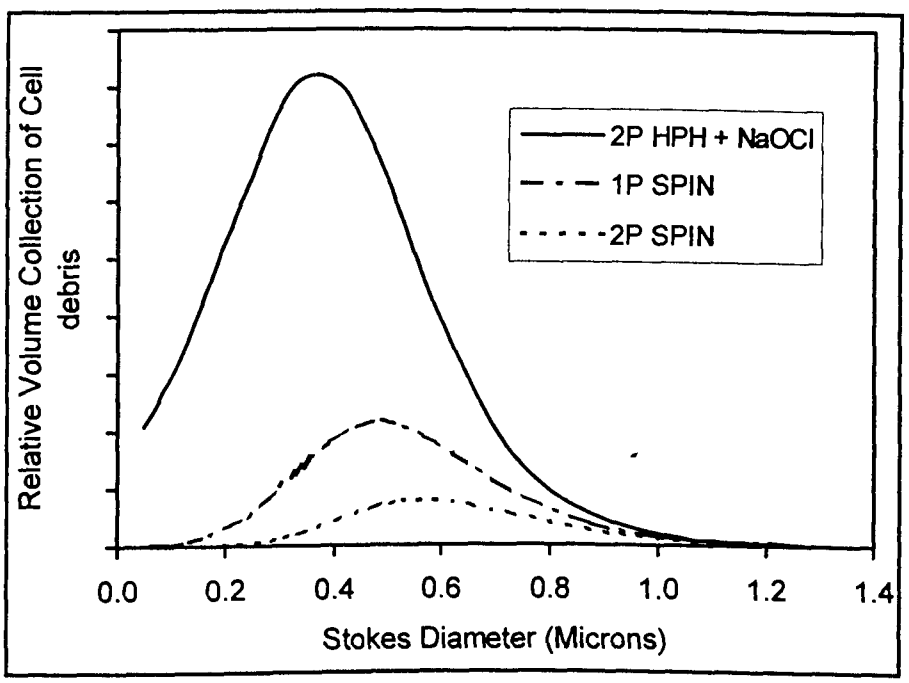

Figure 4. 16. Simulation of cell debris collection in PHB paste by each unit operation in Process B.

The improvement of PHB collection by NaOCl treatment was mainly due to the reduced suspension viscosity. According to the simulation, PHB collection was enhanced from 89.6% to 93.7% as the viscosity reduced from 1.5 $\times 10^{-3}$ Pa.s to 1.3 $\times 10^{-3}$ Pa.s, assumed PHB size is unchanged during NaOCl treatment.

The simulation result of relative debris volume collection in the concentrates in Process B was presented in Figure 4.16. It was assumed that the suspension viscosity was 1.1 $\times 10^{-3}$ Pa s in the second centrifugation. Again, the re-suspension of collected concentrate after the first centrifugation was assumed to be complete. Cell debris removal occurred mainly in the first centrifugation with 81% by volume, and a further 13% was removed at the second pass, related to a

total of 100% cell debris prior to the centrifugation in a two-pass homogenate. This compares with the actual results of 85.4% for the first pass and another 8.9% for the second one.

4.4.3.3. Process C

Process C was the recovery process designed on the base of experimental results from Processes A and B (Chapters 3). Re-sequencing unit operations was to facilitate protein and DNA removal. The process also aimed to improve PHB collection efficiency through the selection of a low feedrate for the first centrifugation ($Q/\Sigma = 2.21 \times 10^{-9}$ m s^{-1}). Additional centrifuge pass (the third pass) was employed to obtain a high PHB purity.

Figure 4.17 presents the simulated relative volume collection of cell debris in each unit operation, and the debris removal percentage during operation is illustrated in Figure 4.18. After the first centrifugation, the concentrate collected was re-suspended and homogenized prior to NaOCl treatment. As there was no debris size data available for the same operation, the data used in the simulation of the second centrifugation is that from re-suspended concentrate after three passes homogenization, followed by NaOCl treatment and additional homogenizer pass (Table C.1). Under the assumption of complete re-suspension without the addition of homogenization, the swap of homogenization and NaOCl treatment in sequence does not significantly affect the simulation results.

The simulation shows that 67% by volume of total cell debris was removed by the first centrifugation, while PHB recovery was 88.5%. Compared to Process A (73% and 80.2%, respectively), this improvement was due to feedrate decrease from 3.09×10^{-9} m s^{-1} to 2.21×10^{-9} m s^{-1}. NaOCl treatment effected the cell debris digestion. Together with one homogenization step, it reduced the debris median diameter D_{50} from 0.622 micron to 0.398 micron according to the simulation, which resulted in the increase of cell debris removal to 76.2%. The third pass achieved a cell debris removal of 65.6%.

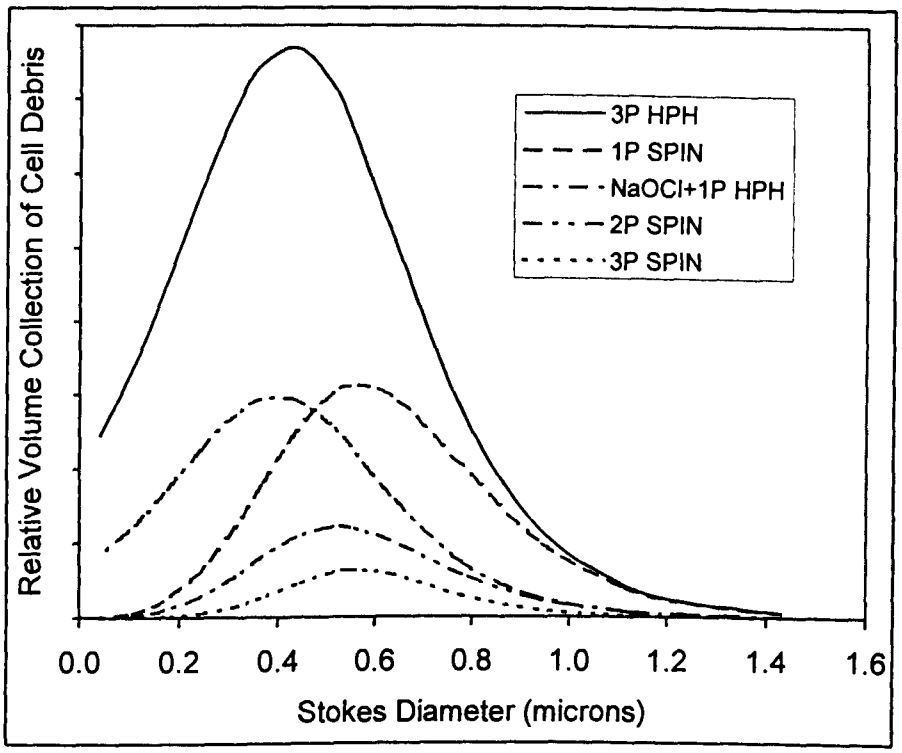

Figure 4.17. Relative volume collection of cell debris as a function of debris size in Process C after three-pass homogenizeation (3P HPH), the first centrifugation (1P SPIN), re-suspension and NaOCl treatment (NaOCl+ 1P HPH), the second (2P SPIN) and the third centrifugation (3P SPIN).

Total cell debris removal in Process C was 97.3%. According to the simulation above and previous reports (Wong, 1996), to achieve 95% by volume of cell debris removal by three centrifugation passes should not be difficult if the operating conditions are well chosen. However, Process C gave only 85% of PHB recovery according to simulation, compared with the actual result of 79.6%. There is approximately 8.3% improvement (from 80.2% to 88.5%) on PHB collection in the first centrifugation pass as the feedrate decreased from 3.09×10^{-9} m s^{-1} to 2.21×10^{-9} m s^{-1}. Modifying the feedrate in the second and third pass can not improve PHB collection efficiency very much due to the insensitivity of PHB collection. PHB recovery in the second centrifugation is 98%, which is significantly higher than that from the first pass. To enhance total PHB recovery, the feedrate for the first centrifugation has to be optimized. High PHB collection can also be achieved by changing the properties of homogenate, such as reducing the homogenate viscosity by using chemical treatment or extensive homogenization. This, in turn, improves cell debris removal.

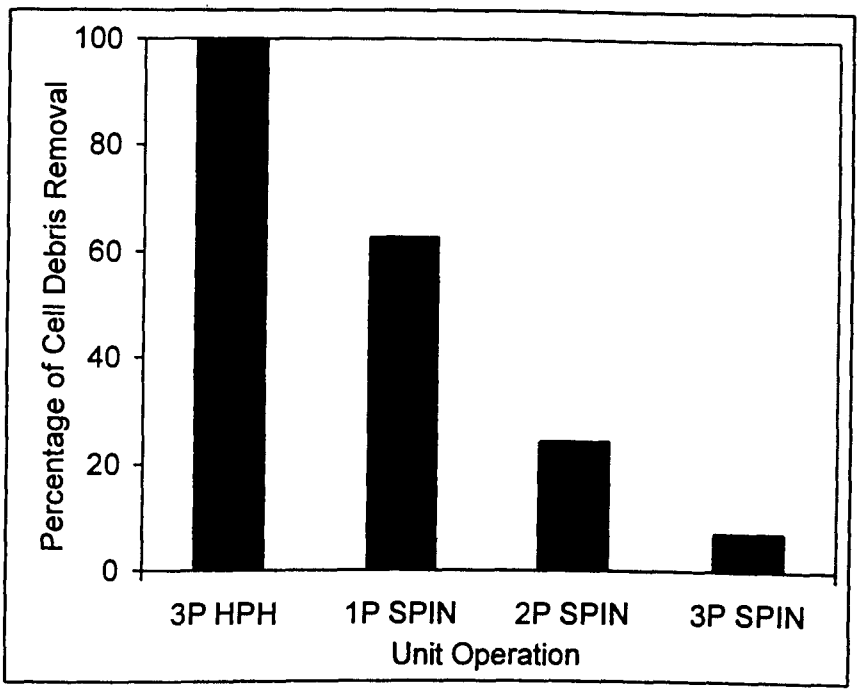

Figure 4.18. The relative fraction of cell debris removal in Process C by the first (1P SPIN), the second (2P SPIN) and third centrifugation (3P SPIN), relating to the 100% of total debris after the third homogenizer pass (3P HPH).

PHB granule size is dictated by fermentation. The formation of large PHB granules will facilitate its fractionation. High centrifuge feedrate thus can be employed without compensating the PHB loss. High feedrate also minimizes operation time and enhances the operation efficiency of centrifuge usage, and thus reducing production cost.

Large PHB granules can also be produced by aggregation or flocculation (Section 1.4.4). The aggregation agents must be very selective to PHB, as non-PHB components incorporated into aggregates may be difficult to subsequently remove. The stability of aggregates is also of concern as intense shear will be experienced during the process. Breakage of aggregates means that product is lost.

4.4.4. Conclusions

Repeated homogenization and centrifugation effected PHB fractionation from cell debris with increased PHB collection and debris removal rate. Since the majority of cell debris removal and PHB loss occurred in the first centrifugation pass, the selection of its operating conditions (e.g., feedrate) and defining the pretreatment prior to the centrifugation (e.g., the number of homogenization passes) were important in terms of the optimization of total PHB collection and cell debris removal. The simulation revealed the effectiveness of incorporating NaOCl treatment into the recovery process for cell debris removal. NaOCl treatment also facilitated PHB collection due to the reduced viscosity.

The simulation was based on the centrifugal fractionation model (Equation 4.12)* and the cell debris size reduction model (Equation 4.1). The simulation matches the experimental results in Chapter 3 reasonably well. This suggests the effectiveness of models used for the prediction, and also the effectiveness of CDS and CSA used for particle size measurement. PHB fractionation in a process involving homogenization and centrifugation can be predicted by the simulation and thus the optimal process regime can be selected.

There is potential for further improvement of PHB collection efficiency and cell debris removal in Process C by optimizing NaOCl treatment conditions and centrifugal feedrate. Since NaOCl treatment was limited only to a concentration of 0.85 g/L active chlorine, it is necessary to explore wider NaOCl concentration range. More work also can be done to define a better centrifugal feedrate. The cell material in the experimental work was at a concentration of 4.2 g/L due to the limitation of available cell material. Actual cell concentration in plant processing could be much higher. PHB fractionation at high cell concentration needs to be investigated when developing an industrially acceptable PHB fractionation process.

CHAPTER 5

OPTIMIZING CELL DEBRIS DIGESTION USING RESPONSE SURFACE METHODOLOGY

NaOCl treatment has been identified as an important unit operation in the PHB extraction process. To optimize the whole PHB extraction process, cell debris digestion and PHB degradation by NaOCl treatment are examined and modelled using response surface methodology. Firstly, a literature review focussing on NaOCl digestion is presented and a preliminary investigation is conducted, to assist in identifying key experimental variables.

5.1. INTRODUCTION

Sodium-hypochlorite (NaOCl) digests microbial cell materials effectively. It has been one of the most commonly-applied methods for the release of intracellular PHB granules from *A. eutrophus* and recombinant *E. coli.* The released PHB granules are then separated by centrifugation from non-PHB biomass, followed by a number of washing steps to remove residual NaOCl and biomass. Severe PHB degradation encountered during the process can be minimized by optimizing the NaOCl treatment regime (Berger *et al.*, 1989 and Ramsay *et al.*, 1990) or by using a dispersion of NaOCl and chloroform to solubilize and isolate the PHB from NaOCl attack (Hahn *et al.*, 1994). A literature review about the use of NaOCl for PHB recovery is given in Section 1.3.

NaOCl has been employed in Chapter 3 to effect a size reduction of recombinant *E. coli* cell debris following homogenization of PHB-containing cells. NaOCl treatment facilitated cell debris removal in the centrifugal PHB purification process, and also improved the removal of other intracellular contaminants such as protein and DNA, with acceptable PHB loss. The effect of *E. coli* cell debris digestion by NaOCl treatment was confirmed in Appendix C by measuring cell debris size reduction using CSA. It was found that NaOCl (0.85 g/L) coupled with homogenization effected a better debris size reduction than that achieved solely with homogenization. Large cell debris is difficult to centrifugally fractionate from PHB granules, thus reducing the efficiency of the recovery process and raising total PHB production cost. In order to optimize the PHB recovery process established in Chapter 3, the NaOCl treatment regime needs to be studied further to achieve a strong cell-debris size reduction with minimal PHB loss. Existing studies have only examined PHB release rate from cells and the diminution of PHB degradation under a fixed NaOCl condition. No comprehensive studies have been conducted into the effects of NaOCl treatment on the subsequent purification process and the resulting PHB quality.

The digestion of cell material by NaOCl relies on both oxidation and alkaline saponification of cell-material components, such as carbonaceous materials

(White, 1972). NaOCl digestion capacity varies greatly with the state of the cell, cell concentration, the type of pretreatment, NaOCl concentration, pH, incubation time and temperature (Berger *et al.*, 1989). Response Surface Methodology (RSM) (Mason *et al.*, 1989) is employed in this study to examine the effect of key factors (cell concentration, NaOCl concentration and the number of homogenization prior to treatment) on the size reduction of recombinant *E. coli* cell debris in a PHB-containing suspension (both homogenized and intact cells). The resulting model will aid in the selection of appropriate NaOCl digestion conditions by permitting the trade-off between debris size reduction and PHB digestion to be examined in detail. The resulting model is used to define an optimal process by simulation in Chapter 6, which is then demonstrated experimentally.

5.2. LITERATURE REVIEW OF CHLORINATION AND PRELIMINARY INVESTIGATION

5.2.1. Chemistry of Chlorination

When chlorine gas is dissolved in water, the following chemical reactions occur:

$$Cl_2 + H_2O \longrightarrow HOCl + H^+ + Cl^- \quad (5.1)$$

$$HOCl \longrightarrow ClO^- + H^+ \quad (5.2)$$

At low Cl_2 concentration, Equation 5.1 proceeds rapidly to the right, allowing complete conversion to dissociated hydrochloric acid. Hypochlorous acid (HOCl) is classified as a weak acid and dissociates partially according to Equation 5.2. The relative amount of HOCl and OCl^- (hypochlorite ion) is a function of pH. Both HOCl and OCl^- are defined as free available chlorine.

Figure 5.1 shows the dependence of relative HOCl and OCl^- concentration as a function of pH. At pH 7, about 70% of the chlorine is present as HOCl, whereas the remaining 30% is present as OCl^-. The higher the pH value, the greater the concentration of OCl^- ion, while the amount of HOCl becomes proportionately less.

Commercial sodium hypochlorite (NaOCl) solution is normally formed by dissolving chlorine gas Cl_2 in aqueous alkaline NaOH solution. The reactions proceed as follows:

$$2NaOH + Cl_2 \longrightarrow NaOCl + NaCl + H_2O \quad (5.3)$$

$$NaOCl + H_2O \longrightarrow HOCl + OH^- \quad (5.4)$$

NaOCl solution is unstable to some extent. Its deterioration can be minimised by controlling the solution alkalinity. Greatest stability is attained at pH close to 11.0 and with an absence of heavy-metal cations. At pH 11, HOCl is almost completely dissociated to hypochlorite ion (OCl^-) (White, 1972). The stability of

hypochlorite solution is also affected by heat, light, and storage time. The concentration of the effective species (HOCl and OCl^-) in NaOCl solution is collectively expressed as the actual weight percent of available chlorine.

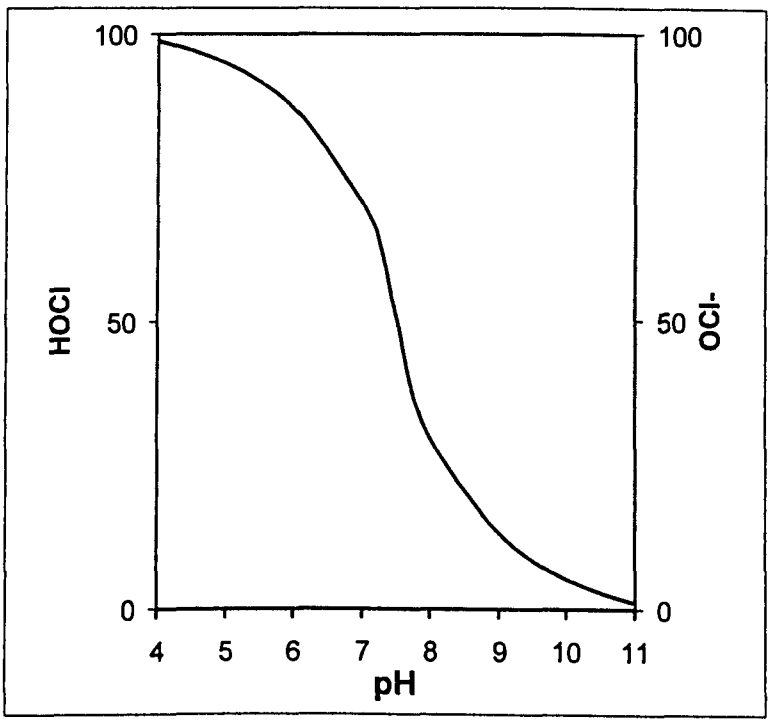

Figure 5.1. Distribution of HOCl and OCl^- in water as a function of pH (Bitton, 1980)

Nitrogenous compounds (N-compounds) in the solution will react with OCl^-, forming by-products known collectively as chloramines. The reaction of chlorine with inorganic nitrogen, such as ammonia, in dilute solution forms three types of chloramines:

$$NH_3 + HOCl \longrightarrow NH_2Cl \text{ (monchloramine)} + H_2O \qquad (5.5)$$

$$NH_2Cl + HOCl \longrightarrow NHCl_2 \text{ (dichloramine)} + H_2O \qquad (5.6)$$

$$NHCl_2 + HOCl \longrightarrow NCl_3 \text{ (trichloramine)} + H_2O \qquad (5.7)$$

In addition to the ratio of chlorine to ammonia, the relative amounts of the three forms of chloramines depend on solution pH. Organic nitrogen compounds such as amino acids, peptides and protein can react with HOCl, but at much slow speeds, giving chloramines with more complex molecular structure (White, 1978).

As strong oxidation agents, the effective components in both NaOCl and chlorine gas solution are OCl^- and HOCl, which convert the positive Cl^+ radical into a stable chloride radical with a valence of −1. Oxidation is the predominant reaction for water disinfection using chlorine. Chloramines with a positively charged chlorine atom function as strong oxidizing agents as well. An extensive literature search failed to find a direct comparison of the relative oxidizing capacities of HOCl, OCl^- and chloramines.

5.2.2. Mechanism of chlorination for cell material

5.2.2.1. Chlorine as a disinfectant

Chlorine has been used as an effective disinfectant in wastewater treatment since early this century. 1 mg/L chlorine or less for about 30 minutes was generally efficient in significantly reducing the number of viable bacteria in water (Bitton, 1994). Considerable information is available on the physical chemistry of chlorine aqueous solution at low concentration, as well as the kinetics of bactericidal action (White, 1972). Generally, chlorine causes two types of damage to bacterial cells (Bitton, 1994). Firstly, chlorine disrupts the integrity of the bacterial cell wall, thus leading to a loss of cell permeability control and to the disruption of other cell functions. Since the initial interaction of active chlorine when exposed to bacteria is to react with the cell wall or membrane, existing research indicates that chlorine at a concentration sufficient for bactericidal action can cause physical, chemical, or even biochemical damage to cell wall. Venkobachar *et al.* (1977) observed the leakage of *E. coli* cellular components (e.g., protein and RNA) after chlorine treatment even at a low chlorine concentration of 1.5 mg/L. Release of DNA occurred at higher chlorine doses. Secondly, the action of chlorine on bacterial cells can also involve damage to nucleic acids and enzymes, resulting in a high level of inactivation. Factors that influence chlorine's effectiveness in inactivating bacteria include chlorine concentration, contact time, pH, temperature, and the presence of interfering substances.

As mentioned above, oxidation is the dominant reaction at conditions used for water disinfection by chlorine. The cell components that might be involved in reactions with chlorine include carbonaceous materials such as lipids, and organic nitrogen compounds, such as amino acids, peptides, and protein.

Lipids are major structural components of the cell wall. Chlorine reacts with organic carbon in the same manner as it reacts with inorganic carbon. The reaction is rapid, and can be expressed by Equations 5.8 and 5.9 according to White (1972):

$$C + 2\,HOCl \longrightarrow 2\,HCl + CO_2 \qquad (5.8)$$

$$2\,NaOCl + C + OH^- \longrightarrow 2\,NaCl + CO_3^{2-} + H^+ \qquad (5.9)$$

As chlorine concentration at bactericidal doses is very low, the reaction of chlorine with organic carbon may result in only minor physical disruption of the cell wall barrier, allowing chlorine further access to the intracellular materials. The chlorine reaction will be enhanced at higher NaOCl concentration. pH drift will be observed in poorly-buffered solution due to the release of H^+ as the reaction proceeds.

Organic nitrogen is one of the main components making up amino acids and thus protein. Organic nitrogen components contained in cell materials may also be involved in the reactions with chlorine. However, these reactions are comparatively slow and less significant in terms of cell wall destruction. Unlike the nitrogen in ammonia nitrogen, which is lost completely within a short contact time (Section 5.2.1), the simple and unsubstituted amino nitrogen of many common amino acids is consumed more slowly with only negligible reaction even after many days. Protein is relatively stable compared with other simple, smaller, nitrogen sources such as amino acids. Protein is considerably more resistant to decomposition by chlorine. In other words, the chlorination of protein at normal reaction times is negligible. Increasing the concentration of chlorine may promote its reaction with protein. The experiment conducted in Chapter 3 demonstrated that protein removal was enhanced by NaOCl treatment.

The insensitivity of protein to chlorination provides the strong confidence for the use of CSA to assay debris size after chlorine treatment. The assay, based on the quantification of insoluble cell wall protein, was used in Appendix C for sizing cell debris in an NaOCl-treated homogenate, and will be the major experimental technique used in this chapter to quantify the effect of NaOCl treatment on cell debris size.

The chlorination of nucleic acids such as DNA and RNA is also important in terms of chlorine disinfection. The presence of DNA and RNA is of major concern at processing scale as it determines cell-suspension viscosity and hence centrifugation performance. The chlorination of DNA and RNA will be addressed in the latter part of this section.

It has been found that HOCl differs to OCl^- in the effectiveness of bacterial inactivation. According to White (1978), the germicidal efficiency of HOCl is attributed to its relative ease of cell-wall penetration, which is comparable to that of water. However, OCl^- is a poor disinfectant because of its inability to diffuse through the cell wall due to its negative electrical charge. Since the relative amounts of HOCl and OCl^- in a solution depend on pH, pH will affect the disinfection effectiveness. It is also postulated that the formation of neutral alkali cation-hypochlorite ion pairs possessing biocidal potency greater than OCl^- may occur. This is based on the fact that the addition of alkali cations to hypochlorite solutions enhanced disinfection efficiency (Haas *et al.*, 1986). Chloramines have a disinfection capacity intermediate to HOCl and OCl^-.

5.2.2.2. Solubilisation of cellular materials by hypochlorite

The research reviewed above is focused on the use of chlorine at bactericidal doses. Chlorine oxidation becomes more effective as chlorine concentration increases. Hypochlorite (NaOCl) lysis of cellular materials has been widely employed for the recovery of PHB from a wide range of bacteria (Section 1.3.1). Early research showed that NaOCl solution with a high active chlorine concentration can dissolve nearly all cell components, resulting in the liberation

of intracellular PHB granules (Williamson and Wilkinson, 1958). PHB degradation can be minimized by optimizing the NaOCl treatment conditions (Berger *et al.*, 1989).

The mechanism of cellular material digestion by NaOCl treatment at high NaOCl concentration is not well known at this stage. NaOCl in alkaline conditions reacts with cellular material in a complex manner, generally attributed to a combination of alkaline saponification and oxidization (Belter *et al.*, 1988). Stronger cellular material digestion occurs at higher pH. Williamson and Wilkinson (1958) observed that oxidation capacity increased as pH rose from pH 8.4 to pH 11.6. The enhanced oxidation of NaOCl at high pH is likely due to the higher oxidation capacity of OCl^- compared to HOCl. The existing studies on NaOCl digestion have focused on alkaline conditions. It is postulated that oxidation is the dominant mechanism at mild pH, whereas at high pH, both oxidation and saponification efficiency are enhanced.

High pH promotes the saponification of cell wall lipids, converting it into detergent and leading to cell-wall dissolution. The effect of saponification on cellular material was demonstrated by Lee *et al.* (1995). They tested the digestion of *A. eutrophus* cellular material containing PHB treated with either acidic (HCl, H_2SO_4, or H_3PO_4) or alkaline (NaOH, KOH, or NH_4OH) solution at a concentration of 0.1 N. For both non-PHB cellular material and PHB, alkaline conditions always gave higher digestion than acidic solution. NaOH gave the highest digestion performance. The saponification of cell-wall material was also demonstrated in this study by measuring cell debris size after incubation with 0.2 M NaOH (Appendix C). Significant digestion was obtained. After 0.5 h, the total volume fraction of *E. coli* cell debris in a homogenate suspension dropped to 42% and the median diameter of residual cell debris decreased from 0.50 μm to 0.33 μm. Unfortunately, PHB granule aggregation occurred, so this system was not examined further. However, due to the significance of pH during NaOCl treatment, pH effects on the digestion of non-PHB cellular material and PHB stability will be tested in Section 5.2.4.

The reaction between NaOCl and non-PHB cellular material when using NaOCl for the treatment of PHB-containing cells can be described by simplified second order kinetics (Equation 5.10) (Jin *et al.*, 1997),

$$\beta.\ \text{NaOCl} + \text{non-PHB} \longrightarrow \text{Products} \qquad (5.10)$$

where β is an undetermined stoichiometric reactant ratio between NaOCl and non-PHB material.

The higher the NaOCl and cell debris concentration, the bigger the digestion capacity will be. Increasing treatment time will lead to an increase in cell debris digestion until NaOCl is depleted. At low NaOCl concentration, NaOCl will be depleted completely before termination. The digestion of cell material by NaOCl is therefore affected by the concentration of NaOCl and the reaction time.

5.2.2.3. Chlorination of nucleic acids

Apart from investigations into the mode of chlorine action on bacterial cell walls and cell membranes, the modification and destruction of intracellular nucleic acids by chlorination has also drawn some research attention as it relates to the mutagenic potential of this disinfectant. At processing scale, the release of intracellular nucleic acids including DNA and RNA after cell disruption causes a significant increase in suspension viscosity (Agerkvist and Enfors, 1990). This impacts dramatically on the subsequent particle fractionation. Multiple homogenization passes can break the DNA chains thus reducing suspension viscosity (Kleinig *et al.*, 1995). Initial research showed that NaOCl treatment of homogenate can improve cell debris removal and also facilitate the removal of other intracellular contaminants such as protein and DNA (Chapter 3). A rational understanding of DNA chlorination will aid to optimization of the NaOCl treatment process and hence the whole PHB recovery process.

Chlorination significantly affects nucleic acids (DNA and RNA) *in vivo* and *in vitro*. DNA transforming activity was reduced after treatment with hypochlorous acid (HOCl), and NaOCl treatment broke DNA strands and reduced DNA molecular weight (Lu Shih and Lederberg, 1976). Hayatsu *et al.* (1971) reported

a rapid decrease in the absorbence of ultraviolet light for both calf thymus DNA and yeast transfer RNA after NaOCl treatment. Lu Shih and Lederberg (1976) also reported single-strand breaks and a few double strand scissions (at higher chlorine doses) accompanied by a loss of DNA transforming activity following treatment with chloramine. Chloramine was about three times more efficient in inducing single-strand DNA *in vitro* breaks compared to that *in vivo*. These trends imply employing homogenization prior to NaOCl treatment will be more efficient in inducing DNA single-strand breaks and thus in reducing suspension viscosity, because of the chloramine-induced release of DNA and RNA. It is also worth noting that the rate of DNA breakage induced by chloramine is time dependent. Clearly, the length of chemical treatment will affect the final viscosity.

5.2.3. Dechlorination

Dechlorination is the process of removing the remaining free and combined chlorine after chlorination. To quantify cell-wall material digestion by chlorination, dechlorination is required after the assigned treatment period to effectively quench the reaction. Dechlorination can be accomplished by the addition of sulfur dioxide or other sulfur-bearing compounds such as sodium sulfite (Na_2SO_3). Sodium sulfite is more easily controlled and is often used at small scale.

Sodium sulfite reacts with chlorine as follows:

$$Na_2SO_3 + Cl_2 + H_2O \longrightarrow Na_2SO_4 + 2\,HCl \qquad (5.11)$$

$$Na_2SO_3 + NaOCl \longrightarrow Na_2SO_4 + NaCl \qquad (5.12)$$

The reaction of Na_2SO_3 with free residual chlorine is complete nearly instantaneously, or within seconds. The conversion of active chlorine to negative chloride radicals requires a stoichiometric amount or excess of Na_2SO_3.

As stated in Section 5.2.1, the N-compounds present in the samples react with OCl^-, which generates by-product chloramines having oxidation capacity.

Na_2SO_3 can also deactivate the combined chlorine along with free chlorine in the sample solution. The speed of these reactions is similar to that with free chlorine. Completion can be indicated by the use of the iodometric method (Vogel, 1987). Na_2SO_3 reacts with chloramines as follows:

$$NH_2Cl + Na_2SO_3 + H_2O \longrightarrow NH_4HSO_4 + HCl \qquad (5.13)$$

Similar products are formed in the dechlorination of dichloramine and other poly-N-chlorine compounds.

White (1972) summarized dechlorination as follows: once sulfur dioxide or related compounds are added to the solution, the first reaction is simultaneously to remove the free chlorine (HOCl and OCl^-); next is the removal of monochloramine, followed by dichloramine, trichloramine and poly-N-chlor compounds. The total overall reaction time to remove all of these compounds is no more than a few minutes.

The point of chemical equilibrium of the oxidation reaction can be indicated by the use of the iodometric method (Vogel, 1987). Na_2SO_3 solution is titrametrically added until a negative reaction is obtained with potassium iodine-starch paper. A bluish-black colour will be formed in neutral or weakly alkaline solution as the result of separation of iodine:

$$OCl^- + 2\,I^- + H_2O \longrightarrow I_2 + 2\,OH^- + Cl^- \qquad (5.14)$$

If the solution is too alkaline, the colour disappears because hypochlorite and iodide ions are formed:

$$I_2 + 2\,OH^- \longrightarrow OI^- + I^- + H_2O \qquad (5.15)$$

The use of Na_2SO_3 for dechlorination does not introduce additional insoluble contaminants to the sample solution. As will be described in the later sections of this chapter, NaOCl is employed for *E. coli* cell wall digestion, which is measured using CSA. CSA is based on the quantitation of insoluble cell wall protein (Section 2.4.3). The use of Na_2SO_3 does not affect the subsequent protein quantification. The by-products, such as Na_2SO_4 and NaCl, are all soluble and thus removed from the samples prior to analysis.

5.2.4. Factors affecting NaOCl digestion

NaOCl digestion capacity for cellular material has been addressed in general terms in previous sections. In this section, the factors affecting cell-material digestion during NaOCl treatment will be summarized. This will help identify factors during NaOCl treatment that must be included in an experimental design or assigned to fixed, controlled values.

NaOCl digestion of cell material is affected by numerous factors. Key factors will be as follows:

- Cell condition (the state of the cells, concentration),
- NaOCl treatment conditions (NaOCl concentration, pH, treatment time and temperature),
- type of pretreatment (homogenization, freeze-thaw cycle, lyophilized, wet cell paste or cell broth, etc.).

Cell condition encompasses the cell type, cell wall structure and cell concentration. Cell wall composition and structure are dictated by fermentation. Differences in digestion are expected for the cells taken from different fermentation stages due to variations in cell-wall composition. Cell concentration is one of the most important factors affecting cell digestion. With reference to Equation 5.10, high cell concentration will accelerate the reaction to the right side of the equation and form new products, resulting in preferential cell-material solubilisation.

NaOCl concentration is obviously another major factor as illustrated by Equation 5.10. pH, treatment time, and temperature are also factors that should be considered. pH is strongly correlated with NaOCl digestion capacity as discussed in the previous sections. It will be identified experimentally in Section 5.3.3. Treatment time also appears to be an important factor especially when high NaOCl concentration is applied. Increasing treatment time will lead to an increase in cell digestion until NaOCl is depleted. At a low NaOCl concentration, NaOCl will be depleted completely before the reaction is terminated. Under a

condition of excess cell material, digestion will clearly be the function of NaOCl concentration and the treatment time if pH is fixed. Treatment time can be precisely fixed by the use of Na_2SO_3 for dechlorination (Section 5.2.3), regardless of the time necessary for subsequent analysis.

It should be mentioned that organic and inorganic N-compounds are prone to react with NaOCl, thus reducing the available free chlorine and generating products with low oxidation capacity. Their oxidation capacity is very time dependent compared to that of free chlorine (White, 1972). This increases the dependence of cell digestion on treatment time.

Cell pretreatment before exposure to NaOCl is also very important. Ramsay *et al.* (1990) reported that the pretreatment of *A. eutrophus* cells containing PHB using surfactants prior to NaOCl digestion can improve NaOCl digestion of non-PHB cellular material due to the weakened cell wall. To extract PHB from *Azotobacter Chroococcum* using NaOCl treatment, the attained PHB molecular weight from lyophilized cells was 5 times higher than that from wet cell mass (Nuti *et al.*, 1972). A significant difference is therefore expected in cell debris digestion between lyophilized and wet cell. Freeze-thaw cycle affects the attainable debris size as well (Section 4.3.4). Homogenization is the most widely used mechanical method for cell-wall comminution. To monitor the effect of cell debris digestion by NaOCl, the cell debris size following homogenization (i.e., before treatment) needs to be quantified.

Note that the cell system studied in this work is *E. coli* with cytoplasmic PHB granules. PHB content can reach over 50% by weight in most of PHB accumulating cells. There is no doubt that PHB also undergoes NaOCl digestion, but at a different rate to non-PHB cellular material. In assigning values to fixed parameters, and in examining an experimental design, it is therefore necessary to also consider the effect of NaOCl digestion on PHB. The target is to achieve a high level of cell-debris digestion, while minimizing product loss.

5.3. FACTORIAL EXPERIMENTAL DESIGN AND RESPONSE SURFACE METHODOLOGY

5.3.1. Factorial design and response surface methodology

To optimize the multifactor process, the effect of several factors and their interaction has to be considered. The traditional method using one-factor-at-one-time design is often inconclusive, or even misleading for such complex processes. It does not provide information about factor interactions, and the true factor effects are often masked by the variation in the observed responses. It also involves a large amount of experimental work. However, factorial design allows the analysis of a multiple-factor process incorporatively, and the dominant factors and possible interactions related to a special response can be identified and integrated into an empirical model. The statistical approach of factorial design requires a relatively small series of experimental runs to reveal responses, allowing a large and complex experiment to be divided into a series of small experiments that can be conducted easily with no or minimal loss of information.

The empirical model established through factorial design is referred to as a response surface. A response surface is the geometric representation obtained when a response variable is plotted as a function of one or more quantitative factors. The general form of this type of response function is

$$y = f(x_1, x_2, ..., x_k),$$

where y is the response and $x_1, x_2, ...x_k$ are quantitative levels of the factors of interest. The function, f, is found by fitting models to data obtained from the designed experiments. The available function allows one to both summarize the results of the experiment and predict the response for values of the quantitative factors. The response surface may be graphed as a curve in one dimension (one factor) or a surface or a contour map in two dimensions (two factors). The response surface can be explored to determine important characteristics such as optimum operating conditions (i.e., factor levels that produce the maximum or minimum estimated response) or relevant trade-off when there are multiple responses.

Response surface methodology (RSM) includes factorial designs, model regressions, the evaluation of factor effects, and searching for optimum conditions of factors for desirable responses. It is a good method for analyzing multiple-factor system.

5.3.2. Selection of factors and response variables

Of the factors listed in Section 5.2.4, cell mass concentration, NaOCl concentration, and the number of homogenizer passes at a fixed homogenization condition prior to NaOCl treatment were considered dominant and selected in the experimental design as the variables. The maximum cell concentration attainable was 43.3 g/L from Fermentation III (Section 5.4.1). It was justified to 3 levels. 5 levels were set for NaOCl concentration. NaOCl at 0.85 g/L was assigned as the lowest. This was the concentration used for PHB extraction without significant impact on PHB degradation (Middelberg *et al.*, 1995) and it was also the concentration employed for PHB extraction in Chapter 3. The number of homogenizer passes prior to NaOCl treatment was assigned to 0, 1 and 3. Table 5.1 summarizes the selected factors and their level settings. Incubation time is arbitrarily fixed at 1 h according to the previous research (Section 1.3.1), and to reduce the design complexity. This seems a reasonable process time scale. pH 7 is maintained throughout the treatment period on the basis of Section 5.3.3.

The response variables of interest are the attainable debris size and PHB stability. In the first experiment, only debris size was analyzed. Cell debris size was monitored by using CSA, and was presented in the form of an oversize cumulative size distribution which was then regressed to the Boltzmann equation (2.8), giving the median diameter D_{50} and distribution width w. D_{50} and w were then used as the specific responses related to the variation of the selected three factors in the design. PHB stability was also considered in the second experiment, quantified by the ratio, R, of the PHB after NaOCl treatment to that initially present. It provides information about PHB stability against NaOCl digestion.

Table 5.1: Factors and their level settings, and responses in factorial design

		Unit	Code	Actual level
Factors	Homogenization (N)	pass	A	0 1 3
	cell concentration (C_{cell})	g/L	B	4.3 21.7 43.3
	NaOCl concentration (C_{NaOCl})	g/L	C	0.85 1.7 3.4 6.8 13.6
Response	Median diameter	micron (μm)	D_{50}	
	Boltzmann parameter	micron (μm)	w	
	PHB stability	%	R	

5.3.3. The effect of pH during NaOCl treatment on cell debris digestion and PHB stability

pH is one of the major factors affecting NaOCl performance during digestion. The actual lysis capacity of NaOCl is generally attributed to both alkaline saponification and hypochlorite oxidation, as reviewed in Section 5.2.2. For a homogenate system containing insoluble cell debris and PHB inclusion bodies, differences in composition and molecular structure will lead to varied resistances to NaOCl digestion. Different responses to pH are expected. In our case, strong cell-debris digestion and minimal PHB loss are desired. Unfortunately, little information is available in the literature on the relative effects. Furthermore, inclusion of this factor in the experimental design in Section 5.3.4 leads to an impractical design in terms of available time and sample. Consequently, a simple experiment is conducted to define a pH that gives a high level of cell debris digestion with minimal PHB loss. This pH is used subsequently.

Experimental procedure

E. coli cells containing PHB granules were from Fermentation I (Section 2.1) with a cell concentration of 42.3 g/L (DCW) and a PHB content of 52% (w/w). It was diluted to a cell concentration of 4.2 g/L with MilliQ water before being homogenized at 55 MPa in an APV-Gaulin high-pressure homogenizer (15 MR, CD value) with a feed temperature of approximate 15°C. The homogenate was then separated into seven samples of 200 mL and stored in 500 mL bottles.

A stock NaOCl solution with 57 g/L active chlorine was prepared from concentrated NaOCl (100 g/L active chlorine) immediately before use as described previously (Section 3.2). NaOCl treatment started by pipetting 6 mL NaOCl stock solution into each of 6 samples, which gave a final NaOCl concentration of 1.7 g/L active chlorine. pH was adjusted to 6, 7, 8, 9, 10, or 11 using aqueous NaOH (2M) and HCl (2M) solution, and was maintained throughout the treatment period by careful addition as necessary. Suspensions were incubated for 1 h at room temperature with stirring by magnetic fleas. The treatment ended by adjusting pH to 7, followed by deactivation of residual NaOCl by titration with Na_2SO_3 (0.5M) until a negative reaction was obtained on potassium iodine-starch paper. A control sample was treated in parallel where 6 mL of MilliQ water was used in place of NaOCl. All the samples were adjusted to pH 7 before subsequent PHB and cell debris analysis.

To quantify the remaining cell debris, 20 mL of suspension was collected from each sample and centrifuged at 27,600×g for 4 h in a Sorvall RC-5C refrigerated centrifuge (Du Pont Instruments, USA) using a HB-6 swing-out rotor. SDS-PAGE analysis was then conducted as described in Section 2.4.3. Density scanning of one of the specific cell-wall protein bands (Section 2.5.3) gave the relative volume of sedimented cell debris.

In parallel with cell-debris quantification, PHB was also measured. 1.0 mL of sample was taken from each suspension using a pipette and centrifuged at 13,000 rpm for 10 min in a Micromax bench centrifuge. Supernatants were discarded and pellets were then washed twice with MilliQ water prior to removal into clean

glass tubes for freeze drying and PHB quantitation by GC (Section 2.6.1).

Results

The density of a specific protein band appearing on the SDS-PAGE gels representing one of the insoluble cell wall protein is proportional to the volume of *E. coli* cell debris with a size larger than 0.04 micron under the treatment conditions described above (Section 2.5.3). The relative percentages of detectable PHB and remaining cell debris compared to the control sample are presented as a function of pH in Figure 5 2.

As shown, the curve representing PHB stability is above that of cell debris, implying PHB is less sensitive to NaOCl digestion than cell debris over the pH range investigated (pH 6 -11). PHB is relatively stable between pH 7 and pH 9. Strong acidic and alkaline conditions promote PHB degradation significantly. At pH 11, only 73% of the initial PHB remains. Cell debris digestion follows a similar trend. By plotting the ratio of relative percentages of remaining PHB and cell debris (Figure 5.3), it is found that the maximum value appears when pH is 7. On the basis of these results, pH is set to 7.0 in this study. This reflects the desire to minimize PHB degradation, while ensuring sufficient cell debris digestion.

Strong digestion of PHB and cell debris was observed in both acidic and alkaline conditions. Saponification may dominate the digestion at alkaline conditions as discussed previously. In the pH range of 5 to 9, the percentage of HOCl and OCl^- varies greatly (Figure 5.1). The presence of free chlorine is mainly in the form of HOCl when pH is less than 7. It is postulated that HOCl may have stronger oxidation capacity for cellular materials than OCl^-. The quick increase in available HOCl may lead to the strong digestion. However, chlorine, especially at high concentrations, is less stable under acidic conditions. Neutral or alkaline conditions are therefore preferred for use in cellular-material digestion.

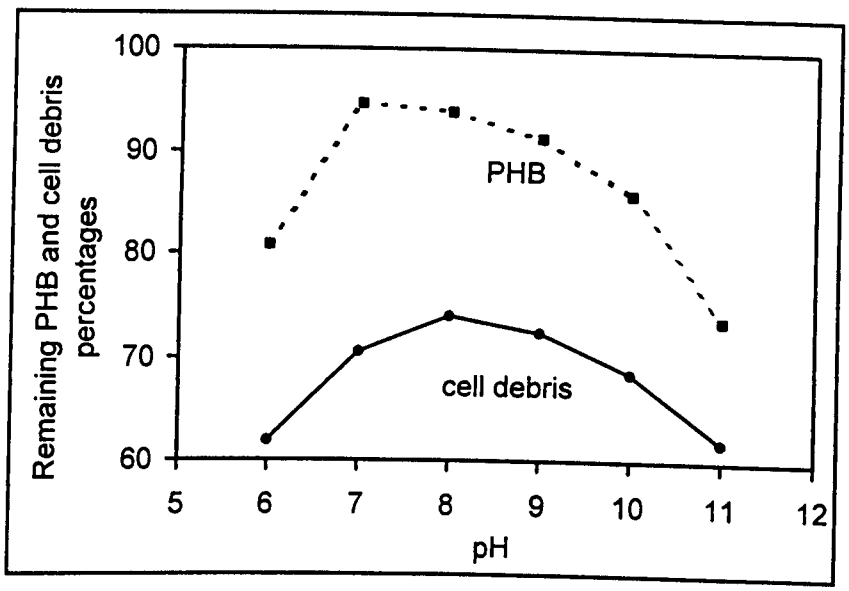

Figure 5.2. PHB and cell debris digestion during NaOCl treatment as a function of pH.

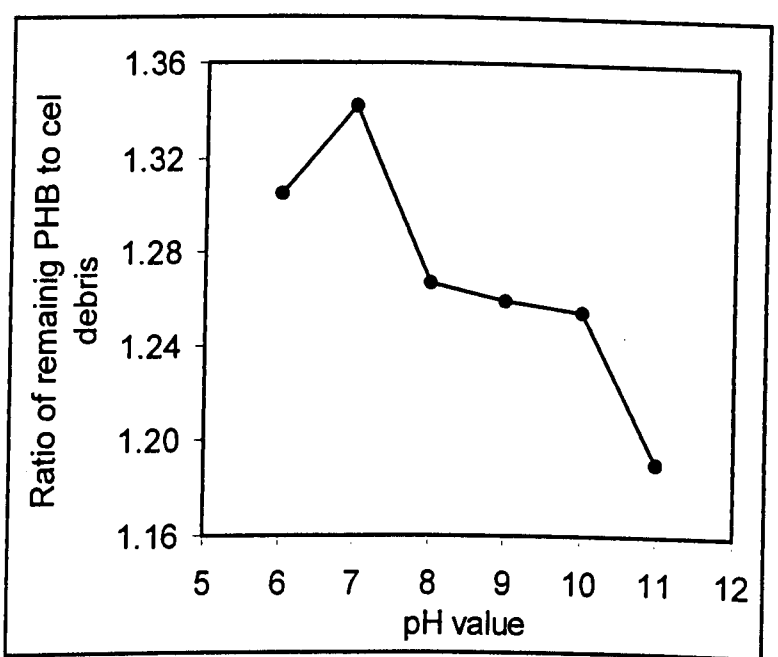

Figure 5.3. The ratio of relative volume percentages of remaining PHB and cell debris after NaOCl treatment as a function of pH.

5.3.4. Experimental Design

5.3.4.1. Overview

The whole experimental work splits into two parts. In the first part (Experiment I), three main factors at the following levels were considered:

Number of homogenizer passes: 1, 3;
Cell mass concentration (g/L): 4.3, 21.7, and 43.3;
NaOCl concentration (active chlorine, g/L): 0.85, 1.7 and 3.4.

Experiment II covered an adjacent region in terms of the values of the three main factors in the first experiment. As low cell debris size reduction was achieved in the first experiment, the use of high NaOCl concentration was then considered. Furthermore, at production scale high cell concentration is normally employed to meet the capacity of each operational unit such as homogenizers and centrifuges, for economical production. The use of high cell concentration was therefore investigated in the second experiment. Levels were set as below:

Number of homogenizer passes: 0 and 1;
Cell mass concentration (g/L): 21.7 and 43.3;
NaOCl concentration (g/L): 3.4, 6.8, and 13.6.

In the following analysis, the three factors, the number of homogenizer passes, cell mass concentration and NaOCl concentration are represented by A, B and C, respectively, for the convenience of presenting the experimental design and model development.

5.3.4.2. Design for Experiment I

For Experiment I, the complete factorial design including all possible factor-level combinations had the full 18 runs generated by the 2×3×3 combinations. However, there was an additional operational constraint that the runs must be

blocked into 6 runs in a batch, and the cell material for the 6 runs derived from one master sample. Among the 6 runs in a batch, 3 runs used only the material from one-pass homogenate while the other 3 used the three-pass homogenate. During sample analysis using CSA, the centrifuge used for performing sample fractionation can only process 6 samples at a time. Blocking into 6 runs in a batch can utilize the centrifuge capacity efficiently and thus shorten the assaying time.

Three batches were then formed as listed in Table 5.2 (Batches 1, 2 and 3). The design enables each batch of 6 to contain 3 runs at each level of factor 'homogenization'. The master sample in each batch can thus have 3 samples withdrawn after 1 homogenizer pass, and another 3 taken out after 3 passes as required. As a result, the large differences due to the master samples were confounded with the differences between the batches of 6.

As stated above, blocking is due to the limitation of experimental operation. The need to block into 6 runs per batch partially confounds the interaction between factors B and C. In the design proposed, each batch contains two runs at each level of factors B and C. However, only 6 out of 9 combinations of B and C are included in each batch of 6.

The confounded effect can be identified through algebraic analysis of the defined effects. The terms below cover 13 different effects, corresponding to A, B(2), C(2), the AB(2), AC(2) interactions, plus the BC(4) interaction. The numbers in brackets represent the number of degrees of freedom for that effect, and correspond to the number of contrasts needed to specify that term. Using an information matrix, it is found that all terms except the BC interaction are unaffected by blocking. The BC interaction splits into two parts, and about 25% of the information is lost into blocking. Detailed analysis is given in Appendix D. The 3 batches of tests were conducted in a random order and 6 runs within each batch were also arranged in a random order, avoiding additional confounding.

5.3.4.3. Design for Experiment 2

Similar to the first experiment, 12 complete combination runs were formed in the second experiment from a 2×2×3 factorial design with one degree of freedom confounded with batches. The 12 runs split into 2 batches of 6, and the batch effect was thus expected. The design is shown in Table 5.2 (Batches 4 and 5). The third response variable LN(1-R) representing PHB stability is included in the second experiment in addition to D_{50} and w. There are two design points replicated in both experiments, namely (Run 1 and Run 28) which occurs in Batches 1 and 5, and (Run 8 and Run 22) which occurs in Batches 2 and 4. This may provide information on the batch effects.

Table 5.2. The experimental design containing 30 test combinations conducted in two experiments

Experiment	Run No.	Coded variables			Actual variable levels		
		A	B	C	A (pass)	B (g/L)	C (g/L)
1	1	1	1	1	1	43.3	3.4
1	2	1	2	2	1	21.7	1.7
1	3	1	3	3	1	4.3	0.85
1	4	2	1	2	3	43.3	1.7
1	5	2	2	3	3	21.7	0.85
1	6	2	3	1	3	4.3	3.4
1	7	1	1	3	1	43.3	0.85
1	8	1	2	1	1	21.7	3.4
1	9	1	3	2	1	4.3	1.7
1	10	2	1	1	3	43.3	3.4
1	11	2	2	2	3	21.7	1.7
1	12	2	3	3	3	4.3	0.85
1	13	1	1	2	1	43.3	1.7
1	14	1	2	3	1	21.7	0.85
1	15	1	3	1	1	4.3	3.4
1	16	2	1	3	3	43.3	0.85
1	17	2	2	1	3	21.7	3.4
1	18	2	3	2	3	4.3	1.7
2	19	0	1	1	0	43.3	3.4
2	20	0	2	0	0	21.7	6.8
2	21	0	1	−1	0	43.3	13.6
2	22	1	2	1	1	21.7	3.4
2	23	1	1	0	1	43.3	6.8
2	24	1	2	−1	1	21.7	13.6
2	25	0	2	1	0	21.7	3.4
2	26	0	1	0	0	43.3	6.8
2	27	0	2	−1	0	21.7	13.6
2	28	1	1	1	1	43.3	3.4
2	29	1	2	0	1	21.7	6.8
2	30	1	1	−1	1	43.3	13.6

5.4. EXPERIMENTAL WORK

5.4.1. Fermentation

E. coli Topp1[pJM9123] described in Section 2.1 was used in this fermentation (Fermentation III). Similar to Fermentation I and II, the fed-batch fermentation was conducted in a 20 L Chemap CF-2000 fermenter with an initial medium volume of 12.5 L. The medium composition and operating conditions were given previously (Section 2.1). The feeding solution contained glucose (700 g/L), yeast extract (35 g/L) and $MgSO_4.7H_2O$ (20 g/L), and was dosed to bring the glucose concentration in the culture up to 20 g/L as soon as the pH rose up to 6.95 from the control set-point of 6.9. Dissolved O_2 concentration was maintained at 80% saturation by automatically adjusting aeration. Compressed 25% air balance oxygen (75% oxygen/25% air) was used when required. During the fermentation, samples were taken regularly for the measurement of PHB concentration (2.6.1), DCW (Section 2.4.5), optical density (OD) (600 nm, UNICAM 8625 spectrophotometer) and glucose concentration (Section 2.4.6). The fermentation was terminated by the addition of formaldehyde (0.02% v/v final concentration) at an optical density (A_{600}) of 124, corresponding to a dry cell weight (DCW) of 43.3 g/L and PHB content of 60.5% w/w. The total volume of 18 L culture was stored overnight at 10 °C in the fermenter before being separated into 2 L bottles and frozen at -18°C for storage. This fermentation provided all cell material for the remaining experimental work described in this thesis (Chapter 5 and 6).

5.4.2. Homogenization and NaOCl treatment

The experiment was blocked into 5 batches for practical and design consideration (Table 5.2). For each batch, 2 L of cell broth was taken and defrosted at 4°C before use. Homogenization was conducted at the conditions described in Section 2.2. The homogenates were then diluted to the concentration required with MilliQ water. NaOCl treatment started by pipetting fresh NaOCl stock solution into the homogenates. The volume of NaOCl solution added was dependent on

the NaOCl concentration required in each sample. The suspension was stirred using a magnetic stir plate at room temperature. pH for all samples was maintained at 7 by manual addition of concentrated NaOH and HCl solution throughout the treatment. The treatment lasted for 1 h. The remaining NaOCl was deactivated by the addition of 0.5M Na_2SO_3 solution titrimetrically until a negative reaction was obtained on potassium iodine-starch paper. The treated suspensions were then further diluted to the same concentration, facilitating true cell debris size measurement by CSA.

The NaOCl stock solution contained 57 g active chlorine/L, was diluted from the concentrated sodium hypochlorite solution (100 g active chlorine/L) with MilliQ water immediately before treatment (Middelberg *et al.*, 1995).

5.4.3. Cell debris size measurement by CSA

Cell debris size was measured by CSA. The detailed procedure is described in Section 2.4.2. After NaOCl treatment, the suspension was pipetted into 11 centrifuge tubes with each containing 25 mL. The fractionation was conducted in a HB-6 swing-out rotor in a Sorvall RC-5C (Du Pont Instruments) refrigerated centrifuge, with the assigned series of spin speeds and times given in Table 2.7, which covers a broad range of debris size (≥0.05 μm). For the first 10 samples, 20 mL of supernatant was discarded and the remaining 5 mL of concentrate was further pelleted at 27,600 ×g for the sedimentation of all cell debris to 0.05 μm. Sample 11 was the control sample (i.e., not treated with NaOCl). Its total supernatant was discarded after centrifugation and the cell debris contained in the pellet represented the total cell debris in calculation. The pellets were then boiled with SDS-PAGE sample buffer for 10 min prior to SDS-PAGE analysis. Gel bands representing cell-wall associated protein (i.e., sedimentable as identified by Wong (1997)) were then quantified by scanning densitometry. The resulting cell debris size was presented as a cumulative oversize distribution. The density of cellular debris was taken as 1085 kg/m^3 (Wong *et al.*, 1997). The viscosity of sample supernatant was measured by a Haake Rotovisco RV 100 concentric cylinder viscometer. Only 10 samples plus one control sample, instead of 15

(Wong, 1997), were collected for each treatment for constructing cumulative distribution, as the basic distribution range is already known. Furthermore, only concentrate samples instead of both concentrate and supernatant samples after the first CSA fractionation were analyzed. This simplifies the experimental work, but with no impact on the presentation of the size results. These therefore represent the simplification of the original CSA procedure developed by Wong (1997).

5.4.4. PHB stability analysis

PHB stability against NaOCl treatment was determined by measuring the total PHB before and after treatment using the method of Braunegg *et al.* (1978). 1.0 mL of sample was taken from each suspension before and after NaOCl treatment, and centrifuged at 16,750×g for 10 min in a Micromax Bench Centrifuge. The pellets were then washed twice with MilliQ water prior to removal into clean glass tubes for lyophilizing and PHB quantification. GC operating conditions are given elsewhere (Section 2.6.1). The results were presented as the ratio of detected PHB amounts before and after NaOCl treatment, R.

5.5. DEVELOPING REGRESSION MODELS

The observed responses in 30 treatment runs are presented in Table 5.3. The data analysis in this section involves identifying contrasts representing various treatment effects and blocks, and calculating their values; and doing Normal probability plots to determine which effects are important and to estimate the associated standard deviations. The regression models for the responses D_{50}, w and LN(1–R) are generated in algebraic form and also illustrated in contours. The data from the first and second experiments are analyzed separately, giving models suited to different variable ranges. The effect of the ratio of cell concentration and NaOCl concentration to response surfaces (D_{50} and w) are also investigated based on the data from both experiments.

Details about contrast calculations and the normal probability plots for the determination of effect significance, and also the procedure for the model development, are given in Appendix D.

5.5.1. Analysis for Experiment I

To analyze Experiment I (Batches 1, 2 and 3) 17 contrasts between the 18 observations were firstly identified, representing all of the treatment effects. The values of these contrasts were calculated. To determine the importance of these contrasts to the response D_{50}, normal probability plots were then employed. It revealed that the main effects A (A1), B (B1), C (C1), and the quadratic term in B (B2) were important. AB1 and AC1, representing the interaction between A and the linear effects of B and C, were moderately important. The quadratic term in C (C2) was not important (Appendix D).

To fit this D_{50} model, the coefficients of the model and the possible standard errors were estimated and listed in Table 5.4. Again, this suggests that there are some block effects (Bl1 and Bl2), but they are not large. The main effects of the 3 main factors are significant (A1, B1 and C1), with C appearing only to have a linear effect. There are interactions between A and the linear effects of B and C

(AB1 and AC1).

Table 5.3. Responses observed during 30 runs of NaOCl treatment combination (R = fractional recovery of PHB following treatment)

No. of run	Batch No.	Responses		
		D_{50} (μm)	w (μm)	R
1	1	0.7921	0.2863	
2	1	0.8032	0.2900	
3	1	0.6070	0.2238	
4	1	0.7844	0.2706	
5	1	0.7878	0.2709	
6	1	0.2983	0.1327	
7	2	1.0523	0.4028	
8	2	0.7010	0.2623	
9	2	0.4798	0.1907	
10	2	0.7096	0.2501	
11	2	0.7194	0.2533	
12	2	0.5243	0.2038	
13	3	0.9204	0.3685	
14	3	0.9154	0.3588	
15	3	0.3313	0.1422	
16	3	0.8520	0.3169	
17	3	0.6207	0.2239	
18	3	0.4362	0.1810	
19	4	0.8719	0.2964	0.9854
20	4	0.6143	0.2165	0.9225
21	4	0.6101	0.2152	0.9118
22	4	0.6968	0.2613	0.9389
23	4	0.6919	0.2601	0.9312
24	4	0.2678	0.1314	0.7861
25	5	0.7624	0.2640	0.9637
26	5	0.7613	0.2635	0.9613
27	5	0.4109	0.1634	0.8309
28	5	0.7862	0.2833	0.9630
29	5	0.5087	0.2062	0.8864
30	5	0.4938	0.1984	0.8652

Table 5.4. Coefficient estimates and the standard errors for D_{50} regression model

Variable	Coefficient value	Standard errors	t value	Pr (>| t |)
intercept	0.6853	0.0036	188.7585	0.0000
Bl1	0.0009	0.0154	0.0584	0.9547
Bl2	0.0374	0.0154	2.4258	0.0382
A1	_0.2050	0.0154	_13.3101	0.0000
B1	_0.7026	0.0154	_45.6142	0.0000
B2	_0.2179	0.0154	_14.1455	0.0000
C1	0.3711	0.0154	24.0952	0.0000
AB1	0.0749	0.0154	4.8639	0.0009
AC1	_0.0620	0.0154	_4.0273	0.0030

Residual standard error: 0.0154 on 9 degrees of freedom
Multiple R-squared: 0.9971
F-statistic: 385.5 on 8 and 9 degrees of freedom, the p-value is 1.715e-10

To express the response surface in an algebraic form, the factors A, B and C were coded as displayed in Table 5.5. The fitted equation (Equation 5.16) is:

$$D_{50} = 0.6853 - 0.2050*A - 0.7026*B - 0.2179*(36*B^2 - 2)/6 + 0.3711*C + 0.3178*A*B - 0.2630*A*C \quad (5.16)$$

where $A = 0.235*(N - 2)$

$B = 0.289*(7 - 2*(C_{cell}/4.33)^0.778)/5$

$C = 0.289*(1 - \log(C_{NaOCl}/0.85)/0.693)$

C_{cell} and C_{NaOCl} represent cell concentration (g/L) and NaOCl concentration (g/L), respectively. N is the number of homogenizer passes. The log is base 10. D_{50} can also be expressed as follows:

$$D_{50} = 0.4240 + 0.0257*N + 0.0678*C_{cell}^0.778 - 0.0018*C_{cell}^1.556 - 0.2063*\log(C_{NaOCl}) + 0.0258*N*\log(C_{NaOCl}) \quad (5.17)$$

For the response variable w, 6 major effects were identified by the use of normal probability plotting as for D_{50}. The analysis for the fitted model including blocks plus the identified effects was conducted. The estimated coefficients for the regression model and the corresponding standard errors are presented in Table 5.6. Note that the same effects are identified as being important for D_{50} and w, implying a strong correlation between D_{50} and w.

Table 5.5. Actual factor levels corresponding to the coded factor values

	Actual values			Coded values		
N (pass)	1	3		_0.235	+0.235	
C_{cell} (g/L)	43.3	21.7	4.3	_0.289	0	+0.289
C_{NaOCl} (g/L)	3.4	1.7	0.85	_0.289	0	+0.289

Table 5.6. Coefficient estimates and the standard errors for *w* regression model

Variable	Coefficient value	Standard errors	t value	Pr (>| t |)
intercept	0.2572	0.0014	189.2806	0.0000
Bl1	0.0338	0.0058	5.8618	0.0002
Bl2	0.0100	0.0058	1.7434	0.1152
A1	0.0995	0.0058	_17.2646	0.0000
B1	_0.2370	0.0058	_41.1111	0.0000
B2	_0.0582	0.0058	_10.0935	0.0000
C1	0.1384	0.0058	24.0191	0.0000
AB1	0.0522	0.0058	9.0551	0.0000
AC1	_0.0317	0.0058	_5.4978	0.0004

Residual standard error: 0.005764 on 9 degrees of freedom
Multiple R-squared: 0.9968
F-statistic: 352.1 on 8 and 9 degrees of freedom, the p-value is 2.576e-10

5.5.2. Analysis for Experiment II

11 contrasts representing all the treatment effects from the factorial design of Experiment II were identified, and the values of these contrasts were then calculated. Normal probability plots for the response variables D_{50}, *w* and LN(1_R) were plotted to identify the important effects. The standard deviations were also estimated. This allows the establishment of a response surface in algebraic form.

5.5.2.1. Response D_{50}

Among the 11 identified effects, five major effects corresponding to all main factors (A1, B1, C1 and C2) plus the interaction BC were defined as the main effects for D_{50} through a normal probability plot. Table 5.7 shows the estimated coefficients for the D_{50} regression model.

Table 5.7. Coefficient estimates and standard deviations for D_{50} regression model.

Variable	Coefficient estimate	Standard error	t value	Pr (>| t |)
intercept	0.6230	0.0056	110.7687	0.0000
A1	−0.0488	0.0056	−8.6787	0.0001
B1	−0.0795	0.0056	−14.1404	0.0000
C1	0.1362	0.0056	24.2203	0.0000
BC	0.0231	0.0056	4.1055	0.0063
C2	−0.0149	0.0056	−2.6441	0.0383

Residual standard error: 0.01948 on 6 degrees of freedom

The effect of C2 could be ignored. The fitted model can be expressed by Equation 5.18,

$$D_{50} = 0.6230 + 0.0488*A - 0.0795*B + 0.1362*C + 0.0231*B*C \quad (5.18)$$

where $A = 2*N - 1$

$B = 2*\log(21.7/C_{cell})/\log(2) + 1$

$C = \log(6.8/C_{NaOCl})/\log(2)$

D_{50} can also be rewritten as follows (Equation 5.19):

$$D_{50} = 1.0235 + 0.0976*N - 1.0482*\log C_{cell} - 1.4832*\log C_{NaOCl} + 0.6246*\log C_{cell}*\log C_{NaOCl} \quad (5.19)$$

5.5.2.2. Response *w*

Similar to the analysis of D_{50}, major effects for the response *w* were confined to B1, C1 and the interaction of B and C (BC), from the 11 identified effects by a normal probability plot. Table 5.8 presents the coefficient estimates and standard errors for the regression model. The influence from A is small and ignored.

Table 5.8. Coefficient estimates and standard errors for *w* regression model.

variable	Coefficient estimates	Standard error	t value	Pr (>| t |)
intercept	0.2300	0.0034	68.1084	0.0000
B1	−0.0229	0.0034	−6.7680	0.0001
C1	0.0405	0.0034	11.9910	0.0000
BC	0.0066	0.0034	1.9473	0.0874

Residual standard error: 0.0117 on 8 degrees of freedom.

The value of w is not dependent on the effect of A according to this model. This analysis also suggests that the interaction of B and C is not important. The fitted model can be expressed by Equations 5.20,

$$w = 0.2308 - 0.0229*B + 0.0405*C + 0.0066*B*C \quad (5.20)$$

where the values of B and C are calculated as for Equation 5.18. Equation 5.20 can be rewritten as Equation 5.21.

$$w = 0.1329 + 0.1412*\log C_{cell} - 0.1542*\log C_{NaOCl} + 0.0132*\log C_{cell}*\log C_{NaOCl} \quad (5.21)$$

5.5.2.3. Response LN(1–R)

This analysis takes the values of LN(1–R) for modelling convenience, as most of the R values are close to 1. Similar to the analysis of D_{50} and w, the 11 contrasts identified in the initial analysis were calculated for the response LN(1–R). The major effects were confined to three main effects (A1, B1 and C1) and AC interaction through normal probability plotting. The coefficients estimated for fitting this model, and the associated standard errors are presented in Table 5.9.

Table 5.9. Coefficient estimates and standard errors for LN(1–R) regression model.

Variables	Coefficient value	Standard error	t value	Pr (>| t |)
intercept	–2.6706	0.0296	–90.0790	0.0000
A1	0.2556	0.0296	8.6223	0.0001
B1	0.3101	0.0296	10.4588	0.0000
C1	–0.6004	0.0296	–20.2528	0.0000
AC	0.0808	0.0296	2.7244	0.0296

Residual standard error: 0.1027 on 7 degrees of freedom

The best equation is given by Equation 5.22.

$$LN(1-R) = -2.6706 + 0.2556*A + 0.0301*B - 0.6004*C + 0.0808*AC \quad (5.22)$$

The values of B and C are calculated as for Equation 5.18. The equation can also be rewritten as Equation 5.23.

$$LN(1-R) = -0.8273 + 0.5112*N + 2.0603*\log C_{cell} + 2.2629*\log C_{NaOCl} \quad (5.23)$$

5.5.1. Effect of B/C as a single factor on cell debris digestion

Since cell debris digestion by NaOCl is based on the interaction between NaOCl and the cell debris, the responses D_{50} and w should rely heavily on the ratio of cell concentration to NaOCl concentration. B/C effect on cell debris digestion was analyzed using the data from two experiments. The results thus apply to the whole experimental range. The analysis procedure is given in Appendix D and only the result is presented below.

The analysis of variance indicates that the contribution of B and C to the responses D_{50} and w can be well summarized by the single factor B/C, and B/C is the major determinant. The regression study which includes B/C as a single factor in the modelling of responses D_{50} and w is thus explored. Tables 5.10 and 5.11 present the analysis results.

Table 5.10. Coefficient estimates and standard errors for D_{50} regression model

Variables	Coefficient value	Standard error	t value	Pr (>| t |)
intercept	0.6666	0.0058	115.8345	0.0000
A1	−0.0602	0.0058	−10.3195	0.0000
(B/C)1	−1.0861	0.0327	−33.1982	0.0000
(B/C)2	−0.1030	0.0319	−3.2248	0.0036
A1*(B/C)1	0.1317	0.0343	3.8452	0.0008
A1*(B/C)2	−0.0125	0.0333	−0.3763	0.7100

Residual standard error: 0.02945 on 24 degrees of freedom

Table 5.11. Coefficient estimates and standard errors for w regression model

Variables	Coefficient value	Standard error	t value	Pr (>| t |)
intercept	0.2511	0.0026	96.0085	0.0000
A1	−0.0307	0.0038	−8.1119	0.0000
(B/C)1	0.0165	0.0145	1.1381	0.2663
(B/C)2	−0.3809	0.0149	−25.6147	0.0000
A1*(B/C)1	0.1215	0.0222	5.4624	0.0000
A1*(B/C)2	−0.0469	0.0216	−2.1694	0.0402

Residual standard error: 0.01339 on 24 degrees of freedom

The fitted equations are given by Equations 5.24 and 5.25.

$$D_{50} = 0.6841 \_ 0.0829*(A \_1.1) \_ 0.1354*(B/C \_ 0.866) \_ 0.0079*(B/C \_ 0.866)\text{^}2 + 0.0227*(A \_ 1.1)*(B/C \_ 0.866) \_ 0.0014*(A \_ 1.1)*(B/C \_ 0.866)\text{^}2 \quad (5.24)$$

$$w = 0.2483 \_0.0227* (A \_1.1) \_ 0.0466*(B/C \_ 0.866) + 0.0013*(B/C \_ 0.866)\text{^}2 + 0.0141*(A \_ 1.1)*(B/C \_ 0.866) \_ 0.0036*(A \_ 1.1)*(B/C \_ 0.866)\text{^}2 \quad (5.25)$$

where B/C = 1.67 _ $\log(C_{cell}/C_{NaOCl})$ and the log is base 2; A is 0, 1 or 2 corresponding to 0, 1 or 3 homogenizer passes.

Compared with the D_{50} models generated from Experiments I and II, Equation 5.24 does not fit to the same accuracy. The residual standard deviation for Equation 5.24 (0.02945) is larger than that for Equation 5.16 (0.0154) and for Equation 5.18 (0.01948) (Appendix D). The analysis shows that most of the deviation is due to a major outlier, the point corresponding to the treatment Run 27 in Batch 5. However, Equations 5.24 and 5.25 enable the prediction of responses D_{50} and w over a wide range of treatment conditions. In particular, the effect of high cell concentration and the strong trade-off between NaOCl and cell concentration are of great interest.

5.6. DISCUSSION

5.6.1. The effect of cell concentration and NaOCl concentration on cell debris digestion

It has been suggested in the previous section that the effect of both cell concentration (B) and NaOCl concentration (C) on cell debris size during NaOCl treatment can be summarized by a single factor B/C, and expressed using the empirical equations 5.24 and 5.25. In this section, B/C as a single factor will be further studied in terms of its effect on cell debris digestion.

The investigation is based on data from both experiments. As stated before, B/C is coded as $B/C = 3.67 - \log(C_{cell}/C_{NaOCl})$. Figures 5.4 and 5.5 show the plots of D_{50} and w against log(B/C), respectively, illustrating their correlation. For clear expression, the points corresponding to each treatment combination are represented with three coded digits defined in Table 5.2 in the order of factors A (the coded number of homogeniser passes), B and C. To refine Figures 5.4 and 5.5, it is interesting to note that the points with same number of homogenizer passes are almost located on one line for both D_{50} and w (Figures 5.6 and 5.7). The effect of factor A on D_{50} and w is thus clearly revealed. For a given B/C, a lower value of A tends to give higher value of D_{50} and w, which is consistent with the comminution effect of homogenization. Furthermore, there is more divergence of these lines at the left end and less at the right for both D_{50} and w. It generally indicates that the homogenization has less effect as the value of C_{cell}/C_{NaOCl} decreases, and conversely, a high effect from homogenization is expected if the value of C_{cell}/C_{NaOCl} increases. In other words, since both homogenization and NaOCl treatment are attributed to the cell debris micronization, the contribution of NaOCl treatment becomes significant at a low cell concentration, while the use of homogenization is more effective at a high cell concentration. This is consistent with the report of Kleinig *et al.* (1995) that the disruption efficiency of homogenization decreases slightly with cell concentration. The effect of homogenization on debris size reduction becomes small compared to that from NaOCl treatment if low cell concentration is

employed. The contribution of homogenization on cell debris size reduction (e.g., D_{50} and w) can be illustrated by the gap between the lines representing each homogenizer pass. Comparing Figures 5.5 and 5.6, it is noted that homogenization results in more decrease in the value of D_{50} than that of w following an increase in C_{cell}/C_{NaOCl}.

These relationships between log(B/C) and A are not reflected from Equations 5.24 and 5.25. As the analysis of variance and the regression are an artifact of the order of fitting, it can not provide realistic meaning to the fitted models. It is also noted that in the analysis of variance for D_{50} and w, homogenization (A) does not appear to be an important effect, especially for w, which is even not relevant to A (Equations 5.20 and 5.21). The relationship between log(B/C) and A illustrated in Figures 5.5 and 5.6 gives a rational understanding of the contribution of A to cell debris size reduction.

Because of the strong effect from B/C on D_{50} and w, a trade-off between B and C is expected which can also be observed in Figures 5.4 and 5.5. An increase in levels of both B and C by 1, leaves the responses D_{50} and w almost unchanged, such as the overlapped pairs (112, 123), (212, 223), (111, 122). This does not extend to the case of B = 3 (C_{cell} = 4.33 g/L) because of the non-proportional relation. The use of B/C as a single factor instead of B and C simplifies the model and also makes it easier to predict NaOCl performance on cell debris digestion.

In conclusion, cell concentration and NaOCl concentration are the major effects on D_{50} and w according to both modelling study and the data analysis above, especially at low cell concentration. The ratio of C_{cell}/C_{NaOCl} is clearly the major determinant. The effects due to the number of homogenization passes will become dominant if a high cell concentration is employed.

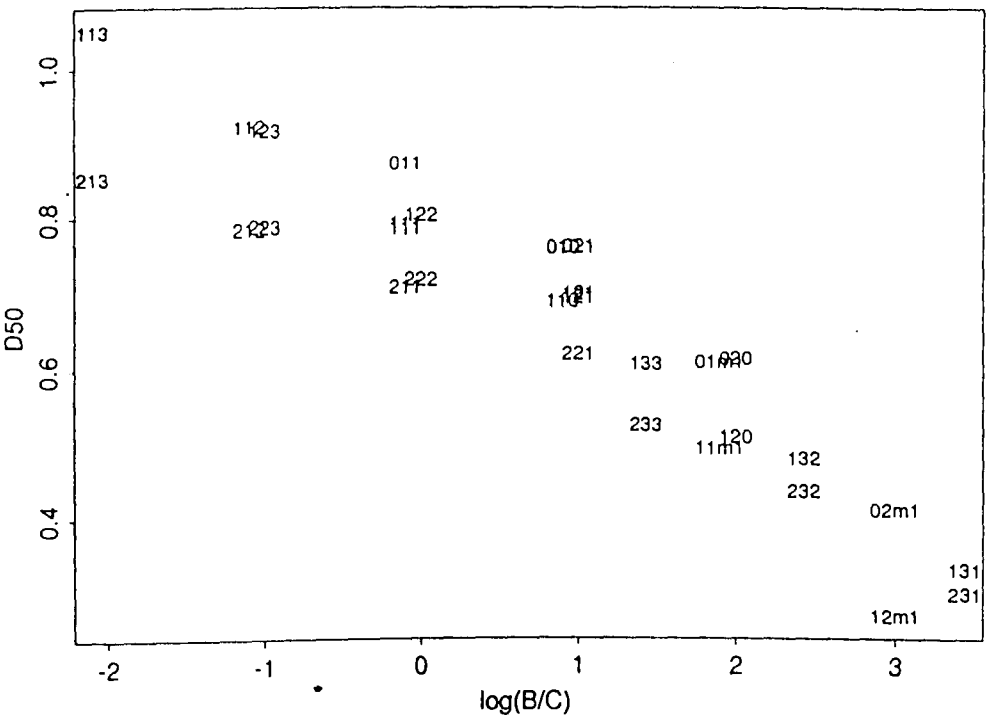

Figure 5.4. The correlation between the median diameter D_{50} and log(B/C).

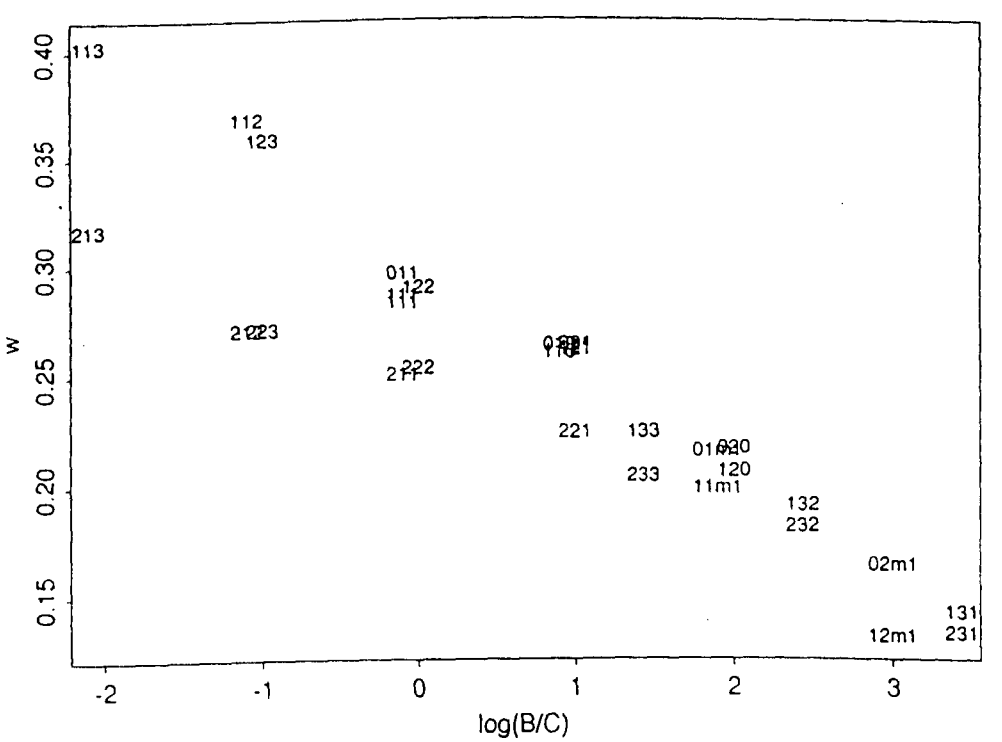

Figure 5.5. The correlation between Boltzmann parameter *w* and log(B/C).

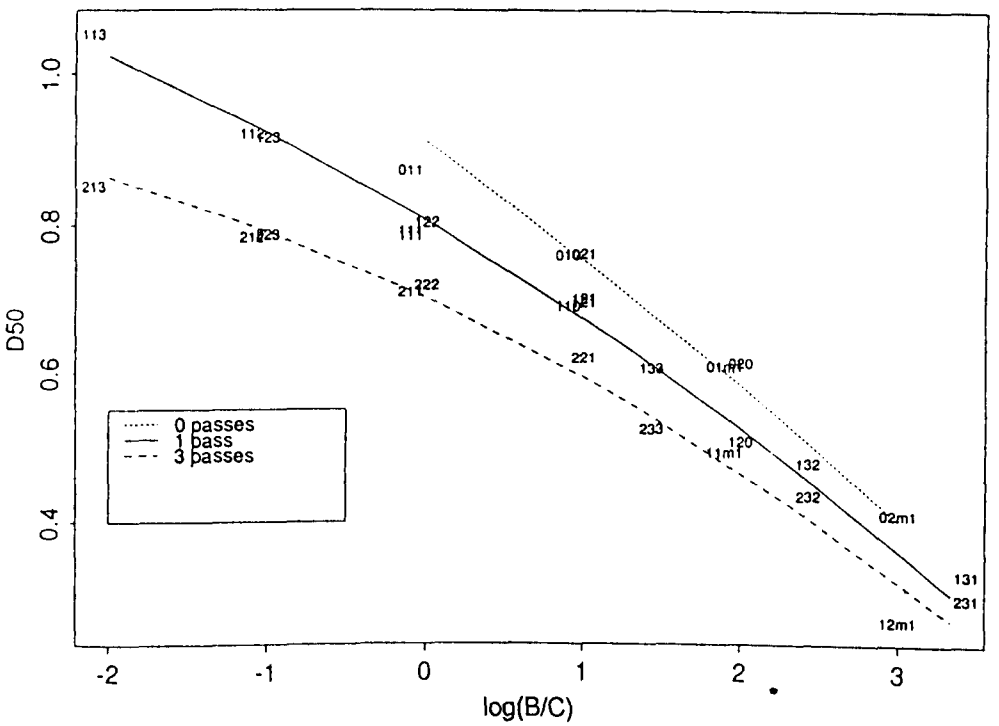

Figure 5.6. The correlation between the median diameter D_{50}, log(B/C) and homogenization passes

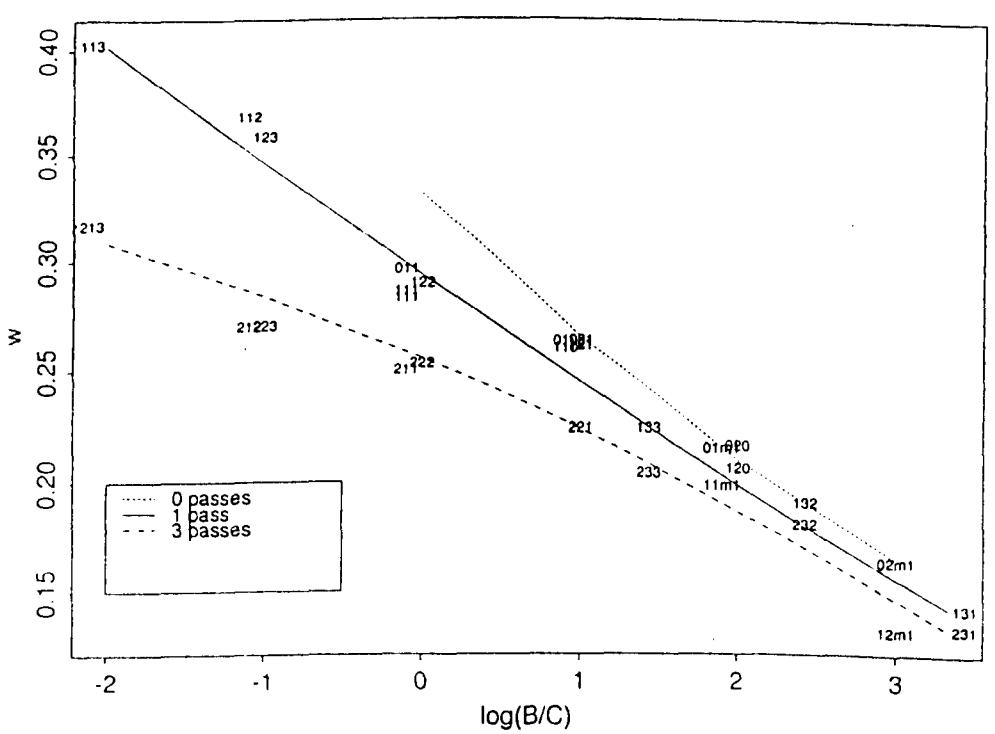

Figure 5.7. The correlation between Boltzmann parameter w, log(B/C) and homogenization passes.

5.6.2. Contour plotting analysis

In Section 5.5.2, the empirical models for D_{50}, w and LN(1−R) as a function of NaOCl treatment conditions are developed using the data from the second experiment (Equations 5.18, 5.20 and 5.22). The contour maps are plotted according to these models and presented in Figures 5.8, 5.9 and 5.10, respectively. They suggest a general trend that lower cell concentrations and higher NaOCl concentrations will give lower D_{50} and w values, and lower PHB recovery (R) as the contour lines diverge at the right side.

Overlapping Figures 5.8 and 5.10, it is found that the contour lines for D_{50} = 0.8 μm and R = 0.96 are almost coincident for both N = 0 and N = 1, implying that to maintain PHB collection at 96% or higher, the available D_{50} after NaOCl treatment will not be less than 0.8 μm in the whole experimental range. In the cell concentration range of 20 - 50 g/L, the lowest D_{50} is 0.6 μm for whole cell suspension (N = 0) and 0.5 μm for one pass homogenate (N = 1), corresponding to PHB recoveries of 92% and 88%, respectively. Furthermore, for one pass homogenate (N = 1), to maintain PHB collection rate over 90%, the lowest D_{50} and w will be 0.6 μm and 0.24 μm, which can be achieved by adjusting the NaOCl concentration within 9 to 14 g/L. Furthermore, the cell concentration has to be in the range of 20 to 28 g/L. This required NaOCl treatment condition is obviously impractical. There are three main disadvantages. Firstly, the achievable cell debris size compared to the size of PHB granules (D_{50} = 0.86 μm, and w = 0.11 μm) is not small enough to ensure good fractionation,. Secondly, 90% PHB recovery is unacceptably low. Since the first centrifugation is the major source of PHB loss in a repeated centrifugation process (Section 4.4.2), a combination of both NaOCl treatment and centrifugation will push the total PHB collection down significantly. Thirdly, a high cell concentration needs to be employed in the production scale for economic processing (see Chapter 6). The required cell concentration range of 20 to 28 g/L is not high enough.

In conclusion, the sole use of NaOCl treatment or NaOCl treatment combined with few homogenization passes is unlikely to generate a sufficient cell debris

size reduction while maintaining a high PHB collection. As a high level of cell debris size reduction is required to ensure efficient PHB fractionation, other unit operations such as multiple homogenization need to be involved in association with NaOCl treatment, especially when a high cell concentration is employed.

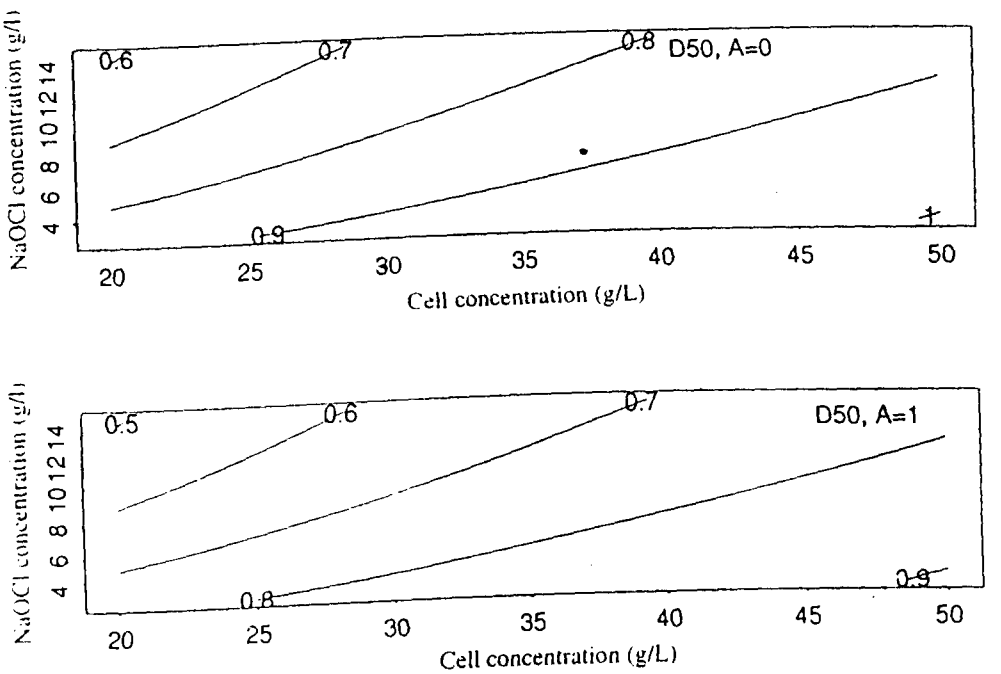

Figure 5.8. Contour map for D_{50} (Equation 5.18)

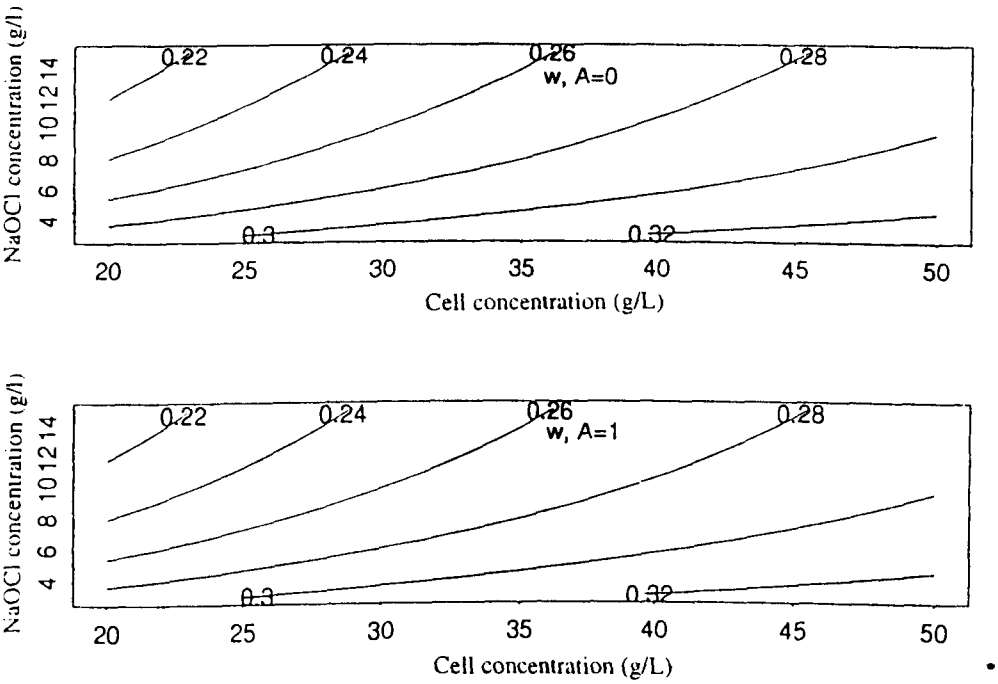

Figure 5.9. Contour map for *w* (Equation 5.20)

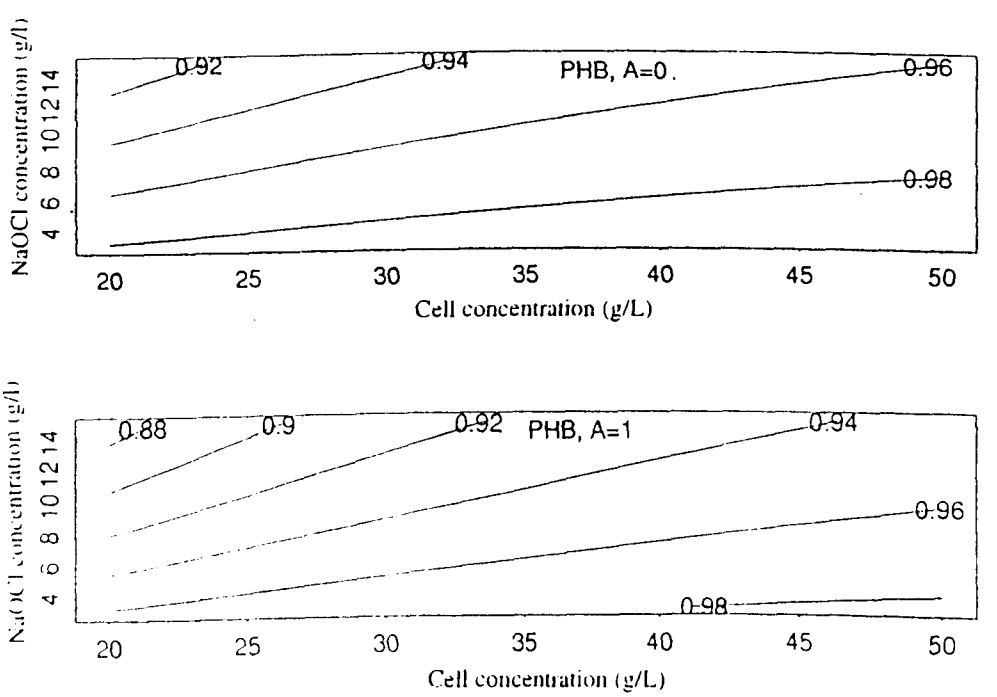

Figure 10. Contour map for LN(1-R) (Equation 5.22)

5.6.3. Cell debris size distribution and Boltzmann function

Figure 5.11 shows a plot of D_{50} against the corresponding values of w using the data collected from both Experiments I and II. It reveals a strong linear correlation between D_{50} and w. A higher value of D_{50} corresponds to higher value of w. w is generally very close to 40% of the value of D_{50}. This is consistent with the observation of the cell debris minimisation by multiple homogenisation (Section 4.3.2).

The Boltzmann function (Equation 2.8) has been successfully used in this study for describing particle size (*E. coli* cells, PHB granules and cell debris) in Chapter 4. D_{50} representing the median diameter and w describing the spread of the distribution are obtained by minimizing the sum of squared differences between the observed cumulative size distribution $W(D)$ and the theoretical values.

$$W(D) = \frac{1}{1 + \exp((D - D_{50})/\omega)} \tag{2.8}$$

Equation 2.8 can be transformed into a logit formation as expressed in Equation 5.26.

$$\log(\frac{1-W}{W}) = \frac{D - D_{50}}{\omega} = a + bD \tag{5.26}$$

where $b = 1/w$ is the slope of a linear regression and $a = -D_{50}/w$ is the intercept. The transformed proportions $\log((1-W)/W)$ should lie on a straight line when plotted against D, and where these lines cross the horizontal line at 0 should correspond to $-D_{50}/w$ and the slope of the lines should be $1/w$. Figure 5.12 shows such a plot using the 18 sets of data from the first experiment. As observed, these lines are close to linear although most are slightly concave, suggesting Equation 2.8 does not express the size distribution of cell debris digested by NaOCl treatment very well. The transformation of the D scale into logD was considered (Figure 5.13). The lines appear convex instead of concave, suggesting that the size distribution is skewed to the right. The results are confirmed by plotting the 12 sets of data from the second experiment (Figures 5.14 and 5.15). Using sqrt(D) on the horizontal axis gives straight lines and provides a more consistent fit to the experimental data. The analysis indicates that the Boltzmann function may not be the best model to describe the size of cell

debris treated with NaOCl. The deviation may become serious when high NaOCl concentration and low cell concentration are employed, where strong debris digestion occurs.

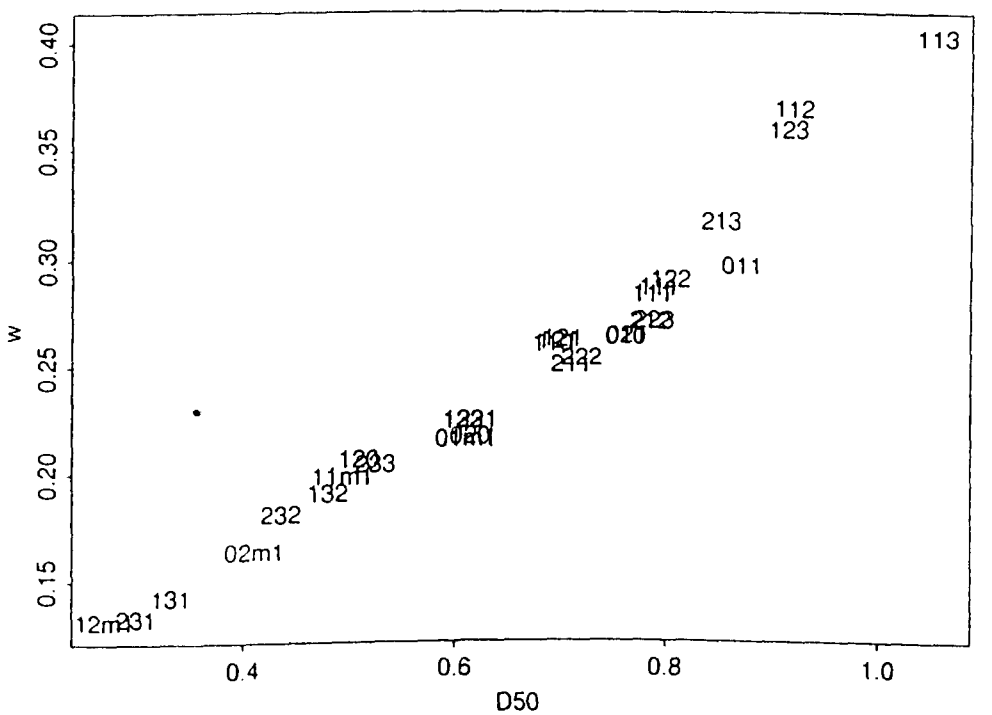

Figure 11. Plot of D_{50} versus *w*.

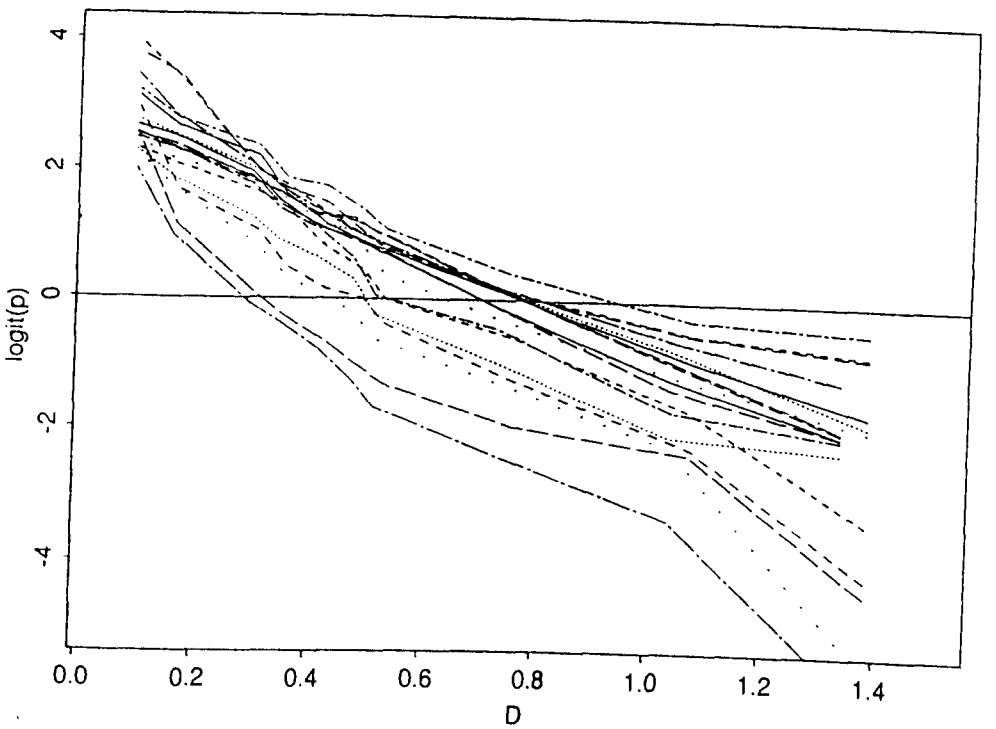

Figure 12. Plot of log((1−*W*)/*W*) against D for the first experiment.

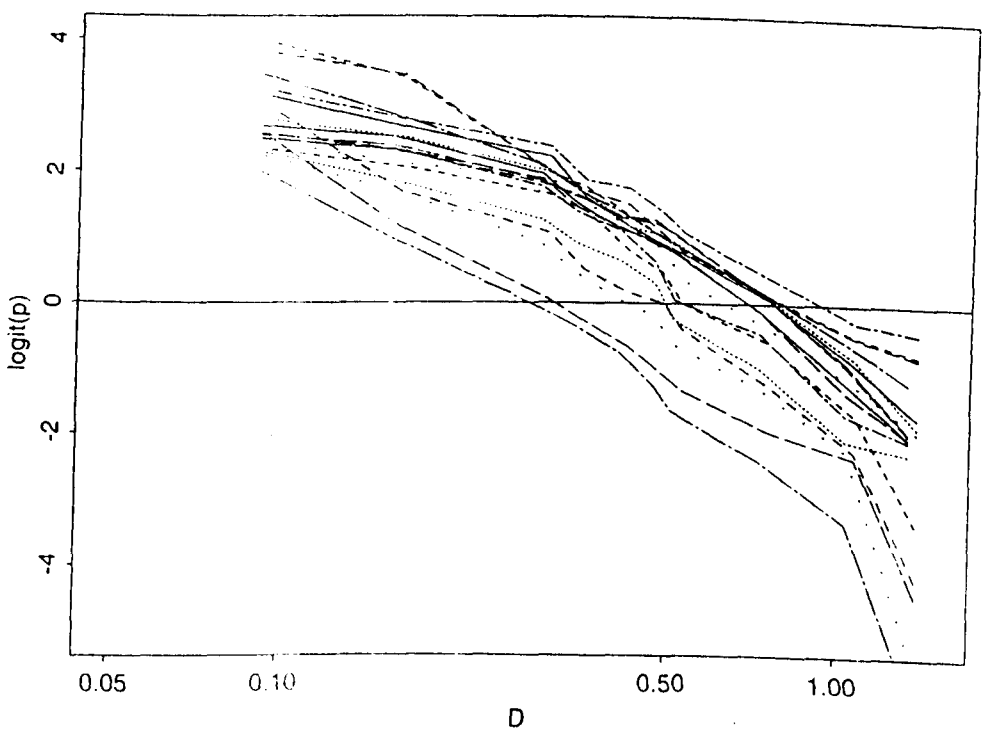

Figure 13. Plot of log((1−*W*)/*W*) against logD for the first experiment.

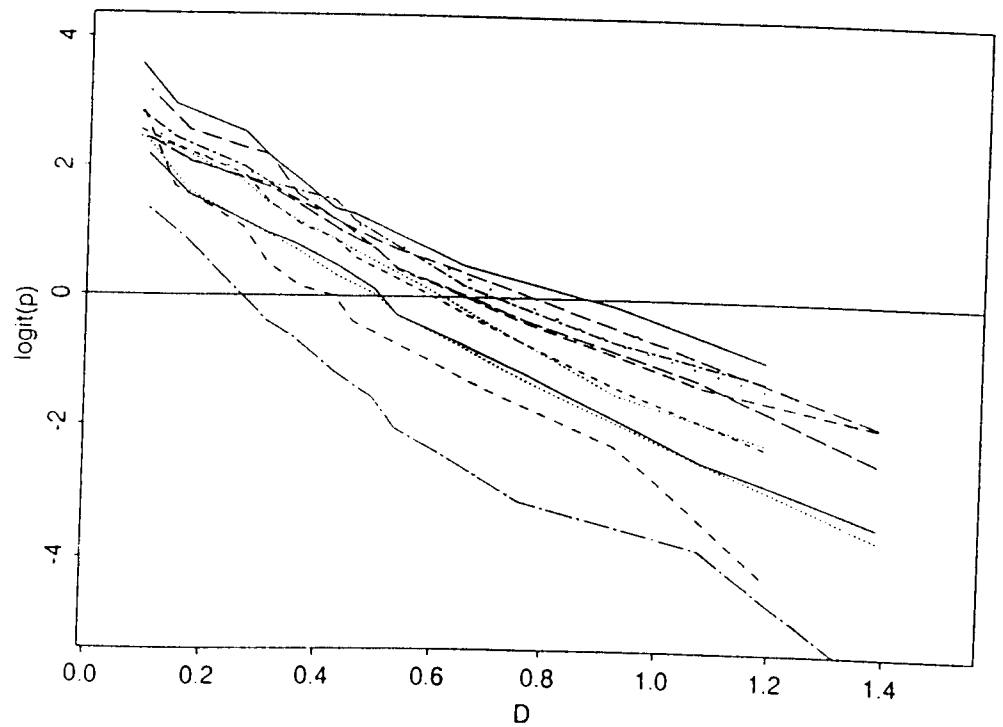

Figure 14. Plot of log((1−*W*)/*W*) against D for the second experiment.

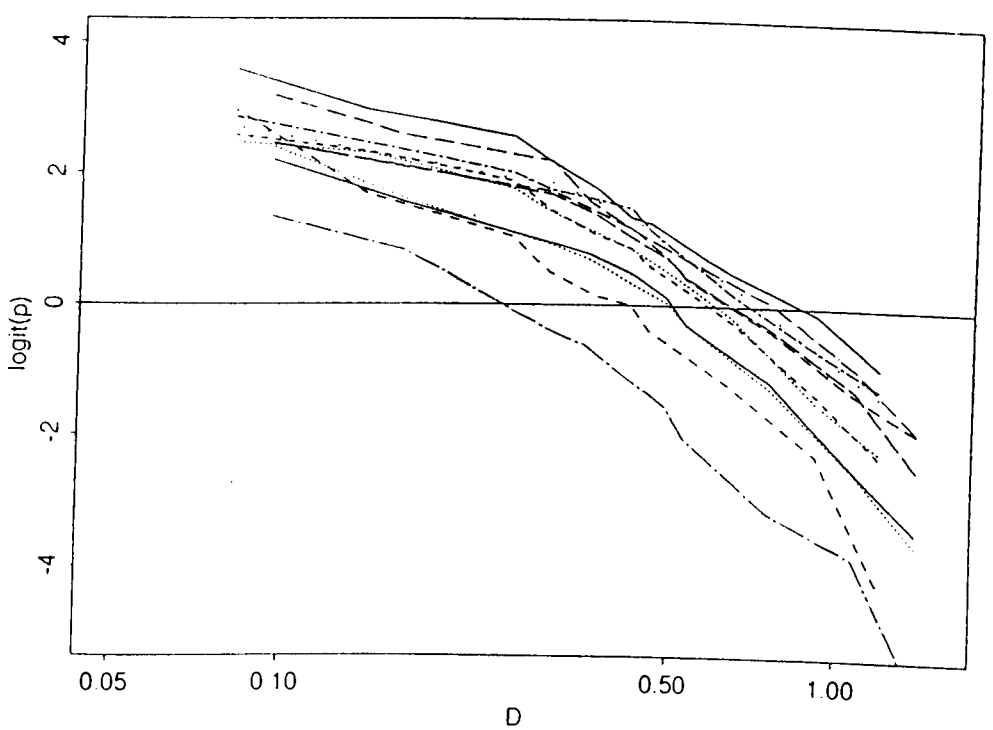

Figure 15. Plot of log((1−*W*)/*W*) against logD for the second experiment.

CHAPTER 6

OPTIMIZATION OF THE PHB RECOVERY PROCESS

A preliminary investigation of PHB recovery by homogenization and centrifugation was conducted in Chapter 3. Particle fractionation during the recovery processes was studied in Chapter 4 and the improvement in cell debris size reduction thus cell debris removal by NaOCl treatment was identified. The first centrifugation was identified as the most important unit operation in terms of cell debris removal and PHB collection. In Chapter 5, cell debris digestion by NaOCl was modeled as a function of NaOCl treatment conditions using response surface methodology. This provides an empirical model enabling the prediction of cell debris size as a function of NaOCl concentration, cell concentration and the number of homogenizer passes prior to centrifugation. In this chapter, the preceding studies will be used to optimize the PHB recovery process by simulation. PHB collection and cell debris removal are estimated for each unit operation as a function of key operational variables. The impact of each variable choice on overall production cost is also estimated. The process which meets a performance target (in this case 95% cell debris removal) at lowest overall cost will be selected as optimal. This optimal process is then demonstrated at pilot scale, and is characterized in terms of the removal of non-PHB cellular materials in each unit operation. The optimal process selected involved 6 homogenizer passes, and 2 centrifuge passes, incorporating NaOCl treatment at a concentration of 0.85 g/L active chlorine before the second homogenizer pass. An overall production cost of US$6.57 /kg PHB was estimated. A PHB purity of 93.6%, with cell debris removal of 95.3% and PHB recovery rate of 91.8% was achieved, and good removal of DNA and protein was also attained. As this study is conducted at semi-industrial pilot scale, the final process can be easily extrapolated to full industrial application.

6.1. SIMULATION AND OPTIMIZATION OF PHB RECOVERY

To simulate the PHB recovery process, a basic process flowsheet comprising homogenization, NaOCl treatment and centrifugation is firstly defined in Section 6.1.1, followed by a description of the simulation strategy (Section 6.1.2), and selection of the key simulation parameters (Section 6.1.3). Since overall production cost depends strongly on the available PHB quality, a cell-debris removal target of 95% is defined as the key goal of process optimization. Coupled with an estimate of overall PHB production cost, the optimal PHB recovery process which meets the cell debris removal criteria at minimum production cost is then obtained by simulation (Section 6.1.4).

6.1.1. Defining the basic process flowsheet

The PHB recovery process developed in Chapter 3, combining 5 homogenizer passes, 3 centrifuge passes and NaOCl treatment (Figure 3.1), achieved an overall PHB recovery fraction and cell debris removal fraction of about 79.6% and 96.5%, respectively. DNA and protein contaminant levels were acceptable (<0.01% and 0.03%, respectively). Flowsheets for simulation of PHB recovery are based on the topology of this process. The three major unit operations (homogenization, NaOCl treatment, and centrifugation) are re-sequenced and grouped as Part I and Part II in terms of their function: cell debris minimization for Part I and particle fractionation for Part II (Figure 6.1). This re-organization does not affect the final fractionation performance very much in a multiple-pass centrifugation strategy (Wong, 1996).

A significant reduction in cell debris size prior to the first centrifugation is necessary to improve PHB fractionation efficiency (Section 4.4). The preliminary objective of Part I is to micronize cell debris through both homogenization and NaOCl treatment. Size is regulated by adjusting the number of homogenizer passes (N) and NaOCl treatment conditions, and can be estimated using the cell-

debris size-reduction models for NaOCl treatment and homogenization (Section 6.1.2). In addition, both homogenization and NaOCl treatment change the suspension properties, facilitating PHB fractionation (see Appendix F). Extensive homogenization reduces the suspension viscosity (Kleinig *et al.*, 1995), and the use of NaOCl treatment can also destroy long-chain nucleic acids (Lu Shih and Lederberg, 1976) thus lowering suspension viscosity. Moreover, NaOCl treatment facilitates DNA and other non-PHB cellular materials removal (Sections 3.3.4 and 5.2.2).

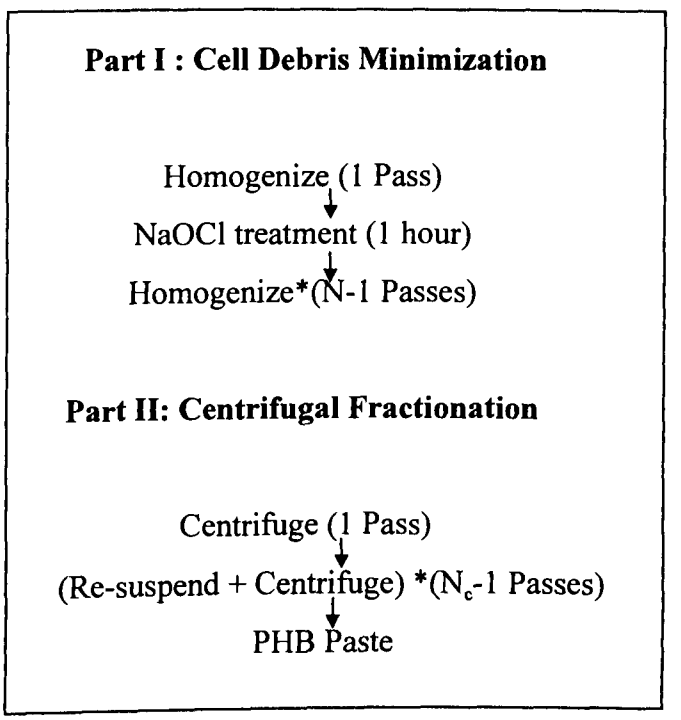

Figure 6.1. Basic design of the PHB recovery process to be optimized by simulation.

Part II involves multiple cycling of centrifugation and re-suspension to meet the performance target of ≥95% cell debris removal. The number of cycles (N_c) depends on the cell debris removal efficiency per pass. As discussed in Appendix C, inserting homogenization in between centrifugation passes in Process C improved the re-suspension of the discharged PHB paste obtained from the solid bowl disc-stack centrifuge employed in this work. In practice, however, incorporating homogenization between centrifugation passes complicates batch scheduling. Furthermore, the concentrate discharged from production scale centrifuges is in the form of a slurry, thus removing problems of paste re-

suspension. For these reasons, only the flowsheet based on the design in Figure 6.1 is considered.

Strong interactions are expected between homogenization, NaOCl treatment, and centrifugation with regards to cell-debris removal, PHB collection, and the resulting PHB production cost. For example, high cell debris removal can be achieved by increasing either the number of homogenizer passes, the NaOCl concentration, the feedrate or number of centrifuge passes, or by decreasing the cell concentration during NaOCl treatment. However, these changes will lower PHB collection efficiency thus increasing overall PHB production cost. Due to the process complexity and the number of variables involved, it was decided to restrict the variable range before conducting the simulation.

6.1.2. Simulation strategy

6.1.2.1. Criteria for particle fractionation

The recovery process determines final PHB purity and production cost to a large extent. The objective of optimization by simulation is to select the process which recovers PHB with acceptable purity at minimum cost. A performance specification must be defined in terms of the target non-PHB contaminant removal before starting the simulation. A target of 95% by volume of cell debris removal is suggested. Since the PHB content for the starting cell material in this study is 60.5% (w/w), a cell debris removal of 95% means that the concentration of cell debris in the final product will be less than 1.2%. Compared with a final PHB purity of 90% obtained from the industrial process described by Harrison (1990), and 96.5% obtained in Process C described in Chapter 3, this target is acceptable. Due to the lack of models for protein and nucleic-acid removal, these contaminants cannot be included in the simulation. It is assumed that the cell debris removal target will lead to acceptable protein and DNA concentration, as debris is the most difficult to remove. This was certainly the case in Process C (Chapter 3). After simulating the technical performance for a given set of operational parameters, the associated overall PHB production cost per kilo of the

purified PHB is then estimated. The optimal process will be the one that meets the cell debris removal constraint of 95% at minimum production cost.

6.1.2.2. Models and parameters used in simulation

Three major unit operations are involved in the basic PHB recovery process: homogenization, NaOCl treatment and centrifugation. Models and parameters used for the simulation of cell debris micronisation and its fractionation from PHB during each unit operation will now be summarized (Table 6.1).

Homogenization is based on an APV-Gaulin 15MR high-pressure homogenizer with a ceramic cell-disruption valve, operated at a pressure of 55.2 MPa, which is the maximum continuous pressure for this system. The feed temperature is approximately 10°C. Debris size reduction by homogenization can be estimated by Equation 4.1 with α and a_d equal to 2.29 and 0.96, respectively (Section 4.3.4).

Cell debris size after NaOCl treatment is predicted with Equations 5.17 and 5.18 at high NaOCl concentrations (≥3.4 g/L NaOCl) and Equations 5.21 and 5.22 for low NaOCl concentrations (<3.4 g/L NaOCl) (Section 5.5). PHB digestion at high NaOCl concentration (≥3.4 g/L NaOCl) is calculated with Equation 5.20, while at low NaOCl concentration it is estimated proportionally to the ratio of NaOCl concentration against cell concentration.

The density of whole cells is taken as 1085 kg/m^3 (Hwang, 1996), while PHB granule density is taken as 1260 kg/m^3 (Middelberg *et al.*, 1995). These densities are approximate and only used to transform distributions to a size basis for presentation. In simulation, the settling-velocity distribution is the critical determinant of performance, and this is not affected by the assumed density (Middelberg, 1998).

Table 6.1. Functions of unit operations and corresponding models for the simulation of PHB recovery and cell debris removal.

Function	Unit Operation	Models	Parameters
Cell debris minimization	NaOCl treatment	Cell-debris size-reduction models (Equations 5.17, 5.18, 5.21 and 5.22)	
		PHB digestion model (Equation 5.20)	
	Homogenization	Cell-debris size - reduction model (Equation 4.1)	$\alpha = 2.29$ $a_d = 0.96$
Centrifugal fractionation	Centrifugation	Grade-efficiency for a disc-stack centrifuge (Equation 4.12)	PHB granules: k=0.13, n=2.1; Cell debris k=0.16, n=2.6.

The centrifugal fractionation of PHB from cell debris is based on the models for a Veronesi KLE-160 solid-bowl disc-stack centrifuge with an average bowl rotational speed of 8400 rpm (Σ=3775 m^2). This was employed in Chapter 3 for the preliminary investigation of PHB recovery. The normalized feedrate (Q/Σ) in the simulation ranges from 1.32×10^{-9} m s^{-1} to 3.97×10^{-9} m s^{-1} as this is the range of model and parameter confidence. Settling behavior of PHB granules and *E. coli* cell debris in the disc-stack centrifuge is predicted using the grade-efficiency curve for the centrifuge (Equation 4.12). The values of parameters k and n are given in Table 6.1. These parameters were obtained for recombinant *E. coli* cell debris and protein inclusion bodies fractionated in the same centrifuge used in this study (Wong, 1996). As demonstrated in Section 4.4, the parameters for both recombinant *E. coli* cell debris and inclusion bodies perform well for cell debris simulation and PHB granules.

6.1.2.3. Variables involved in PHB recovery process

The variables, involved in the basic process defined in Section 6.1.1 and affecting final cell debris removal and PHB production cost, can be classified as uncontrollable, operational and response variables.

Uncontrollable variables mean the variables that can not be adjusted in the simulation but which affect fractionation performance. Some uncontrollable variables are determined by the starting cell material, including PHB granule size, density, and cell wall characteristics. Cell pretreatments such as freeze-thaw also affect PHB granule size and cell-wall characteristics (Section 4.3.3). Other variables are restricted due to the limitation of models applied (Table 6.1). For example, the models for cell debris size reduction and PHB stability during NaOCl treatment allow only the variation of cell concentration and NaOCl concentration at fixed treatment duration and temperature.

Operational variables include the variables that can be adjusted in the simulation: NaOCl concentration, cell concentration, the feedrate for each homogenizer and centrifuge pass, and the number of homogenizer and centrifuge passes.

Key response variables are affected by both the operational and uncontrollable variables. These include the attainable cell debris size and recovery, PHB degradation and recovery, and suspension characteristics such as viscosity.

As discussed in previous chapters, the bulk of the cell debris removal is achieved through the first centrifugation and mainly depends on feedrate. Fractionation efficiency is also dependent on key response variables (cell debris size and suspension viscosity) which, in turn, rely on the homogenization and NaOCl treatments. Clearly, a strong interaction exists between these variables. Cell debris size during NaOCl treatment and homogenization is estimated by the models indicated in Table 6.1. It is assumed that homogenization does not have impact on the PHB size distribution on the basis of our previous study. It is also assumed that NaOCl treatment digests PHB and reduces the total PHB collection, but does not change the PHB size distribution. It is clearly an approximation, but reasonably valid considering the low amount of PHB degradation and the cubed relation between PHB diameter and PHB volume. For example, when the total PHB recovery is 93.1% after NaOCl treatment (cell concentration, 43.3 g/L and NaOCl concentration, 6.8 g/L active chlorine) (Table 5.3), the resulted reduction of PHB mean diameter should be less than 2.4%. It is also postulated during the

simulation that size distribution of particles including whole cells, PHB granules and cell debris from either homogenization or NaOCl treatment, can be described by the Boltzmann function. The suspension viscosity is affected by both homogenization and NaOCl treatment conditions, and affects the subsequent fractionation. Due to the limitation of experimental conditions, the suspension viscosity used in the simulation was assumed and the details are given in Appendix F.

To be able to simulate the recovery process and present meanful results, the simulation range of some variables has to be restricted while other variables need to be fixed. The uncontrollable variables determined by the starting cell material can easily be fixed by assuming the same starting material with the same pretreatment. Cell material referred to in this simulation is from Fermentation III (Section 5.4) with a cell concentration of 43.3 g/L and a PHB content of 60.5% (w/w). The median diameter D_{50} and Boltzmann parameter w used in the simulation are 1.93 μm and 0.210 μm for the defrosted *E. coli* cells, and 0.865 μm and 0.111 μm for PHB granules after three homogenizer passes, respectively. Note that both the whole-cell and PHB-granule size are larger than those from Fermentations I and II (Table 4.2). The PHB size and the parameters for cell debris size reduction models used in the simulation are all from the cells following freeze-thaw pretreatment as specified above.

Operational variables can be controlled during the process, and directly affect the fractionation performance. Their valid simulation range is discussed in the following section (Section 6.1.3).

6.1.3. Operational variables selection

There are five operational variables determining cell debris removal and PHB collection in the basic process defined in Section 6.1.2.3: cell concentration, NaOCl concentration, the feedrate for each centrifugation, and the number of homogenizer (N) and centrifuge passes (N_c). In the following part of this section,

the range of these variables are restricted and justified for the purpose of simulation.

Feed cell concentration

The cell concentration employed in Process C (Chapter 3) was low at 4.3 g/L due to the low amount of cell material available. It is obviously not practical at production scale. High cell concentration needs to be employed in practice to minimize the operating scale and thus manufacturing cost. The cell concentration of choice employed in practice will depend on operational constraints on the homogenizer and centrifuge. Homogenization performance for PHB release and cell debris comminution is relatively insensitive to feed cell concentration (Kleinig *et al.*, 1995; Wong *et al.*, 1997). In practice, the optimal cell concentration for homogenization will be determined by the operational handling constraints due to a high feed viscosity (Kleinig *et al.*, 1995). Moreover, NaOCl treatment followed by extensive homogenization prior to the first centrifugation will destroy the released nucleic acids, thus reducing suspension viscosity and allowing a higher cell concentration to be handled by centrifugation. In addition to the increased viscosity, at high cell concentration, hindered sedimentation of particles in a homogenate becomes an important factor governing fractionation efficiency because of decreased particle settling velocity. Poor fractionation of PHB from cell debris may be thus expected. However, increased feed cell concentration only slightly decreased granule collection but not purity in a multiple centrifuge-pass process (Wong, 1996). The feed concentration for the first centrifugation in the simulation is therefore set to 40 g/L. This is a reasonable practical constraint for disc-stack centrifuges (maximum solids load ca. 4-5% w/w dry basis). This also approximates the final cell concentration achieved in the fermentation conducted in this study, thereby removing the need for batch dilution. After re-suspension prior to the second centrifuge pass, the viscosity is further reduced and the allowable feed concentration is increased. A feed concentration of 70 g/L is thus assumed for subsequent centrifugations. Cell concentration affects PHB overall production cost significantly at process scale, as discussed subsequently (Section 6.1.5.2).

NaOCl concentration

NaOCl concentration varies in the range of 0 to 13.6 g/L active chlorine in the simulation, which is the confidence range of cell debris digestion models established in Chapter 5.

Centrifuge feedrate

Centrifuge feedrate (Q/Σ) greatly influences PHB and cell-debris fractionation. It is restricted between 2.65×10^{-9} m s^{-1} and 3.97×10^{-9} m s^{-1} in the simulation for the first centrifugation, as this is the range of feedrate for which the grade-efficiency curves for the Veronesi solid-bowl centrifuge are known with confidence (Wong, 1996). The feedrate for subsequent centrifuge passes is fixed to the maximum of this range (3.97×10^{-9} m s^{-1}). After the first centrifugation, suspension viscosity is reduced significantly and its impact on particle fractionation becomes less pronounced. PHB collection and cell debris removal are thus mainly determined by centrifuge feedrate and particle size. As stated in Section 4.4.1, PHB collection will be less sensitive to the variation of centrifuge feedrates when PHB size increases. PHB size used for this simulation (D_{50} = 0.865 μm) is much larger than that from Fermentation I (D_{50} = 0.377 μm). Fixing the feedrate to the maximum value for the centrifuge system gives high cell debris removal while maintaining a high PHB collection efficiency.

The number of homogenizer and centrifuge passes

The number of homogenizer (N) and centrifuge passes (N_c) will be adjusted in the simulation to achieve the PHB fractionation target specified earlier.

The operational variables for the PHB recovery process are finally limited to four. Table 6.2 lists these variables and the allowable simulation range.

Table 6.2. Summary of operational variables considered in simulation.

Variables	Simulation Range
NaOCl concentration (g/L)	0 - 13.6 g/L of active chlorine
The first centrifuge feedrate (Q/Σ)	$2.65 - 3.97 \times 10^{-9}$ m s^{-1}
The number of homogenizer passes (N)	N: integer/0
The number of centrifuge passes (N_C)	N_C: integer/0

6.1.4. Simulation

In this section, cell debris removal and PHB recovery are simulated as discussed above. An example is given in Appendix D for the simulation of cell debris fractionation. A general scan is conducted to search for candidate processes that meet the performance target of >95% cell debris removal. The cost for each candidate process is estimated according to the economic analysis procedure of van Wegen *et al.* (1998) for the same basic conditions. Costs are presented in 1995 US$ per kilo of purified PHB. This enables the optimal process that meets the cell debris removal target at minimum cost to be selected.

6.1.4.1. The effect of NaOCl concentration on CDR and PC

Simulation starts with an investigation of cell debris removal (CDR) and the corresponding overall PHB production cost per kg (PC) in response to changes in NaOCl concentration. Figure 6.2 illustrates CDR and PC as a function of both NaOCl concentration and the number of homogenizer passes. The target CDR of 95% is achieved after three centrifuge passes at a feedrate of 2.65×10^{-9} m s^{-1} for the first pass and 3.97×10^{-9} m s^{-1} for subsequent passes as discussed earlier. The fractions of cell debris solubilized and PHB degraded during NaOCl treatment (before centrifugation) are also estimated and included in the overall cell debris removal and PHB recovery.

In general, CDR increases with an increase in NaOCl concentration with the exception of NaOCl concentrations close to zero. NaOCl concentration influences CDR greatly at fewer homogenizer passes. For one-pass homogenate,

CDR changes from 68% at an NaOCl concentration of 0.85 g/L to a maximum of 93% at an NaOCl concentration of 13.6 g/L. After two passes of homogenization, CDR is affected less by NaOCl treatment. The effect is reduced further as the number of homogenizer passes increases further. At a NaOCl concentration of 0.85 g/L, there is almost a 20% improvement in CDR from one to two homogenizer passes, while only a 2% improvement is achieved by increasing from 3 passes to 4.

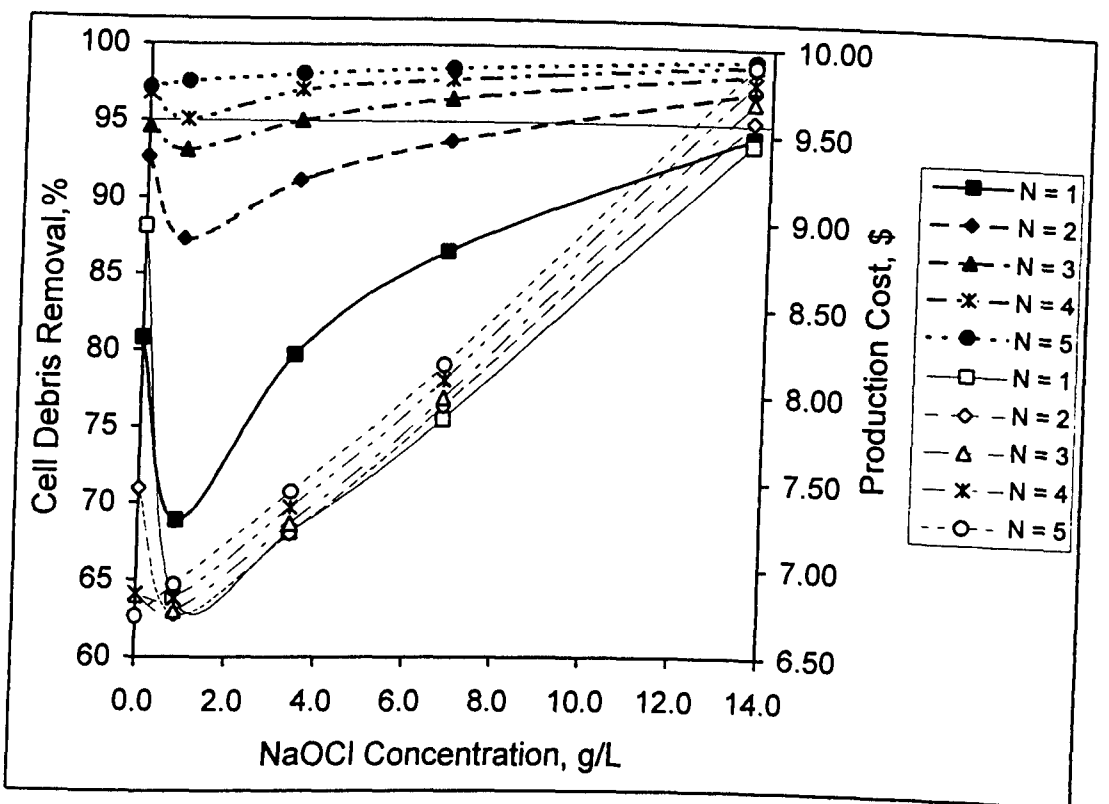

Figure 6.2. Simulation of cell debris removal (solid symbols) and production cost (open symbols) as a function of NaOCl concentration after three centrifuge passes. N is the number of homogenizer passes. The normalized centrifuge feedrate (Q/Σ) is 2.65×10^{-9} m s^{-1} for the first pass and 3.97×10^{-9} m s^{-1} for subsequent passes.

Since both homogenization and NaOCl treatment function to micronize cell debris, a strong trade-off between NaOCl concentration and the number of homogenizer passes is expected. As shown, four homogenizer passes are required to meet the CDR target of 95% at a NaOCl concentration of 0.85 g/L. Three homogenizer passes are required at 3.4 g/L NaOCl, reducing to two homogenizer passes at 13.6 g/L. A low NaOCl concentration with a high number of homogenizer passes, or vice versa, achieves the CDR target of 95%.

Production cost increases dramatically with increasing in NaOCl concentration. For three-pass homogenate, PC rises from US$6.85 /kg to US$9.69 /kg as NaOCl concentration increases from 0.85 g/L to 13.6 g/L. The increase in PC for the one and two passes homogenates at low NaOCl concentration (less than 0.85 g/L) is due to a low PHB collection (64.3% and 80.6%, respectively, at 0 g/L NaOCl). Comparatively, homogenization has less effect on PC with an increase of approximate US$0.10 /kg PHB for each additional pass.

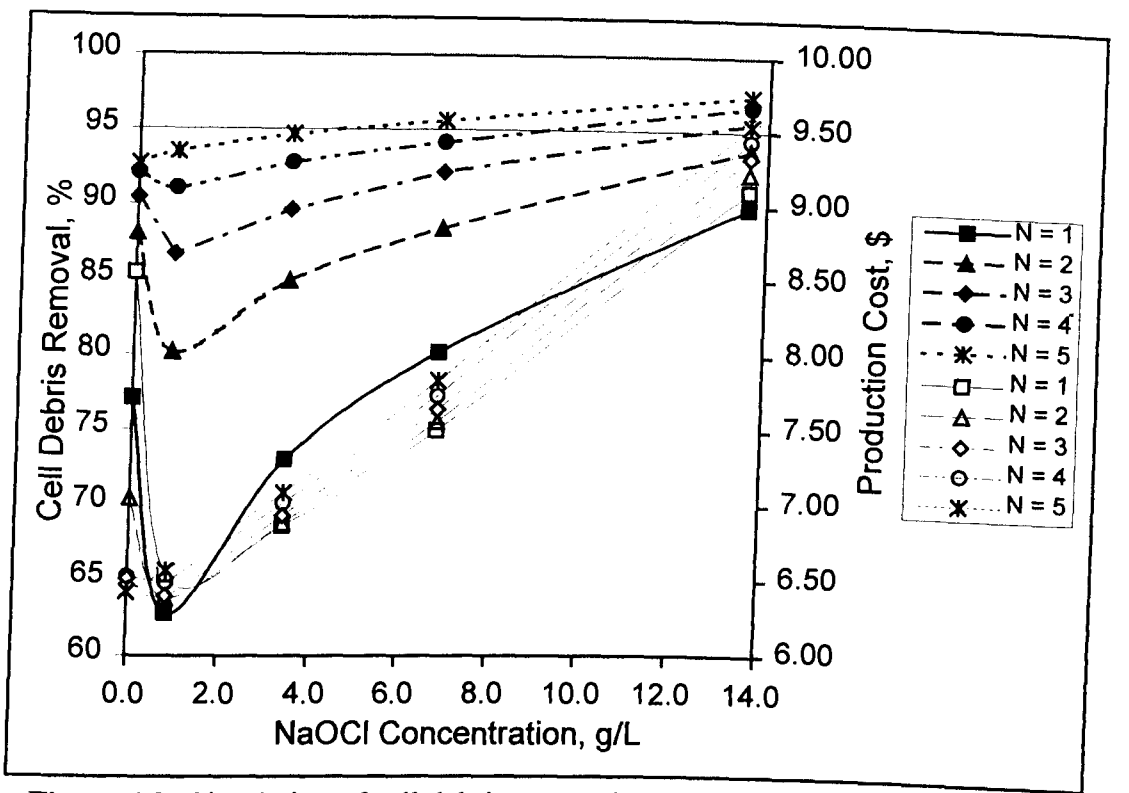

Figure 6.3. Simulation of cell debris removal (solid symbols) and production cost (open symbols) as a function of NaOCl concentration after two centrifuge passes. N is the number of homogenizer passes. The normalized centrifuge feedrate (Q/Σ) is 2.65×10^{-9} m s^{-1} for the first pass and 3.97×10^{-9} m s^{-1} for subsequent passes.

In Figure 6.2, the curves representing PC appear as almost parallel straight lines, implying an almost linear dependence of PC on NaOCl concentration. The significant rise in production cost is mainly attributed to the cost of NaOCl purchase and wastewater treatment after NaOCl digestion. It is estimated that the use of NaOCl treatment at a concentration of 13.6 g/L active chlorine increases PC by US$1.80 /kg (US$1.50 /kg for NaOCl purchase and at least US$0.30 for

wastewater treatment). The use of NaOCl at 0.85 g/L adds only US$0.09 /kg to the total PHB production cost.

A similar simulation is also conducted for processes utilizing 2 or 4 centrifuge passes (Figures 6.3 and 6.4). Similar trends are revealed. These indicate clearly that the higher the NaOCl concentration, the higher the production cost. Homogenization has less effect on PC. The use of a low NaOCl concentration, therefore, is preferred to reduce PC. A low CDR can be improved by using a high number of homogenizer passes without significantly increasing PC.

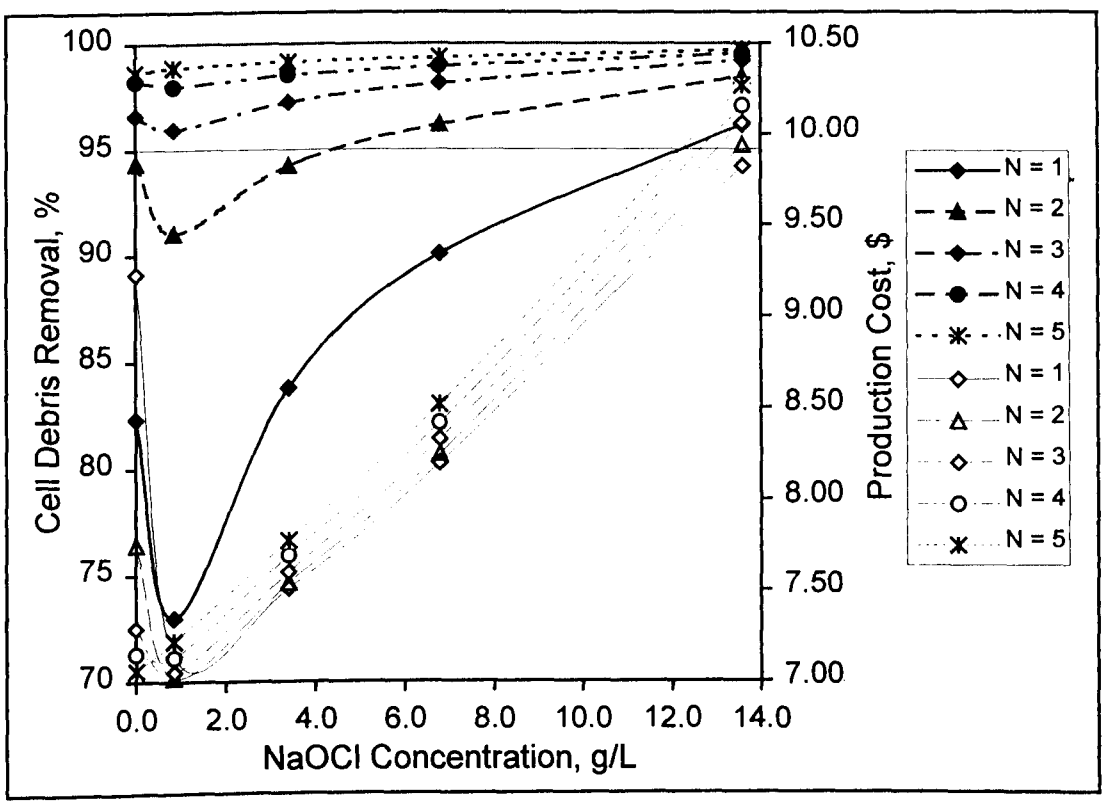

Figure 6.4. Simulation of cell debris removal (solid symbols) and production cost (open symbols) as a function of NaOCl concentration after four centrifuge passes. N is the number of homogenizer passes. The normalized centrifuge feedrate (Q/Σ) is 2.65×10^{-9} m s^{-1} for the first pass and 3.97×10^{-9} m s^{-1} for subsequent passes.

6.1.4.2. The effect of first-centrifuge feedrate on CDR and PC

Since the use of a high NaOCl concentration places a heavy toll on overall production cost, only low NaOCl concentrations are considered in the following

search for an optimal PHB recovery process. Apart from NaOCl concentration, the feedrate during the first centrifugation is another major variable affecting CDR and PC. Figure 6.5 shows the simulated CDR and PC against the first-pass feedrate with subsequent passes operated at the maximum feedrate of 3.97 $\times 10^{-9}$ m s^{-1}. The simulation assumes an NaOCl concentration of 0.85 g/L and three homogenizer passes prior to centrifugation. To reveal the developing trends of CDR and PC, the feedrate is extended beyond the region of model development to 6.18 $\times 10^{-9}$ m s^{-1}.

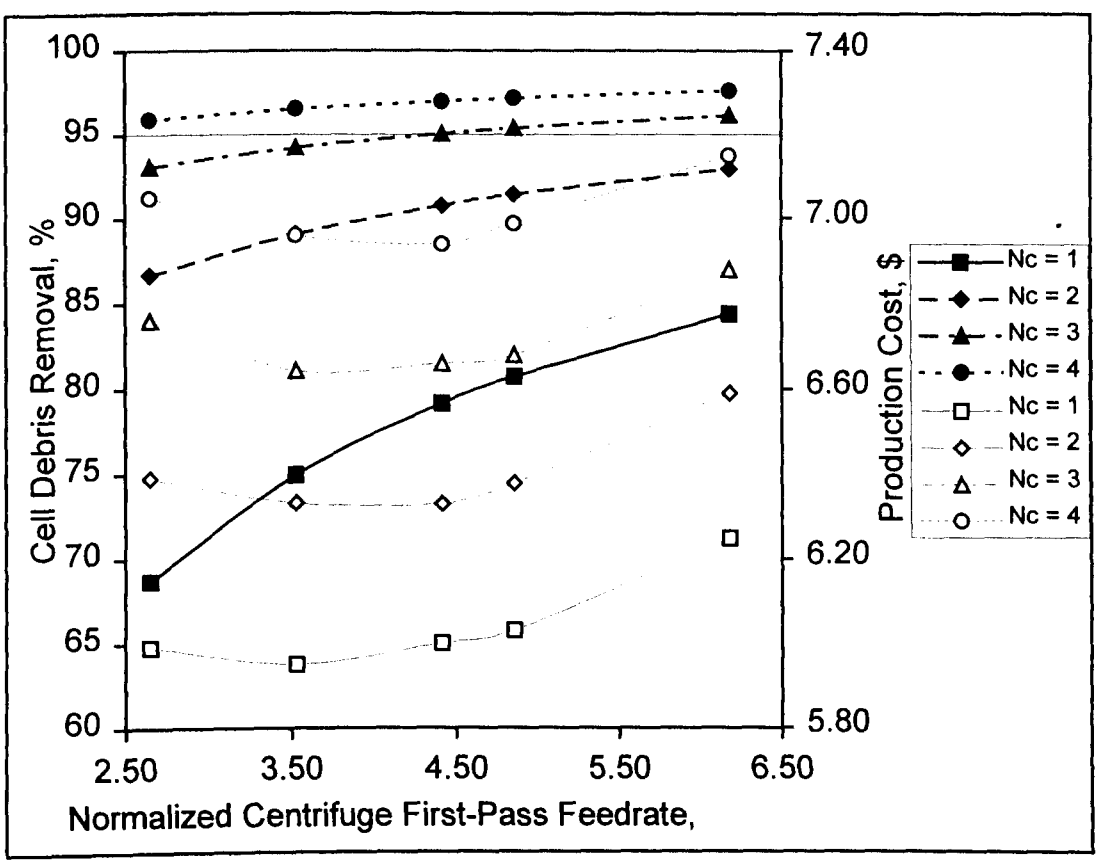

Figure 6.5. Simulation of cell debris removal (solid symbols) and production cost (open symbols) as a function of the normalized feedrate for first centrifuge pass (Q/Σ, $\times 10^{9}$ m/s). Nc is the number of centrifuge passes. Other conditions as follows: N = 3, NaOCl concentration = 0.85 g/L, centrifuge feedrate for passes 2 and 3 = 3.97 $\times 10^{-9}$ m s^{-1}.

Clearly, CDR rises smoothly as the feedrate increases from 2.65 $\times 10^{-9}$ m s^{-1} to 6.18 $\times 10^{-9}$ m s^{-1}. The benefit is reduced as the number of centrifuge passes increases. Increasing the feedrate up to 6.18 $\times 10^{-9}$ m s^{-1} is unlikely to achieve the 95% CDR target using two centrifuge passes. Further, the initial two centrifuge

passes affect CDR significantly. This is a result of the homogenate characteristics (e.g., viscosity). The high viscosity of the homogenate prior to the first centrifugation will facilitate CDR in the first centrifugation. It is also found in this simulation study that CDR is very sensitive to the change in centrifuge feedrate at high viscosity, resulting in the significant increase in CDR corresponding to the increase in feedrate. This trend becomes less obvious as the viscosity decreases in subsequent centrifugations. After the third centrifugation, additional centrifugation has less improvement on CDR. This is consistent with the previous discussion in Chapters 3 and 4 confirming the importance of the first centrifuge pass on CDR.

As illustrated in Figure 6.5, the concave curves for PC indicate an optimal feedrate between 3.53 $\times 10^{-9}$ m $s^{-1}$and 4.42 $\times 10^{-9}$ m s^{-1}. The effect of centrifugal feedrate on PC is less significant compared to that of NaOCl concentration in Figure 6.2, but is nevertheless important. It is interesting to find that increasing the number of centrifuge passes results in a PC increase of an almost fixed rate of US$0.30 /kg to US$0.40 /kg, which is significant compared with PC variation due to the change of feedrate in the simulation range. It is also larger than the increase of approximately US$0.10 /kg in PC for each additional homogenizer pass. This indicates that fewer centrifuge passes are preferred to minimize production cost.

A similar trend is revealed at an NaOCl concentration of 0 g/L (Figure 6.6). PC increases continuously as the feedrate increases from 2.65 $\times 10^{-9}$ m $s^{-1}$and 6.18 $\times 10^{-9}$ m s^{-1}, and the feedrate corresponding to the lowest PC is below the lower limit of the simulation range. The influence of feedrate on PC is obviously large relative to that at an NaOCl concentration of 0.85 g/L. Note that the corresponding PC is generally higher than that at a similar process condition but with NaOCl at 0.85 g/L, mainly as a consequence of lower PHB collection. For example, at a feedrate of 3.53 $\times 10^{-9}$ m s^{-1}, PHB collection is 95.3%, 93.6%, 92.3% and 91.2% after one, two, three and four centrifuge passes, respectively. This corresponds to a PC of US$5.95, US$6.33, US$6.64 and US$6.96, respectively,

for an NaOCl concentration of 0.85 g/L. In comparison, PHB collection is 90.6%, 87.5%, 85.0% and 84.3%, corresponding to US$6.10, US$6.57, US$7.01 and US$7.27, when NaOCl concentration is 0 g/L. Moreover, the use of NaOCl treatment facilitates the removal of other important contaminants such as DNA and protein as reported in Chapter 3. Consequently, the process without NaOCl treatment is not considered further as it does not yield a significant cost benefit. NaOCl concentration is therefore set to 0.85 g/L, and the feedrate for the first centrifugation is restricted to lie between 3.53 $\times 10^{-9}$ m s^{-1} and 4.42 $\times 10^{-9}$ m s^{-1}. These results further narrow the search space for defining an optimal PHB recovery process.

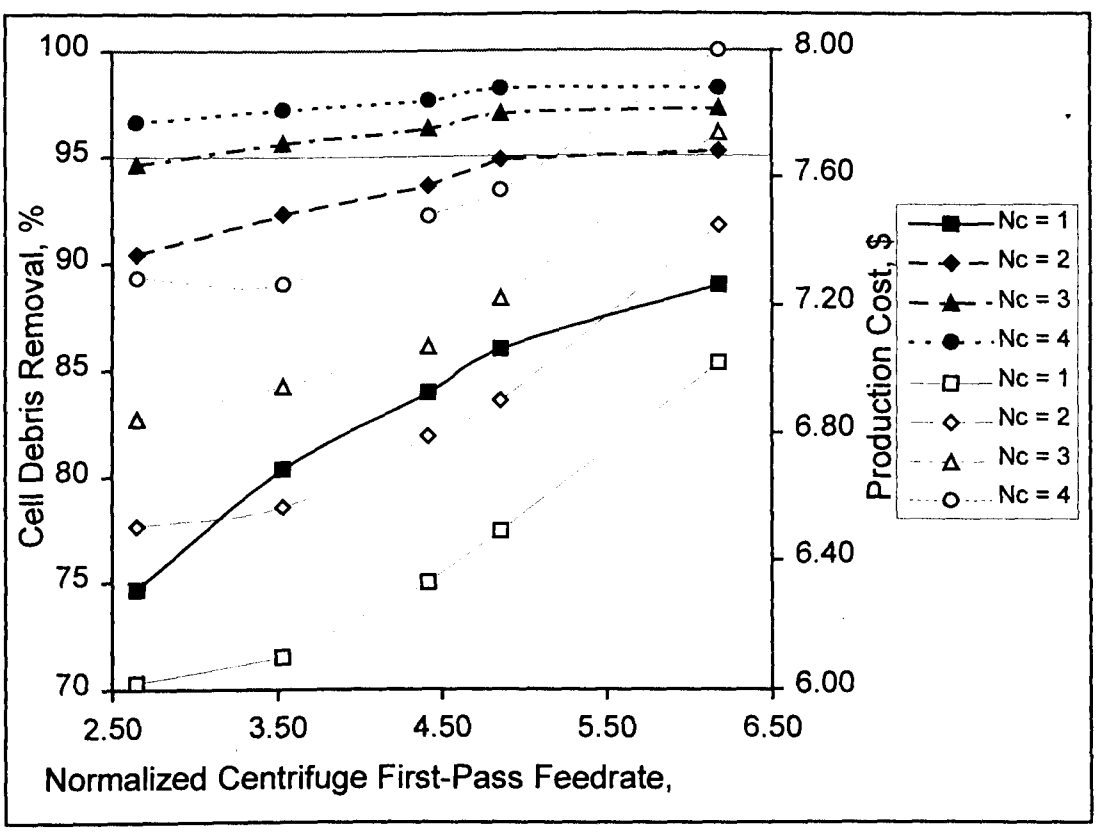

Figure 6.6. Simulation of cell debris removal (solid symbols) and production cost (open symbols) as a function of the feedrate of the first centrifuge pass ($Q/\Sigma, \times 10^9$ m/s). Nc is the number of centrifuge passes. Other conditions as follows: N = 3, NaOCl concentration = 0 g/L, centrifuge feedrate for passes 2 and 3 = 3.97 $\times 10^{-9}$ m s^{-1}.

6.1.4.3. The effect of homogenization and centrifugation

Following the earlier simulation, the remaining decision variables are the number of homogenizer and centrifuge passes. Different combinations result in different CDR and PC responses.

A strong relation exists between the number of centrifuge and homogenizer passes required, as stated above. An increase in both the number of homogenizer and centrifuge passes increases both CDR and PC. However, PC is less sensitive to increases in homogenization. As a result, a reduction in CDR due to fewer centrifuge passes can be compensated by the use of a high number of homogenizer passes, resulting in a relatively low production cost.

Figure 6.7 presents the simulation results for CDR and PC as a function of the number of homogenization passes at different centrifugation passes, under the assumption that the feedrate is 3.53×10^{-9} m s^{-1} for the first centrifuge pass and 3.97×10^{-9} m s^{-1} for subsequent passes, and the NaOCl concentration is 0.85 g/L. As shown, the CDR target of 95% can not be achieved even after 6 homogenizer passes if only one centrifuge pass is employed. The use of two centrifuge passes achieves the CDR target (96.1%) if the number of homogenizer passes is increased to 6. The corresponding overall production cost is US$ 6.57 /kg PHB. Only 4 homogenizer passes are needed to achieve a CDR of 96.8% with 3 centrifuge passes, but PC rises to US$ 6.72. The lowest production cost is therefore achieved with two centrifuge passes and six homogenizer passes.

Obviously, the use of fewer homogenizer passes and more centrifuge passes results in a steady increase in overall PC, which is consistent with the discussion above. A relatively large increase in CDR from one to two homogenizer passes is a consequence of the significant reduction in viscosity. This corresponds to a rise in PC due to low PHB collection. Viscosity, therefore, has a significant effect on both fractionation and production cost.

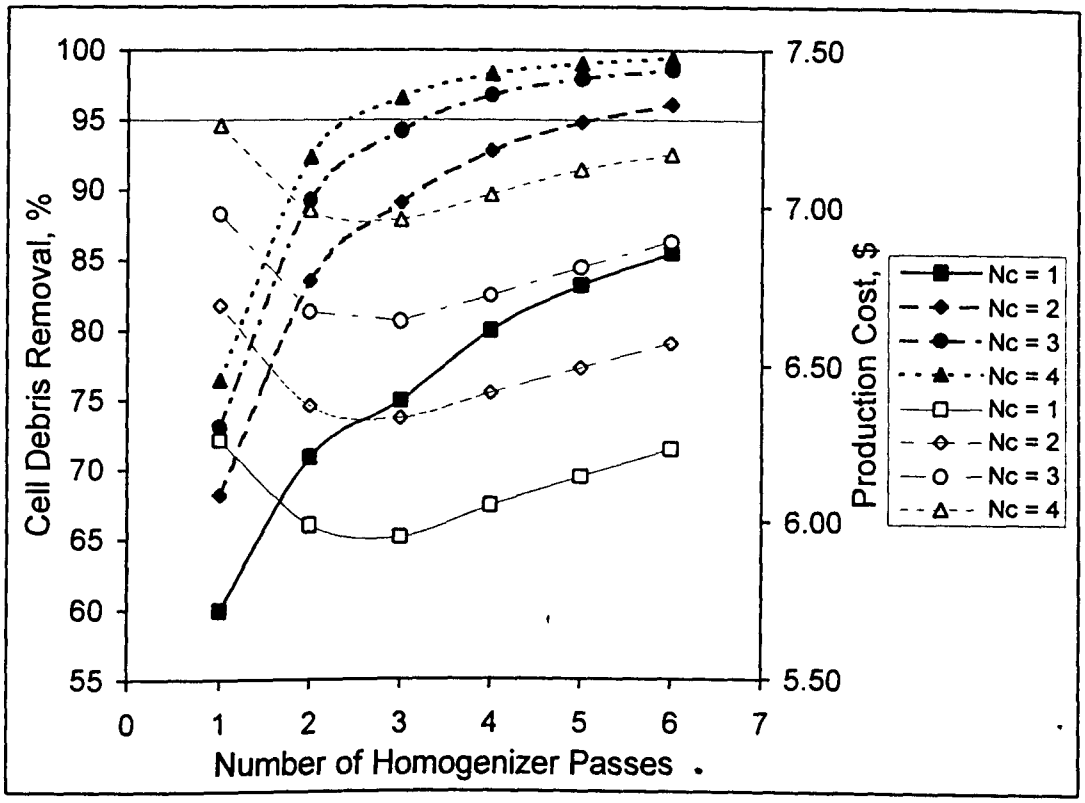

Figure 6.7. Simulation of cell debris removal (solid symbols) and overall production cost (open symbols) as a function of the number of homogenizer passes. Nc is the number of centrifuge passes. Other conditions as follows: NaOCl concentration = 0.85 g/L, centrifuge feedrate is 3.53 $\times 10^{-9}$ m s^{-1} for the first pass and 3.97 $\times 10^{-9}$ m s^{-1} for subsequent passes.

A similar simulation is also conducted at a feedrate of 4.42 $\times 10^{-9}$ m s^{-1} (Figure 6.8). The use of 5 homogenizer passes and 2 centrifuge passes achieves the CDR target of 95% at a production cost of US $6.51 /kg PHB, which is not significantly different to that for Figure 6.7.

Now we consider the process without NaOCl treatment. Figure 6.2 shows that the overall production cost will be very low if the number of homogenizer passes is higher than 2 in the case without NaOCl treatment. Figure 6.5 reveals the general trend of PC increase following the increase of the feedrate in the simulation range. The feedrate (Q/Σ) at 2.65 $\times 10^{-9}$ m s^{-1} gives the lowest PC. Figures 6.9 and 6.10 present the simulated cell debris removal and the overall production cost as a function of homogenizer passes under the assumption that feedrate for the first centrifugation is 2.65 $\times 10^{-9}$ m s^{-1} and 3.53 $\times 10^{-9}$ m s^{-1}, respectively. In Figure 6.9,

the lowest PHB overall production cost is US$6.73 with a CDR of 97.1%. In Figure 6.10, PC is US$6.58 at a CDR of 96.2%.

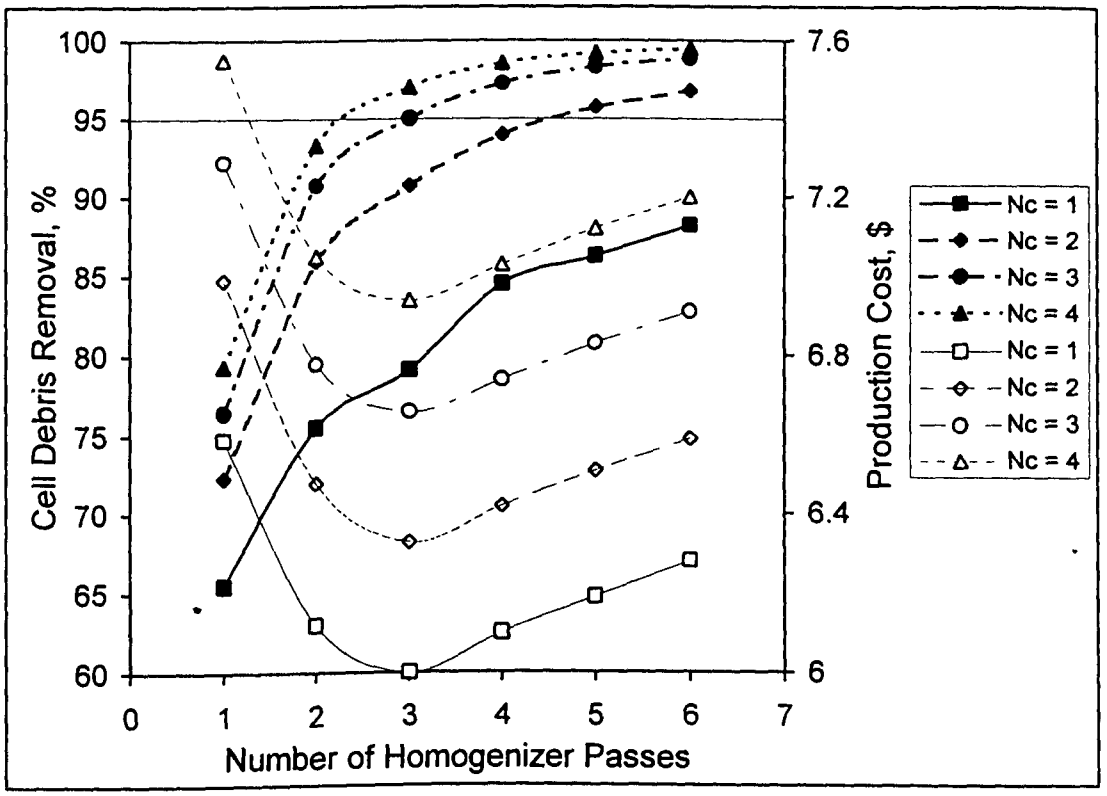

Figure 6.8. Simulation of cell debris removal (solid symbols) and overall production cost (open symbols) as a function of the number of homogenizer passes. Nc is the number of centrifuge passes. Other conditions as follows: NaOCl concentration = 0.85 g/L, centrifuge feedrate is 4.42×10^{-9} m s^{-1} for the first pass and 3.97×10^{-9} m s^{-1} for subsequent passes.

Note that the process without NaOCl treatment can also achieve the CDR target with acceptable production cost but without significant reduction in production cost. Moreover, as mentioned previously, the use of NaOCl treatment can improve the removal of other major cellular components (DNA and protein), which is also a major concern in terms of PHB quality improvement.

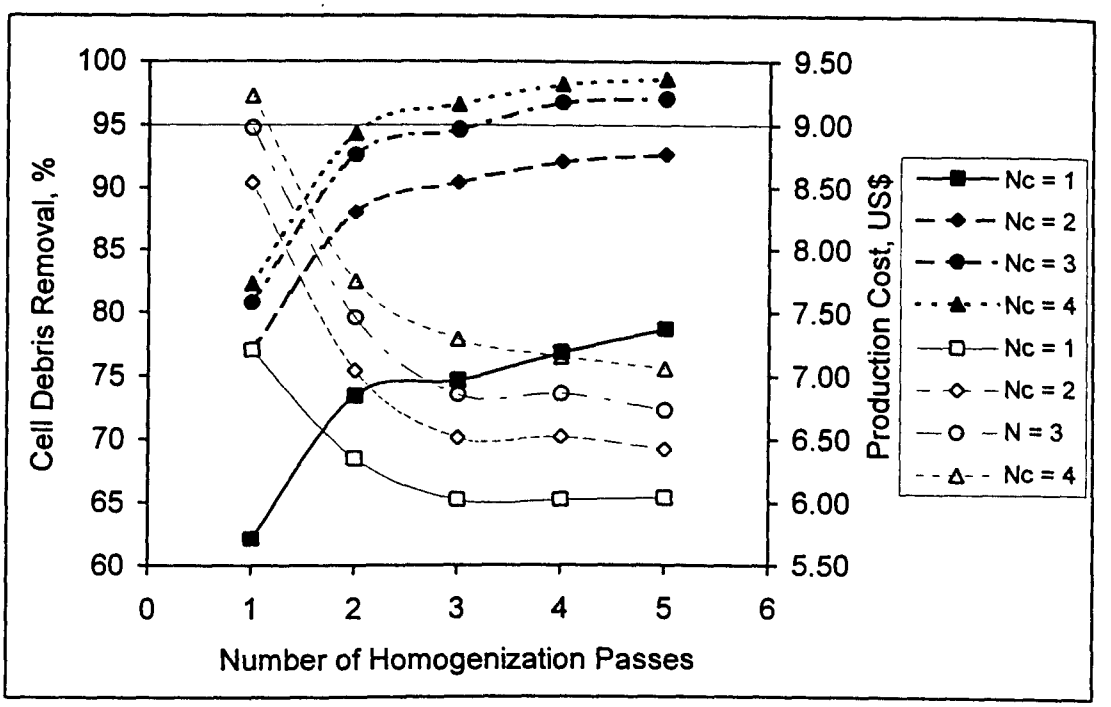

Figure 6.9. Simulation of cell debris removal (solid symbols) and overall production cost (open symbols) as a function of the number of homogenizer passes. Nc is the number of centrifuge passes. Other conditions as follows: NaOCl concentration = 0 g/L, centrifuge feedrate is 2.65×10^{-9} m s^{-1} for the first pass and 3.97×10^{-9} m s^{-1} for subsequent passes.

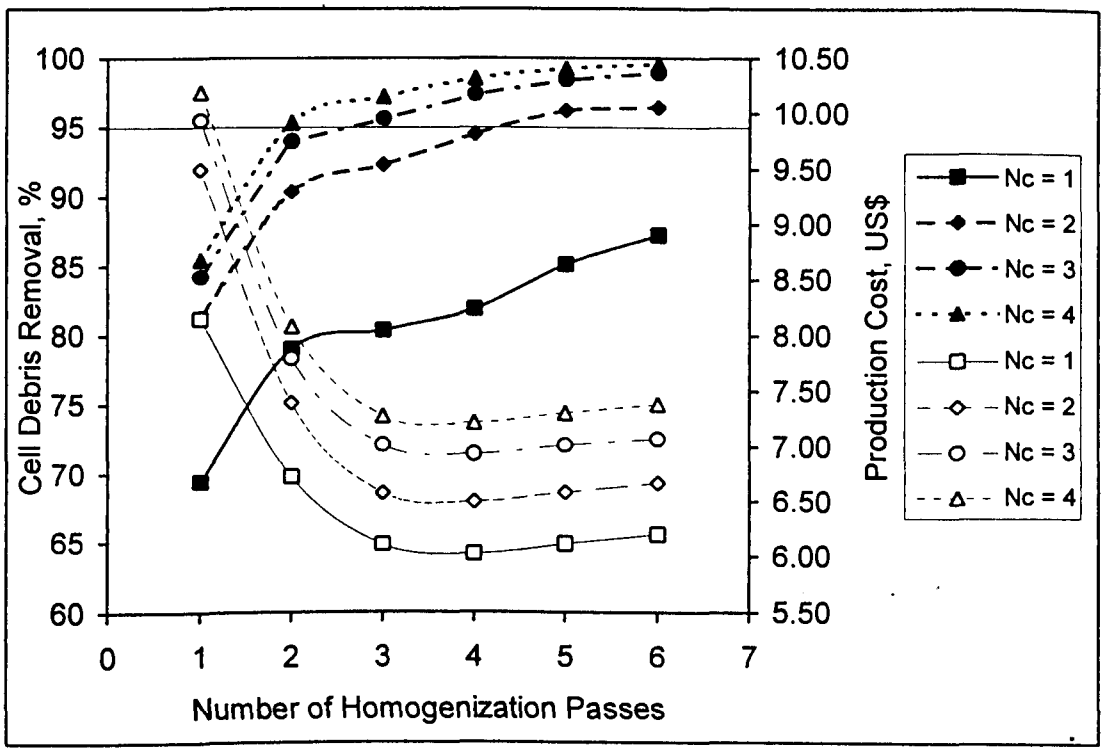

Figure 6.10. Simulation of cell debris removal (solid symbols) and overall production cost (open symbols) as a function of the number of homogenizer passes. Nc is the number of centrifuge passes. Other conditions as follows: NaOCl concentration = 0 g/L, centrifuge feedrate is 3.53×10^{-9} m s^{-1} for the first pass and 3.97×10^{-9} m s^{-1} for subsequent passes.

6.1.5. Summary: Process conditions for the optimized PHB recovery process

The preceding simulation enables a process to be selected that meets the cell debris removal target of >95% at minimum PHB production cost. The operating conditions are: cell concentration, 40 g/L; NaOCl concentration, 0.85 g/L active chlorine; treatment time, one hour; feedrate for the first centrifugation, 3.53×10^{-9} m s^{-1}; feedrate for the second centrifugation, 3.97×10^{-9} m s^{-1}; homogenizer passes, 6. The simulated PHB collection and cell debris removal during each unit operation is given in Table 6.3. A diagram of this process is also presented in Figure 6.11. The process achieves a total cell debris removal of 96.1% at a PHB recovery of 93.65%. The PHB overall production cost is estimated to be US$6.57 /kg PHB.

Table 6.3. The simulation of PHB fractionation in the optimal recovery process.

Extraction step	Simulated cell debris removal (% total)	Simulated PHB collection efficiency (% per pass)
NaOCl treatment	3.8	98.9
The first centrifuge pass	85.5	96.3
The second centrifuge pass	96.1	98.3
Overall	96.1	93.65

Since a low NaOCl concentration is employed, there is no need to consider the effect of corrosion of NaOCl on process equipment. Jack corrosion would substantially increase process cost. Furthermore, at a NaOCl concentration of 0.85 g/L active chlorine is fully consumed in less than one hour according to our experiment. Less attention is therefore needed to wastewater treatment. The duration of NaOCl treatment is very much adjustable, to suit the overall processing needs. A delay prior to centrifugation will not increase PHB loss due to excess NaOCl digestion, as would be the case at higher NaOCl concentration, thus improving process operability.

PHB production cost from this optimal recovery process is sensitive to the PHB granule size distribution. A large PHB mean diameter with narrow distribution is preferred to reduce production cost. Feed cell concentration has a strong influence on production cost as well. Increasing cell concentration can reduce the production cost. However, if the cell concentration exceeds the handling limit of the centrifuge employed, the production cost will rise because dilution is required.

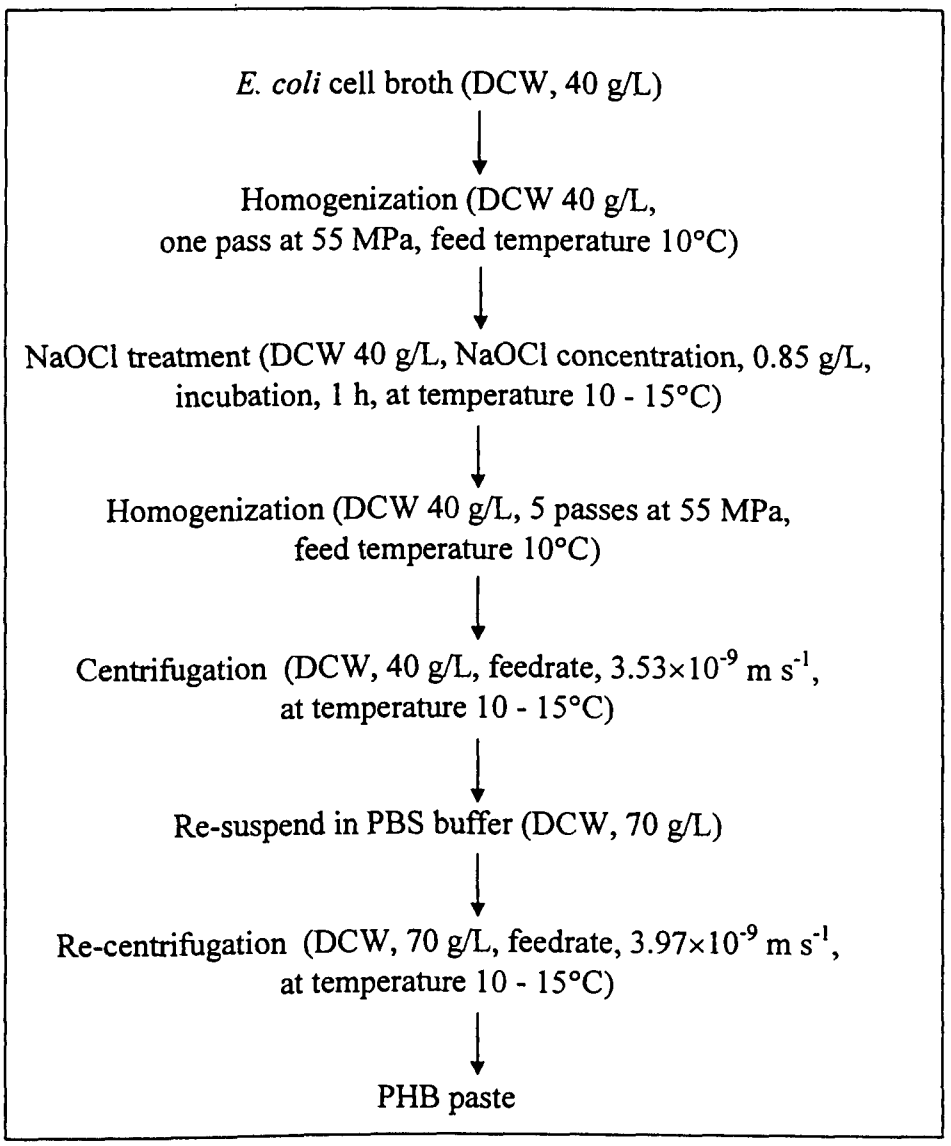

Figure 6.11. The optimal PHB recovery process defined by simulation.

6.2. EXPERIMENTAL DEMONSTRATION OF THE PROCESS

Experimental demonstration of the PHB recovery process optimized in the last section will be conducted in this section and characterized in terms of PHB purity, contaminant levels in the extracted PHB, and PHB collection efficiency during the centrifugal fractionation. Comparison will also be made between this process and the existing PHB recovery process described by Harrison (1990.

6.2.1. Definition for the optimal PHB recovery process

The optimal PHB recovery process has been defined in early sections of this chapter by simulation. The flowsheet organization and operating conditions are summarized in Figure 6.11. In consideration of the removal of nucleic acids and protein, NaOCl treatment in the optimal process is conducted between the first and second homogenizer pass based on the information obtained in Chapter 3. It does not change the final PHB fractionation performance significantly (Wong, 1996).

6.2.2. Experimental work

In this section, the experimental demonstration for the optimal PHB recovery process is described. *E. coli* cell material used in this test was from Fermentation III with a cell concentration of 43.3 g/L (DCW) and a PHB content of 60.5% w/w. The full description of the fermentation conditions is given in Section 5.4.1. 2 L of frozen cell broth stored at -18°C was thawed at 4°C before use. PBS buffer (1.37 g/L KH_2PO_4; 6.5 g/L NaCl, adjusted pH to 6.9 with NaOH) was used for the dilution of cell broth and re-suspension of the sedimented paste after the first centrifuge pass. Figure 6.12 summarizes the operating conditions.

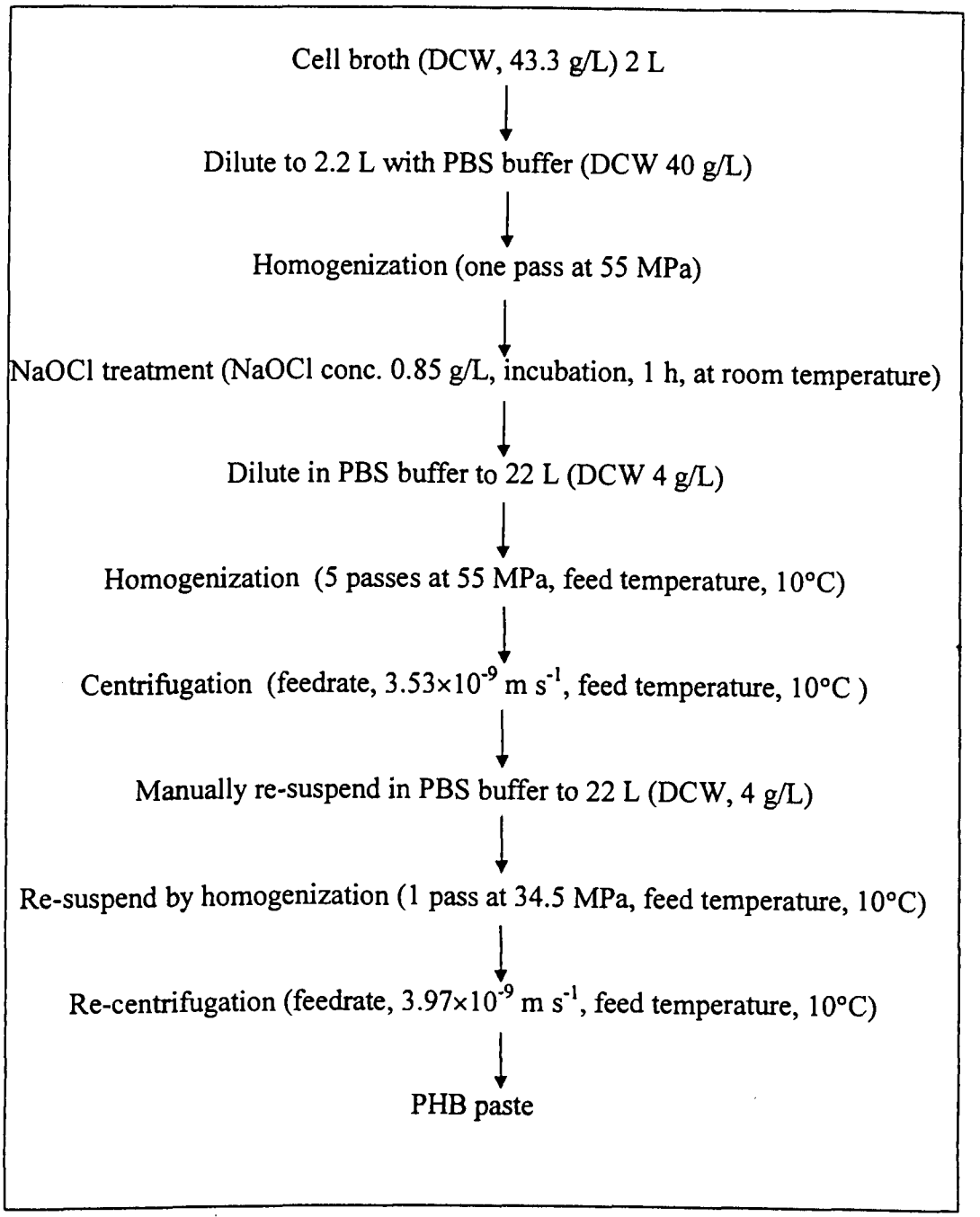

Figure 6.12. Operating conditions for demonstration of the PHB extraction process

There are some differences between the optimal process defined by simulation (Figure 6.11) and the actual experimental conditions described in Figure 6.12. Due to the limited cell material available for this experiment, the homogenate after NaOCl treatment was diluted to 4 g/L (DCW) for further processing. The dilution will not cause significant variation in recovery performance as explained in Section 6.1.3. Moreover, additional homogenization (34.5 MPa) was inserted

between the two centrifugation passes to re-suspend the PHB paste because of the particular centrifuge system used (see Appendix C for further discussion). In addition, the cell material employed was stored frozen and thawed before use, which is consistent with the simulation assumptions (Section 6.1.2). In practice, using fresh harvested cell material could bring some variation to the simulation results. The effect of freeze-thaw on cell disruption and cell debris minimization was discussed in Section 4.3.3.

During operation, samples were taken after each centrifugation pass and were lyophilized for analysis (PHB, cell debris, DNA, and total protein). A detailed description of the operating conditions for each unit operation is now presented.

Homogenization and centrifugation

Homogenization was conducted at 55.2 MPa for PHB release and cell debris comminution and 34.5 MPa for later re-suspension in an APV-Gaulin high pressure homogenizer (15 MR, CD valve). A Veronesi KLE-160 solid-bowl disc-stack centrifuge with a fixed operating speed of 8400 r.p.m. (Σ = 3775 m^2) was employed for PHB fractionation. The feed temperature was approximately 10°C for each homogenization and centrifugation pass. Cell disruption and the size distribution of the released PHB by homogenization were monitored with an Applied Imaging DCF4 Disc Centrifuge (CDS) (Gateshead, U.K.) with the standard water spin fluid scheme (Middelberg *et al.*, 1990). The density of whole cells and PHB granules were taken as 1085 kg/m^3 (Hwang, 1996) and 1260 kg/m^3 (Middelberg *et al.*, 1995), respectively. No extinction correction was applied to the data (Middelberg *et al.*, 1995). PHB collection efficiency by centrifugation was determined by comparing CDS output of feed and supernatant samples.

NaOCl treatment

After cooling to room temperature, the one pass homogenate was treated with NaOCl at a concentration of 0.85 g/L active chlorine, by the addition of fresh NaOCl stock solution. NaOCl stock solution contained 57 g/L active chlorine, diluted from the commercial sodium hypochlorite solution (Fistons technical grade, 100 g/L active chlorine) with MilliQ water immediately before treatment

(Middelberg *et al.*, 1995). The suspension was stirred using a magnetic stirrer at room temperature, and pH was maintained at 7.0 by manual addition of concentrated NaOH and HCl during the one hour incubation. Any residual NaOCl was deactivated by the addition of 0.5 M Na_2SO_3 solution titrimetrically until a negative reaction was obtained on potassium iodine-paper.

PHB Measurement

PHB in the concentrates after each centrifugation was quantitated using the GC method of Braunegg *et al.* (1978). The sample preparation and GC operating procedures are given in Section 2.6.2.

Protein and DNA Quantification

A commercial protein kit (Bio-Rad, Australia, Catalogue No. 500-0002) was used to analyze total protein remaining in the concentrate after each centrifugation. The concentration of contaminating DNA was determined by diphenylamine assay using calf thymus DNA sodium salt (Sigma, Sydney, Australia) as a standard. Samples were incubated with 7% (w/v) $HClO_4$ at 70°C for 30 min. The detailed procedure is given in Sections 2.5.1 and 2.5.2. Protein and DNA concentrations are given on a dry weight basis.

Cell Debris Quantification

Relative cell debris concentration in the concentrates after each centrifugation was approximated by SDS-PAGE with a 12% acrylamide separating gel and a 4% stacking gel, followed by densitometry of an outer-membrane protein band between 31 and 45 kDa (Wong *et al.*, 1997). Cell debris content was determined relative to the initial homogenate. The experimental procedure is detailed in Section 2.5.3.

6.2.3. Characterization of the optimized PHB recovery process

The demonstration test started with the dilution of thawed cell broth to a concentration of 40 g/L to match the condition in the defined PHB recovery process (Figure 6.11). After NaOCl treatment, the cell suspension was further diluted to 4 g/L prior to 5 homogenizer passes and two centrifuge passes, because only limited cell material was available. Since both homogenization and centrifugation performance are relatively insensitive to cell concentration, the dilution would not result in big variations in the final PHB recovery and cell debris removal compared to the simulation. Incorporating extra homogenization at a low operating pressure (34.5 MPa) in between two centrifugation passes aimed to improve the re-suspension of the PHB paste recovered from the solid bowl disc-stack centrifuge. Its contribution to cell debris size reduction and thus PHB fractionation can be negligible. At production scale, extra homogenization is not necessary for re-suspension as explained in Section 6.1.1.

Figure 6.13 shows particle size distributions of whole cells and homogenates before centrifugation determined with the analytical disc centrifuge. The mean diameters D_{50} of PHB granules and the whole cells are approximately 0.844 μm and 1.91 μm, respectively. With reference to Table 6.4, these sizes match the sizes used in the simulation very well. This is, of course, expected as the starting material was previously characterized. Clearly, three homogenization passes at 55 MPa are sufficient to achieve complete PHB release.

Table 6.4. Actual particle size of the thawed cell broth from Fermentation III between the simulation value and that measured in the demonstration test.

		Simulation	Actual Test
Whole Cells	D_{50} (μm)	1.93	1.91
	w (μm)	0.210	0.201
PHB	D_{50} (μm)	0.865	0.844
	w (μm)	0.111	0.103

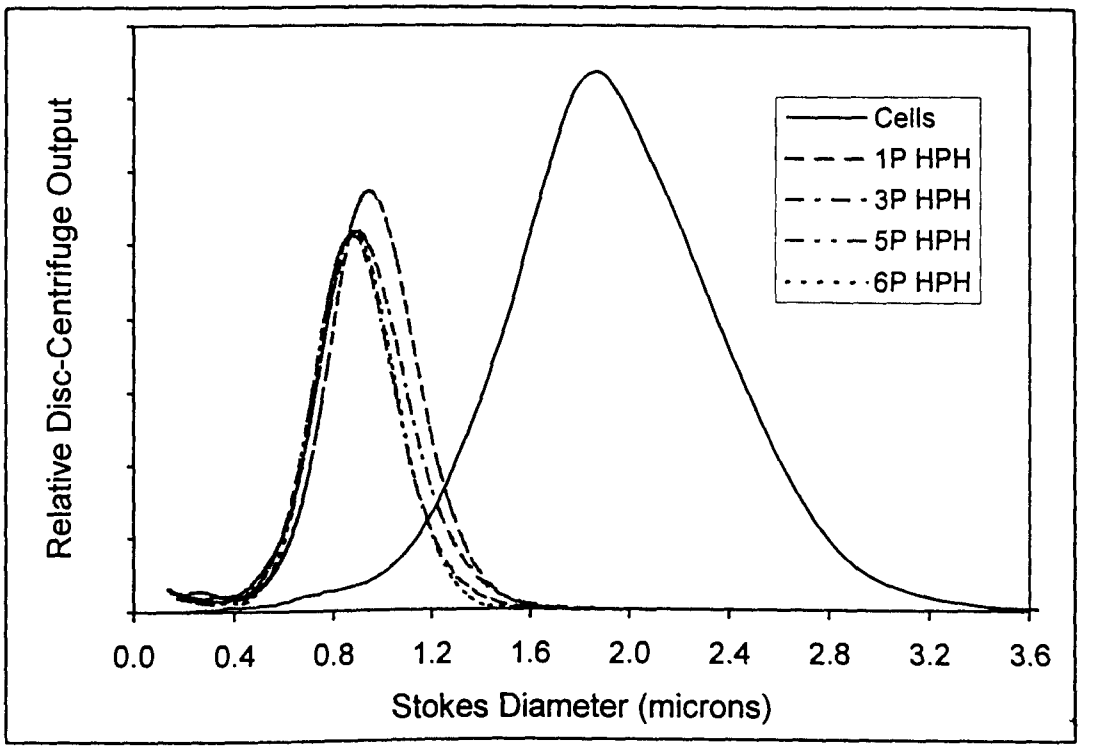

Figure 6.13. Size distribution of homogenizer feed (Cells) and homogenate samples after one (1P HPH), three (3P HPH), five (5P HPH) and six (6P HPH) homogenizer passes.

PHB breakage under extensive homogenization was observed for the cells from Fermentation I and further discussion about PHB stability was given in Section 4.3.1. Due to the lack of models, the possible change in PHB size during homogenization was ignored in the simulation study. In this case, PHB granules are relatively stable under the conditions tested (Figure 6.13). This suggests multiple homogenization will not reduce PHB granule size and hence collection efficiency. The difference in PHB breakage under homogenization from different fermentations may relate to PHB formation conditions during the fermentation, and also to different pretreatments, as postulated in Section 4.3.1. Moreover, NaOCl treatment at the optimized conditions did not result in significant PHB granule degradation as shown in Figure 6.13. PHB degradation was reported at the same NaOCl concentration (0.85 g/L active chlorine), but at a considerably lower cell concentration (Middelberg *et al.*, 1995).

The composition of PHB paste recovered in the extraction process is detailed in Table 6.5. The simulation results of PHB collection efficiency and cell debris

removal from Table 6.4 are also included for comparison. PHB with a purity of 93.6% w/w (dry basis) was achieved after two centrifuge passes. This is comparable to that obtained by Harrison (1990) for *A. eutrophus*. The overall PHB collection efficiency was about 91.8% which is much higher than that in Process C (Section 3.3.4, 79.6%), even though the feedrate for both centrifugation passes increased greatly. It is seen that the actual PHB collection efficiency in each unit operation matches the simulated result very well. Due to the large PHB granule size and low viscosity, PHB collection is high in both centrifugation passes. For the second centrifugation, both simulated and experimental values exceed 98% providing justification of a high feedrate for re-centrifugation (Section 6.1.3). This indicates that the grade-efficiency model used in the simulation (Equation 4.12) describes PHB settling behavior well, even though the parameters k and n were obtained for smaller protein inclusion bodies from recombinant *E. coli* (0.4μm). This suggests that the parameters in the grade-efficiency model (k and n) may be approximately particle size-independent for the centrifuge system used. Differences between the simulated and the experimental PHB recoveries in Chapter 4 are therefore probably due to errors in the assumed suspension viscosity.

In terms of cell debris removal, the simulation matches the experimental result very well. The first centrifugation pass was predicted to remove 85.5% by volume of cell debris, and 73.1% on the second pass. Actual values for cell debris removal were 88.4% and 59.5% on the first and second passes, respectively. The importance of the first centrifuge pass on cell debris removal is again clear. The lower cell debris removal efficiency in the second centrifugation results from reduced viscosity and a shift in the debris size distribution to larger sizes following the first centrifuge pass. The total cell debris removal (95.3%) (Table 6.5) is comparable to that in Process C (96.5%) (Table 3.1).

Protein and nucleic acids (DNA and RNA) are still major concerns in terms of contaminant removal, even though their removal was not considered in the simulation due to the lack of models. The first centrifuge pass reduced protein content to 14 % of the initial value, compared to a 36.4% result for Process C

(Section 3.3.4). This confirms the effectiveness of NaOCl treatment on protein removal. A similar result was obtained in Process B (Section 3.3.3), where 15.6% of total protein removal was achieved by the first centrifugation. A further 91% removal of protein was achieved in the second centrifugation. Complete protein removal was not achieved after the second centrifuge pass under the specified conditions, but the remaining protein (0.32% w/w) is much below the acceptable limit of 2% reported to result in considerable PHB browning during heat processing (Harrison, 1990).

Similarly, approximate 77% of DNA was removed in Process C after the first centrifugation, compared with about 89% of total DNA removal achieved in the optimized process. The hindered removal of DNA during NaOCl treatment observed in Process B did not occur possibly as the consequence of the. subsequent extensive homogenization improving their solubilisation. This was further decreased through the second centrifugation by another 89% yielding a final DNA content of 0.06% by weight. This indicates that the optimal process is also more efficient at removing DNA than Process C. NaOCl treatment and extensive homogenization may result in the total liberation and destruction of nucleic acids (DNA and RNA).

It is interesting to note that PHB loss and cell debris digestion are negligible during NaOCl treatment (1.3% and 3.5%, respectively). Cell debris size minimization by NaOCl treatment at 0.85 g/L is also less effective than that achieved by one homogenization pass (simulation result not shown). NaOCl treatment in this PHB recovery process is therefore not included primarily for cell debris digestion as originally proposed in Section 1.3. Rather, its benefit in separation primarily derives from viscosity reduction. This improves the handling properties and particularly the centrifuge feedrate, thus minimizing production cost. Furthermore, NaOCl treatment under the sepcified conditions significantly enhances protein and DNA removal, although this is a benefit not foreseen by simulation.

A possible limitation of the current test is the low cell concentration employed. At high concentration, problems may arise due to the increased viscosity and other factors in Section 6.1.3. Using high feed concentration affects PHB recovery, and attainable PHB collection could be lower than the value in this experiment. However, high concentration does not affect the relative recovery rate of cell debris and PHB greatly according to Wong (1996). It remains a question whether acceptable removal of protein and DNA can be achieved at high cell concentration. It is difficult to predict at this stage as no data are available about protein and DNA removal in centrifugal fractionation.

Table 6.5. Results of PHB fractionation from the optimized recovery process

Extraction Process	PHB (% w/w)	Protein (% w/w)	DNA (% w/w)	Simulated cell debris removal (%)	Cell debris removal (%)	Simulated PHB collection efficiency (% per pass)	PHB collection efficiency (% per pass)
Cell material	60.5	26.4	4.91	0	0		
NaOCl treatment				3.8	3.5	98.9	98.7
The first pass centrifugation	89.2	3.6	0.53	85.5	88.4	96.3	94.5
The second pass centrifugation	93.6	0.32	0.06	96.1	95.3	98.3	98.4

6.2.4. Conclusion

The optimized PHB recovery process was demonstrated and characterized at semi-industrial scale. A good agreement between predicted and experimental results, in terms of cell debris removal and PHB collection, was obtained. PHB with a final purity of 93.6% (w/w) was obtained. DNA and protein removal efficiency were also higher than in the preliminary investigation in Chapter 3 (Process C). NaOCl plays an important role in DNA and protein removal, and in viscosity reduction. The corresponding production cost estimate was US$6.57 /kg PHB.

6.3. SENSITIVITY ANALYSIS AND FURTHER DISCUSSION

The optimal PHB recovery process that meets the fractionation performance target at minimum cost has been defined by simulation and characterized experimentally in Sections 6.1 and 6.2, respectively. In this section, a breakdown of PHB overall production cost is given, and the sensitivity of PHB fractionation and the corresponding production cost to some key parameters is also discussed.

6.3.1. The effect of PHB size distribution on PHB production cost

PHB granule size is one of the major factors affecting PHB collection efficiency during centrifugal fractionation. The size-dependent particle collection can be described by a grade efficiency curve (Equation 4.12). The simulation presented in Section 6.1.4 was based on an assumed PHB granule size (D_{50} = 0.865μm, w = 0.111μm). It was assumed that the size distribution was unchanged throughout the whole fractionation process. In contrast, cell debris size was regulated through multiple homogenization and NaOCl treatment, with the aim of enlarging the size difference between the two particulate species, thus facilitating fractionation.

PHB granule size can be highly variable, and depends greatly on the fermentation conditions and host-vector characteristics. A sensitivity study is thus conducted to investigate the effect of PHB size on PHB fractionation efficiency and overall production cost. The analysis is based on the optimized process involving six homogenizer passes, two centrifuge passes, and NaOCl treatment at a concentration of 0.85 g/L active chlorine (see Figure 6.11 for detailed processing conditions). Figure 6.14 presents the simulated PHB collection and production cost as a function of PHB mean diameter with the distribution width fixed at 0.11 μm. The result suggests that mean diameter has a significant impact on overall collection efficiency and hence the corresponding production cost. Overall PHB recovery obtained is only 44% if the mean diameter is 0.40 μm, corresponding to

a production cost of US$13.2 /kg. When the mean diameter exceeds 1.0 μm, PHB recovery and the corresponding production cost tend to stabilize, more than 97% of the PHB will be recovered at a production cost of less than US$ 6.30 /kg.

A similar analysis is conducted to investigate the effect of size-distribution width (Figure 6.15). PHB mean diameter is fixed at 0.80 μm. Note that w has less influence on collection efficiency and production cost than D_{50}. A decrease of about 9% in overall PHB collection is observed when w increases from 0.06 μm to 0.16 μm, while PHB cost rises about US$ 0.60 /kg. The simulation suggests that a large PHB granule size with a narrow size distribution is preferred to maximize collection efficiency and thus lower production cost.

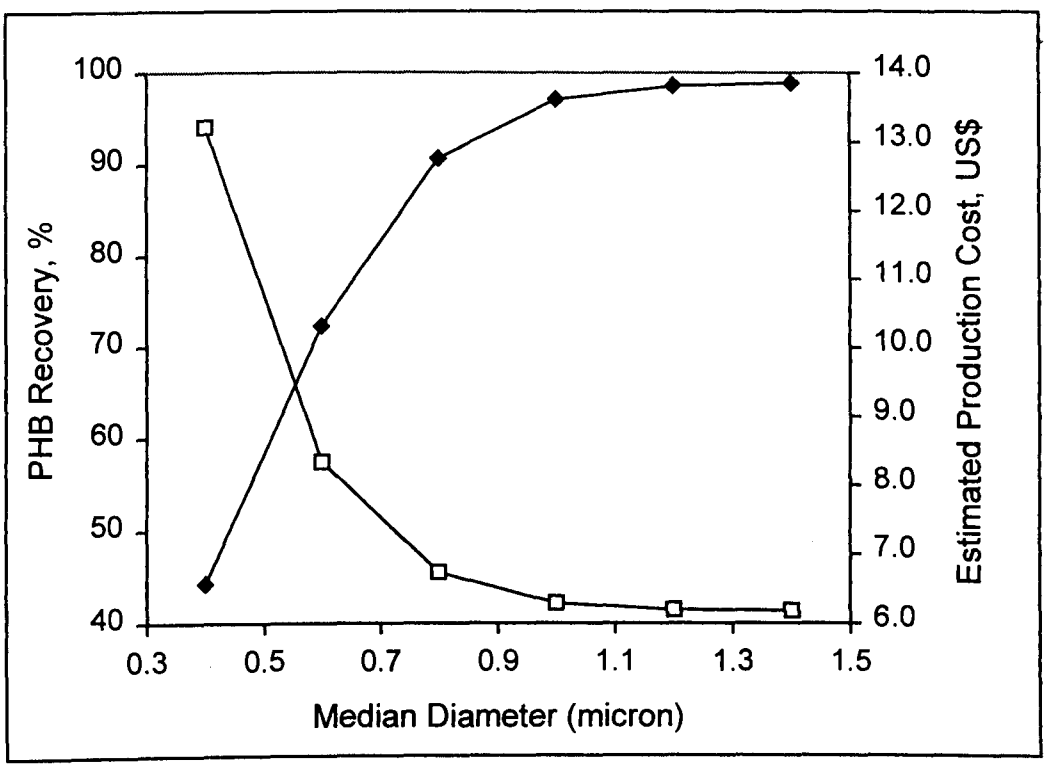

Figure 6.14. Simulation results of PHB recovery (solid symbols) and the estimated production cost (open symbols) as a function of PHB mean diameter with distribution width fixed at 0.11 μm. Operating conditions are the same as that described in Figure 6.11.

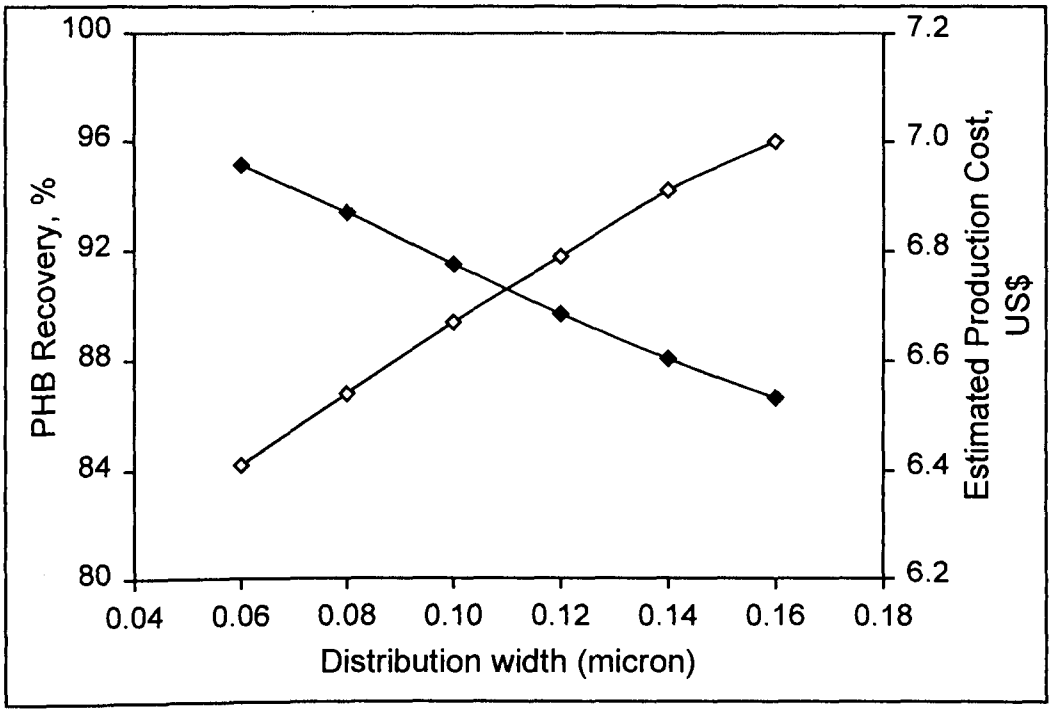

Figure 6.15. Simulation results of PHB recovery (solid symbols) and estimated production cost (open symbols) as a function of PHB distribution width, with mean diameter fixed at 0.80 μm. The operating conditions are the same as that described in Figure 6.11.

PHB granule size is dictated by fermentation conditions. As reviewed in Section 1.4.2, granules from recombinant *E. coli* and *A. eutrophus* have different size distributions because of different PHB accumulation mechanisms. PHB accumulated in *A. eutrophus* is highly homogeneous in size with a relatively low distribution width due to the two-stage accumulation mechanism. PHB from recombinant *E. coli* is highly heterogeneous because of one-stage accumulation control, resulting in a broad distribution width. However, PHB from recombinant *E. coli* has a large mean diameter because of its accumulation mechanism. Middelberg *et al.* (1995) reported the size of PHB granules from recombinant *E. coli* in a range of 1.13 μm to 1.25 μm, which is larger than that from wild-type microorganims. PHB synthesized in *A. eutrophus* or *Bacillus megaterium* were spherical with a diameter of 0.10 to 0.80 μm (Lafferty *et al.*, 1988).

The dominant effect of PHB median diameter compared to the distribution width suggests that the reduction in PHB production cost will result by increasing granule size. The production cost for *E. coli* will be lower than for *A. eutrophus*.

It has been found that PHB granule size in *A. eutrophus* was strongly influenced by granule-associated phasin protein (Wieczorek *et al.*, 1995; Wieczorek *et al.*, 1995). If it becomes possible to increase PHB granule size in recombinant *E. coli* through genetic manipulation, further significant improvement in the recovery will result with a consequent reduction in production cost.

6.3.2. The effect of cell concentration on production cost

As indicated in Section 6.1.3, feed cell concentration for homogenization and centrifugation in the recovery process has a significant impact on overall PHB production cost. The simulation conducted in Section 6.1.4 limited the cell concentration to 40 g/L (DCW). As the available cell concentration is 43.3 g/L from Fermentation III, choosing 40 g/L enabled experimental demonstration of the simulated process (Section 6.2). Since much work has been done to obtain a high cell concentrations in fermentation (e.g., a cell concentration of 101.4 g/L (DCW) was reported with a PHB concentration of 81.2 g/L using recombinant *E. coli* (Lee, 1996)), there is quite a wide range of cell concentrations to choose as a feed cell concentration in the recovery process. The use of low cell concentration increases process volume due to dilution, and thus processing scale. In practice, the concentration limits are set by each unit operation to ensure the acceptable performance. The maximum concentration for homogenization, for example, is determined by the practical constraints due to high feed viscosity, because disruption efficiency is insensitive to the feed concentration (Kleinig *et al.*, 1995).

The following simulation study therefore investigates the effect of cell concentration on PHB fractionation and production cost. Figure 6.16 illustrates overall cell debris removal and production cost as a function of cell concentration. The simulation is based on the process defined in Section 6.1.4 with processing conditions presented in Figure 6.11. The suspension viscosity is affected by cell concentration. The viscosity increases following the increase in cell concentration. The value of viscosity in the simulation is approximated by using an empirical model (Middelberg, 1989). In the simulation, it is also assumed that cell debris size reduction by homogenization is not affected by the change in cell

concentration in the range of 10 g/L to 50 g/L (Kleinig *et al.*, 1995). The effect of NaOCl treatment on cell debris size reduction is estimated by the models developed in Chapter 5 (Table 6.1).

Figure 6.16. Simulation of cell debris removal (solid symbols) and the estimated

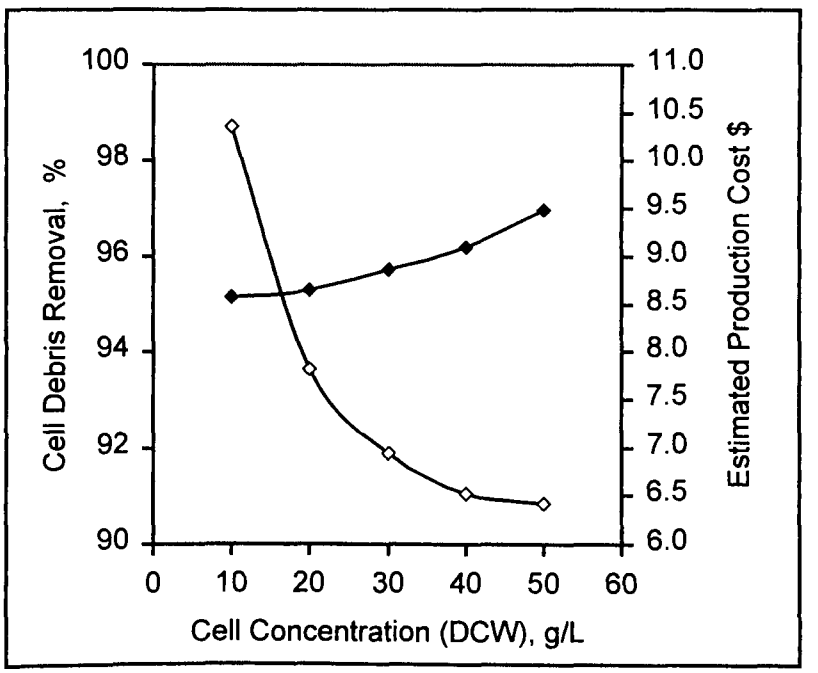

production cost (open symbols) as a function of cell concentration, with PHB mean diameter and distribution width fixed at 0.87 μm and 0.11 μm, respectively.

The influence of cell concentration on PHB fractionation is mainly due to the viscosity. Since the large and dense PHB granule is less sensitive to the change in viscosity, the overall PHB recovery decreases only slightly following the increase in cell concentration. Cell debris removal was enhanced by 2% as the concentration increases from 10 g/L to 40 g/L. It is consistent with the observation of Wong (1996) that the use of high feed cell concentration decreases centrifuge performance slightly.

Cell concentration is of vital importance to production cost as shown in Figure 6.16. Significant decrease in production cost occurs in the high cell concentration range with only slight increase in cell debris removal. The production cost reduced from US$10.36 /kg to $6.95 /kg as the cell concentration increases from 10 g/L to 30 g/L. Since the cell concentration increases to 30 g/L, further increases result only in a slight cost reduction. In the estimation of the overall

production cost, the maximum cell concentration of 50 g/L (DCW) for the first pass centrifugation is assumed. Dilution is required before centrifugation if this limit is exceeded. Therefore, high cell concentration (>50 g/L) attained from fermentation does not benefit the downstream recovery process in terms of fractionation performance improvement and production cost reduction because of the need for dilution. It will raise the production cost slightly if the dilution is considered in the cost estimation (ven Wegen *et al.*, 1998).

In conclusion, feed cell concentration in PHB recovery process is of vital importance to production cost. Increasing cell concentration can reduce the production cost without compromising PHB recovery and cell debris removal. However, if the cell concentration exceeds the handling limit of the centrifuge employed, dilution is required and this will raise the production cost.

6.3.3. PHB production cost allocation

The estimated overall production cost for the optimal process (Figure 6.11) was US$6.57 /kg PHB on the basis of the economic analysis of van Wegen *et al.* (1998). Under the same assumption, the breakdown of overall cost and allocation to associated production unit operations were conducted. Figure 6.17 and Table 6.6 present the breakdown of the total capital cost and the operating cost to each unit operation section of the assumed PHB production plant, while Figure 6.18 shows the overall PHB production cost allocated to each unit operation.

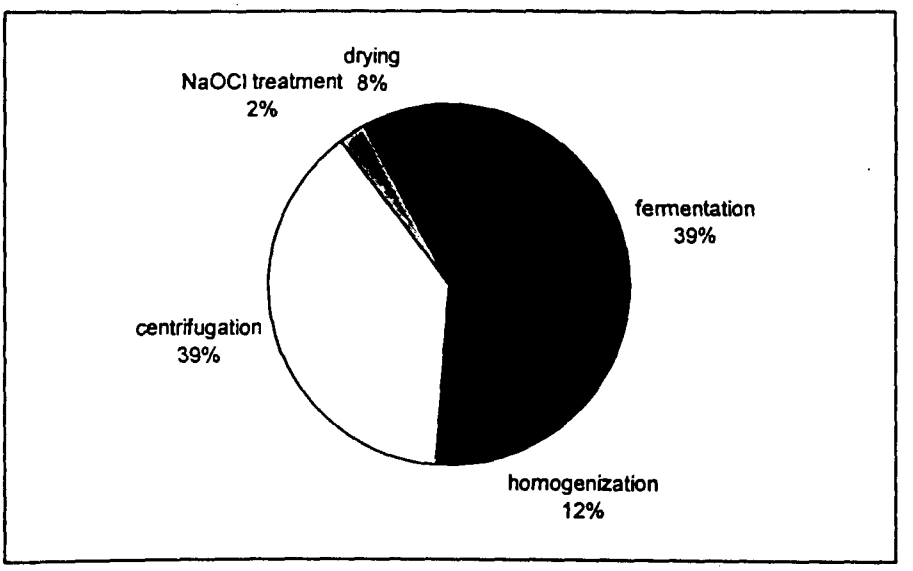

Figure 6.17. The breakdown of capital cost to each unit operation

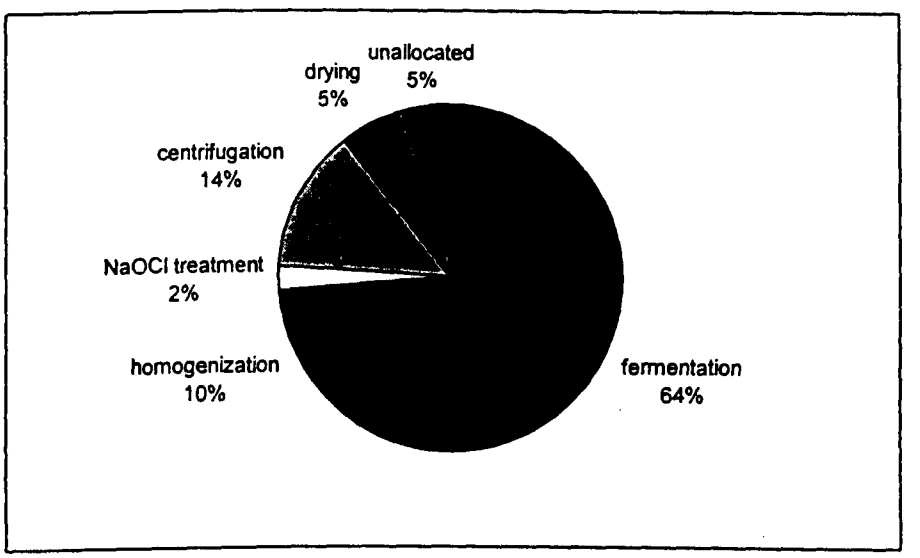

Figure 6.18. The breakdown of overall PHB production cost to each unit operation

Table 6.6. Operating cost breakdown for each unit operation (US$)

	steam	electricity	chemicals	waste	maintenance, labour etc.
fermentation	$237.3k	$1,437k	$14,767k		$1087k
homogenization		$2,084k			$326k
centrifugation		$273k			$1,070k
NaOCl treatment		$2.4k	$425k	$103k	$64k
drying	$912k				$217
unallocated				$975k	$676k

This shows clearly that fermentation contributes almost two thirds of the overall PHB production cost (64%), whereas one third of total cost is allocated to the recovery process (32%). The cost of homogenization is mainly due to the electricity assumption (64% of the total contribution). Since 6 homogenization passes were involved in the optimized recovery process (Figure 6.11), the average operating cost for each homogenization pass is about US$0.08 /kg PHB. In terms of the centrifugation, about 13.6% of the overall cost is allocated, of which the capital cost is a fraction of 67.8%. The average operating cost for one centrifugation pass is about US$0.15 /kg PHB in the total PHB production cost of US$6.57. Only US$0.15 in PHB cost (2.4% of the overall production cost) is due to the NaOCl treatment.

6.3.4. Sensitivity analysis and further reduction of PHB production cost

On the basis of the optimized PHB recovery process, a sensitivity analysis is conducted to reveal potential for further reduction in overall production cost. In terms of the recovery process, a reduction in PHB cost can be achieved through the following changes:

- Increasing the feed cell concentration for homogenization and the first centrifugation from 40 g/L to 50 g/L, the total cost drops by US$0.25. It confirms again the significance of cell concentration on overall production cost as discussed in Section 6.3.2. A cell concentration of 50 g/L is the assumed maximum capacity of the centrifuge in simulation. An increase in feed concentration to 50 g/L does not generate significant variation in the PHB fractionation according to the simulation.

- The attainable overall PHB recovery affects the cost greatly. If PHB recovery rises from 93.65% (simulation value) to 94.65%, the cost could drop by US$0.09. This can be simply achieved by slightly

increasing the PHB granule size according to the discussion on Section 6.3.1.

- Increasing the first pass centrifuge feedrate from 3.53 $\times 10^{-9}$m s^{-1} to 3.97 $\times 10^{-9}$m s^{-1} drops the attainable PHB recovery by about 1% according to the simulation, keeping the overall cost about the same. Further increase in feedrate results in an increase in production cost.

- Decreasing NaOCl concentration from 0.85 g/L to 0.425 g/L can drop the cost by US$0.06. This decrease does not affect cell debris removal and PHB collection. Its influence on the removal of other cellular components is unknown.

6.3.5. Conclusion

The economic analysis shows PHB recovery process optimized in this study allocates less than one third of the overall production cost, with 10.3%, 13.6% and 2.4% of the total cost to each unit operation: homogenization, centrifugation and NaOCl treatment, respectively. The feed cell concentration for homogenization and centrifugation is very sensitive to the overall PHB cost. PHB cost is also dependent greatly on the attainable PHB granule size, which is determined by the fermentation conditions. The cost for PHB recovery from *E. coli* will generally be lower than from *A. eutrophus* due to the large PHB size. PHB production cost reduction can be achieved by increasing feed cell concentration and the PHB granule size.

Chapter 7

OVERALL CONCLUSIONS

The impediment of expanding PHB production and market as a bulk plastic material is its high production cost. The process for intracellular PHB recovery is the major cost involved. The recovery can also significantly alter the properties of the final product and their use.

PHB recovery methods reported involve either the solubilisation of PHB using selective solvents or digestion of the insoluble non-PHB cellular components, followed by solid-liquid fractionation by centrifugation. These approaches are generally hard to scale up, and raise the overall production cost. In this thesis, an alternative approach was considered using homogenization and centrifugation as the basic unit operations for PHB recovery from recombinant *E. coli*. A PHB recovery process involving homogenization, centrifugation and NaOCl treatment was developed with acceptable PHB quality and competitive production cost. The work conducted and findings made during this study are summarized in the following.

7.1. PHB host --recombinant *E. coli* cells

The PHB host cell employed in this study was a non-K-12 *E. coli* strain Topp1 [F', *proAB*, *lacI*^{q}, ZΔ *M15*. In*10*, (*tet*^{R})] transformed with plasmid pJM9123. Plasmid pJM9123 contains the *phb* operon originally isolated from *A. eutrophus*. Fed-batch fermentation was employed in this study to achieve a high cell concentration with high PHB content using the pH-stat method. Unlike *A. eutrophus*, PHB accumulation in recombinant *E. coli* does not require the limitation of an essential nutrient source and no induction is needed. The expression system used a semi-defined medium containing yeast extract to improve PHB production. Glucose was the major carbon source. Three

fermentations were conducted and cell concentration (DCW) obtained were around 42.0 g/L with the maximum PHB content of 60.5%. This provided cell material for downstream recovery study.

7.2. A summary of PHB recovery methods

There are generally two approaches to achieve the PHB recovery. One is to solubilize PHB using specific PHB solvents followed by precipitation (i.e., solvent extraction) and another is to solubilize non-PHB cell material and maintain PHB granules intact followed by solid-lipid fractionation (i.e., differential digestion). The dispersion of hypochlorite and chloroform is the combination of solvent extraction and differential digestion. A common disadvantage of these methods is the need to use a large amount of chemical, thus raising production cost. Scale up of these methods has not been attempted.

The only industrial method reported for PHB recovery from *A. eutrophus* involves the release of PHB granules by homogenization, enzymatic and detergent digestion of non-PHB cell material, followed by extensive washing and centrifugation. A high cell disruption efficiency is obtained using homogenization and the stability of PHB granules remains. However, the contaminants levels in the recovered product are over the limits which causes PHB thermal decolouration. Foreign contaminants are also introduced because of the insufficient removal of the chemicals after their use. This approach raises total production cost and still yields a relatively low quality PHB, which is unacceptable for many applications.

7.3. Homogenization

Cell disruption by homogenization

Homogenization was confirmed to be efficient for PHB release from recombinant *E. coli*, while maintaining PHB granule stability. Similar to *A. eutrophus*, the initial stage of cell disruption may involve a point break in the cell wall envelope, and some cell wall remaining associated with PHB, which can be removed

through further homogenization. The stability of PHB granules under homogenization may depend on fermentation and the treatment prior to homogenization. Extensive homogenization may result in some breakage of PHB granules.

Cell debris comminution by homogenization

The cell debris size was reduced with each homogenization pass. The efficiency of debris size comminution varied with the strain, cell growth phase and whether or not cells are induced. The Boltzmann function describes the debris size distribution for *E. coli* homogenate containing PHB granules very well, and the parameters D_{50} and w can be obtained by regression of the experimental data. The debris size distribution after homogenization can be predicted as a function of the number of homogenization passes using the cell debris size reduction model developed by Wong (1996), if the initial whole cell distribution and the cell disruption efficiency of each homogenizer pass are known. The value of the model parameters α, a_c and a_d depend upon cell material and homogenizer operation conditions and design, and can be obtained by the regression of the experimental data. CSA was a good means for the measurement of cell debris size.

Cell debris comminution by homogenization was affected by the strain and fermentation conditions. *E. coli* containing PHB granules has a weaker cell wall structure than *A. eutrophus* because of different genetic background, and a small debris size is expected. Cell growth phase and PHB content are also the factors affecting available debris size under homogenization. Large cells with high PHB content will generate large debris size after multiple-pass homogenization, while small cells with small PHB granules give small debris size. Cell debris size is also affected by the pretreatment. Freeze-thaw causes extensive cell wall damage and gives small debris size compared to the untreated cells.

7.4. NaOCl treatment

NaOCl Digestion

NaOCl digests *E. coli* cellular material effectively, generally due to the combination of oxidation and alkaline saponification. pH is one of the major factors affecting NaOCl digestion. Both acidic and alkaline conditions tend to improve digestion capacity, but differentiates in PHB and cell debris digestion rate. NaOCl at a reasonable concentration can reduce DNA transforming activity, yield broken DNA strands and reduce DNA molecular weight. Incorporating NaOCl treatment into the PHB recovery process after homogenization improves not only cell debris removal but also reduces homogenate viscosity, which facilitating the handling of cell suspensions and improving PHB recovery. The removal of other intracellular contaminants such as nucleic acids and protein is also improved.

Cell debris micronization

NaOCl was efficient on *E. coli* cell debris size reduction. NaOCl at a mild condition (0.85 g/L active chlorine) showed less effect on cell debris micronisation compared with NaOH (0.2 M), but both NaOCl and NaOH are more effective than multiple homogenization in terms of debris size reduction. PHB aggregation was observed in PHB homogenate after NaOH treatment.

Modelling cell debris digestion by NaOCl treatment

E. coli cell debris micronization by NaOCl treatment was modelled using response surface methodology with the pH fixed at 7.0. After NaOCl treatment, the attainable cell debris size can be expressed as a function of cell concentration (B), NaOCl concentration (C) and the number of homogenizer passes prior to treatment (cell concentration, 0-43.3 g/L; NaOCl concentration, 0-13.6 g/L; the number of homogenization, 1-3). Cell concentration and NaOCl concentration are the major factors affecting debris size, and their effect can be well summarized by the ratio B/C. In other words, the ratio of B/C is the major determinant. A strong trade-off between cell and NaOCl concentration exists.

Since both NaOCl treatment and homogenization are attributed to cell debris micronization, the contribution of NaOCl treatment becomes significant at a low cell concentration, while the use of homogenization is more effective at a high cell concentration. The modelling study also indicates that in a PHB-containing *E. coli* homogenate, the sole use of NaOCl treatment or NaOCl treatment combined with few homogenization passes does not generate a sufficient debris size reduction, while maintaining a high PHB stability. To achieve a high level of debris size reduction in order to ensure the efficient fractionation of PHB and cell debris, other unit operations such as multiple homogenization have to be involved in association with NaOCl treatment, especially when a high cell concentration is employed. It is suggested that the NaOCl digestion method described in Section 1.3.1 is unlikely to be adapted in a scale-up process as it causes either significant PHB degradation or insufficient cell debris removal.

The cell debris digestion model can also find application for the analysis of other intracellular inclusion bodies recovery if the product of interest is resistant to the degradation of NaOCl treatment.

7.5. Centrifugal fractionation

The particle fractionation in a centrifuge is size-dependent, which can be described by a grade-efficiency curve. A grade efficiency model based on an assumption of plug flow with lateral mixing in a disc-stack centrifuge describes the fractionation of PHB granule and cell debris in a homogenate well.

For a given PHB homogenate system, PHB collection decreases concomitantly with the increase of cell debris removal as the centrifuge feedrate increases. With an increase in PHB granule size, PHB collection will become less sensitive to feedrates. At a fixed centrifuge feedrate, multiple homogenization prior to centrifugation effects cell debris removal. However, the collection efficiency of PHB remains stable due to the insensitive PHB size under homogenization. The relationship of cell debris removal and PHB collection with centrifugation

feedrate and the number of homogenizer passes prior to centrifugation is illustrated by simulation.

Both experimental work and simulation study indicate that cell debris removal from PHB homogenate is effected by repeated centrifugation while a reasonable PHB collection efficiency is ensured. Since the majority of cell debris removal is achieved by the first centrifugation, the feedrate of the first centrifugation and the number of homogenizer passes prior to the centrifugation are the major factors in terms of optimizing the efficiency of overall PHB collection and cell debris removal.

Cell debris removal in a centrifugal fractionation depends greatly on the available debris size. Significant cell debris micronization prior to the first centrifugation pass is required to maximize debris removal. The reduction of cell debris size can be achieved by multiple homogenization and NaOCl treatment.

7.6. Simulation and optimization of PHB extraction process

The basic PHB recovery process

A basic process comprising homogenization, NaOCl treatment and centrifugation was defined based on preceding studies. Due to the process complexity and the number of variables involved, the simulation range of some variables was restricted while other variables were fixed. The operational variables were restricted to four: NaOCl concentration, the feedrate of the centrifugation, and the number of homogenization passes and the number of centrifugation passes. Feed cell concentration for homogenization and centrifugation was 40 g/L (DCW). The key response variables were the cell debris removal and PHB collection

Cell debris micronization in PHB recovery process

Both homogenization and NaOCl treatment are needed for the cell debris micronization in the PHB fractionation process. The use of high NaOCl concentration has a great influence on cell debris removal through cell debris micronization and the homogenate viscosity reduction, but causes PHB

degradation and yields a low product recovery. Comparatively, homogenization has less effect on cell debris micronization and almost no impact on PHB degradation. Homogenization and NaOCl treatment differ also remarkably in their operation cost. The use of NaOCl at high concentration raises overall PHB production cost significantly due to the purchase cost of NaOCl and the subsequent wastewater treatment. The combination of multiple homogenization and NaOCl treatment at a low concentration can achieve the sufficient cell debris micronization and minimize the PHB loss through degradation at a reasonable expense, while the NaOCl treatment on the reduction of suspension viscosity can be functioned.

Process simulation

The simulation was to determine the necessary process operating conditions to achieve a target product purity at minimum production cost. A cell debris removal target of 95% was set as the key goal of process optimization. PHB collection and cell debris removal in the defined basic process were simulated as a function of key operational variables and the corresponding production cost was then estimated. The process which met a performance target at minimum cost was selected as optimal. The optimal process was then demonstrated at pilot scale, and characterized in terms of PHB collection and the removal of non-PHB cellular material in each unit operation.

In the simulation, the debris size reduction model by homogenization and NaOCl treatment was used. Cell debris and PHB fractionation was simulated with a grade efficiency curve for a disc stack centrifuge. The simulation matches the experimental results reasonably well.

7.7. A process for PHB recovery from recombinant *E. coli*

The optimized PHB extraction process

A process for PHB recovery from recombinant *E. coli* was developed involving 6 passes homogenization, 2 passes centrifugation and NaOCl treatment at a concentration of 0.85 g/L active chlorine before the second homogenization.

Demonstration of the optimal process was achieved at pilot scale. The process yielded 95.3% cell debris removal and 91.8% PHB recovery. Good removal of DNA and protein was also achieved (0.06% and 0.32% final concentration, respectively). An overall production cost of US$6.57/kg PHB was estimated, which is considerably lower than the advertised cost of US$ 16/kg PHB (Lee, 1995a). This process can be extrapolated to industrial scale for the recovery of PHB.

Sensitivity analysis

The performance of the optimal PHB extraction process is PHB size dependent. The demonstration and overall production cost estimation are based on the PHB granules with mean diameter of 0.86 μm and distribution width of 0.11 μm. A large PHB size with narrow size distribution is recommended to achieve a high PHB collection at a low overall PHB production cost without compromising cell debris removal and PHB quality.

Feed cell concentration of homogenization and centrifugation is also of vital importance on PHB overall production cost. Simulation and production cost estimation conducted are based on a cell concentration of 40 g/L. Further reduction on overall PHB production cost can be achieved by increasing the cell concentration. At a low cell concentration, significant increase in production cost results with almost no improvement in PHB collection and quality.

Production allocation

The economic analysis shows PHB recovery process optimized in this study allocates less than one third of overall PHB production cost (32%), and fermentation contributes two third of the total production cost (64%). Three major unit operations, homogenization, NaOCl treatment and centrifugation, allocate 10.3%, 2.4% and 13.6% of the total production cost, respectively.

7.8. Areas of interest for further research

NaOCl treatment on protein and nucleic acid removal

Protein and nucleic acid (DNA and RNA) are the major contaminants as they give PHB an offensive odour and cause decolouration during thermal processing. In this study NaOCl treatment was found to facilitate the removal of protein and nucleic acid in the PHB homogenate. A good removal of protein and nucleic acid was achieved in the optimized extraction process which incorporates NaOCl treatment (at a concentration of 0.85 g/L active chlorine) into the process. Further work is required to investigate protein and nucleic acid removal at different NaOCl treatment conditions and minimize the levels of remaining protein and nucleic acid in harvested PHB paste.

Cell debris size distribution

The Boltzmann function describes the debris size distribution of *E. coli* containing PHB granules disrupted by homogenization. However, statistical analysis indicates that the Boltzmann function was not good enough to describe the size distribution of *E. coli* cell debris digested by NaOCl. A new size distribution model needs to be explored.

PHB granule size and stability

PHB collection efficiency in centrifugation is size dependent and large PHB granules facilitate PHB fractionation. The formation of large PHB granules needs to be investigated. Since PHB size is primarily affected by fermentation, fermentation condition needs to be manipulated to obtain large PHB granules. Large PHB granules can also be produced by aggregation or flocculation. The aggregation agents must be very selective to PHB to avoid the incorporation of non-PHB components.

PHB stability during homogenization and centrifugation is of some concern. It determines the suitability for the process scale-up. PHB breakage not only represents PHB yield loss but also complicates the fractionation process. Since

PHB granules or PHB aggregates experience extensive shear during homogenization, the stability of PHB or PHB aggregates is worth further study.

Suspension viscosity

The suspension viscosity is one of the key factors affecting cell debris and PHB fractionation. The reduction of suspension viscosity by NaOCl treatment (at a NaOCl concentration of 0.85 g/L active chlorine) was identified and its contribution to PHB fractionation was emphasized in this thesis. The assumption of viscosity reduction by NaOCl treatment at different NaOCl concentration made in the simulation study was reasonable as the simulation matches the experimental results well. Similar to cell debris size reduction, viscosity reduction was affected by NaOCl concentration, cell concentration and homogenization. A modelling study of viscosity is needed to present better simulation results.

REFERENCES

Agerkvist, I and Enfors, S. -O. 1990. Characterisation of *E. coli* cell disintegrates from a bead mill and high pressure homogenizers. ***Biotech. Bioeng.*** **36**: 1083-1089.

Akita, S.; Einaga, Y.; Miyaki, Y. and Fujita, H. 1976. Solution properties of poly(D-β-hydroxybutyrate). 1. Biosynthesis and characterization. ***Macromolecules.*** **9**: 774-780.

Ambler, C.M. 1959. The theory of scaling up laboratory data for the sedimentation type centrifuge. ***J. Biol. Microbiol. Technol. Eng.*** **1**: 185-205.

Anderson, A.J. and Dawees, E.A. 1990. Occurrence, metabolism, metabolic role, and industrial uses of bacterial polyhydroxyalkanoates. ***Microbiol. rev.*** **54**(4): 450-472.

Anderson, K.W.; Grulke, E. and Gerhardt, P. 1984. Microfiltration culture process for enhanced production of rDNA receptor cells of *Escherichia. coli*. ***Bio/Technology.*** **2**: 891-896.

Arronsson, G. and Zadorecki, P. 1987. Scaling down for production scale up of downstream processing. ***Aust. J. Biotechnol.*** **1**(2): 20.

Ballard, D.G.H.; Holmes, P.A. and Senior, P.J. 1987. Formation of polymers of β-hydroxybutyric acid in bacterial cells and a comparison of the morphology of growth with the formation of polyethylene in the solid state. **In**: ***Recent advances in mechanistic and synthetic aspects of polymerization.*** Fontanille, M. and Guyot, A. (eds.). 215: 293-314. Reidel (Kluwer) Publishing. Co., Lancaster, U.K.

Barham, P.G.; Keller, A.; Otum, E.L. and Holmes, P.A. 1984. Crystallization and morphology of a bacterial thermoplastic: poly-β-hydroxybutyrate. ***J. Mater. Sci.*** **19**: 2781-2794.

Barham, P.J. 1990. Physical properties of poly (hydroxybutyrate) and poly (hydroxybutyrate-co-hydroxyvalerate) **In**: ***Novel biodegradable microbial polymers.*** Edwin A.D (ed.). Kluwer Academic Publishers.

Barnard, G.N. and Sanders, J.K.M. 1988. Observation of mobil poly(β-hydroxybutyrate) in the storage granules of methylobacterium AMI by *in vivo* ^{13}C-NMR spectroscopy. ***FEMS. Microbiol. Lett.*** **23**(1): 16-18.

Barnard, G.N. and Sanders, J.K.M. 1989. The poly-β-hydroxybutyrate granules *in vivo.* ***J. Biol. Chem.*** **264**(6): 3286-3291.

Belter, P.A.; Cussler, E.L. and Hu, W.S. 1988. Cell disruption **In**: ***Bioseparations: Downstream processing for Biotechnology***. John Wiley (New York). 77-98.

Berger, E.; Ramsay, B.A.; Ramsay, J.A. and Chavarie, C. 1989. PHB recovery by hypochlorite digestion of non-PHB biomass. ***Biotechn. Techni.*** **3**(4): 227-232.

Bio-Rad Laboratories, 1997. Instruction Manual for Bio-Rad Protein Assay.

Bitton, G. 1980. Introduction to environmental virology. Wiley, New York.

Bitton, G. 1994. Wastewater microbiology. Wiley-liss, New York.

Bradford, M.M. 1976. A rapid and sensitive method for the quantitation of microgram quantities of protein utilizing the principle of protein-dye binding. ***Anal. Biochem.*** **72**: 248-254.

Braunegg, G.; Sonnleitner, B.; and Lafferty, R.M. 1978. A rapid gas chromatographic method for the determination of poly-β-hydroxybutyric acid in microbial biomass. ***European J. Appl. Microbiol. Biotechnol.*** **6**: 29-37.

Burton, K. 1956. A study of the conditions and mechanism of the diphenylamine reaction for the colorimetric estimation of deoxyribounucleic acid. ***Biochemistry*** **62**: 315-323.

Burton, K. 1968. Determination of DNA concentration with diphenylamine. **In**: ***Methods in Enzymology***, Grossman, L. and Moldave, K. (eds) **12B**: 163-166.

Byrom, D. 1987. Polymer synthesis by microorganisms: Technology and economics. ***TIBTECH***. **15**: 246-250.

Byrom, D. 1992. Production of poly-β-hydroxybutyrate : poly-β-hydroxyvalerate copolymers. ***FEMS Microbiol. Rev.*** **103**: 247-250.

Chang, H.N. 1994. Biodegradable plastics and biotechnology. **In:** ***Proceedings of 3rd Asia-Pacific Biochemical Engineering Conference***, Singapore. June 1994. 24-30.

Dennis, D. 1991. Improved production of poly-beta-hydroxybutyrate in transformed *Escherichia coli*. PCT No: PCT/US91/03547.

Doi, Y.; Kawaguchi, Y.; Nakamura, Y. and Kunioka, M. 1989. Nuclear magnetic resonance studies of poly(3-hydroxybutyrate) and polyphosphate metabolism in *Alcaligenes eutrophus*. ***Appl. Environ. Microbiol.*** **55:** 2932-2938.

Doi, Y. 1990. Microbial Polyester. ***VCH Publishers Inc.*** New York.

Doi, Y.; Kumagai, Y.; Tanahashi, N. and Mukai, K. 1992. Structural effects on biodegradation of microbial and synthetic poly(hydroalkanoates). **In**:

Biodegradable polymers and plastics Vert, M. (ed.). Royal Society of Chemistry. G.B.

Dwivedi, C.P.; Imanaka, T.and Aiba, S. 1982. Instability of plasmid-harboring strain of *E. coli* in continuous culture. ***Biotechnol. Bioeng.*** **24**: 1465-1468.

Fidler, S. and Dennis, D. 1992. Polyhydroxyalkanoate production in recombinant *Escherichia coli*. ***FEMS Microbiol. Lett.*** **128**: 231-236.

Fieschko, J.; Ritch, T.; Bengston, D.; Fenton, D. and Mann, M. 1985. The relationship between cell dry weight concentration and culture turbidity for a recombinant *E. coil* strain producing high levels of human alpha interferon analogue. ***Biotechnol. Prog.*** **1**: 205-208.

Finar, I.L. 1963. The fundamental principles **In***:* ***Organic chemistry*** (vol. 1), published by Longmans. 451-456.

Frampton, G.A. 1963. Evaluating the performance of industrial centrifuges. ***Chem. Process. Eng.*** **August**: 402-412.

Griebel, R.J.; Smith, Z. and Merrick, J.M. 1968. ***J.M. Biochem.*** **7**: 3676.

Grubisic, Z.; Remp, P. and Benoit, H. 1967. A universal calibration for gel permeation chromatography. ***Polym. Lett.*** **5**: 753-759.

Guerrero, R.; Mas, J. and Pedros-Alio, C. 1984. Buoyant density changes due to intracellular content of sulfur in chromatium warmingii an chromatium vinosum. ***Arch. Microbiol.*** **137**: 350-356,

Haas, C.N.; Kerallus, M.G.; Brnclch, M.D. and Zapkin, M.A. 1986. Alteration of chemical and disinfectant properties of hypochlorite by sodium, potassium and lithium. ***Environ. Sci. Technol.*** **20**(8): 822-826.

Haenggi, U.J. 1990. Pilot scale production of PHB with *Alcaligenes latus*. **In**: ***Novel Biodegradable Microbial Polymers***, 65-70. (Dawes E.A. ed.). Kluwer Academic Publishers.

Hahn, S.K.; Chang, Y.K.; Kim, B.S.; Lee, K.M. and Chang, H.N. 1993. The recovery of poly(3-hydroxybutate) by using dispersion of sodium hypochlorite solution and chloroform. ***Biotechnol. Techn.*** 7(3): 209-212.

Hahn S.K.; Chang Y.K.; Kim B.S. and Chang H.N. 1994. Optimisation of microbial poly(3-hydroxybutyrate) recovery using dispersion of sodium hypochlorite solution and chloroform. ***Biotech. Bioeng.*** **44**: 256-261.

Hahn, S.K.; Chang, Y.K. and Lee, S.Y. 1995. Recovery and characterization of poly(3-hydroxybutyric acid) synthesized in *Alcaligenes eutrophus* and recombinant *Escherichia coli*. ***Appl. Environ. Microbiol.*** **61**(1): 34-39.

Hahn, S.K. and Chang Y.K. 1995. A themogravimetric analysis for poly(3-Hydroxybutyrate) quantification. ***Biotechnol. Techniq.*** 9(12): 873-878.

Harrison, S.. L. 1990. The extraction and purification of poly-β-hydroxybutyrate from *Alcaligenes eutrophus*. PhD Thesis, University of Cambridge, Cambridge, UK.

Harrison, S.T.L.; Chase, H.A.; Dennis, J.S. 1991. The disruption of *Alcaligenes eutrophus* by high pressure homogenization: Key factors involved in the process. ***Bioseparation***. **2**: 155-166.

Harrison, S.T.L.; Chase, H.A.; Amor, S.R.; Bonthrone, K.M. and Snaders, J.K.M. 1992. Plasticization of poly(hydroxybutyrate) *in vivo*. ***Int. J. Biol. Microl.*** **14**: 50-56.

Hayatsu, H.; Pan, S. and Ukita, T. 1971. Reaction of sodium hypochlorite with nucleic acids and their constituents. ***Chem. Pharm. Bull. Jpn***. **19**: 2189-2192.

Higgins, J.J.; Lewis, D.J.; Daly, W.H.; Mosqueiro, F.G.; Dunnill, P and Lilly, M.D. 1978. Investigation of the unit operations involved in the continuous flow isolation of β-galactosidase from *Escherichia coli*. ***Biotech. Bioeng.*** **20**: 159-182.

Hoare, M. and Dunnill, P. 1989. Biochemical engineering challenges of purifying useful proteins. ***Phil. Trans. R. Soc. Lond.*** **B 324**: 497-507.

Holmes, P.A. 1985. Applications of PHB---a microbially produced biodegradable thermoplastic. ***Phys. Technol.*** **16**: 32-36.

Holmes, P.A. and Lim, G.B. 1990. Separation process. United States Patent: 4,910,145.

Hopkins, M. 1991. Cell disruption and protein recovery **In**: ***Purification and analysis of recombinant proteins***. Seetharam, R. and Sharma, S.K. (eds). NY.

Hwang, S.O. 1996. Effect of inclusion bodies on the buoyant density of recombinant *Escherichia coli*. ***Biotechnol. Techn.*** **10**(3): 157-160.

Kawaguchi, Y. and Doi, Y. 1990. Structure of native poly(3-hydroxybutyrate) granules characterized by X-ray diffraction. ***FEMS microbiol. lett.*** **70**: 151-156.

Kawaguchi, Y. and Doi, Y. 1992. Kinetics and mechanism of synthesis and degradation of poly(3-hydroxybutyrate) in *Alcaligenes eutrophus*. ***Macromolecules*** **25**: 2324-2329.

Kemnitzer, J.K.; McCarthy, S.P. and Gross, R.A. 1992. Poly(β-hydroxybutyrate) stereoisomers: a model study of the effects of stereochemical and morphology variables on polymer biological degradability. ***Macromolecules***. **25**: 5927-5934.

Kim, B.S.; Lee, S.Y. and Chang, H.N. 1992. Production of poly-β-hydroxybutyrate by fed-batch culture of recombinant *E.coli*. ***Biotechnol. Lett.*** **14**(9): 811-818.

Kim, B.S.; Lee, S.C.; Lee, S.Y.; Chang, H.N.; Chang, Y.K. and Woo, S.I. 1994a. Production of poly(3-hydroxybutyric-co-3-hydroxyvaleric acid) by fed-batch culture of *Alcaligenes eutrophus* with substrate control using on-line glucose analyser. ***Enzyme Microb. Technol.*** **6**: 556-561.

Kim, B.S.; Lee, S.C.; Lee, S.Y.; Chang, H.N.; Chang, Y.K. and Woo, S.I. 1994b. Production of poly(3-hydroxybutyric acid) by fed-batch culture *of Alcaligenes eutrophus* with glucose concentration control. ***Biotechnol. Bioeng.*** **43**: 892-898.

Kleinig, A.R.; Mansell, C.J.; Nguyen, Q.D.; Badalyan, A.; Middelberg, A.P.J. 1995. Influence of broth dilution on the disruption of *Escherichia coli*. ***Biotechnol. Tech.*** **9**: 759-762.

Kleinig, A.R. and Middelberg, A.P J. 1998. On the mechanism of microbial cell disruption in high-pressure homogenisation. ***Chem. Eng. Scien.*** **53**(5): 891-898.

Koning, G.J.M. and Lemstra, P.J. 1992. The amorphous state of bacterial poly(3-hydroxyalkanoate) *in vivo*. ***Polymer*** **33**(15): 3292-3294.

Kunioka, M.; Kawaguchi, Y. and Doi, Y. 1989. Production of biodegradable copolyesters of 3-hydroxybutyrate and 4-hydroxybutyrate by *Alcaligenes eutrophus*. ***Appl. Microbiol. Biotechnol.*** **30**: 569-573.

Jan, S.; Roblot, C.; Goethals, G.; Courtois, J.; Courtois, B.; Saucedo, J.E.N.; Seguin, J. and Barbotin, J. 1995. Study of parameters affecting poly(3-hydroxybutyrate) quantification by gas chromatography. ***Anal. Biochem.*** **225**: 258-263.

Janes, B.; Hollar, J. and Dennis, D. 1990. Molecular characterization of poly-β-hydroxybutyrate biosynthetic pathway of *Alcaligenes eutrophus* H16. **In**: ***Novel biodegradable Microbial Polymers.*** Dawes, E.A. (ed.) Kluwer Academic Publishers. 175-190.

Lafferty, R.M.; Korsatko, B. and Korsatko, W. 1988. Microbial production of poly-β-hydroxybutyric acid. **In**: ***Biotechnology***, Rehm, H.J. and Reed, G. (eds.). **6b**: 136-176. Verlagsgesellschaft Weinheim.

Law, J.H. and Slepecky, R.A. 1961. Assay of poly-β-hydroxybutyric acid. ***J. Bacteriol.*** **82**: 33

Lee, I.Y.; Chang, H.N. and Park, Y.H. 1995. A simple method for recovery of microbiol poly-β-hydroxybutyrate by alkaline solution treatment. ***J. Microbiol. Biotechnol.*** **4**: 238-240.

Lee, S.Y.; Chang, H.N. and Chang, Y.K. 1994. Production of poly(β-hydroxybutyric acid) by recombinant *Escherichia coli*. ***Annals N. Y. Acad. Scien.*** **721**: 43-53.

Lee, S.Y. 1995a. Polyhydroxyalkanoates as biodegradable plastic material: Academic and industrial effort. **In**: ***Proceeding of Chemca 95 Adelaide*** 3-8.

Lee, S.Y. and Chang, H.N. 1995b. Production of poly(3-hydroxybutyric acid) by recombinant *Escherichia coli* strain: genetic and fermentation studies. ***Can. J. Microbiol.*** **41**(Suppl.1): 207-215.

Lee, S.Y. 1996a. High cell-density culture of *Escherichia coli*. ***TIBTECH.*** **14**: 98-105.

Lee, S.Y. 1996b. Poly(3-hydroxybutyrate) extrusion by cells of recombinant *E. coli*. ***J. Microbiol. Biotechnol.*** **6**(2): 147-149.

Lee, S.Y. 1996c. Plastic bacteria? Progress and prospects for polyhydroxyalkanoate production in bacteria. ***TIBTECH.*** **14**: 431-438.

Lee, S.Y. and Chang, H.N. 1996d. Characteristics of poly(3-hydroxybutyric acid) synthesis by recombinant *Escherichia coli*. ***Annals N. Y. Acad. Scien.*** **782**: 133-142.

Licht, W. 1980. Air pollution control engineering--Basic calculations for particle collection. **In**: ***Pollution engineering and technology***/10. Marcel Dekker, Inc. New York.

Lu Shih, K. and Lederberg, J. 1976. Effects of chloramine on *Bacillus Subtilis* Deoxyribonucleic acid. ***J. Bacteriol.*** **125**(3): 934-945.

Lundgren, D.G.; Pfister, R.M. and Merrick, J.M. 1964. Structure of poly(β-hydroxybutyric acid) granules. ***J. Gen. Microbiol.*** **34**: 441-446.

Lundgren, D.G.; Alper, R.; Schnaitman, C. and Marchessault, R.H. 1965. Characterization of poly-β-hydroxybutyrate extracted form different bacteria. ***J. Bacteriol.*** **89**(1): 245-251.

Mannweiler, K. 1989. The recovery of biological particles in high-speed continuous centrifuges with special reference to feed-zone break-up effects. Ph.D. Thesis. University of London, London, UK.

Marchessault, R.H.; Okamura, K. and Su, C.J. 1970. Physical properties of poly(β-hydroxybutyrate). 2. Confirmational aspects in solution. ***Macromolecules.*** **3**: 735-740.

Mas, J.; Pedros-Alio, C. and Guerrero, R. 1985. Mathematical model for determining the effects of intracytoplasmic inclusions on volume and density of microorganisms. ***J. Bacteriol.*** **164**(2): 749-756.

Mason, R.L.; Gunst, R.F. and Hess, J.L. 1989. Statistical design and Analysis of experiments with applications to engineering and science. John Wiley & Sons, Inc. N.Y.

Merrick, J.M. and Doudoroff, M. 1964. Depolymerisation of poly-β-hydroxybutyrate by an intracellular enzyme system. ***J. Bacteriol.*** **88**(1): 60-71.

Middelberg, A.P.J. 1988. Simulation of a novel biochemical process. Honours Thesis. University of Adelaide.

Middelberg, A.P.J.; Bogle, I.D.L. and Snoswell, M.A. 1989. Simulation of a novel biochemical process. **In**: ***Proceedings of CHEMCA'89***, Broadbeach, Qld. The Institute of Engineers Australia, 671-678.

Middelberg, A.P.J.; Bogle, I.D.L. and Snoswell, M.A. 1990. Sizing biological samples by photosedimentation techniques. ***Biotechnol. Prog.*** **6**: 255-261.

Middelberg, A.P.J.; O'Neill, B.K.; Bogle, I.D.L. and Snoswell, M.A. 1991. A novel technique for the measurement of disruption in high-pressure homogenization: Studies on *E. coli* containing recombinant inclusion bodies. ***Biotech. Bioeng.*** **38**: 363-370.

Middelberg, A.P.J.; O'Neill, B.K.; Bogle, I.D.L.; Gully, N.J.; Rogers, A.H. and Thomas, C.J. 1992. A new model for the disruption of *Escherichia coli* by high-pressure homogenization Part II: A correlation for the effective cell strength. ***Trans IChemE.*** partC. **70**: 213-218.

Middelberg, A.P.J. 1995. Process-scale disruption of microorganisms. ***Biotechnol. Advan.*** **13**(3): 491-551.

Middelberg, A.P.J.; Lee, S.Y.; Martin, J.; Williams, D.R.G and Chang, H.N. 1995. Size analysis of poly(3-hydroxybutyric acid) granules produced in recombinant *Escherichia coli*. ***Biotechnol. Lett.*** **17**(2): 205-210.

Middelberg, A.P.J. 1996. Large-scale recovery of recombinant protein inclusion bodies expressed in *Escherichia coli*. ***J. Microbiol. Biotechnol.*** **6**: 225-231.

Middelberg, A.P.J. 1998. Large-scale recovery of protein inclusion bodies by continuous centrifugation. **In**: ***Downstream Processing Methods.*** (Desai, M.A. ed.). Publisher: The Human Press Inc.

Mitomo, H.; Barham, P.J. and Keller, A. 1987. Crystallization and morphology of poly(β-hydroxybutyrate) and its copolymer. ***Polymer J.*** **19**(11): 1241-1253.

Miyaki, Y.; Einaga, Y.; Hirisye, T and Fujita, H. 1977. Solution properties of poly(D-β-hydroxybutyrate). 2. Light scattering and viscosity in trifluoroethanol and behavior of highly expended polymer coils. ***Macromolecules***. **10:** 1357-1364.

Nuti, M.P.; de Bertoido, M. and Lepidi, A.A. 1972. ***Can. J. Microbiol.*** **18:** 1257-1261.

Olbrich, R. 1989. The characterization and recovery of protein inclusion bodies from recombinant *Escherichia coli*. PhD thesis, University of London, London, UK.

Ostle, A.G. and Holt, J.G. 1982. Nile blue A as a fluorescent stain for poly-β-hydroxybutyrate. ***Appl. Environ. Microbiol.*** **44**(1): 238-241.

Page, W.J. and Tenove, C.J. 1996. Quantitation of Poly-β-hydroxybutyrate by fluorescence of bacteria and granules stained with Nile blue A. ***Biotechnol. Techniq.*** **10**(4): 215-220.

Peoples, O.P. and Sinskey, A.J. 1989a. Poly-β-hydroxybutyrate biosynthesis in *Alcaligenes eutrophus* H16. Characterisation of the genes encoding β-ketothiolase and acetoacetyl-CoA reductase. ***J. Biol. Chem.*** **264**: 15293-15297.

Peoples, O.P. and Sinskey, A.J. 1989b. Poly-β-hydroxybutyrate biosynthesis in *Alcaligenes eutrophus* H16. Identification and characterisation of the PHB polymerase gene (phbC). ***J. Biol. Chem.*** **264**: 15298-15303.

Petros-Alio, C.; Mas, J. and Guerrero, R. 1985. The influence of poly-β-hydroxybutyrate accumulation on cell volume and buoyant density in *A. eutrophus*. ***Arch. Microbiol.*** **143**: 178-184.

Prat, R.; Nofre, C. and Cier, A. 1968. Effects of sodium hypochlorite ozone and ionizing radiation on pyrimidines of *Escherichia coli*. ***Ann. Inst. Pasteur.*** **114**: 595-607.

Ramsay, J.A.; Berger, E.; Ramsay, B.A. and Chavarie, C. 1990. Recovery of poly-3-hydroxyalkanoic acid granules by a surfactant-hypochlorite treatment. ***Biotechnol. Techn.*** **4**(4): 221-226.

Riis, V and Mai, W. 1988. Gas chromatographic determination of poly-β-hydroxybutyric acid in microbial biomass after hydrochloric acid propanolysis. ***J. Chrom.*** **445**: 285-289.

Roh, K.S.; Yeom, S.H. and Yoo, Y.J. 1995 The effects of sodium bisulfite in extraction of PHB by hypochlorite. ***Biotechnol. Techniq.*** **9**(10): 709-712.

Saito, T.; Suzuki, K.; Yamamoto, J.; Fukui, T.; Miwa, K.; Tomita, K.; Nakanishi, S.; Odani, S.; Suzuki, J.-I. and Ishikawa, K. 1989. Cloning, nucleotide sequence, and expression in *Escherichia coli* of the gene for poly(3-hydroxybutyrate) depolymerase from *Alcaligenes faecalis*. ***J. Bacteriol.*** **171**: 184-189.

Schubert, P.; Steinbuchel, A. and Schlegel, H.G. 1988. Cloning of *the Alcaligenes eutrophus* genes for synthesis of poly-β-hydroxybutyric acid (PHB) and synthesis of PHB in *Escherichia coli*. ***J. Bacteriol.*** **170**: 5837-5947.

Shirakura, Y; Fukui, T.; Saito, T.; Okamoto, Y.; Narikawa, T.; Koide, K.; Tomita, K.; Takemasa, T. and Masamune, S. 1986. Degradation of poly(3-hydroxybutyrate) by poly(3-hydroxybutyrate) polymerase from *Alcaligenes faecalis*. ***Biochem. Biophys. Acta.*** **748:** 331-339.

Siddiqi, S.F.; Titchener-Hooker, N.J. and Shamlou, P.A. 1996. Simulation of particle size distribution changes occurring during high-pressure disruption of bakers' yeast. ***Biotechnol. Bioeng.*** **50**: 145-150.

Slater, S.C.; Gallaher, T. and Dennis, D.E. 1992. Production of poly(3-hydroxybutyrate-co-3-hydroxyvalerate) in a recombinant *Escherichia coli* strain. ***Appl. Environ. Microbiol.*** **58**: 1089-1094.

Steinbuchel, A. 1991. Polyhydroxyalkanoates, 124-213. **In**: ***Biomaterials***: ***Novel materials from biological sources***. Byrom, D. (ed). Stockton Press, NY.

Steinbuchel, A. and Valetin, H.E. 1995. Diversity of bacterial polyhydroxyalkanoic acids. ***FEMS Microbiol. Lett.*** **128**: 219-228.

Stryer, L. 1981. Biochemistry, published by Stanford University.

Sulo, P; Hudecova, D.; Propperova, A. and Basnak, I. 1996. Rapid and simple analysis of poly-β-hydroxybutyrate content by capillary isotachophoresis. **10**(6): 413-418.

Suzuki, T.; Yamane, T. and Shimizu, S. 1986. Mass production of poly-β-hydroxybutyric acid by fully automatic fed-batch culture of methylotroph. ***Appl. Microbiol. Biotechnol.*** **23**: 322-329.

Taylor, G.; Hoare, M.; Gray, D.R. and Marston, F.A.O. 1986. Size and density of protein inclusion bodies. ***Bio/technology***. **4**: 553-557.

Thomas, J.C.; Middelberg, A.P.J.; Hamel, J.F. and Snoswell, M.A. 1991. High-resolution particle size analysis in biotechnology process control. ***Biotechnol. Prog***. **7**: 377-379.

Valax, P. and Georgiou. 1993. Molecular characterisation of β-lactamase inclusion bodies produced in *Escherichia coli*. 1. composition. ***Biotechnol. Prog***. **9**: 539-547.

Venkobachar, C.; Invegar, Z. and Prabhakara Raj, A.V.S. 1976. Mechanism of disinfection: effect of chlorine on cell membrane functions. ***Water Res.*** **11**: 727-729.

ven Wegen, R.; Ling, Y. and Middelberg, A.P.J. 1998. Industrial production of poly-hydroxyalkanoates using *Escherichia coli:* an economic analysis. ***Trans IchemE.*** Part A, **76**: 417-426.

Vogel, A.I. 1987. Vogel's qualitative inorganic analysis. 6th ed/rev. by Svehla, G. Scientific & Technical, Wiley. 1987.

White, G.C. 1972. Handbook of Chlorination: for potable water, wastewater, cooling water, industrial processes and swimming pool. Van Nostrand Reinhold Company, N.Y.

White, G.C. 1978. Disinfection of wastewater and water for reuse. Van Norstrand Reinhold Co. New York.

Wieczorek, R.; Pries, A.; Steinbuchel, A. and Mayer, F. 1995. Analysis of a 24-kilodalton protein associated with the poly-hydroxyalkanoic acid granules in *Alcaligenes eutrophus*. ***J. Bactieriol.*** **177**(9): 2425-2435.

Wieczorek, R.; Steinbuchel, A. and Schmidt, B. 1996. Occurrence of polyhydroxyalknoic acid granules-associated proteins related to the *Alcaligenes eutrophus* h16 ga24 protein in other bacteria. ***FEMS Microbiol. Lett.*** **135**(1): 23-30.

Williamson, D.H. and Wilkinson, J.F. 1958. The isolation and estimation of the poly-β-hydroxybutyrate inclusions of *Bacillus species*. ***J. Gen. Microbiol.*** **19**: 198

Wong, H.H. 1996. Modelling studies of the interaction between homogenization, centrifugation, and inclusion body dissolution. PhD thesis. The University of Adelaide, Australia.

Wong, H.H.; O'Neill, B.K.; Middelberg, A.P.J. 1996. Centrifugal recovery and dissolution of recombinant Gly-IGF-II inclusion-bodies: The impact of feedrate and re-centrifugation on protein yield. ***Bioseparation***. **6**: 185-192.

Wong, H.H.; O'Neill, B.K. and Middelberg, A.P.J. 1997. Cumulative sedimentation analysis of *Escherichia coli* debris size. ***Biotech. Bioeng***. **55**(3): 556-564.

Wong, H.H.; van Wegen R.J.; Choi, J.I.; Lee, S.Y. and Middelberg, A.P.J. Metabolic analysis of poly(3-hydroxybutyate) production by recombinant *Escherichia coli*. Submitted, 1998.

Appendix A

A1 OPERATING PROCEDURE FOR SDS-PAGE ANALYSIS

A1.1. Gel casting procedure

1. Prepare stock solutions listed in Table A.1.
2. Clean thoroughly the glass plates (20 × 20 cm^2 and 20 × 22.3 cm^2) and spacers (1.00 mm) with ethanol and assemble them after dry; Clamp them onto the mould base; Use alignment card to ensure the flush bottom of the sandwich assembly.
3. Make up monomer mixture for the separating gel (12%) (see Table A.2) by mixing all reagents except ammonium persulfate and TEMED using a Buchner flask; Degas the mixture for about 15 min using a vacuum pump and a vapour trap.
4. Add the freshly-made ammonium persulfate solution (1 g/mL) and TEMED to the monomer mixture, swirling gently for mixing.
5. Immediately inject the ready mixture into the mould using a 50mL syringe, tilting the mould back at a slight angle to avoid bubbles. Fill until about 1 cm above the arrows on the side clamps.
6. Cover the mixture with about 1cm of isobutanol using a squirt bottle for the alignment of the gel top line. Allow to stand for at least 1 h for full polymerization.
7. Pour out the isobutanol from the top of the polymerized gel. Rinse with MilliQ water and drain the water out. Place the well combs into the mould at an angle of approximately 10°.

8. Prepare the monomer mixture for stacking gels (see Table A.2) and degas it for about 10 min. Add ammonium persulfate and TEMED with gentle stirring.
9. Slowly inject the mixture using a 5 mL pipette. Release any bubbles trapped. Stand for at least 30 min for polymerization.
10. Take the well combs out. Rinse the wells thoroughly with MilliQ water and drain out the water.

A1.2. Sample preparation

1. Mix the sample pellet with sample buffer (see Table A.1 for composition). Crush and scrape the pellets on the tube bottom using a ceramic stick for protein dissolution.
2. Heat water in a waterbath. After boiling place the samples into the bath and stand for 10 min. Take the sample out and wait for cooling.
3. Spin the samples at 13,000 rpm for 5 min in a Micromax Bench Centrifuge prior to loading them onto gels.

A1.3. Electrophoresis procedure

1. Dilute 300 mL of the 5× running buffer (Table A.1) with MilliQ water to 1500 mL and pour 1000 mL into the electrophoresis tank.
2. The electrophoresis core should be placed in a fridge for 2 h before assembling to the gel mould. Clamp the gel mould onto the cold electrophoresis core and place it into the tank. Pour the remaining dilute running buffer into the top dam.
3. Load samples using a Finnpipette with loading tips.
4. Put the lid on the tank matching the electrode connections. Attach the system to a Bio-Rad model 1000/500 power supply. Set the power pack to maximum voltage (1000 V), maximum power (250 W) and current 20 Amps for one gel or 40 Amps for two gels. Press RUN to start.

5. When the sample front moves to about 2 cm from the bottom of the glass plate, stop the power supply. Remove the electrophoresis core system with gels from the tank and pour off the buffer in the top dam. Unclamp the gel mould from the core. Remove the gels from the glass plates by side the spacers and gently twist the plates apart.

A1.4. Gel staining and post treatment

1. Fill a tank with 500 mL coomassie blue R-250 stain solution (see Table A.1). Immerse the gels in the solution. Leave overnight with gentle agitation.
2. Fill destaining tank with 1 L of destain solution and place in a magnetic stirrer plate. Adjust the stirrer to ensure stable stirring inside the tank. The stained gel is rinsed in MilliQ water prior to transferring into the destaining tank. Leave it to destain for 3 to 5 h.
3. Fill a tank with 500 mL of gel conditioner and place the gel in it after finishing the destain. Allow the gel to condition for 3 h, agitating gently. The gel is then further hydrated in a gel hydrator for about 10 min prior to vacuum drying.
4. Dry the gel with a gel dryer (Model 583, BioRad Laboratories, Sydney, Australia). Wet a cellophane sheet with hydrating solution and place it onto the dry base. Place the gel on the top of the cellophane and cover it with another wet cellophane sheet. Replace the transparent gasket and close the dryer lid.
5. Switch the vacuum pump, vapour trap and the dryer. Set the dryer to Gradient cycle, temperature at 60°C and time to 8 h. Start the dry cycle.
6. Scan the intensity of the specific protein bands on the dried gel using a densitometer (Model 300A, Molecular Dynamics, California, USA).

Table A.1. Stock reagents for SDS-PAGE analysis and preparation

Number	Stock solutions	Composition and storage
1	Acrylamide/Bis	Acrylamide, 73.0 g and N,N'-Methylene-bis Acrylamide, 2.0 g. Add MilliQ water to 250 mL. Filter and store at 4°C in the dark.
2	1.5 M Tris-HCl, pH 8.8	Tris base, 45.41 g and MilliQ water, 200 mL; adjust to pH 8.8 with concentrated HCl and then add water to 250 mL. Store at 4°C.
3	0.5 M Tris-HCl, pH 6.8	Tris base, 6 g and MilliQ water 60 mL; adjust to pH 6.8 with concentrated HCl and then add water to 100 mL. Store at 4°C.
4	10% (w/v) SDS	Dissolve SDS 5 g in 50 mL MilliQ water with gentle heat/stirring. Store at room temperature.
5	10%(w/v) Ammonium persulfate	Dissolve 100 mg ammonium persulfate in 1.0 mL milliQ water. Use only freshly prepared.
6	Sample Buffer (62.5 mM Tris-HCl pH 6.8/20% Glycerol/2%SDS/5 % β-merceptoethanol)	480 mL solution contains: MilliQ water, 180 mL; 0.5 M Tris-HCl, pH6.8, 60 mL; Glycerol, 96 mL; 10% SDS, 96%; β-merceptoethanol, 24 mL and 0.5 % bromophenol blue water solution, 24 mL. Store at 4°C.
7	5 × Running buffer (1× =25mMTris, 192mM Glycine, 0.1% SDS, pH8.3)	Tris base, 15.0 g; Glycine, 72.0 g and SDS, 5.0 g. Dissolve in 1 L MilliQ water. Store at 4°C. Dilute before use.
8	Coomassie Blue stain solution	Coomassie Blue R-250, 0.5 g; Methanol, 200 mL and Acetic acid, 50 mL. Add MilliQ water to 500 mL. Store at room temperature. Reuse for many gels.
9	Destain solution	Methanol, 800 mL; Acetic acid, 200 mL and MilliQ water 1 L. Store at room temperature. Reuse for many gels.
10	Gel Conditioner	Methanol, 200 mL; Acetic acid, 50 mL; Glycerol, 15 mL and MilliQ water, 235 mL. Store at 4°C. Reuse for many gels.
11	Gel Hydrator	Glycerol, 15 mL and MilliQ water, 485 mL. Store at 4°C. Reuse for many gels.

Table A.2 Formulations for SDS-PAGE separating and stacking gels

	Separating gel (0.375 M Tris, pH 8.8)	**Stacking gel (0.125 M Tris, pH 6.8)**
Monomer Concentration	12% T (or 2.67% C)[a]	4.0 % (or 2.67% C)[a]
Acrylamide/bis (30% T or 2.67% C stock solution)[a]	40.0 mL	1.3 mL
MilliQ water	33.5 mL	6.1 mL
1.5 M Tris-HCl, pH 8.8	25.0 mL	
0.5 M Tris-HCl, pH 6.8		2.5 mL
10% (w/v) SDS	1.0 mL	100 µL
10% Ammonium Persulfate	500 µL	50 µL
TEMED	50 µL	10 µL
Total Volume	100 mL	10 mL

[a] % T= [(gm Acrylamide + gm Bis-Acrylamide)/Total Volume] ×100
% C= [(gm Bis-Acrylamide/(gm Acrylamide + gm Bis-Acrylamide)]×100

A2 MODIFICATION OF SAMPLE PREPARATION FOR SDS-PAGE ANALYSIS

A2.1 Sample boiling time

The protein sample should be denatured and solubilized by boiled with sample buffer containing SDS prior to loading onto the gel. The boiling conditions affect the protein solubilisation yield and thus the sensitivity of the analysis results. Overboiling may result in the protein degradation. A reasonable boiling condition is thus required to ensure the analysis sensitivity.

Experiment

Samples (12×25 mL) were taken from a fresh two pass-homogenate with a cell concentration of about 4 g/L and centrifuged at 27,600 ×g for 60 min in a HB-6 swing-out rotor using a Sorvall RC-5C refrigerated centrifuge (Du Pont, USA). After re-suspending the pellets with SDS-PAGE sample buffer, the samples were boiled in a water bath for 2, 5, 10, 15, 20 and 30 min, respectively. After cooled to room temperature, SDS-PAGE analysis was conducted using the procedure detailed in Appendix A1. The measurement was repeated in duplicate and the average value was taken. The intensity of protein band was measured and normalized to that of the sample boiled for 10 min. Data are shown in Figure A.1.

Results

Protein intensity varied with sample boiling time. Under this condition, 10 min gave the highest response and thus highest protein solubilisation yield. Times other than 10 min resulted in a lower sensitivity, possibly due to incomplete protein solubilisation or protein degradation. A boiling time of 10 min was applied for all samples prepared for SDS-PAGE analysis in this study.

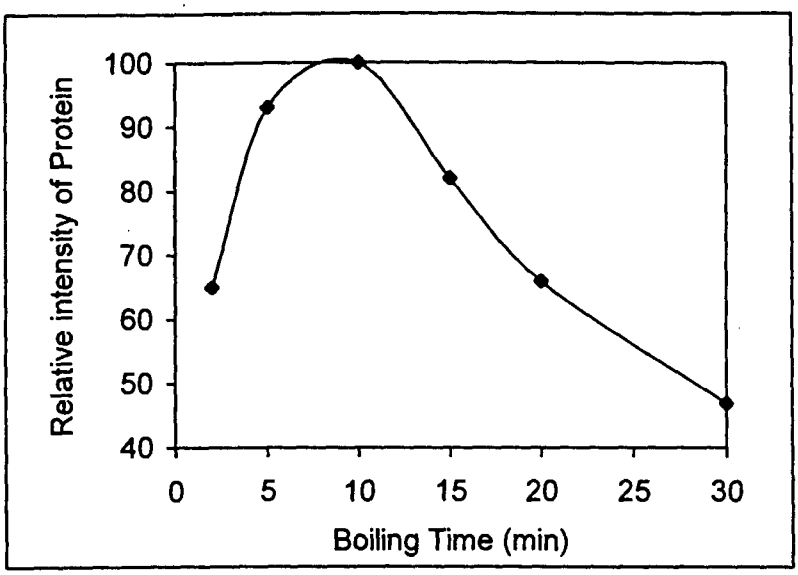

Figure A.1. Relative protein intensity as a function of boiling time.

A2.2. Effect of storage time on protein stability

Due to the large number of samples involved and the long fractionation time required for each batch of CSA analysis, protein stability during storage has to be considered. The following experiment was therefore conducted to examine prolonged storage effects prior to SDS-PAGE analysis.

Experiment

The sampling procedure was same as that described in Section A2.1. Samples were stored in a fridge at 4°C for different time intervals, varying from 1 day to 8 days, before they were sedimented and mixed with sample buffer. Samples were boiled for 10 min before loading onto the gel.

Results

Figure A.2 shows the detected *E. coli* outer membrane protein as a function of storage time. The data were normalized to that of the sample stored for 1 day. Obviously, cell membrane protein becomes unstable after prolonged storage. Within the first five days, detectable protein dropped to 93% of the original

intensity. Only 70% was detectable after 8 days. As a result, it was important to complete the sample preparation within 5 days, thus minimizing errors.

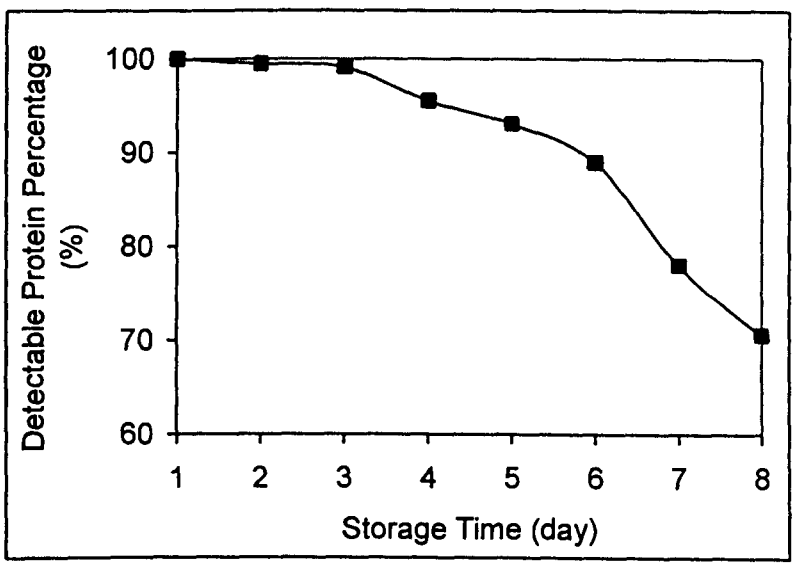

Figure A.2. Protein stability versus storage time before SDS-PAGE analysis.

Appendix B

DETERMINATION OF PHB CONCENTRATION BY GC

B.1. Preparation of samples

B.1.1 Reagents and solutions

PHB (Aldrich Chem. Co., NSW, Australia)
Chloroform (AnalaR) (BDH Chemicals, VIC, Australia)
Methanol (AnalaR) (BDH Chemicals, VIC, Australia)
Benzoic acid (C_6H_5COOH) (Merck, Darmstadt, Germany)
Sulphuric acid
Methanol solution containing 3% v/v sulphuric acid
Internal standard solution (0.2 g benzoic acid dissolved in 50 mL methanol)

B.1.2 Sample preparation

1. Pipette a certain volume of cell culture into an 8 mL Kimble glass culture tube. The volume depends on cell density. It is required to keep the cell mass in a range of 4-10 mg based on DCW. Record the volume used.
2. Freeze-dry the broth for one and half days.
3. Crush the cell sample into a fine powder and suspend it by the addition of tion, and 200 μm internal standard solution in a glass tube, using a vortexer.
4. Seal the tube tightly, and place it in an oven at 100°C for 3.5 h. Shake the tube two or three times during the incubation.
5. Add 1 mL MilliQ water into the tube and vortex for 3 min after cooling to

ambient temperature.

6. Allow to stand for 10 min until three phases are clearly formed. Remove the top and the debris phase. The bottom phase is ready for GC.

B.1.3 PHB calibration standard sample preparation

1. Dissolve 15-30 mg PHB powder in chloroform in a waterbath at 508C, using a 5 mL volumetric flask.
2. Pipette 200 μl, 400 μl, 600 μl, 800 μl and 1000 μl PHB solution into five tubes and add chloroform, methanol and internal standard as if the standards are normal samples.

B.2. Analytical technique

B.2.1 Preparation of standard curve

1. Inject 0.5-1.5 μl for each standard solution into the GC and obtain the thermographs containing the peaks representing PHB and internal standard.
2. Calculate the peak-area ratio (HB peak area against internal standard) and the pure PHB amount in each standard sample. Plot the curve of PHB (mg) vs peak-area ratio as a calibration curve.

B.2.2 Analysis

1. Inject the samples as if the samples are standards as above.
2. Use the calibration curve to determine the PHB amount in each sample
3. Calculate the PHB concentration based on dry cell weight.

Appendix C

IMPACTS OF CHEMICAL TREATMENT AND INCOMPLETE RE-SUSPENSION ON PHB GRANULES AND CELL DEBRIS SIZE

Sodium hypochlorite (NaOCl) and sodium hydroxide (NaOH) have been used for the digestion of insoluble cell debris for PHB recovery from *A. eutrophus* and recombinant *E. coli* (Section 1.3.1). However, most of the research has focused on attaining high PHB purity, recovery rate and stability. No studies of the effect on debris size have been reported. In this study, cell debris size reduction by NaOH and NaOCl treatment, and their impact on PHB granules were investigated.

PHB centrifugal fractionation was performed in a solid bowl Veronesi disc-stack centrifuge in this research. PHB paste was sedimented onto the innerface of the rotating bowl, and removed after batch operation. Obviously, complete re-suspension of PHB paste prior to the subsequent operations was hardly achieved and this could lead to inherent limitations in modelling the true process. A single homogenization step to break aggregates prior to re-centrifugation may be needed between centrifugation passes. To monitor the re-suspension under these experimental conditions, and testify the impact of incomplete suspension on cell debris size, a scaled-down process was designed and conducted.

These experiments will provide the information for the selection of chemicals and assist the process design for the PHB recovery conducted in Chapter 3.

C.1. Experimental conditions

Experiment One

Fresh cell material from Fermentation I (Section 2.1) was homogenized under the conditions described in Section 2.2. 1 L of the homogenate after two passes was then taken and 2M NaOH aqueous solution was gradually added to give a final NaOH concentration of 0.2M. The suspension was incubated at room temperature for 1 h on a magnetic stirring plate. The treatment was terminated by neutralization with 2M HCl solution. Samples were taken prior to and after the treatment to monitor the change of PHB granules by CDS analysis (Section 2.4.1). CSA analysis (Section 2.4.2) was conducted after the treatment.

To quantify the remaining cell debris after NaOH treatment, samples were collected prior to and after NaOH treatment, and then centrifuged in a swing-out rotor for a sufficient time to ensure the collection of all cell debris with a size down to 0.04 μm. The concentrates were analyzed by SDS-PAGE. Details are given in Section 2.5.3.

Experiment Two

After thawing at 4°C overnight, the frozen cell material from Fermentation I (Section 2.1) was diluted ten times with PBS buffer, followed by three discrete homogenizer passes under the conditions described in Section 2.2. Six samples were taken from the homogenate and analyzed by CSA. The first two samples were from the two-pass homogenate, and treated with NaOH and NaOCl, respectively. Samples 3 and 4 were taken from the two-pass and the three-pass homogenate, respectively, and then centrifuged at 27,600×g for 2 h in a Sorvall RC-5C refrigerated centrifuge (Du Pont, USA) using a HB-6 swing out rotor. Supernatant was discarded, and the pellets were re-suspended in the same volume of PBS buffer using a hand-held mixer. The samples were further treated with NaOCl. Samples 5 and 6 were taken from the two and three pass homogenate but without additional treatment before CSA analysis. PHB size distribution was monitored prior to and after chemical treatment by CDS, and a PHB density of 1260 kg/m^3 was applied to present the results.

NaOH treatment conditions were the same as those described above. NaOCl stock solution was added to the homogenate to give 0.85 g/L active. The homogenate was then incubated for 1 h at room temperature with magnetic stirring, prior to the deactivation of active chlorine by the titration of Na_2SO_3 (0.5M) using the potassium iodine-starch paper as an indicator. NaOCl stock solution with 57 g/L active chlorine was diluted from the NaOCl (Fistons technical grade, FSE Australia, 100 g/L active chlorine) with MilliQ water (Middelberg *et al.*, 1995).

C.2. Results and discussion

C.2.1. NaOH treatment

CSA result shows that the debris size was significantly reduced by NaOH treatment (Figure C.1). The median diameter (D_{50}) of cell debris in the two-pass homogenate decreased from 0.50 μm to 0.33 μm after NaOH treatment. The distribution width *w* was also narrowed, and the size overlap of PHB and debris significantly reduced. The result also shows that the volume fraction of cell debris after NaOH treatment dropped to only 42% relative to the untreated homogenate sample. The remainder was out of the detectable size limit due to strong solubilisation by NaOH.

It is also interesting to find that the NaOH treatment changed the PHB size distribution, as shown in Figure C.2, probably due to aggregation. The PHB size distribution shifted to a large median size and a definite population of large particles was formed. This may aid subsequent fractionation, provided that the aggregated granules do not have a large fraction of cell debris incorporated into them. As it is likely that these aggregates incorporate entrapped cellular debris, further study of NaOH digestion was not undertaken (note that both the PHB and lipid surfaces are hydrophobic, and selective aggregation of PHB without entrapped lipid from a mixed population seems improbable).

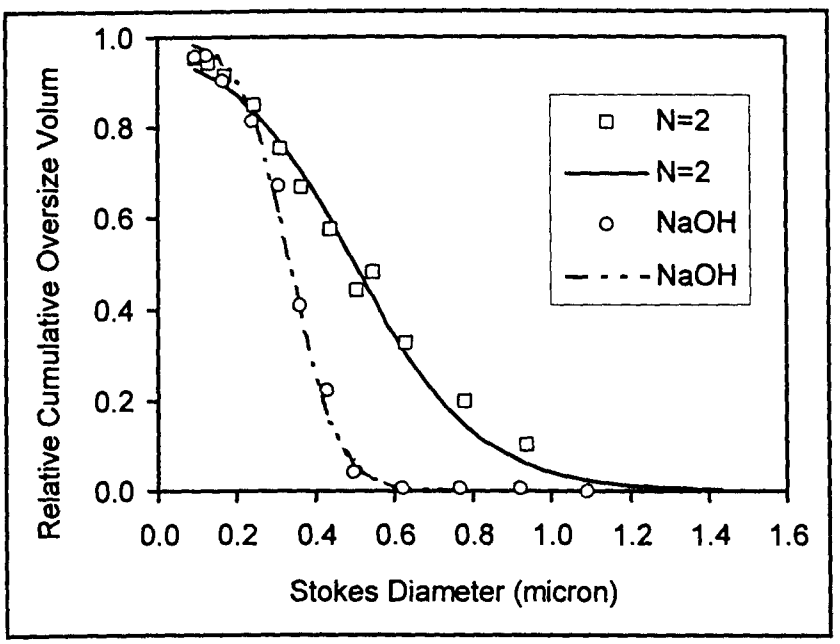

Figure C.1. Cumulative oversize debris distributions by CSA for two-pass homogenate prior to (N=2) and after (NaOH) treatment. Smooth curves were obtained by the regression to the Boltzmann equation.

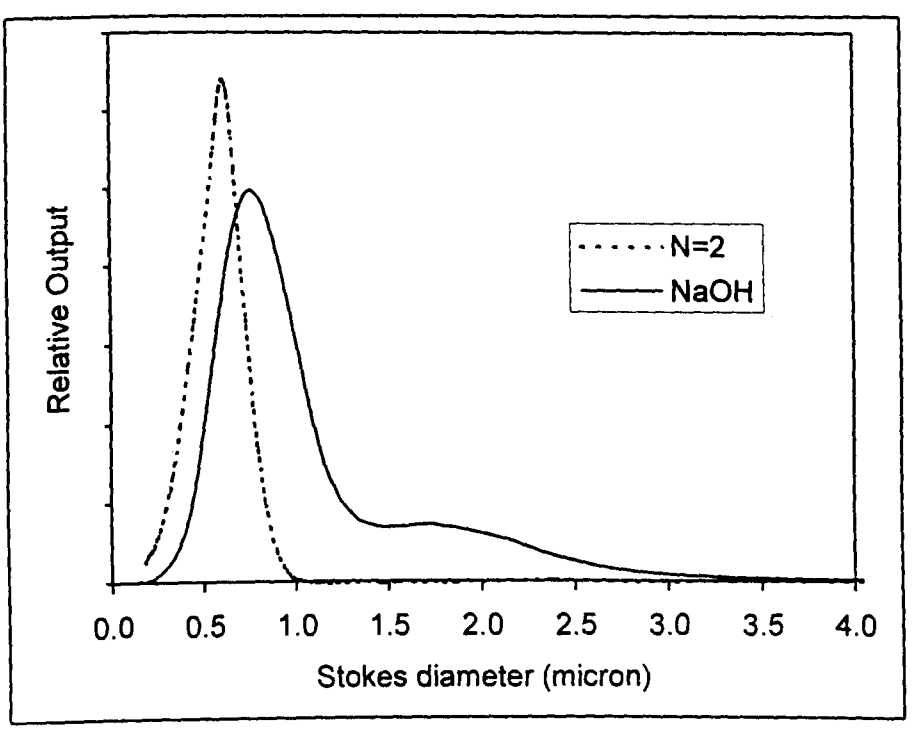

Figure C.2. Particle size distributions by CDS for two-pass homogenate prior to and after NaOH treatment.

C.2.2. The comparison of NaOCl and NaOH Treatment

Figure C.3 shows the cumulative debris size distribution with regressed parameters D_{50} and w listed in Table C.1. Note that size reduction by NaOH was more significant than that by NaOCl. The NaOH treatment resulted in a decrease in median diameter from 0.480 μm after two homogenizer passes to 0.309 μm. The decrease was less with NaOCl, dropped to 0.371 μm. Both reductions are significant when compared with the value of 0.421 μm measured after three homogenizer passes without chemical treatment. It suggests that the chemical treatment is more effective than multiple homogenization in terms of cell debris size reduction under the conditions tested. There was no aggregation found in the homogenate after NaOCl treatment by CDS analysis, and the resultant PHB digestion was also negligible as observed by Middelberg *et al.* (1995).

In the above tests, NaOCl and NaOH were used at different concentrations. It is unreasonable to compare digestion capacities at different concentrations, even though both NaOCl and NaOH are efficient at cell debris digestion. However, the result provides general information on the effect of chemical treatment on PHB homogenates. The observed aggregation of PHB during NaOH treatment is of concern, so more work is required before selecting it for PHB extraction. As NaOCl treatment led to a significant debris size reduction without aggregation, it is selected as the digestion method for further study in Chapter 3.

Table C.1. Median diameter (D_{50}) and Boltzmann parameter (w) for cell debris from thawed cells of Fermentation I.

Sample No.	Treatment			D_{50} (μm)	w (μm)
	Homogenization Passes	Chemical Digestion	Centrifugation and Re-suspension		
1	N=2	-	-	0.480	0.172
2	N=3	-	-	0.421	0.152
3	N=2	NaOH	-	0.309	0.078
4	N=2	NaOCl	-	0.371	0.123
5	N=2	NaOCl	√	0.465	0.168
6	N=3	NaOCl	√	0.458	0.162

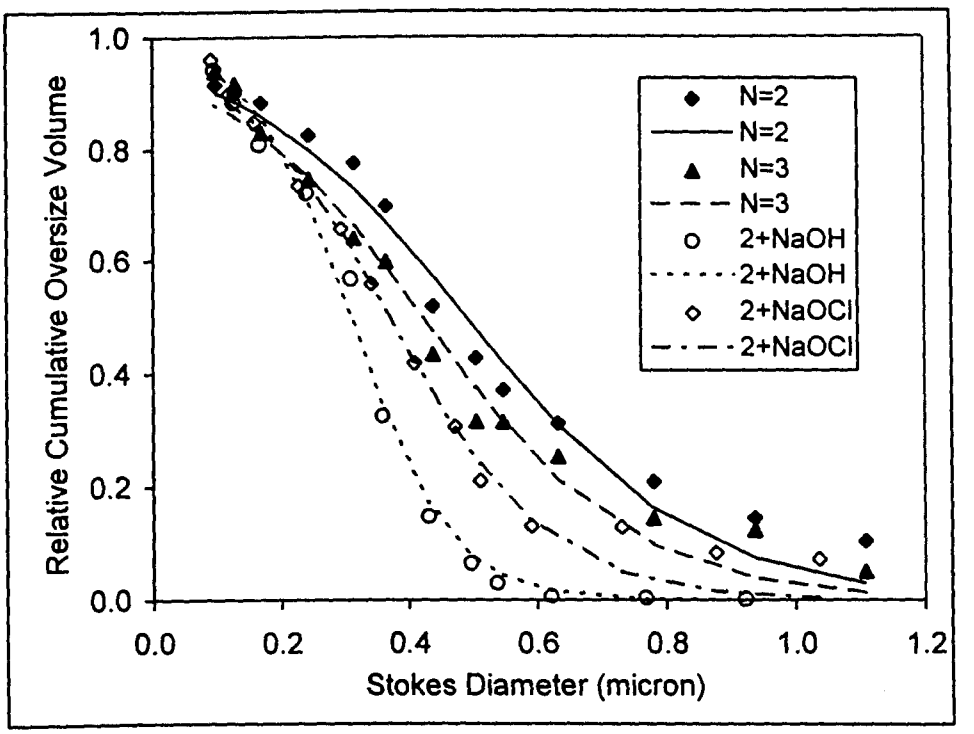

Figure C.3. The cumulative oversize debris distributions for two-pass homogenates treated with NaOH (N=2+NaOH) and NaOCl (N=2+NaOCl). Smooth curves are the regressions of Boltzmann equation. The distribution for two-pass and three-pass homogenates without chemical treatment are included for comparison.

C.2.3. Impact of incomplete re-suspension on cell-debris size

Repeated centrifugation is often employed for the fractionation of protein inclusion bodies and cell debris with enhanced product purity (Middelberg, 1996; Wong *et al.*, 1996). The efficient removal of both insoluble cell debris and soluble intracellular contaminants depends on the complete re-suspension of product paste after each centrifugation. Incomplete re-suspension traps contaminants, preventing them from further removal and giving high contamination in products. For some processes, additional homogenizer passes has to be incorporated between centrifugations. This could ensure complete suspension of product paste, and also contribute to further reduction in cell debris size, thus facilitating subsequent fractionation.

To clarify the impact of incomplete suspension on cell debris size, a scale-down process was conducted. Instead of the Veronesi centrifuge, a batch centrifuge with a swing-out rotor was employed for sedimenting homogenates, followed by re-suspension in PBS buffer with a hand-held mixer. Homogenization was not incorporated due to the experimental limitation (inability to scale-down the homogenizer).

Figure C.4 illustrates the debris size distribution of the two-pass and three-pass homogenate with pre-centrifugation and NaOCl treatment measured by CSA, compared to that of the two-pass homogenate without pre-centrifugation and re-suspension prior to NaOCl treatment. The regressed D_{50} and w are listed in Table C.2 (Samples 4, 5 and 6). Re-suspension does have a significant impact on debris size for these experimental conditions. It is noted that the debris median diameter rises from 0.371 μm (Sample 4) up to 0.465 μm (Sample 5) due to incomplete suspension. A difference of debris size between the second and third homogenizer pass was also offset by re-suspension, from 0.067 μm (Samples 1 and 2) to 0.007 μm (Samples 5 and 6). Incomplete re-suspension also reduced the efficiency of NaOCl treatment on cell debris size reduction. There is only less than 0.04 μm reduction in debris size for the two-pass homogenate with pre-centrifugation and NaOCl treatment (Samples 1 and 5) compared with 0.12 μm without pre-centrifugation (Samples 1and 4).

In conclusion, incomplete re-suspension in a repeated centrifugal process should be avoided because it has an impact on cell debris micronization and consequently cell-debris removal. More seriously, it may hinder the removal of other soluble contaminants and therefore lowered the product quality. Fortunately, the incomplete re-suspension will not be a serious issue in practice as industrial-scale centrifuge discharges slurry instead of paste. The results obtained are limited to only these specific experimental conditions. Nevertheless it provides a general indication of the influence of insufficient re-suspension on cell debris. It assists the design of the processes conducted in Chapter 3.

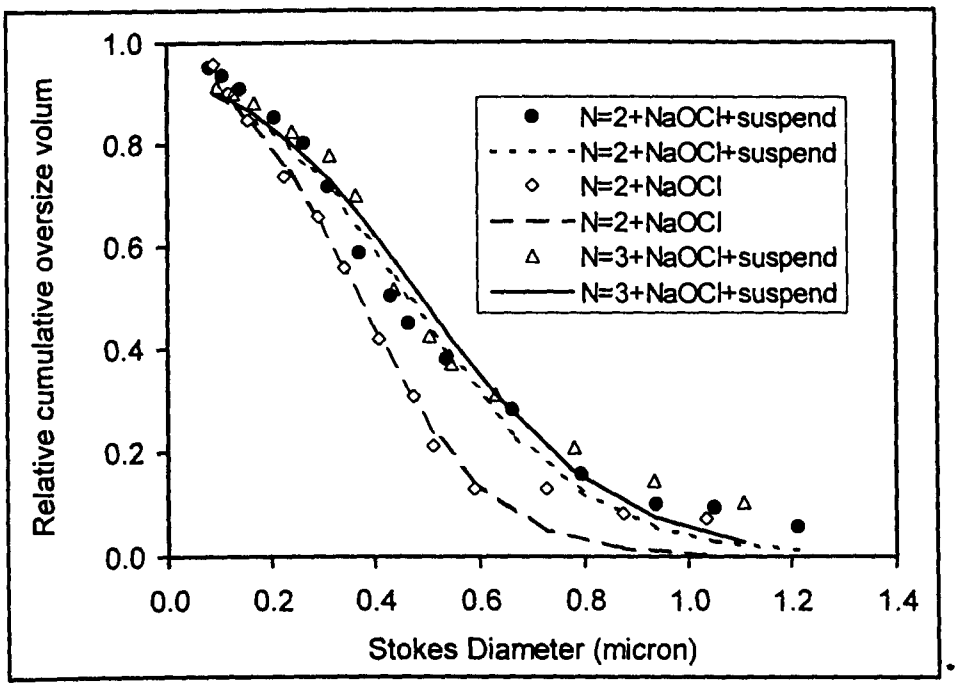

Figure C.4. Cumulative oversize debris distribution for the two or three-pass homogenates with pre-centrifugation and re-suspension followed by NaOCl treatment (N=2+NaOCl+suspend and N=3+NaOCl+suspend). The distribution for the two-pass homogenate without pre-centrifugation prior to NaOCl treatment is also included (N=2+NaOCl). The smooth curves are obtained by regression to the Boltzmann equation.

Appendix D

SIMULATION PROCEDURE OF CELL DEBRIS FRACTIONATION

The simulation study of PHB granules and cell debris fractionation was conducted in Chapter 4 and Chapter 6. The fractionation process involves unit operations of homogenization, centrifugation and NaOCl treatment. In this appendix, a detailed description of simulation procedure for cell debris is provided based on Process A (Chapter 3). Process A involves three homogenization passes, followed by two passes of centrifugation at feedrate of 3.09×10^{-9}m s^{-1} (700 mL/min) and 2.21×10^{-9}m s^{-1} (500 mL/min), respectively. A homogenization step was inserted between centrifugation.

Simulation procedure

1. The cumulative size distribution of cell debris after three homogenization passes is measured by CSA and expressed by the Boltzmann function (D_{50} = 0.44 μm and w = 0.16 μm in Table 4.1 of Section 4.3.2). The cumulative distribution is converted into a fractional distribution for the convenience of subsequent simulation (Table D.3).

2. The grade efficiency of *E. coli* cell debris T(D) in the first and second centrifugation pass is predicted using Equation 4.12 (k = 1.3 and n = 2.1) (Table D.2). The critical particle size D_c is calculated using Equation 4.11 (Table D.1).

3. The cell debris fractionation during the first centrifugation (3.09×10^{-9} m s^{-1}) can be then predicted (Equations 4.13, 4.14 and 4.15). The cell debris size distribution (D_{50} and w) changes from D_{50} = 0.444 μm to D_{50} =0.641 μm, and from w = 0.171 μm to w = 0.134 μm, respectively (Table D.3). The

fraction of remaining cell debris in the concentrate is also estimated related to the initial 100% before the first centrifugation (73.0%).

4. The size distribution of the remaining cell debris is re-expressed in a cumulative format, which allows the use of the cell debris size reduction model (Equation 4.1) for the prediction of the resulted debris size distribution following one pass of homogenization (α= 2.12, and a_d = 0.844 from Section 4.3.2,) (Table D.4).

5. After transforming the cumulative size distribution to a fractional format, cell debris fractionation in the second centrifugation pass (2.21×10^{-9} m s^{-1}) is estimated and the fraction discharged through the supernatant is obtained (72.0%). The final cell debris size distribution remained in the concentrate is also obtained (D_{50} = 0.726 μm and w = 0.118 μm) (Table D.5)

Table D.1, Calculation of the critical cell debris size D_c in the first and second centrifugation (Density difference $\Delta\rho$ = 85 kg/m^3, the settling area Σ = 3775 m^2)

	The first centrifugation	The second centrifugation
Viscosity$\times10^3$ (Pa.s)	1.4	1.2
Flowrate Q (mL/min)	700	500
$Q/\Sigma\times10^9$ (m s^{-1})	3.09	2.21
D_c (μm)	0.306	0.239

Table D.2, The grade-efficiency T(D) of the cell debris during the two passes centrifugation in the disc-stack centrifuge (k = 1.3 and n = 2.1)

Size(D)	T(D)(700)	T(D)(500)
1.43024	0.963803	0.996133
1.345259	0.945968	0.992439
1.238624	0.914011	0.983542
1.107859	0.856446	0.961191
1.045789	0.820879	0.943786
0.936312	0.744193	0.897928
0.863251	0.683203	0.853998
0.780058	0.60511	0.788874
0.70237	0.52547	0.712856
0.631933	0.44958	0.631914
0.54727	0.356871	0.522349
0.505542	0.311809	0.465014
0.437812	0.241387	0.370253
0.364839	0.171699	0.270449
0.312734	0.127417	0.203993
0.243226	0.07725	0.125914
0.168387	0.036461	0.060279
0.127289	0.020427	0.033957
0.097219	0.011651	0.019425
0.042587	0.002069	0.00346

Table D.3, The simulation for the first pass of centrifugation

Size(D)	Initial cumulative distribution	Fractional distribution	T(D)(700)	Sedimented fraction	Cumulative distribution
1.43024	0.003124	0.018204	0.963803	0.017545	0.002793
1.345259	0.005123	0.029798	0.945968	0.028188	0.005246
1.238624	0.009514	0.055090	0.914011	0.050353	0.011534
1.107859	0.020214	0.115782	0.856446	0.099161	0.029978
1.045789	0.028801	0.163525	0.820879	0.134234	0.046772
0.936312	0.053247	0.294709	0.744193	0.219321	0.099827
0.863251	0.079367	0.427156	0.683203	0.291834	0.160437
0.780058	0.122967	0.630471	0.605110	0.381504	0.262050
0.70237	0.180870	0.866126	0.525470	0.455123	0.387768
0.631933	0.249986	1.096092	0.449580	0.492781	0.516975
0.54727	0.353488	1.336020	0.356871	0.476786	0.667858
0.505542	0.411007	1.415211	0.311809	0.441275	0.732884
0.437812	0.509036	1.461032	0.241387	0.352674	0.819619
0.364839	0.613668	1.385977	0.171699	0.237970	0.886683
0.312734	0.682950	1.265839	0.127417	0.161289	0.920223
0.243226	0.763815	1.054635	0.077250	0.081470	0.950879
0.168387	0.833580	0.810986	0.036461	0.029569	0.971265
0.127289	0.864301	0.685651	0.020427	0.014006	0.978681
0.097219	0.883631	0.601132	0.011651	0.007004	0.982886
0.042587	0.912668	0.465961	0.002069	0.000964	0.988541

Table D.4, Simulation of cell debris size distribution after one pass of homogenization
(The cell debris size distribution after homogenization is:
D_{50} = 0.538 μm and w = 0.134 μm)

Size (D)	Undersize cumulative distribution	Cumulative distribution after homogenization	Boltzmann function	Residue
1.43024	0.997207			
1.345259	0.994754	0.999379	0.997632	3.05E-06
1.238624	0.988466	0.998193	0.994756	1.18E-05
1.107859	0.970022	0.993538	0.98617	5.43E-05
1.045789	0.953228	0.985749	0.978174	5.74E-05
0.936312	0.900173	0.964768	0.951822	0.000168
0.863251	0.839563	0.928521	0.919594	7.97E-05
0.780058	0.737950	0.866074	0.859892	3.82E-05
0.70237	0.612232	0.772266	0.774366	4.41E-06
0.631933	0.483025	0.659836	0.669543	9.42E-05
0.54727	0.332142	0.519187	0.518161	1.05E-06
0.505542	0.267116	0.421402	0.440402	0.000361
0.437812	0.180381	0.327018	0.321632	2.9E-05
0.364839	0.113317	0.230542	0.215469	0.000227
0.312734	0.079777	0.161833	0.156815	2.52E-05
0.243226	0.049121	0.109521	0.099555	9.93E-05
0.168387	0.028735	0.063926	0.059406	2.04E-05
0.127289	0.021319	0.036756	0.044378	5.81E-05
0.097219	0.017114	0.025314	0.035757	0.000109
0.042587	0.011459	0.015916	0.024048	6.61E-05
			sum	0.001507

Table D.5. The fractionation of cell debris by the second centrifugation
(The cell debris size distribution remained in concentrate is: D_{50} = 0.726 μm and w = 0.118 μm)

Size (D)	Oversize cumulative distribution	Fractional distribution	T(D)(500)	The fraction of sedimented debris	Oversize cumulative distribution	Boltzmann function	residue
1.43024	0.002798	0.020778	0.996133	0.020697			
1.345259	0.005256	0.038928	0.992439	0.038634	0.005995	0.00522	6E-07
1.238624	0.011553	0.085031	0.983542	0.083632	0.014989	0.0128	4.79E-06
1.107859	0.030018	0.216802	0.961191	0.208388	0.046646	0.037824	7.78E-05
1.045789	0.046828	0.332351	0.943786	0.313668	0.07351	0.062401	0.000123
0.936312	0.099917	0.669645	0.897928	0.601293	0.156552	0.144167	0.000153
0.863251	0.160550	1.003526	0.853998	0.857009	0.24488	0.238417	4.18E-05
0.780058	0.262177	1.440359	0.788874	1.136261	0.382355	0.388008	3.2E-05
0.70237	0.387884	1.767907	0.712856	1.260264	0.536705	0.55065	0.000194
0.631933	0.517058	1.859337	0.631914	1.174941	0.678907	0.690141	0.000126
0.54727	0.667891	1.651621	0.522349	0.862722	0.821927	0.82038	2.39E-06
0.505542	0.732896	1.457629	0.465014	0.677818	0.875219	0.866791	7.1E-05
0.437812	0.819606	1.100907	0.370253	0.407614	0.936166	0.920371	0.000249
0.364839	0.886658	0.748294	0.270449	0.202375	0.973069	0.955485	0.000309
0.312734	0.920196	0.546798	0.203993	0.111543	0.986629	0.970925	0.000247
0.243226	0.950855	0.347953	0.125914	0.043812	0.995581	0.983665	0.001633
0.168387	0.971247	0.207942	0.060279	0.012535	0.999077	0.991275	0.003266
0.127289	0.978665	0.155471	0.033957	0.005279	0.999684	0.993827	0.006527
0.097219	0.982872	0.125353	0.019425	0.002435	0.999876	0.99521	0.012975
0.042587	0.988531	0.084422	0.00346	0.000292	1	0.996981	0.025827
						sum	0.051861

Appendix E

STATISTICAL ANALYSIS FOR MODEL DEVELOPMENT

Response surface methodology was employed in Chapter 5 for factorial experimental design and model establishment of cell debris size reduction by NaOCl treatment. Three variable factors (A, B and C) were selected with three responses (D_{50}, w, and LN(1–R)). The observed responses during the 30 treatment combinations are presented in Table 5.3. In this appendix, the statistical analysis about the contrast calculation and normal probability plotting for the determination of effect significance, and also the detailed procedure for model development, are described.

E.1. Analysis for Experiment I

In Experiment I, 18 treatment combinations were conducted in three batches (Batches 1, 2 and 3). 17 contrasts were firstly identified, representing all of the treatment effects shown in Table E.1. The 17 contrasts include Bl1 and Bl2 representing linear and quadratic contrasts between blocks, B1 and B2 (C1 and C2) representing linear and quadratic contrasts of B (and C), AB1 and AB2 (AC1 and AC2) representing the linear and quadratic interaction between A and B (and C), BC1–BC2 representing four contrasts for BC interaction, ABC1 and ACB2 representing 4 contrasts for the ABC interaction. The values of these contrasts were calculated and included in Table E.1.

A normal probability plot of these effects for the response D_{50} is shown in Figure E.1. All of the effects that lie along the line are negligible, whereas the large

effects are far from the line. The important effects that emerge from this analysis are main effects A1, B1 and C1, the quadratic term in B (B2), with the exception of the quadratic term in C, and AB1 and AC1 are moderately important. After taking the 6 largest effects, and re-plotting the 11 remaining effects on a normal probability paper, it is found that they are close to a straight line (Figure E.2). This confirms that the 6 identified effects capture most of effects given to the response D_{50}. Figures E.3 and E.4 repeat the analysis for the response w. Considering the close correlation with D_{50}, it is not surprising that the same effects are identified for w as important.

Table E.1. Contrast identification and effect estimation for Experiment I.

	D_{50} (μm)	w (μm)
Mean	0.6853	0.2572
A1	−0.2050	−0.0995
B1	−0.7026	−0.2370
B2	−0.2179	−0.0582
C1	0.3711	0.1384
C2	−0.0159	−0.0056
AB1	0.0749	0.0522
AB2	0.0009	0.0111
AC1	−0.0620	−0.0317
AC2	−0.0132	0.0018
BC1	−0.0040	0.0203
BC2	0.0371	−0.0004
CB1	0.0107	0.0043
CB2	0.0107	0.0043
ABC1	−0.0217	−0.0118
ABC2	0.0033	0.0273
ACB1	−0.0131	−0.0065
ACB2	0.0136	−0.0043

For D_{50}, a formal analysis involving blocking effects and 6 main effects is conducted and summarized in Table E.2. This suggests that there are some block effects, but they are not large. Again, the main effects of the 3 main factors are significant, with C appearing only to have a linear effect. There are interactions between A and the linear effects of B and C.

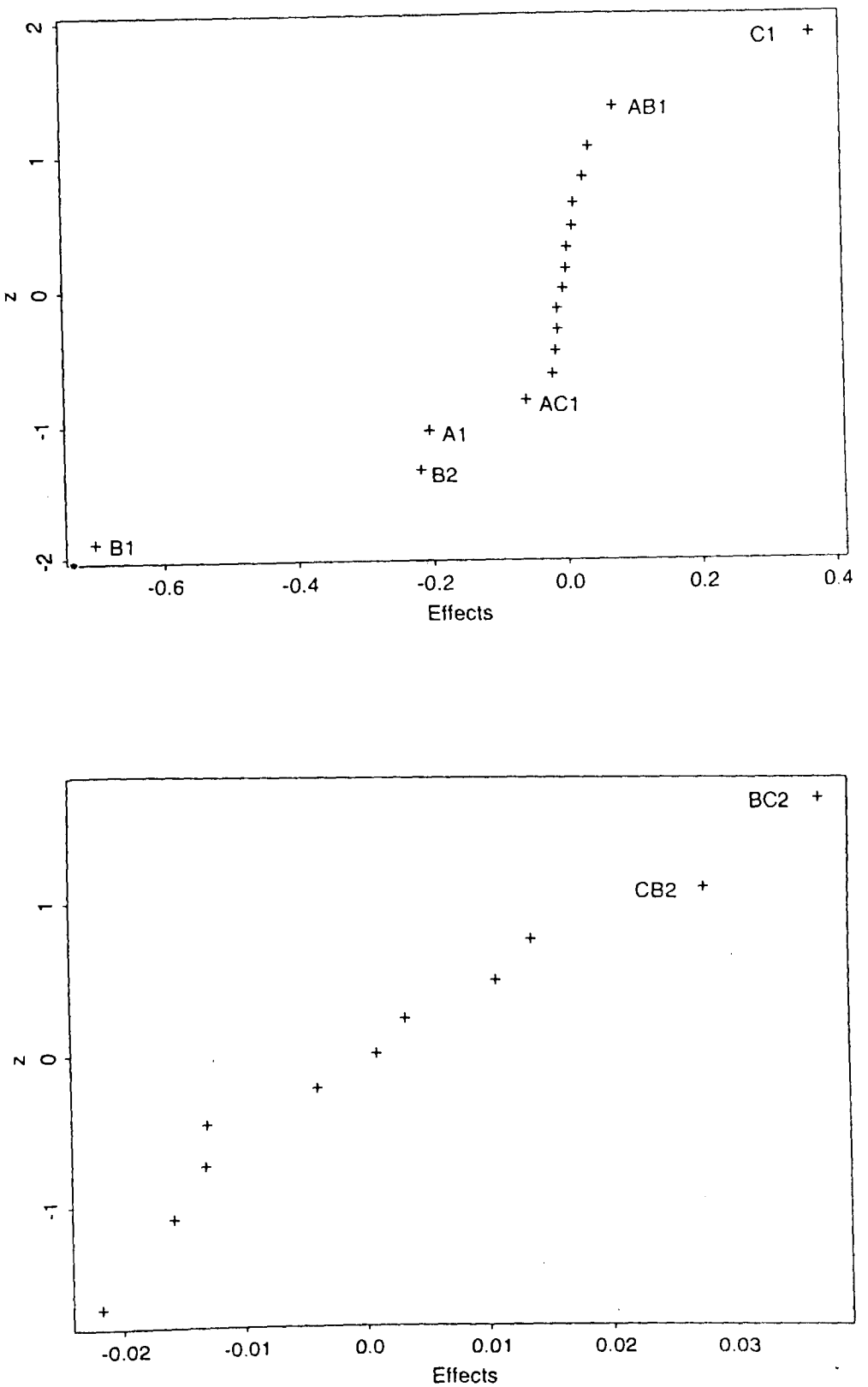

Figure E.2. Q-Q plot of the remaining 11 small effects for the response D_{50} in the first experiment

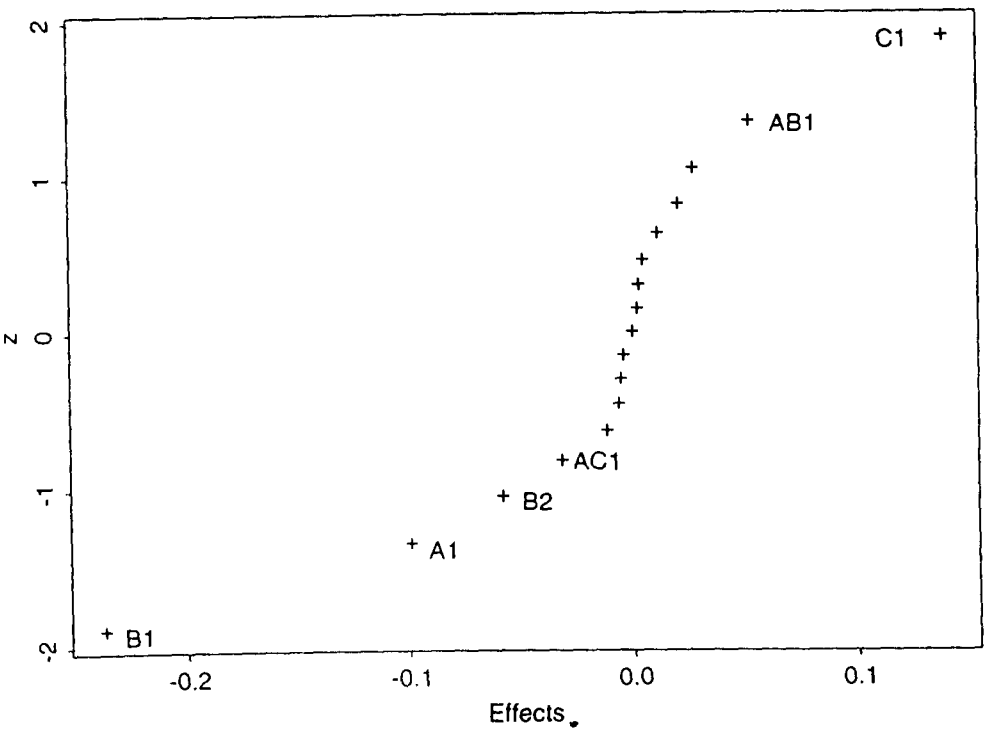

Figure E.3. Q-Q plot of 17 effects for the response *w* in the first experiment.

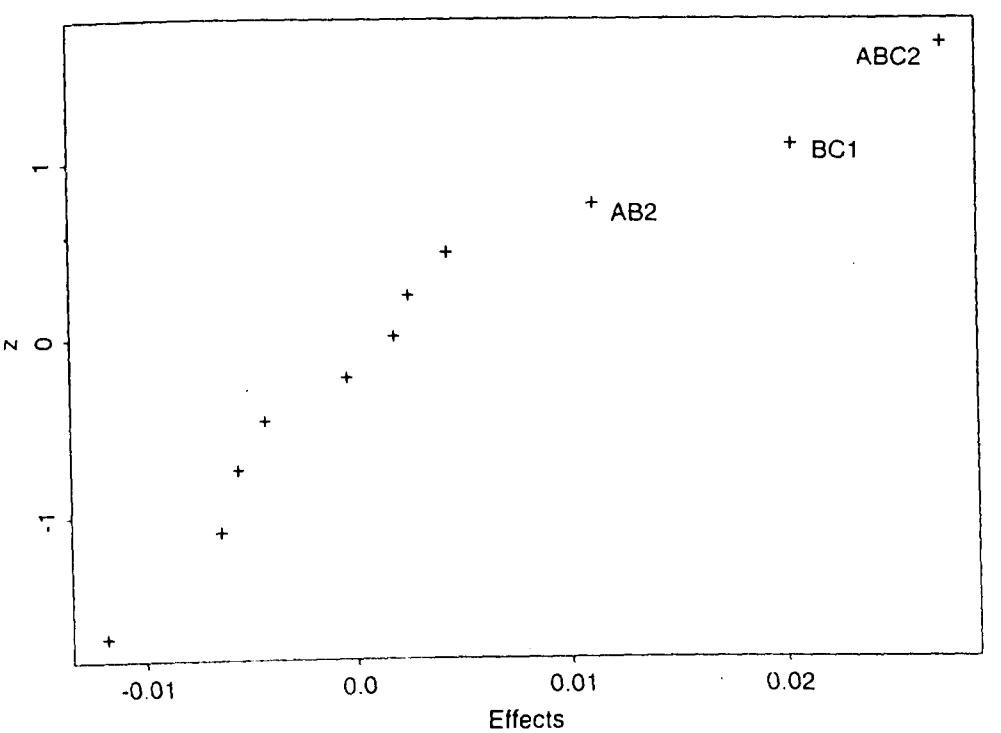

Figure E.4. Q-Q plot of the remaining 11 small effects for the response *w* in the first experiment

Table E.2. Coefficient estimates and the standard errors for D_{50} regression model

Variable	Coefficient value	Standard errors	t value	Pr (>| t |)
intercept	0.6853	0.0036	188.7585	0.0000
Bl1	0.0009	0.0154	0.0584	0.9547
Bl2	0.0374	0.0154	2.4258	0.0382
A1	−0.2050	0.0154	−13.3101	0.0000
B1	−0.7026	0.0154	−45.6142	0.0000
B2	−0.2179	0.0154	−14.1455	0.0000
C1	0.3711	0.0154	24.0952	0.0000
AB1	0.0749	0.0154	4.8639	0.0009
AC1	−0.0620	0.0154	−4.0273	0.0030

Residual standard error: 0.0154 on 9 degrees of freedom
Multiple R-squared: 0.9971
F-statistic: 385.5 on 8 and 9 degrees of freedom, the p-value is 1.715e-10

For the response w, further analysis involving blocking effects plus the identified main effects are also conducted and presented in Table E.3.

Table E.3. Coefficient estimates and the standard errors for w regression model

Variable	Coefficient value	Standard errors	t value	Pr (>| t |)
intercept	0.2572	0.0014	189.2806	0.0000
Bl1	0.0338	0.0058	5.8618	0.0002
Bl2	0.0100	0.0058	1.7434	0.1152
A1	−0.0995	0.0058	−17.2646	0.0000
B1	−0.2370	0.0058	−41.1111	0.0000
B2	−0.0582	0.0058	−10.0935	0.0000
C1	0.1384	0.0058	24.0191	0.0000
AB1	0.0522	0.0058	9.0551	0.0000
AC1	−0.0317	0.0058	−5.4978	0.0004

Residual standard error: 0.005764 on 9 degrees of freedom
Multiple R-squared: 0.9968
F-statistic: 352.1 on 8 and 9 degrees of freedom, the p-value is 2.576e-10

Using these effects plus the overall mean, but ignoring the block effects, both responses D_{50} and w are estimated for each specific combination and compared with the experimental values (Table E.4).

Table E.4. The estimation of responses D_{50} and w compared with the experimental values

No. of run	Responses (μm)			
	D_{50}	Prediction	w	Prediction
1	0.7921	0.7967	0.2863	0.3053
2	0.8032	0.8062	0.2900	0.3000
3	0.6070	0.5979	0.2238	0.2366
4	0.7844	0.7818	0.2706	0.2773
5	0.7878	0.7988	0.2709	0.2839
6	0.2983	0.3302	0.1327	0.1398
7	1.0523	1.0468	0.4028	0.4035
8	0.7010	0.6812	0.2623	0.2509
9	0.4798	0.4728	0.1907	0.1874
10	0.7096	0.6926	0.2501	0.2465
11	0.7194	0.7096	0.2533	0.2531
12	0.5243	0.5087	0.2038	0.2015
13	0.9204	0.9217	0.3685	0.3544
14	0.9154	0.9313	0.3588	0.3491
15	0.3313	0.3478	0.1422	0.1383
16	0.8520	0.8711	0.3169	0.3082
17	0.6207	0.6204	0.2239	0.2223
18	0.4362	0.4195	0.1810	0.1707

E.2. Analysis for Experiment II.

In Experiment II, a 2×2×3 complete factorial design was formed with one degree of freedom confounded with batches. 11 contrasts were identified, including A1, B1, and C1 representing linear effects of A, B and C, C2 representing quadratic effect of C, and AB, AC, BC, AC2, BC2, ABC and ABC2 representing interactions between A, B and C, which capture all the effects and all the interactions. For C, a linear and quadratic effect are separated and repeated in the interactions. Each contrast has a squared length of 12. The matrix of contrasts including batch effect is presented in Table E.5.

Table D.5. The matrix for contrasts and their estimates for Experiment II

A1	B1	C1	C2	AB	AC	BC	AC2	BC2	ABC	ABC2	bch
−1	−1	1.225	0.707	1	−1.225	−1.225	−0.707	−0.707	1.225	0.707	−1
−1	1	0.000	−1.414	−1	0.000	0.000	1.414	−1.414	0.000	1.141	−1
−1	−1	−1.225	0.707	1	1.225	1.225	−0.707	−0.707	−1.225	0.707	−1
1	1	1.225	0.707	1	1.225	1.225	0.707	0.707	1.225	0.707	−1
1	−1	0.000	−1.414	−1	0.000	0.000	−1.414	1.414	0.000	1.141	−1
1	1	−1.225	0.707	1	−1.225	−1.225	0.707	0.707	−1.225	0.707	−1
−1	1	1.225	0.707	−1	−1.225	1.225	−0.707	0.707	−1.225	−0.707	1
−1	−1	0.000	−1.414	1	0.000	0.000	1.414	1.414	0.000	−1.414	1
−1	1	−1.225	0.707	−1	1.225	−1.225	−0.707	0.707	1.225	−0.707	1
1	−1	1.225	0.707	−1	1.225	−1.225	0.707	−0.707	−1.225	−0.707	1
1	1	0.000	−1.414	1	0.000	0.000	−1.414	−1.414	0.000	−1.414	1
1	−1	−1.225	0.707	−1	−1.225	1.225	0.707	−0.707	1.225	−0.707	1

In Table E.5, each column gives a contrast with the 12 readings obtained. As each column has the same squared length, so the estimates of the effects can be compared on an equal footing. The estimation of coefficients for the full models of D_{50}, w and LN(1−R) is then analyzed, and results presented in Table E.6. For the prediction in terms of cell concentration C_{cell} and NaOCl concentration C_{NaOCl} in unit of g/L, the following conversions are needed:

- A is replaced by 2*N−1, where N is the number of passes,
- B is replaced by $2*\log(21.7/C_{cell})/\log(2)+1$, where C_{cell} is given in g/L,
- C is replaced by $\log(6.8/C_{NaOCl})/\log(2)$, where C_{NaOCl} is given in g/L.

The following analysis is to determine the major effects for D_{50}, w and LN(1−R) using normal probability plotting and establish best fitted expression equations.

Response D_{50}

Figure E.5 shows a Q-Q plot of the effects and reveals that there are five major effects, corresponding to all main factors (A, B, C and C2) plus the interaction. Table E.7 shows the estimated coefficients.

Table E.6. The estimated coefficients for the full fit models of D_{50}, w and LN(1−R).

	D_{50}	w	LN(1−R)
Intercept	0.6230	0.2300	−2.6706
A1	−0.0488	−0.0065	0.2556
B1	−0.0795	−0.0229	0.3101
C1	0.1362	0.0405	−0.7354
C2	−0.0149	−0.0047	−0.0038
AB	−0.0036	−0.0010	−0.0659
AC	0.0110	0.0034	0.0989
BC	0.0231	0.0066	0.0375
AC2	−0.0036	−0.0022	0.0114
BC2	0.0021	0.0017	0.0078
ABC	0.0048	0.0026	−0.0275
ABC2	0.0039	0.0005	−0.0125

Table E.7. Coefficient estimates and standard deviations for D_{50} regression model.

Variable	Coefficient estimate	Standard error	t value	Pr (>| t |)
intercept	0.6230	0.0056	110.7687	0.0000
A	−0.0488	0.0056	−8.6787	0.0001
B	−0.0795	0.0056	−14.1404	0.0000
C	0.1362	0.0056	24.2203	0.0000
BC	0.0231	0.0056	4.1055	0.0063
C2	−0.0149	0.0056	−2.6441	0.0383

Residual standard error: 0.01948 on 6 degrees of freedom

The effect of C2 could be ignored. The fitted model can be expressed by Equation E.1. Table E.8 lists the tested values of D_{50} and their prediction by Equation E.1 for comparison.

$$D_{50} = 0.6230 - 0.0488*A - 0.0795*B + 0.1362*C + 0.0231*B*C \qquad (E.1)$$

where $A = 2*N - 1$

$B = 2*\log(21.7/C_{cell})/\log(2) + 1$

$C = \log(6.8/C_{NaOCl})/\log(2)$

Response *w*

The initial analysis provided a list of 11 effects of w (Table E.6) which are plotted in Figure E.6. This suggests that the major effects can be confined to B, C and the interaction of B and C (BC), without much influence for A. Table E.9 presents the coefficient estimates and standard errors for the regression model.

This analysis also suggests that the interaction of B and C is not important either. The fitted equation can be written as below (Equation E.2). The fitted w values to Equation E.2 are listed in Table E.10 and compared to the observed values.

$$w = 0.2308 - 0.0229*B + 0.0405*C + 0.0066*B*C \qquad (E.2)$$

where the values of B and C are calculated as for Equation E.1.

Table E.8. The comparison of the tested values D_{50} with the fitted values to Equation E.1.

A	B	C	D_{50} (μm)	Fitted values (μm)	Residuals
−1	−1	1.224745	0.8719	0.8793	−0.0075
−1	1	0.000000	0.6143	0.6134	0.0010
−1	−1	−1.224745	0.6101	0.6022	0.0079
1	1	1.224745	0.6968	0.6793	0.0175
1	−1	0.000000	0.6919	0.6748	0.0171
1	1	−1.224745	0.2678	0.2891	−0.0212
−1	1	1.224745	0.7624	0.7769	−0.0145
−1	−1	0.000000	0.7613	0.7724	−0.0111
−1	1	−1.224745	0.4109	0.3867	0.0242
1	−1	1.224745	0.7862	0.7817	0.0045
1	1	0.000000	0.5087	0.5158	−0.0070
1	−1	−1.224745	0.4938	0.5046	−0.0109

Table E.9. Coefficient estimates and standard errors for *w* regression model.

variable	Coefficient estimates	Standard error	t value	Pr (>| t |)
intercept	0.2300	0.0034	68.1084	0.0000
B	−0.0229	0.0034	−6.7680	0.0001
C	0.0405	0.0034	11.9910	0.0000
BC	0.0066	0.0034	1.9473	0.0874

Residual standard error: 0.0117 on 8 degrees of freedom.

Response LN(1−R)

In this case, it was necessary to analyze LN(1−R) instead of R because of the skewed data, i.e., most of R values are close to 1 and the occasional value substantially lower than 1. The results for the full fit model of all contrasts of LN(1−R) are given in Table E.6. Figure E.7 shows a Q-Q plot of the contrasts against the normal order statistics. Those deviating from a straight line in the middle constitute important effects, namely the three main effects and the AC interaction. The coefficients estimated for fitting this model, and the associated standard errors are presented in Table E.11.

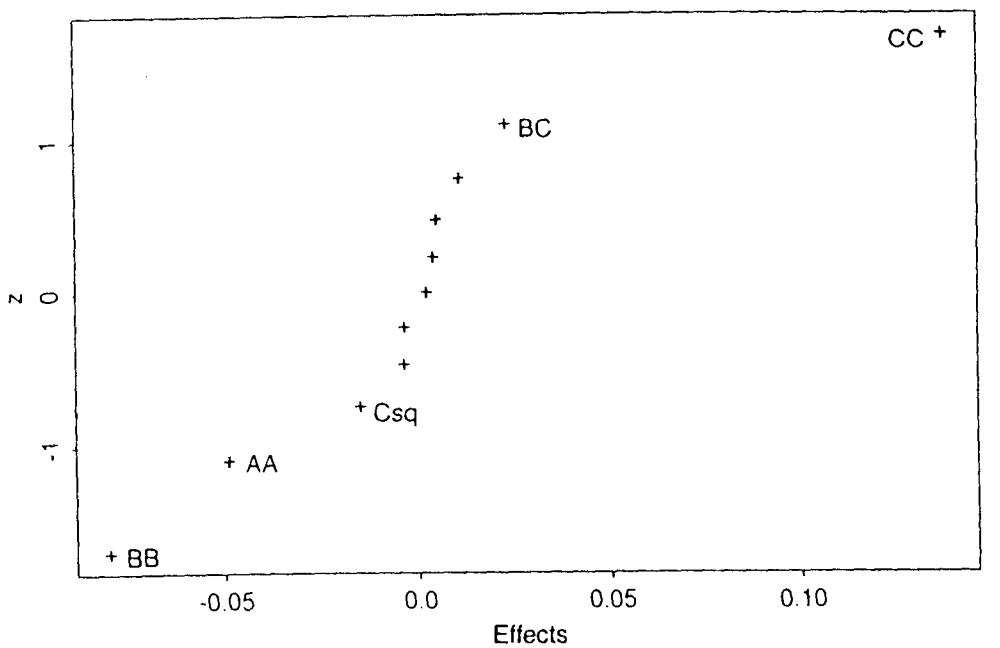

Figure E.5. Q-Q plot of the 11 effects for the response D_{50} in the second experiment.

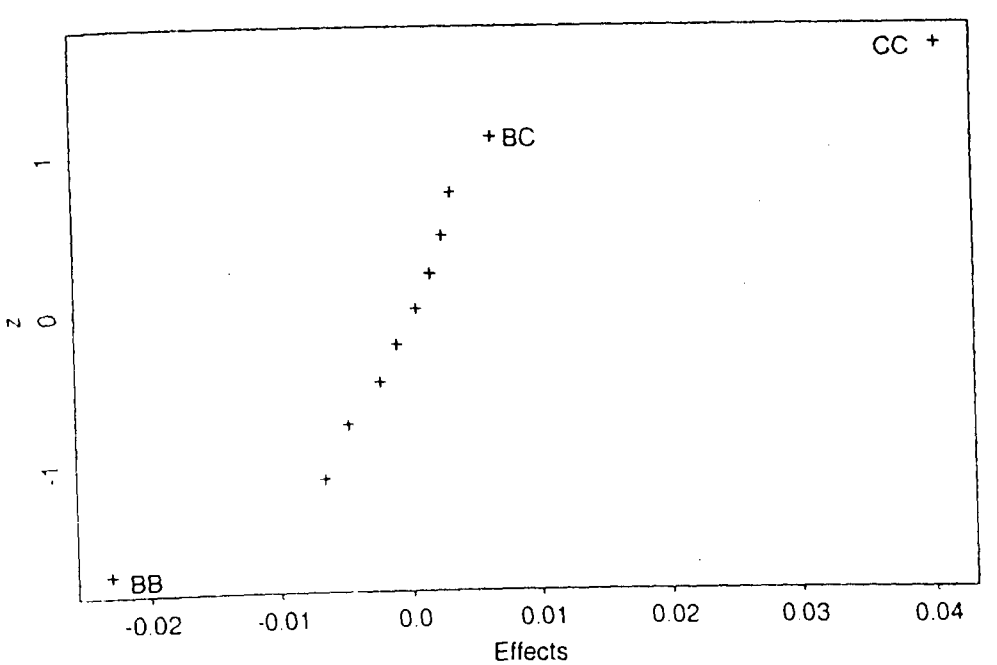

Figure E.6. Q-Q plot of the 11 effects for the response w in the second experiment.

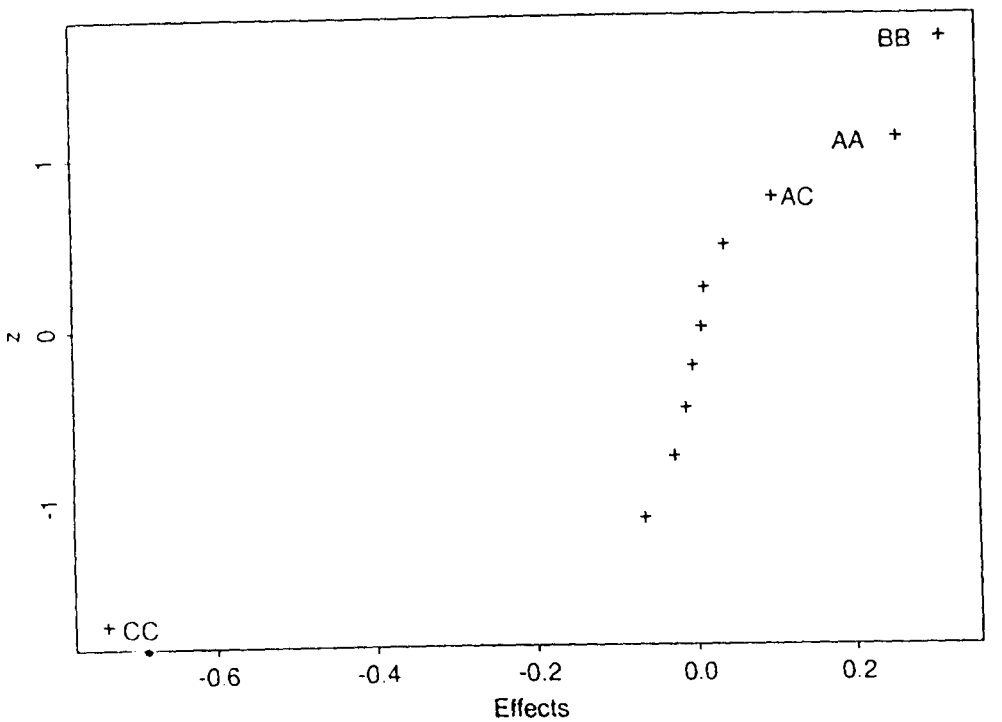

Figure E.7. Q-Q plot of the 11 effects for the response LN(1-R) in the second experiment.

Table E.10. The comparison of the tested values w with the fitted values to Equation E.2.

A	B	C	w (μm)	Fitted values (μm)	Residuals
−1	−1	1.224745	0.2964	0.2944	0.0021
−1	1	0.000000	0.2165	0.2071	0.0093
−1	−1	−1.224745	0.2152	0.2114	0.0039
1	1	1.224745	0.2613	0.2648	−0.0035
1	−1	0.000000	0.2601	0.2529	0.0073
1	1	−1.224745	0.1314	0.1494	−0.0181
−1	1	1.224745	0.2640	0.2648	−0.0008
−1	−1	0.000000	0.2635	0.2529	0.0106
−1	1	−1.224745	0.1634	0.1494	0.0139
1	−1	1.224745	0.2833	0.2944	−0.0110
1	1	0.000000	0.2062	0.2071	−0.0009
1	−1	−1.224745	0.1984	0.2114	−0.0129

Table E.11. Coefficient estimates and standard errors for LN(1−R) regression model.

Variables	Coefficient value	Standard error	t value	Pr (>| t |)
intercept	−2.6706	0.0296	−90.0790	0.0000
A	0.2556	0.0296	8.6223	0.0001
B	0.3101	0.0296	10.4588	0.0000
C	−0.6004	0.0296	−20.2528	0.0000
AC	0.0808	0.0296	2.7244	0.0296

Residual standard error: 0.1027 on 7 degrees of freedom

The best equation is given by Equation E.3. The observed and the fitted values for LN(1-R) and R are listed in Table E.12 for comparison.

$$LN(1-R) = -2.6706 + 0.2556*A + 0.0301*B - 0.6004*C + 0.0808*AC \quad (E.3)$$

Table E.12. The comparison of the tested values LN(1−R) with the fitted values to Equation E.3.

A	B	C	LN(1-R)	Fitted values	R	Fitted R
−1	−1	1.224745	−4.2267	−4.0706	0.9854	0.9829
−1	1	0.000000	−2.5575	−2.6162	0.9225	0.9269
−1	−1	−1.224745	−2.4281	−2.4020	0.9118	0.9095
1	1	1.224745	−2.7952	−2.7414	0.9389	0.9355
1	−1	0.000000	−2.6766	−2.7251	0.9312	0.9345
1	1	−1.224745	−1.5422	−1.4684	0.7861	0.7697
−1	1	1.224745	−3.3159	−3.4505	0.9637	0.9683
−1	−1	0.000000	−3.2519	−3.2363	0.9613	0.9607
−1	1	−1.224745	−1.7773	−1.7819	0.8309	0.8317
1	−1	1.224745	−3.2968	−3.3615	0.9630	0.9653
1	1	0.000000	−2.1751	−2.1049	0.8864	0.8781
1	−1	−1.224745	−2.0040	−2.0886	0.8652	0.8762

E.3. Analysis of overall data

The analysis for the two experiments has been given separately and the associated regression models are presented. In this section, the analysis will focus on the

overall data from both experiments to establish the fitted models covering the whole treatment surface.

E.3.1. Exploring the fitted models

The analysis given here focuses on the response D_{50} using stepwise regression. Initially, only batch effects and a linear term for each of the three main factors were included (Model I). The variance analysis (Table E.13) shows that the batch effect appeared to be very small compared with the other three linear factors. The model (Model II) which dropped the batch effect was then tried. Both the variance analysis (Table E.14) and the coefficient estimation (Table E.15) demonstrate that the batch effect does not appear to be important over the whole treatment surface.

Table E.13. Analysis of variance for Model I

Source of variation	No. of degrees of freedom	Sum of squares	Mean Squares	F value	Pr(F)
batch	4	0.0294035	0.0073509	1.7574	0.1735100
A	1	0.0706198	0.0706198	16.8832	0.0004624
B	1	0.5649597	0.5649597	135.0658	0.0000000
C	1	0.3433521	0.3433521	82.0857	0.0000000
Residuals	22	0.0920227	0.0041828		

Table E.14. Analysis of variance for Model II

Source of variation	No. of degrees of freedom	Sum of squares	Mean Squares	F value	Pr(F)
A	1	0.0053059	0.0053059	1.4746	0.2355411
B	1	0.4307123	0.4307123	119.6989	0.0000000
C	1	0.5707838	0.5707838	158.6260	0.0000000
Residuals	26	0.0935558	0.0035983		

Table E.15. Coefficients estimates and standard errors for Model II

Variables	Coefficient value	Standard error	t value	Pr (>| t |)
intercept	0.9630	0.0308	31.2218	0.0000
A	−0.0986	0.0187	−5.2778	0.0000
B	1.1945	0.0152	−12.7749	0.0000
C	0.1299	0.0103	12.5947	0.0000

Residual standard error: 0.05999 on 26 degrees of freedom

An alternative presentation centres each of these main factors about their mean to find out what is of moving one unit in each factor from the mean. Factor B is also re-coded so it is linear in log value in the analysis region. The coded levels of B are:

Coded levels (B)	4.33,	2,	1,
Actual levels (C_{cell}, g/L)	4.3,	21.7,	43.3

The analysis for the regression model (Model III) (Tables E.16 and E.17) shows that Model III with the re-coded factor B has a much better fit than Models I and II. The residual standard errors decreased from 0.06 for Model II to 0.043 for Model III. Including quadrate effects and also the possible interactions between the variables into Model III, the fit can be improved further with residual standard errors to be 0.0278 (Model VI) (Tables E.18 and E.19). Compared with the models described previously (Sections E.1 and E.2), the models do not quite fit to the same accuracy. A different approach should be considered to find out the best fitted D_{50} model over the entire response surface.

Table E.16. Analysis of variance for Model III

Source of variation	No. of degrees of freedom	Sum of squares	Mean Squares	F value	Pr(F)
A1	1	0.0053059	0.0053059	2.8525	0.103189
b1	1	0.4408671	0.4408671	237.0163	0.0000000
C1	1	0.6058228	0.6058228	325.6988	0.0000000
Residuals	26	0.0483618	0.0018601		

Table E.17. Coefficients estimates and standard errors for Model III

Variables	Coefficient value	Standard error	t value	Pr (>| t |)
intercept	0.6604	0.0079	83.8658	0.0000
A1	−0.0648	0.0094	−6.8711	0.0000
b1	−0.1259	0.0068	−18.4392	0.0000
C1	0.1714	0.0095	18.0471	0.0000

Residual standard error: 0.05999 on 26 degrees of freedom

Table E.18. Analysis of variance for Model IV

Source of variation	No. of degrees of freedom	Sum of squares	Mean Squares	F value	Pr(F)
A1	1	0.0053059	0.0053059	6.8668	0.0163845
b1	1	0.4408671	0.4408671	570.5617	0.0000000
C1	1	0.6058228	0.6058228	784.0442	0.0000000
A2	1	0.0000015	0.0000015	0.0019	0.9657903
b2	1	0.0000025	0.0000025	0.0033	0.9547945
C2	1	0.0195972	0.0195972	25.3623	0.0000633
Ab	1	0.0078238	0.0078238	10.1255	0.0046841
AC	1	0.0004660	0.0004660	0.6032	0.4464667
bC	1	0.0050170	0.0050170	6.4928	0.0191545
Residuals	20	0.0154538	0.0007727		

Table E.19. Coefficients estimates and standard errors for Model IV

Variables	Coefficient value	Standard error	t value	Pr (>| t |)
intercept	0.6604	0.0051	130.1210	0.0000
A1	−0.0629	0.0063	−10.0203	0.0000
b1	−0.1410	0.0057	−24.8480	0.0000
C1	0.1786	0.0064	27.7379	0.0000
A2	−0.0005	0.0080	−0.0680	0.9464
b2	−0.0081	0.0049	−1.6468	0.1152
C2	−0.0260	0.0069	−3.7835	0.0012
Ab	0.0153	0.0059	2.6150	0.0166
AC	−0.0091	0.0107	−0.8511	0.4048
bC	0.0159	0.0063	2.5481	0.0192

Residual standard error: 0.0278 on 20 degrees of freedom

E.3.2. Modelling using B/C as a single factor

The analysis was performed of D_{50} as a linear function of A and B/C using the coded values (B/C = 1.67 − log (C_{cell}/C_{NaOCl}), where the log is base 2). The results are presented in Tables E.20 and E.21.

Table E.20. Analysis of variance

Source of variation	No. of degrees of freedom	Sum of squares	Mean Squares	F value	Pr(F)
A1	1	0.005306	0.005306	2.8657	0.1019939
B/C	1	1.045061	1.045061	564.4379	0.0000000
Residuals	27	0.049991	0.001852		

Table E.21. Coefficients estimates and standard errors

Variables	Coefficient value	Standard error	t value	Pr (>| t |)
intercept	0.7727	0.0092	84.2746	0.0000
A1	−0.0603	0.0081	−7.4413	0.0000
B/C	−0.1297	0.0055	−23.7579	0.0000

Residual standard error: 0.04313 on 27 degrees of freedom

The results show the strong effects for B/C and also for A. There is clearly additional structure to be found. In particular, there might be a quadratic effect to B/C and also an interaction with A. The residual standard deviation of 0.0433 is far too high compared to 0.0278 obtained in the last section, and the 0.0154 obtained in the analysis for the first experiment (Section E.1). However, it is noted that it is comparable to the value of 0.043 found in the analysis which just includes the linear effects of each of A, B and C (Model III). This indicates that the contribution of B and C is well summarized by the single factor B/C.

Further analysis is conducted and presented in Tables E.22 and E.23. The improved model has a residual standard deviation of 0.029, which is comparable with that of Model IV.

Table E.22. Analysis of variance

Source of variation	No. of degrees of freedom	Sum of squares	Mean Squares	F value	Pr(F)
A1	1	0.005306	0.0053059	6.1166	0.02086066
(B/C)1	2	1.061220	0.5306100	611.6811	0.0000000
A1*(B/C)1	2	0.013013	0.0065064	7.5005	0.00294868
Residuals	24	0.020819	0.0008675		

Table E.23. Coefficients estimates and standard errors

Variables	Coefficient value	Standard error	t value	Pr (>| t |)
intercept	0.6666	0.0058	115.8345	0.0000
A1	−0.0602	0.0058	−10.3195	0.0000
(B/C)1	−1.0861	0.0327	−33.1982	0.0000
(B/C)2	−0.1030	0.0319	−3.2248	0.0036
A1*(B/C)1	0.1317	0.0343	3.8452	0.0008
A1*(B/C)2	−0.0125	0.0333	−0.3763	0.7100

Residual standard error: 0.02945 on 24 degrees of freedom

The fitted equation is given by Equation E.4.

$$D_{50} = 0.6841 - 0.0829*(A - 1.1) - 0.1354*(B/C - 0.866) - 0.0079*(B/C - 0.866)\text{^}2 + 0.0227*(A - 1.1)*(B/C - 0.866) - 0.0014*(A - 1.1)*(B/C - 0.866)\text{^}2, \quad \text{(E.4)}$$

where B/C = 1.67– $\log(C_{cell}/C_{NaOCl})$ and the log is base 2; A is 0, 1 or 2 corresponding to 0, 1 or 3 homogenizer passes.

Similar analysis was conducted for *w*. The initial step simply fits a linear term in B/C and a linear term in A as for D_{50}.

Table E.24. Analysis of variance for *w*

Source of variation	No. of degrees of freedom	Sum of squares	Mean Squares	F value	Pr(F)
A1	1	0.0002021	0.0002021	0.5529	0.4635619
(B/C)1	1	0.1166797	0.1166797	319.1257	0.000000
Residuals	27	0.0098718	0.0003656		

Table E.25. Coefficient estimates and standard errors for *w*

Variables	Coefficient value	Standard error	t value	Pr (>| t |)
intercept	0.2838	0.0041	69.6555	0.0000
A1	−0.0261	0.0051	−5.0820	0.0000
(B/C)1	−0.0433	0.0024	−17.8641	0.0000

Residual standard error: 0.01912 on 27 degrees of freedom

Further analysis was made by incorporating additional interaction terms as shown in Tables E.26 and E.27. This reduces the residual standard deviation from 0.01991 down to 0.01339.

The equation fitted is given by Equation E.5.

$$w = 0.2483 - 0.0227*(A - 1.1) - 0.0466*(B/C - 0.866) + 0.0013*(B/C - 0.866)\text{^}2 + 0.0141*(A - 1.1)*(B/C - 0.866) - 0.0036*(A - 1.1)*(B/C - 0.866)\text{^}2, \quad \text{(E.5)}$$

The values of B/C and A are calculated as for Equation E.4.

Table E.26. Analysis of variance for *w*

Source of variation	No. of degrees of freedom	Sum of squares	Mean Squares	F value	Pr(F)
A1	1	0.0002021	0.00020215	1.1282	0.2987412
(B/C)1	2	0.1167198	0.05835992	325.6957	0.000000
A1*(B/C)1	2	0.0055312	0.00276562	15.4344	0.0000490
Residuals	24	0.0043004	0.00017919		

Table E.27. Coefficient estimates and standard errors for *w*

Variables	Coefficient value	Standard error	t value	Pr (>| t |)
intercept	0.2511	0.0026	96.0085	0.0000
A1	−0.0307	0.0038	−8.1119	0.0000
(B/C)1	−0.3809	0.0149	−25.6147	0.0000
(B/C)2	0.0165	0.0145	1.1381	0.2663
A1*(B/C)1	0.1215	0.0222	5.4624	0.0000
A1*(B/C)2	−0.0469	0.0216	−2.1694	0.0402

Residual standard error: 0.01339 on 24 degrees of freedom

Appendix F

SUSPENSION VISCOSITY

The suspension viscosity is determined by both operational and uncontrolled variables, and is one of the factors affecting PHB and cell debris fractionation (Section 6.1.2.3). The significance of suspension viscosity on PHB collection and cell debris removal was simulated and presented in Figures F.1 and F.2. The PHB size used in the simulation is D_{50} = 0.865 μm (w = 0.111 μm) released by three passes of homogenization, and cell debris size is D_{50} = 0.559 μm (w = 0.162 μm) obtained after three homogenization passes. Other conditions are same as described in Section 6.1.2.2.

The effect of suspension viscosity on PHB collection is centrifuge feedrate dependent. Viscosity becomes less important to PHB collection at low feedrate, while significant at high feedrate. However, compared with cell debris, PHB collection is less affected by viscosity.

Suspension viscosity is affected by cell concentration, NaOCl concentration, the number of the homogenization passes in the processing conditions defined in Section 6.1.3. Since cell concentration is fixed at 40 g/L (DCW) (approximately wet weight of 80 g/L) in the simulation conducted in Section 6.1.4, the viscosity is then determined by NaOCl concentration and homogenization conditions. Due to the limitation of workload and experimental conditions, the value of viscosity used in the simulation (Section 6.1.4) was assumed. Some viscosity values are given in Table F.1.

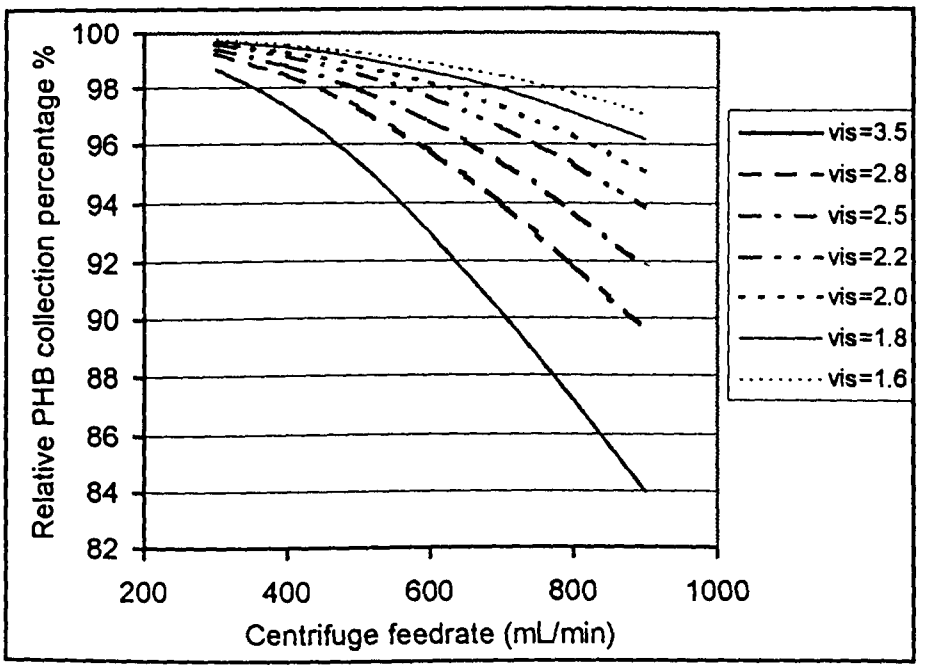

Figure F.1. Simulation of PHB collection as a function of the centrifuge feedrate at different suspension viscosity ($\times 10^{-3}$ Pa s).

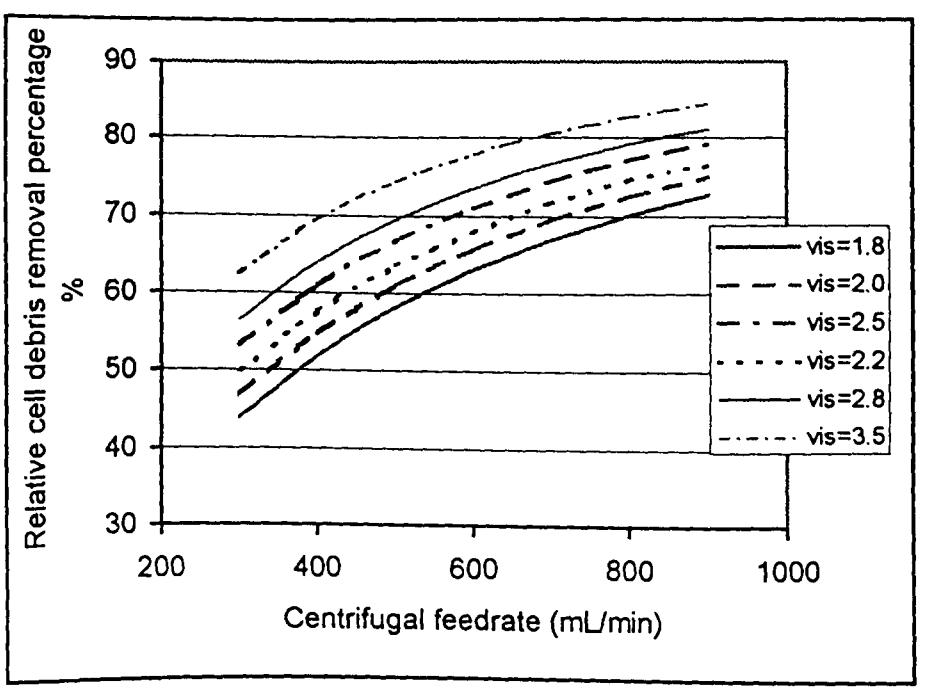

Figure F.2. Simulation of cell debris removal as a function of centrifugal feedtate at different viscosity ($\times 10^{-3}$ Pa s).

The assumed values have a basis in some background information. Viscosity is relatively constant after two homogenization passes according to Kleinig *et al.* (1995). Using an empirical model (Middelberg, 1989), a value of viscosity (2.0×10^{-3} Pa s) was assumed for the suspension (cell concentration of 40 g/L (DCW)) after three homogenization passes. The presence of NaOCl affects suspension viscosity reduction according to results presented in Chapter 3 and the simulation in Chapter 4. Both NaOCl treatment and homogenization effect viscosity reduction by the same mechanism (the destruction of long nucleic acid chains (Section 5.2)). A value of 2.0×10^{-3} Pa s was assumed after NaOCl treatment (at a concentration of 13.6 g/L), which is comparable with the value after three homogenization passes.

The contribution of NaOCl treatment to the viscosity reduction is only limited to the suspension conditions in the first centrifugation pass. The effect of NaOCl treatment on viscosity becomes negligible in the subsequent centrifugation. For the conditions after the first centrifugation pass, a viscosity value of 1.5×10^{-3} Pa s was assumed in the simulation.

Table F.1. The suspension viscosity ($\times10^{-3}$ Pa s) applied in the simulation prior to the first centrifugation (cell concentration, 40 g/L)

		NaOCl concentration (active chlorine, g/L)				
		0	0.85	3.4	6.8	13.6
The number of homogenization passes	1	6.0	4.5	2.8	2.4	2.0
	2	4.5	2.5	2.3	2.2	2.0
	3	2.0	2.0	2.0	2.0	2.0
After the first centrifugation		1.5				

The simulations presented in Section 6.1.4 are based on the above assumed viscosity values. Because most of the operating conditions which meet the requirement of ≥95% cell-debris removal involve multiple homogenization passes and multiple centrifugation passes, where the viscosity variation is less, the inaccuracy in estimating PHB collection and cell debris removal for the prediction of production cost is therefore acceptable. The errors occurred do not affect the simulations significantly.